Assessment of Reanalysis Driven RCM Simulations to Reproduce the Link Between Teleconnection Indices and wet and dry conditions in Mexico

by

Abraham HERNANDEZ-GARCIA

MANUSCRIPT-BASED THESIS PRESENTED TO ÉCOLE DE TECHNOLOGIE SUPÉRIEURE IN PARTIAL FULFILLEMENT FORTHE DEGREE OF DOCTOR OF PHILOSOPHY
Ph.D.

MONTREAL, DECEMBER 19TH, 2024

ÉCOLE DE TECHNOLOGIE SUPÉRIEURE
UNIVERSITÉ DU QUÉBEC

BOARD OF EXAMINERS

THIS THESIS HAS BEEN EVALUATED

BY THE FOLLOWING BOARD OF EXAMINERS

Mrs. Annie Poulin, Thesis Supervisor
Department of Construction Engineering at École de technologie supérieure

Mr. Rabindranarth Romero-Lopez, Thesis Co-supervisor
Faculty of Civil Engineering, Universidad Veracruzana, Mexico

Mr. François Morency, President of the Board of Examiners
Department of Mechanical Engineering at École de technologie supérieure

François Brissette, Member of the jury
Department of Construction Engineering at École de technologie supérieure

Mr. Gerald Augusto Corzo-Perez, External Evaluator
IHE Delft Institute for Water Education, The Netherlands.

THIS THESIS WAS PRENSENTED AND DEFENDED

IN THE PRESENCE OF A BOARD OF EXAMINERS AND PUBLIC

MONTREAL, DECEMBER 13TH, 2024

AT ÉCOLE DE TECHNOLOGIE SUPÉRIEURE

ACKNOWLEDGMENTS

First and foremost, I would like to deeply thank my advisor, Dr. Annie Poulin, and my co-advisor, Dr. Rabindranath Romero-Lopez, for their immense support and guidance. In addition to mentoring and encouraging me, they made great efforts to help me complete this important stage of my life. They exceeded not only my academic expectations but also demonstrated remarkable humanity and passion for their work as scientific mentors.

I would also like to thank Dr. Mariana Castañeda-Gonzalez for her sincere friendship and support throughout the completion of my PhD. Likewise, I would like to express my gratitude to the people I had the chance to meet and with whom I formed bonds of friendship, which helped renew my spirits during challenging times.

I would also like to thank the support provided by the Consejo Nacional de Ciencia y Tecnologia (CONACyT) and the Fonds de recherche du Québec Nature et Technologies (FRQNT) for the financial support granted to pursue my studies and take another step forward in my academic career.

Also, with much love, I want to thank my family for their patience, support, and understanding; they undoubtedly motivated me to continue my studies.

Finalmente, me gustaría dedicar esta tesis a mi hijo Adrián y mi compañera de vida Julia, ya que ellos son el pilar fundamental de mi vida: gracias.

Évaluation des simulations de MCR forcées par les réanalyses pour reproduire le lien entre les indices de téléconnexion et les conditions humides et sèches au Mexique

Abraham HERNANDEZ-GARCIA

RÉSUMÉ

Les effets sociaux, économiques et environnementaux associés aux événements de précipitations extrêmes sont significatifs, ce qui motive le développement de recherches sur des sujets tels que l'adaptation, la mitigation, la vulnérabilité et le changement climatique. Les implications ont été si importantes que le Groupe d'experts intergouvernemental sur l'évolution du climat (GIEC) et l'Organisation météorologique mondiale (OMM) ont publié des rapports compilant à la fois les avancées scientifiques et les pertes liées aux phénomènes hydrométéorologiques. Par conséquent, de nombreuses études abordent non seulement les mécanismes associés aux extrêmes, mais aussi ceux liés aux changements des régimes hydroclimatiques mondiaux. Ces études utilisent des outils numériques tels que les Modèles Climatiques Globaux et Régionaux (respectivement GCM et RCM), qui permettent d'analyser les simulations historiques pour faire des projections sur le comportement atmosphérique et informer la prise de décision. L'un des mécanismes associés aux changements dans les régimes mondiaux de précipitations est l'oscillation des anomalies de la température de surface de la mer (TSM). Une anomalie désigne la différence entre la moyenne climatologique de la température de surface de la mer et la valeur observée à un moment donné. De nombreuses études ont montré que cette anomalie oscille sur différentes échelles temporelles et exerce diverses influences sur les régimes de précipitations mondiaux, y compris les sécheresses, la cyclogenèse des ouragans, les changements dans la largeur de la ceinture tropicale et les événements de précipitations extrêmes, entre autres. Pour cette raison, ces anomalies sont classées comme des indices de téléconnexion (IT). Comprendre les régimes de précipitations à travers les modèles climatiques régionaux (MCR) et leur lien avec les IT est essentiel pour améliorer les prévisions de tels phénomènes. Le Groupe d'experts sur la détection des changements climatiques et des indices (ETCCDI) a développé un ensemble d'Indices d'Extrêmes Climatiques (IEC) pour caractériser les extrêmes en termes d'intensité des précipitations et de durée des conditions humides et sèches. En outre, l'Indice Standardisé des Précipitations (SPI), approuvé par l'OMM et adopté par plusieurs pays, a été largement utilisé pour quantifier les conditions d'humidité, permettant d'évaluer à la fois l'humidité extrême et la sécheresse sur la base de seuils numériques standardisés. Au Mexique, des recherches ont démontré que les indices de téléconnexion (IT), tels que l'oscillation El Niño-Oscillation Australe (ENSO) et l'oscillation décennale du Pacifique (ODP), sont associés aux sécheresses, aux précipitations extrêmes et à des contrastes accrus d'humidité entre les régions nord et sud. Ces relations sont capturées par divers indices de précipitations, y compris les Indices d'Extrêmes Climatiques (IEC) et l'Indice Standardisé des Précipitations (SPI).

Cette étude vise à évaluer la capacité des simulations des MCR, forcées avec les données d'ERA-Interim, à reproduire les modèles spatiaux de la corrélation temporelle entre les IT (ENSO et ODP) et l'Indice Standardisé des Précipitations (SPI) ainsi que les Indices d'Extrêmes Climatiques (IEC) au Mexique, en utilisant quatre simulations de MCR pour la

période de 1980 à 2012. Pour atteindre cet objectif, (1) une évaluation climatologique a été réalisée pour les précipitations issues des simulations et les données de forçage, ainsi que pour la TSM d'ERA-Interim, au cours de la période mentionnée, et (2) le modèle spatial de la corrélation temporelle entre les IT et le SPI et les IEC calculés à partir d'ERA-Interim et des simulations a été comparé aux observations.

La première partie de cette thèse examine la capacité d'ERA-Interim et des simulations des MCR à reproduire le modèle spatial de la corrélation temporelle entre les IT et le SPI. Cela a été réalisé en (1) évaluant la représentation spatiale et temporelle de la TSM en utilisant ERA-Interim et le cycle annuel climatologique des précipitations mensuelles cumulées issues des simulations ; (2) en vérifiant si ERA-Interim représente correctement les IT, et si à la fois les simulations des MCR et ERA-Interim reproduisent correctement les modèles du SPI24 et SPI60 ; et (3) en étudiant la représentation du modèle spatial de la corrélation temporelle entre les IT et le SPI24 et SPI60. Les résultats indiquent qu'ERA-Interim reproduit efficacement les caractéristiques de la TSM et des IT. Malgré certaines surestimations présentes dans les simulations et ERA-Interim, les caractéristiques des précipitations sont correctement reproduites. Cependant, le calcul du SPI24 et du SPI60 est sous-estimé à la fois temporellement et spatialement. Enfin, le modèle spatial de la corrélation entre ENSO et l'ODP avec le SPI24 et le SPI60 montre un contraste entre le nord et le sud du Mexique. Toutefois, ce modèle présente une sous-estimation de la variabilité spatiale.

La deuxième partie de cette thèse a évalué la capacité des MCR à reproduire le modèle de corrélation entre l'ENSO et les CEI. Les CEI utilisés dans cette étude sont le Comptage des Jours Secs (CDD), le Comptage des Jours Humides (CWD), les précipitations maximales en un jour (Rx1) et les précipitations maximales sur cinq jours consécutifs (Rx5). Pour atteindre cet objectif, (1) une évaluation des caractéristiques temporelles des précipitations mensuelles cumulées a été réalisée pour l'ensemble de la période d'étude, ainsi que la représentation temporelle et les phases de l'ENSO avec la TSM d'ERA-Interim ; (2) l'étude a évalué la capacité des simulations des MCR à représenter les caractéristiques spatiales des CEI utilisés ; et (3) elle a analysé si les simulations des MCR et ERA-Interim reproduisent le modèle spatial de la corrélation temporelle entre l'ENSO et les quatre CEI. Les résultats de cette section montrent que l'ENSO et ses phases sont bien reproduits par ERA-Interim. La représentation spatiale des CEI, par ERA-Interim et les simulations, montre des surestimations en termes de variabilité spatiale et de magnitude. Cependant, les principales caractéristiques spatiales observées sont bien représentées. Les simulations du Modèle Climatique Régional Canadien version 5 (CRCM5) représentent mieux le modèle spatial de la corrélation temporelle pour certains indices (CWD et Rx5). Toutefois, la simulation RCA4 montre une meilleure représentation pour la corrélation avec l'indice CDD. Enfin, dans la représentation saisonnière de la corrélation, les simulations de CRCM5 sont plus performantes en été pour les indices CDD et CWD.

Dans la dernière partie de cette thèse, la capacité à représenter les caractéristiques du modèle de corrélation spatiale entre la PDO et les CEI mentionnés précédemment a été évaluée. Ainsi, (1) le jeu de données ERA-Interim a été évalué pour représenter le modèle temporel de la PDO pendant la période considérée dans cette thèse ; (2) la représentation des caractéristiques

climatologiques des précipitations mensuelles et la représentation saisonnière des CEI avec les données ERA-Interim et les simulations ont été étudiées ; et (3) le modèle de corrélation spatiale entre la PDO et les CEI a été analysé. Les résultats de cette partie de la thèse montrent qu'ERA-Interim est capable de reproduire les principales caractéristiques et phases du modèle temporel de la PDO. Pour tous les ensembles de données, une surestimation a été observée dans la représentation des précipitations mensuelles, principalement attribuée aux saisons de printemps et d'été. Les simulations du CRCM5 montrent un meilleur ajustement pour la représentation des CEI saisonniers dans les indices CWD, Rx1, et Rx5, tandis que RCA4 donne de meilleurs résultats pour le CDD. Toutefois, chaque simulation fournit des informations importantes pour chaque saison, chaque indice et chaque région du Mexique. Pour l'ensemble de la période (1980-2012), le modèle de corrélation spatiale ne montre pas de schéma défini. Cependant, dans l'analyse saisonnière, le modèle de corrélation montre qu'au printemps, ERA-Interim et les simulations MCR capturent le principal gradient spatial décrit par les observations. En hiver, ERA-Interim présente une surestimation ; cependant, ERA-Interim et les simulations MCR parviennent à identifier les caractéristiques spatiales de la corrélation.

Dans l'ensemble, il a été observé que les données ERA-Interim et les simulations RCM capturent le principal modèle climatologique de la corrélation temporelle. Cependant, il convient de noter que ces ensembles de données pourraient fournir de meilleures informations en fonction de la saison et de la région considérée au Mexique, ainsi que du cadre temporel spécifique et de l'indice de téléconnexion (TI) étudié. Par conséquent, en raison de ces incertitudes, l'évaluation doit se poursuivre avec différents RCM et différents GCM.

Mots-clés: température de surface de la mer, anomalie, indices climatiques extrêmes, oscillation australe El Niño, oscillation décennale du Pacifique

Assessment of Reanalysis Driven RCM Simulations to Reproduce the Link Between Teleconnection Indices and wet and dry conditions in Mexico

Abraham HERNANDEZ-GARCIA

ABSTRACT

The social, economic, and environmental effects associated with extreme precipitation events are significant, driving the development of research on topics such as adaptation, mitigation, vulnerability, and climate change. The implications have been so substantial that the Intergovernmental Panel on Climate Change (IPCC) and the World Meteorological Organization (WMO) have issued reports that compile both scientific advancements and the losses related to hydrometeorological phenomena. Consequently, there are numerous studies that not only address the mechanisms associated with extremes but also those related to changes in global hydroclimatic patterns. These studies employ numerical tools such as Global and Regional Climate Models (GCM and RCM respectively), which enable the analysis of historical simulations to make projections of atmospheric behavior and inform decision-making. One of the mechanisms associated with changes in global precipitation patterns is the oscillation of Sea Surface Temperature (SST) anomalies. An anomaly refers to the difference between the climatological average of Sea Surface Temperature and the observed value at a specific point in time. Numerous studies have shown that this anomaly oscillates over different temporal scales and exerts various influences on global precipitation patterns, including droughts, hurricane cyclogenesis, changes in the width of the tropical belt, and extreme precipitation events, among others. For this reason, these anomalies are classified as Teleconnection Indices (TIs). Understanding precipitation patterns through Regional Climate Models (RCMs) and their link to TIs is essential for improving predictions of such phenomena. The Expert Team on Climate Change Detection and Indices (ETCCDI) has developed a set of Climate Extreme Indices (CEI) to characterize extremes in both precipitation intensity and the duration of wet and dry conditions. In addition, the Standardized Precipitation Index (SPI), endorsed by the WMO and adopted by several countries, has been widely used to quantify moisture conditions, allowing for the assessment of both extreme wetness and drought based on standardized numerical thresholds. In Mexico, research has demonstrated that Teleconnection Indices (TIs), such as the El Niño-Southern Oscillation (ENSO) and the Pacific Decadal Oscillation (PDO), are associated with droughts, extreme precipitation, and increased moisture contrasts between the northern and southern regions. These relationships are captured by various precipitation indices, including the Climate Extreme Indices (CEI) and the Standardized Precipitation Index (SPI).

This study aims to evaluate the ability of RCM simulations, forced with ERA-Interim data, to reproduce the spatial patterns of the temporal correlation between TI (ENSO and PDO) and SPI and CEIs over Mexico, using four RCM simulations for the period 1980 to 2012. To achieve this objective, (1) a climatological evaluation was conducted for both the precipitation from the simulations and the forcing data, as well as the SST from ERA-Interim, during the aforementioned period, (2) the spatial pattern of the temporal correlation between the TI and

the SPI and CEIs calculated with ERA-Interim and the simulations were compared with observations.

The first part of this thesis examines the ability of ERA-Interim and the RCM simulations to emulate the spatial pattern of the temporal correlation between the TI and SPI. This was carried out by (1) evaluating the spatial and temporal representation of the SST using ERA-Interim and the climatological annual cycle of monthly accumulated precipitation from the simulations; (2) assessing whether ERA-Interim accurately represents the TI, and whether both the RCM simulations and ERA-Interim successfully reproduce the SPI24 and SPI60 patterns; and (3) studying the representation, of the spatial pattern of the temporal correlation between the TI and SPI24 and SPI60. The results indicate that ERA-Interim efficiently reproduces the characteristics of the SST and TI. Despite some overestimations present in both the simulations and ERA-Interim, the characteristics of precipitation are successfully reproduced. However, the calculation of SPI24 and SPI60 is underestimated both temporally and spatially. Finally, the spatial pattern of the correlation between ENSO and PDO with SPI24 and SPI60 displays the contrast between northern and southern Mexico. However, this pattern shows an underestimation in spatial variability.

The second part of this thesis assessed the RCM ability to replicate the correlation pattern between ENSO and the CEIs. The CEIs used in this study are Counting of Dry Days (CDD), Counting of Wet Days (CWD), maximum precipitation in one day (Rx1) and maximum precipitation in five consecutive days (Rx5). To achieve this objective, (1) an evaluation of the temporal characteristics of the monthly accumulated precipitation was conducted throughout the entire study period, as well as the temporal representation and phases of ENSO with SST from ERA-Interim; (2) the study evaluated the RCM simulations capacity to represent the spatial features of the CEI used; and (3) it analyzed whether the RCM simulations and ERA-Interim reproduce the spatial pattern of the temporal correlation between ENSO and the four CEIs. The results of this section show that ENSO and its phases are reproduced by ERA-Interim. The spatial representation of the CEIs, by both ERA-Interim and the simulations, shows overestimations in spatial variability and magnitude. However, it successfully represents the main spatial features observed. The simulations from Canadian Regional Climate Model version 5 (CRCM5) better represent the spatial pattern of the temporal correlation for certain indices (CWD and Rx5). However, the RCA4 simulation shows better representation for the correlation with the CDD index. Finally, in the seasonal representation of the correlation, the simulations from CRCM5 perform better in summer for the CDD and CWD indices.

In the final part of this thesis, the ability to represent the characteristics of the spatial correlation pattern between the PDO and the aforementioned CEIs was evaluated. Therefore, (1) ERA-Interim dataset was evaluated to represent the temporal pattern of the PDO during the period considered in this thesis; (2) the representation of the climatological characteristics of the monthly precipitation and the seasonal representation of the CEI with ERA-Interim data and the simulations were studied; and (3) the spatial correlation pattern between the PDO and the CEIs was analyzed. The results for this part of the thesis show that ERA-Interim is capable of reproducing the main characteristics and phases in the temporal pattern of the PDO. For all

datasets an overestimation was observed in the representation of the monthly precipitation, which is mostly attributed to the spring and summer seasons. The simulations from CRCM5 show a better fit in representing the CEI seasonally in the CWD, Rx1, and Rx5 indices, while RCA4 performs better for CDD. However, each simulation provides important information for each season, each index, and each region within Mexico. For the entire period (1980 - 2012), the spatial pattern of the temporal correlation does not show a defined pattern. Nevertheless, in the seasonal analysis, the correlation pattern shows that in spring, ERA-Interim and the RCM simulations capture the main spatial gradient described by observations. In winter, ERA-Interim presents an overestimation; however, both ERA-Interim and RCM simulations manage to identify the spatial features of the correlation.

Overall, it was observed that both the ERA-Interim data and RCM simulations capture the main climatologically pattern of the temporal correlation. However, it should be noted that these datasets could provide better information depending on the season and the region considered within Mexico and within the specific time frame and TI. Therefore, due to this uncertainties the valuation most continue for different RCM and different GCMs.

Keywords: sea surface temperature, anomaly, climate extreme indices, el Niño-southern oscillation, pacific decadal oscillation

TABLE OF CONTENTS

Page

LIST OF TABLES

Page

LIST OF FIGURES

Page

LIST OF ABREVIATIONS

AMO	Atlantic Multidecadal Oscillation
AOGCM	Atmosphere-Ocean General Circulation Model
AR	Assessment Report
CEI	Climate Extreme Indices
CENAPRED	Centro Nacional de Prevención de Desastres
CMIP	Coupled Model Intercomparison Project
CRCM5	Canadian Regional Climate Model, version 5
CS	Climate Systme
ECMWF	European Centre for Medium-Range Weather Forecasts
ENSO	El Niño-Southern Oscillation
EOF	Empirical Orthogonal Function
ETCCDI	Expert Team on Climate Change and Indices
GCM	Global Climate Models
HadISST	Hadley Centre Sea Ice and Sea Surface Temperature
IPCC	Intergovernmental Panel on Climate Change
MAE	Mean Absolute Error
NASA	National Aeronautic and Space Administration
NCAR	National Center of Atmospheric Research
NOAA	National Oceanic and Atmospheric Administration
PDO	Pacific Decadal Oscillation
RAMS	Regional Atmospheric Modeling System
RCM	Regional Climate Models

XXX

RMSE	Root Mean Square Error
SST	Sea Surface Temperature
SSTA	Sea sSurface Temperature Anomaly
USA	United States of America
UTC	Universal Time Coordinate
WMO	World Meteorological Organizationto insert>

LIST OF SYMBOLS

°C	degree Celsius
mm	millimeters
%	percent

INTRODUCTION

Climate and meteorological extremes continue to pose significant challenges for society and the scientific community. In 2007, the Intergovernmental Panel on Climate Change (IPCC) issued a report (AR4) addressing the impact, adaptation, and vulnerability to climate change. The report highlighted that, as extreme events become more intense and/or frequent, the associated social and economic costs would rise. Furthermore, the AR4 edition mentioned that factors related to extreme weather events, such as low adaptive capacity, exposure to bodies of water, limitations in extreme event preparedness, increased droughts, changes in sea levels, and alterations in precipitation patterns, among others, pose a significant global challenge (IPCC, 2007a).

In 2012, the IPCC published a special report titled "Managing the Risks of Extreme Events and Disasters to Advance Climate Change Adaptation." The report noted a statistically significant trend in the increase of extreme precipitation events over a long period (40 years). Additionally, it reported a low-confidence increase in cyclonic activity and, with medium confidence, highlighted more intense and prolonged droughts in certain regions worldwide (IPCC, 2012).

The 2014 report (AR5) affirmed, with very high confidence, that extreme climatic events such as heatwaves, droughts, and cyclones impact sectors ranging from food production and water supply to ecosystem disruption (IPCC, 2014). In its latest report (AR6) in 2022, the IPCC observed, with high confidence, an increase in extreme climatic and meteorological events. This includes heavy precipitation events, droughts, extreme heat on continents and oceans, which have had impacts on ecosystems, infrastructure, people, and settlements (IPCC, 2022). Specifically, regarding extremes in precipitation, the World Meteorological Organization (WMO) determined in its "Atlas of Mortality and Economic Losses from Weather, Climate and Water Extremes (1970 - 2019)", that droughts ranked first as a cause of death, with up to 650,000 deaths from 1970 to 2019. Storms and floods occupied the second and third positions with 577,232 and 58,700 deaths, respectively, resulting in economic losses of up to US$521

billion (WMO, 2019). Furthermore, the impact of climate change has heightened the various risks and hazards associated with extreme precipitation events (floods and droughts). It has been observed that latitude is a determining factor for vulnerability to these phenomena, and the consequences, in addition to property losses, are linked to agricultural, energy, and human health issues, among others (IPCC, 2012).

Efforts have been made to describe extreme phenomena in precipitation, including both droughts and maximum precipitation events (Deser et al., 2010; Do et al., 2020). Indices have been developed to characterize both extremes, allowing us to understand the variables correlated with the occurrence of extreme precipitation and changes in their patterns (Karl et al., 1999; NCAR, 2024; Peterson et al., 2001). One of these variables is sea surface temperature (SST) anomaly variability, along with its behavior, feedback mechanisms, and interactions across different temporal scales, such as those represented by the El Niño-Southern Oscillation (ENSO), Pacific Decadal Oscillation (PDO), and Atlantic Multidecadal Oscillation (AMO), which are commonly referred to as teleconnection indices. Numerous studies have demonstrated the spatial and temporal association of these oscillations, highlighting how the interaction between atmospheric and oceanic processes influences precipitation patterns, such as droughts across various temporal and spatial scales, as well as changes in the frequency of heavy precipitation events (Abiy et al., 2019; Deser et al., 2010; Do et al., 2020; Méndez & Magaña, 2010). These studies, in addition to contributing to the understanding of precipitation extremes and their relationship with oceanic processes, have spurred research development in both climate models and the relationship between SST variability and changes in precipitation patterns, as well as the reproduction of climate indices.

The influence of teleconnection indices (TIs) has been observed in various regions around the world (Deng et al., 2024; Deser et al., 2010; Gebre et al., 2024; Kashki et al., 2022; Ohba & Sugimoto, 2022; Yan et al., 2024). In Mexico, TIs have been identified as a factor that spatially and temporally affects drought behavior, as well as influencing precipitation patterns (Arroyo-Morales et al., 2023, Englehart & Douglas, 2002; Méndez & Magaña, 2010). Among the TIs most frequently linked to precipitation in Mexico are ENSO and PDO. This thesis focuses on

these TIs not only due to data availability but also because of the evidence of their impact on Mexican precipitation. For instance, ENSO can extend drought conditions during its warm phase, while its cold phase tends to increase precipitation in southern and central Mexico. Similarly, the warm phase of PDO can amplify ENSO's drought effects, whereas its cold phase is associated with increased precipitation across much of Mexico (Méndez & Magaña, 2010, Mantua et al., 1997).

Currently, the ability of climate models to reproduce indices related to precipitation and temperature has been assessed. For instance, Global Climate Models (GCMs) in addition to being used to climate change projections, are also have been evaluated for their ability to reproduce the climatology of stability indices to identify the presence or absence of thunderstorms (Meher & Das, 2019). Nevertheless, for local scale, the capacity of Regional Climate Models (RCMs) has also been assessed for reproduce twelve climate indices based on temperature and nine indices based on precipitation. The conclusion is that certain RCMs have potential applications in climate change and extreme event analysis (Bayissa et al., 2021). The output of the Coupled Model Intercomparison Project Phase 6 (CMIP6) has even been evaluated for its ability to reproduce indices proposed by the Expert Team on Climate Change Detection and Indices (ETCCDI) worldwide (Kim et al., 2020). These indices, proposed for the climatic characterization of extremes under climate change conditions (Karl et al., 1999; Peterson et al., 2001), specifically those related to precipitation, provide insights into moisture conditions in a specific location and time period.

Presently, the ability of RCMs to reproduce the link between TIs and precipitation patterns is still being evaluated, as well as their capacity to capture the connection between TIs and moisture conditions, and extreme events in Mexico. The main objective of this study is to assess the capability of RCM simulations to reproduce the effects of TI on precipitation conditions in Mexico.

CHAPTER 1

LITERATURE REVIEW

1.1 Climate System

The Climate System (CS) consists of various interacting components. However, before understanding its functioning and the interactions between these elements, it is important to first define what climate is. The mean state of the variables that make up the atmosphere, as well as their fluctuations measured through standard deviation or statistical autocorrelation over a certain time interval (approximately 30 years), is referred to as climate (WMO, 2024). The climate is determined by the interaction between the elements of the CS (atmosphere, hydrosphere, cryosphere, biosphere, and geosphere). Most of these interactions are driven by solar radiation, as the sun provides the energy available in the CS (Schneider, 1992). One such interaction occurs, for example, during the day, particularly in the summer season, when the ocean absorbs more heat energy than the land due to the difference in heat capacity between the two elements. This causes the air mass over the land to increase in temperature, generating upward currents, so that the cooler air mass over the ocean moves into the available space over the land, creating a moist air flow from the ocean to the land known as a sea breeze. This example allows us to extrapolate part of the interactions within the CS.

Being fluids, the atmosphere and the oceans exhibit defined circulations, turbulence, and chaotic movements that respond on different timescales, not only between them but also within them. For example, the chemical composition of the atmosphere also affects the climate (Houghton, 1986), as the absorption and emission of solar radiation by the atmosphere are influenced by water vapor, aerosols, carbon dioxide, and ozone. Additionally, the atmosphere exchanges energy with the oceans, and the oceans, in turn, are affected by salinity, which influences water density and, consequently, ocean circulation, leading to complex processes within the CS (Schneider, 1992)

On the other hand, the cryosphere experiences seasonal and interannual variations, causing significant annual alterations in continental heating, the upper ocean mixing, and changes in heat exchange between the atmosphere and the surface. The geosphere and biosphere, due to large orographic barriers and biodiversity, influence the behavior and moisture levels of air masses within the continent and affect the CS on different timescales (Khan & Arsalan, 1966).

Understanding the functioning of each element of the CS, as well as the interactions between these elements, provides us with insight into meteorological and climatological conditions. Consequently, this knowledge enables us to make informed decisions regarding the material context that responds to the impacts of the CS elements and their interactions.

1.2 Natural Climate Variability

A key aspect is recognizing how natural variability within the climate system arises. The CS is driven by solar radiation. The imbalance in net radiation caused by a change in either solar radiation or infrared radiation is known as "radiative forcing". Both solar radiation and the injection of large quantities of aerosols into the atmosphere, as occurs during a volcanic eruption, are considered external forcings, which induce natural variations in radiative forcing. Both external variations and the interactions among the components of the CS can induce climate variability. Therefore, a distinction can be made between internal and external induction of climate change and variability. Each component of the CS responds to these forcings across a broad range of spatial and temporal scales. In the oceans, for example, due to their large heat capacity, the response time is prolonged, potentially spanning decades, centuries, or even millennia. Thus, the CS can vary on different spatial and temporal scales (IPCC, 2001).

1.3 The Ocean and Oceanic Oscillations

Among the components of the CS, the ocean plays a critical role as a vast reservoir of heat energy and a thermal regulator of the atmosphere. The ocean can influence weather and climate, affecting, among other things, the development of tropical cyclones and the spatial

distribution and intensity of precipitation (Stewart, 1997). The ocean exhibits variability in the temperature of its millimeter-thin surface layer, known as Sea Surface Temperature (SST). Various processes, both within and outside the ocean, influence the climatological behavior of SST, resulting in anomalies, which are defined as the difference between the average behavior and the actual SST value at a specific point. These anomalies exhibit variability in their oscillations across different time scales (Deser et al., 2010; Mantua et al., 1997b), and it has been observed that there is a teleconnection between the variability of Sea Surface Temperature Anomalies (SSTA) and changes in precipitation patterns around the world. SSTA oscillations are classified according to the time scale variability being observed and the phase (positive or negative) in which they occur. The El Niño-Southern Oscillation (ENSO), the Pacific Decadal Oscillation (PDO), and the Atlantic Multidecadal Oscillation (AMO) are some of these oscillations. This thesis focuses on ENSO and PDO, which belong to the Pacific basin.

1.3.1 Climate Indices (ENSO and PDO)

Given the ocean's significant role in regulating the climate system, certain oceanic phenomena, such as oscillations in sea surface temperature, are closely linked to broader atmospheric and climatic patterns. The ENSO is an oscillation that occurs on a time scale ranging from two to seven years, not only in terms of the Sea Surface Temperature Anomaly (SSTA) values but also concerning the various associated phenomena (NOAA, 2024). This oscillation is characterized by five continuous three-month anomalies. ENSO has a warm phase (El Niño), a neutral phase, and a cold phase (La Niña) (Trenberth, 2024). It is located in the equatorial Pacific and is classified into four regions: region 1+2 (0°-10°S, 90°W-80°W), region 3 (5°N-5°S, 150°W-90°W), region 4 (150°W-160°E, 5°N-5°S), and, due to its inclusion of parts of regions 3 and 4 as well as the equatorial cold tongue, and its utility in measuring significant SST changes and SST gradients, region 3.4 (5°N-5°S, 170°W-120°W) has been more commonly used (NOAA, 2024), and is utilized in this thesis. ENSO influences atmospheric circulation through deep convection caused by changes in SST, which in turn generate changes in pressure patterns due to the excitation of planetary waves (e.g., Rossby waves) (Deser et al.,

2010). Furthermore, it is associated with changes in precipitation patterns over the continent (Mexico and Central America) (Pan et al., 2018, Mendez, 2010).

The PDO results from a combination of multiple tropical and extratropical processes, including interactions with ENSO through an atmospheric bridge, as well as interactions with pressure systems over the North Pacific (e.g., Aleutian Low) (Newman et al., 2016). This oscillation is understood as a decadal variability pattern of the SSTA, obtained through the principal Empirical Orthogonal Function (EOF) (Mantua et al., 1997a). The spatial pattern of the PDO is located between 20° N and 70° N latitude. The PDO is related to the variation in precipitation patterns across North America (Aryal & Zhu, 2021b; Mccabe et al., 2004); it has even been suggested that the phases of the PDO may be linked to the expansion of the tropical belt and the convective processes inherent to that region (Grassi et al., 2012).

1.3.2 Precipitation Patterns

As these oceanic oscillations influence atmospheric circulation and pressure systems, they also have a notable impact on precipitation patterns. The interaction of these oscillations with atmospheric dynamics can alter regional meteorological conditions, which play a critical role in shaping precipitation behavior. Meteorological conditions determine the atmosphere's ability to develop upward currents that form clouds and eventually rain. These conditions may depend on the susceptibility of atmospheric systems to generate upward currents through orographic forcing and/or convective processes (IPCC, 2001). Each region of the world has different meteorological and topographical characteristics; however, ENSO and PDO, or their interaction, can contribute to developing the necessary atmospheric conditions for changes in precipitation patterns in different parts of the world (Pan et al., 2018; S. Wang et al., 2014).

1.3.2.1 Precipitation Patterns in Mexico

These global influences on precipitation patterns are particularly evident in regions like Mexico, where the interaction of local topography and regional atmospheric conditions with

large-scale oceanic oscillations plays a crucial role in shaping precipitation dynamics. Precipitation in Mexico is attributed to various mechanisms. Orographic conditions, latitudinal factors, and meteorological phenomena specific to the region are among them. Additionally, processes in the tropics that contribute to the generation of tropical disturbances, tropical storms, or hurricanes influence both the intensity and spatial distribution of precipitation. The spatial variability and intensity of annual accumulated precipitation in Mexico (Figure 2.1A) indicate that topography and the advection of moist air from surrounding oceans (Pacific Ocean and Atlantic Ocean) are strongly related to it. In the Mexican rainfall regionalization of Alvarez-Olguin (2017), thought Principal Component Analysis, there are more quantity of precipitation in the regions under the 20° of latitude, which indicates a strong contrast between the north and the south. Furthermore, precipitation in Mexico is associated with both the season and the phases of ENSO, which can favor wet or dry conditions, as the case may be (Deser et al., 2010; Pavia et al., 2006; S. Wang et al., 2014), and may influence precipitation anomalies as well as tropical cyclones (Llanes-Cárdenas et al., 2020). The PDO, in interaction with the weakening of the Caribbean low-level jet and an increase in easterly waves, could interfere with the moisture influx into northern Mexico or vice versa (Méndez & Magaña, 2010). Another factor related to precipitation extremes is the natural variability of ENSO and PDO, which may either intensify or attenuate them (Arriaga-Ramrez & Cavazos, 2010a).

1.4 Precipitation Extremes

Precipitation is part of the phenomena associated with the general circulation of the atmosphere and the interactions among the elements of the CS. Thermal energy from the sun stimulates upward air currents, causing a decrease in pressure and increasing the likelihood of cloud formation. The equatorial region receives the majority of solar radiation, creating a low-pressure belt over the equator. This belt induces upward wind flow toward the poles, as well as a cloud band over this region. The distribution of continents and oceans affects this flow, creating semipermanent pressure systems that, in turn, generate three large-scale circulation cells distributed from the equator to the poles (Hadley cell, Ferrel cell, and Polar cell). As a result, three belts are formed: two low-pressure belts (at the equator and between 50° and 60°

N/S) and one high-pressure belt at 30° N/S latitude. Additionally, with the contribution of Earth's rotation, jet streams are generated in the mid-latitudes, which can not only define the direction of storms but also influence deep convection by stimulating upper-level divergence, thereby creating more severe storms or contributing to wind shear and cloud dispersal. In the same way, large high-pressure systems can cause prolonged periods without precipitation (Wallace & Hobbs, 2006).

As suggested by Gimeno-Sotelo et al (2023), although other factors may be present, atmospheric instability is the key factor that defines the presence of cloudiness associated with extreme precipitation in a single day. Various factors are related to the development of upward air currents in the atmosphere (orography, low-pressure systems, etc.); however, the presence of moisture (precipitable water and vertically integrated water vapor) is essential for cloud formation. Tropical cyclonic phenomena contribute not only to the transport of energy but also to moisture and atmospheric instability.

ENSO and PDO, in addition to being related to changes in seasonal precipitation patterns in short and log time periods, show effects in trend changes of extreme precipitation and deep convection at tropical latitudes (Abiy et al., 2019; Casanueva, 2013; Deser et al., 2010; Do et al., 2020; Huang et al., 2024; Llanes-Cárdenas et al., 2020; Méndez & Magaña, 2010; Pavia et al., 2006; Torres-Alavez et al., 2021; Vega-Camarena et al., 2023), have also been shown to be linked to seasonal extreme precipitation in certain parts of the world. Furthermore, they contribute to moisture availability and transport (DeFlorio et al., 2013; Li et al., 2021; Xiao et al., 2017; Zhang et al., 2010). ENSO and PDO have also been associated with cyclonic activity in the tropics (Llanes-Cárdenas et al., 2020). In Mexico these TI and their phases interaction (cold and warm) have been related with the strengthening of seasonal humidity conditions, drought and effects in moisture transport over the Mexican altiplano (Méndez & Magaña, 2010; Pavia et al., 2006; Vega-Camarena et al., 2023).

1.4.1 Representation of Precipitation through Indices

Extreme precipitation regimes (both maximum and minimum) and their societal impacts have created the need to identify their patterns. Various studies employ different indices to understand these patterns, moisture conditions at specific locations, or to analyze particular characteristics of precipitation (Balling et al., 2016; Colorado-Ruiz & Cavazos, 2021; de Lima et al., 2015; Gajić-Čapka et al., 2015; Ruiz-Alvarez et al., 2020; Tramblay et al., 2013). Some of the characteristics of precipitation indices may be related to meteorological drought, extremes (maximum and minimum), the number of days with or without precipitation, or certain statistical attributes, among others. These indices are used to understand the behavior of droughts, floods, storms, flash rivers, and other hydrological, agricultural, and energy-related applications.

1.4.2 Standardized Precipitation Index

Various indices focused on precipitation deficits have been used to study moisture and drought characteristics. Some indices use only precipitation as an input parameter to analyze these conditions. Table 1 lists the indices that meet this criterion and are identified by the WMO, Global Water Partnership, The National Drought Mitigation Center, and the Integrated Drought Management Programme as the most user-friendly indices (WMO & GWP, 2017).

Table 1.1 Indices with the highest facility of use from the Integrated Drought Management and World Meteorological Organization that considers precipitation as unique parameter

Adapted from *WMO & GWP (2017)*

Index	Type	Strengths	Weaknesses	Reference
Deciles	Meteorology	Simple methodology. Wet and dry situations. Defined thresholds.	Best results with long records.	Gibbs and Maher, 1967
Percent of Normal Precipitation	Meteorology	It is calculated with basic Mathematics	It Confuses with the mean or average. The climate regimes are difficult to compare.	Hayes, 2006
Standardized Precipitation Index (SPI)	Meteorology	It is applicable in any climate regimes. multiple time scales, even short time periods. It allows missing data. It has been used extensively in many scientific articles.	Difficult compare similar scenarios with different temperature conditions. Assumes a prior distribution.	Cheval, 2016; Guttman, 1999; McKee, T.B., Doesken, N.J., Kleist, 1993

In this study, the Standardized Precipitation Index (SPI) was used, which has been documented by various authors. The SPI is capable of detecting both dry and wet conditions, as well as their periodicity, using precipitation as the sole input variable (Cheval, 2016; Guttman, 1999; McKee, T.B., Doesken, N.J., Kleist, 1993). Additionally, it has been employed to study hydrometeorological conditions and their periodicity in different regions of the world with varying geographic characteristics (Giddings & Soto, 2005; Vicente-Serrano & López-Moreno, 2005; Vu & Mishra, 2016). The SPI has also been used to examine agricultural responses to moisture conditions (Duan & Mei, 2014), historical droughts related to oceanic oscillations (Abiy et al., 2019), and even to evaluate RCMs for SPI reproduction (Bayissa et al., 2021).

It is worth mentioning that the SPI is used as a monitoring tool by various countries around the world, including Argentina, Austria, Belize, Bosnia and Herzegovina, Brazil, Bulgaria, Canada, Chile, Croatia, Cyprus, Dominican Republic, Germany, Greece, Hong Kong, Iran, Israel, Jamaica, Jordan, Kazakhstan, Libya, Lithuania, Macedonia, Mexico, New Zealand, Pakistan, Peru, Slovenia, Spain, Sri Lanka, Switzerland, Tanzania, Thailand, Trinidad and Tobago, Turkey, Ukraine, and the USA (WMO & GWP, 2017). Both the practicality of the SPI and the conditions of natural hazards resulting in extreme precipitation values have led the World Meteorological Organization (WMO) to develop a user guide for calculating the SPI (WMO, 2012), thereby enabling monitoring of these phenomena.

1.4.3 Climate Extreme Indices

Due to the impact of extreme events and the subsequent need to understand their behavior, the Expert Team on Climate Change Detection and Indices (ETCCDI) compiled a suite of indices related to extreme climate behavior (Karl et al., 1999; Peterson et al., 2001). These indices are calculated to study both temperature and precipitation; however, this document will focus only on those related to extreme precipitation behavior (Table 2). These indices have been widely used to assess extreme precipitation conditions across various regions (Balling et al., 2016; Colorado-Ruiz & Cavazos, 2021; Lagos-Zúñiga et al., 2022; Ortiz-Gómez et al., 2020; Pita-

Díaz & Ortega-Gaucin, 2020; Ruiz-Alvarez et al., 2020; Tramblay et al., 2013). They have also been used to study local extreme conditions (García-Cueto et al., 2019; Ortiz-Gómez et al., 2020), as well as in the evaluation of GCMs participating in the Coupled Model Intercomparison Project phase (CMIP6) in reproducing the Climate Extreme Indices (Kim et al., 2020).

Table 1.2 Precipitation indices from ETCCDI
Adapted from Karl et al., (1999) and Peterson et al. (2001)

Name	Time window	Definition
Rx1day	one value per month	The maximum precipitation in one day
Rx5day	one value per month	The maximum precipitation in 5 consecutive days
SDII	one value per month	The amount of precipitation in days with more than 1 mm
R10mm	one value per year	Number of days with more tan 10 mm of precipitation
R20mm	one value per year	Number of days with more tan 20 mm of precipitation
Rnmm	one value per year	Number of days with more tan any quantity of precipitation
CDD	one value per month	Maximum consecutive days with less than 1 mm of precipitation
CWD	one value per month	Maximum consecutive days with more than 1 mm of precipitation
R95pTOT	one value per year	The total amount of precipitation of the 95^{th} percentile on wet days
R99pTOT	one value per year	The total amount of precipitation of the 99^{th} percentile on wet days
PRCPTOT	one value per year	Total annual precipitation

In this project, is necessary to obtain extreme humidity conditions related not only to the intensity but also to the presence of precipitation. Additionally, detecting the number of days with and without precipitation is crucial for examining its relationship with teleconnection

indices. Therefore, the Climate Extreme Indices considered are Rx1, Rx5, CDD, and CWD, which not only observe the maximum intensity of precipitation but also its sustained daily presence.

1.4.4 Precipitation Indices Over Mexico

In Mexico, the SPI has been used to monitor humidity conditions across the country. Maps of this index are constructed over a three-month period (CONAGUA, 2024a). Additionally, it serves as one of the indicators for quantifying humidity conditions and monitoring drought in the country (CONAGUA, 2024b). Furthermore, regional studies use the SPI to determine drought classification (Campos-Aranda, 2015), trends in SPI conditions (Magallanes-Quintanar et al., 2019), and the impact of humidity conditions on agriculture (Salas-Martínez et al., 2021; Sierra-Soler et al., 2016). The SPI is so widely used that statistical models, machine learning models, and Narx neural networks have been employed to predict the SPI (Cárdenas, 2023; Magallanes-Quintanar et al., 2023, 2024).

On the other hand, Climate Extreme Indices for Mexico have been studied on a regional scale. These indices have been used to determine patterns of extreme precipitation, as well as their trends over different time windows at a regional scale. It is worth noting that most of these studies have been conducted only for the northwest of the country and for specific hydrometric stations (Arriaga-Ramirez & Cavazos, 2010b; García-Cueto et al., 2019; Ortiz-Gómez et al., 2020; Ruiz-Alvarez et al., 2020) Nevertheless Colorado-Ruiz et al. (2020) shown that the southeastern Mexico is the wettest while the north shown negative trends in the CEI analysis.

1.5 Climate Modeling

Climate models originated from the need to understand surrounding atmospheric phenomena, leading to the creation of the first conceptual models. Subsequently, analog models were developed, providing the initial insight into general circulation. These evolved into radiative-convective and energy balance models, which, in addition to accounting for energy changes

related to Earth's movements, consider radiative interactions and greenhouse gases within the CS. In the early 20th century, general circulation models were developed that incorporated atmospheric dynamics, conservation of momentum, mass, and energy, as well as humidity. After World War II, digital applications were introduced to experiment with numerical weather prediction through the exchange of momentum, energy, and mass among idealized units within the models (Cartesian grid structure), enabling the modeling of general circulation over long periods (Edwards, 2011). This technique is used by GCM, which are employed to model meteorological and climatological phenomena (Edwards, 2011). These models provide a mathematical representation of the CS that not only adheres to physical laws but also ensures that simulations are compared with observations and capable of reproducing past climate patterns and climate changes (IPCC, 2007b).

Currently, there are coupled models that simulate not only the atmosphere but also the ocean, as well as models that incorporate anthropogenic factors influencing the CS. In this context, three main approaches have emerged: Earth System Models (ESMs), Integrated Assessment Models (IAM) and Atmosphere-Ocean General Circulation Model (AOGCM). The ESMs reproduce the processes and cycles biogeochemical and the interaction with physical climate (Flato, 2011); the IAMs consider the link between the ecosystems and crop models and economic models and the AOGCMs use an idealization of the configuration of continent and ocean feedbacks (Edwards, 2011, IPCC, 2007).

Given the diverse social, agricultural, energy, and communication impacts of atmospheric phenomena, it is essential to develop tools that, through climate modeling, allow for an understanding of current phenomena and increasingly accurate projections (Nicholls et. al., 2012). This underscores the importance of utilizing, developing, and evaluating climate models. Furthermore, the existing differences in reliability across various modeled variables make the evaluation and improvement of Climate Models indispensable (Randall et al., 2007).

1.5.1 Global Climate Models

GCMs are tools that use a three-dimensional grid to simulate the exchanges of momentum, heat, and moisture both vertically and horizontally in the atmosphere and the ocean. These models have a spatial resolution ranging from 250 to 600 km, with 10 to 20 vertical layers in the atmosphere and up to 30 layers in the ocean. The inherent uncertainty in GCMs is associated with the modeling of cloud processes and small-scale phenomena. Additionally, there is difficulty in accurately simulating atmospheric feedback mechanisms within GCMs (IPCC, 2024). The applications of GCMs are extensive. However, for the purposes of this thesis, the focus will be on their use in modeling teleconnection indices and Climate Extreme Indices.

The Coupled Model Intercomparison Project (CMIP) provides a platform for comparing different climate models, enabling tracking and evaluation of the modeling of specific phenomena. In the case of ENSO simulation, significant progress has been observed across the various versions of CMIP (CMIP3, CMIP5, and CMIP6). These advancements have not only improved the representation of sea surface temperature but also the ability to simulate the phases of ENSO (Bellenger et al., 2014; Beobide-Arsuaga et al., 2021; De Silva et al., 2023; Hurwitz et al., 2014). Regarding the PDO, CMIP5 simulations can represent the spatial pattern of the PDO but have issues with simulating its phases (T. Wang & Miao, 2018). For CMIP6, there have been some improvements in spatial representation, although there is still room to enhance phase simulation (Song et al., 2021). Additionally, evaluations of CMIP6 model simulations for climate extreme indices have shown improvements in the representation of these indices related to intensity and frequency (Kim et al., 2020).

1.5.2 Regional Climate Models

RCMs are high-resolution climate models used to simulate climate at a regional level. The initial conditions of RCMs depend on the approach used, whether it is nested RCMs or statistical downscaling. The main goal of RCMs is to project and simulate regional atmospheric

patterns. It is also important to note that each region of the world has unique geographical characteristics, so the interaction of RCMs with physiographic, coastal, and terrain features differs from that of GCMs (Salathé et al., 2020).

Nested RCMs are characterized by using the atmospheric state at the beginning and throughout the simulation (initial conditions and time-dependent lateral boundary conditions), as well as surface boundary conditions to determine the interaction of energy and moisture between the soil and the atmosphere. This information comes from GCMs, which provide a framework of initial and boundary conditions to model the climatic behavior of a specific region. Forcing data also include information on greenhouse gases and aerosols (Giorgi et al., 2001).

On the other hand, statistical downscaling is a technique that creates a statistical model linking large-scale variables (e.g., jet streams, pressure patterns, etc.) from Atmospheric-Oceanic Global Climate Models (AOGCM) with local physiographic characteristics. This allows for more detailed simulations and projections by incorporating regional information (Giorgi et al., 2001). The Coordinated Regional Climate Downscaling Experiment (CORDEX) is an initiative aimed at coordinating existing RCMs worldwide to enhance the understanding of regional climate impacts. It employs Empirical Statistical Downscaling driven by GCM and reanalysis data across 14 different domains globally (Giorgi & Jr, 2015).

Studies exist that use RCMs to analyze precipitation simulations across various applications and regions worldwide. For instance, Bayissa et al. (2021) utilized RCMs to reproduce the Standardized Precipitation Evapotranspiration Index in Florida, USA, with RCMs forced by different Global Models. RCMs are also employed to assess their performance in regions with specific topographic conditions (Antic et al., 2006; Stefanidis et al., 2020) or to study the response of their simulations in relation to TI (Aryal & Zhu, 2021a; Meque & Abiodun, 2015). Additionally, the hydrological response of RCMs has been studied in hydrological basins (Teutschbein & Seibert, 2010).

1.5.2.1 RCM simulations over Mexico

Costa et al. (2023) conducted a study with RCMs that cover both Mexico and other countries, using the Regional Atmospheric Modelling System forced with CMIP5 data. The outputs from these regional models were used to simulate precipitation over the tropical region of the American continent, quantifying the intensity and duration of wet and dry events. The representation of precipitation by downscaled RCMs in the Central America domain (including Mexico in this case) has also been evaluated, where it was found that the added value lies in the cumulus parametrization, as it could provide information on the representation of local storms (Llano, 2018). In the same domain, but in 2011, simulations of the Providing Regional Climates for Impacts Studies (PRECIS) RCM were evaluated, showing improvements in the reproduction of precipitation amounts, although with some issues in representing the wet and dry seasons (Karmalkar et al., 2011). Overall, RCMs in Mexico have been used to assess these models in specific regions of the country.

1.6 Research Objectives

The relationship between teleconnection indices (TIs) such as the El Niño–Southern Oscillation (ENSO) and the Pacific Decadal Oscillation (PDO) with precipitation patterns and climate extremes is well-documented globally. However, the understanding of these interactions in Mexico remains limited. Given the acknowledged influence of ENSO and PDO on seasonal precipitation, droughts, and extreme events in this region (Méndez et, al., 2010; Pavia et al., 2006; Vega-Camarena et al., 2023), there is a clear need to evaluate how Regional Climate Model (RCM) simulations reproduce these relationships. Such an evaluation is not only crucial for validating the historical performance of RCMs but also for their reliable application in future climate projections under changing climate conditions.

Evaluating the ability of RCM simulations to reproduce monthly and seasonal ENSO-CEIs and PDO-CEIs relationships is a foundational step in understanding the behavior of RCMs under historical conditions. This assessment serves as the basis for determining the reliability

of RCMs when applied to project future climate. Accurate reproduction of historical patterns, such as the temporal and spatial correlations between TIs and CEIs, ensures that RCMs can capture key physical processes, including teleconnections and extreme precipitation dynamics (Giorgi, 2019; Laprise, 2008).

The validation of RCMs in terms of their ability to reproduce observed phenomena when driven by ERA-Interim, allows for direct comparisons with observed data, identifying biases and limitations in RCM configurations. Additionally, in future studies, comparing RCMs driven by General Circulation Models (GCMs) to those driven by reanalysis datasets provides insights into the sources of variability and errors, particularly in regions with complex topography like Mexico (Ban et al., 2021).

Understanding the mechanisms through which TIs influence precipitation patterns—including wet and dry conditions, as well as extreme precipitation events—is crucial for enhancing water resources management and disaster preparedness in Mexico. In this context, this study seeks to:

Assess the capability of reanalysis driven RCM simulations to reproduce the effects of TI on precipitation conditions in Mexico. To achieve this objective, the following research lines will be implemented:

1) Study the ability of RCM simulations to reproduce the observed link between SPI wet and dry conditions and ENSO and PDO.

2) Assess the reproduction of the observed correlation between ENSO and CEI in Mexico by RCM simulations.

3) Evaluate the reproduction of the observed correlation between PDO and CEI in Mexico by RCM simulations.

The development of these objectives will provide valuable information for improving the credibility of RCMs in simulating teleconnection-driven precipitation patterns. This will enhance their applicability in climate projections, enabling better-informed decision-making for climate adaptation and mitigation strategies. Furthermore, understanding these mechanisms will contribute to global knowledge on teleconnection indices and their regional impacts, with potential applications extending beyond Mexico.

CHAPTER 2

METHODOLOGY

2.1 Experimental set-up

The methodology for developing the aforementioned research lines requires narrowing down this thesis both spatially and temporally. Since this study involves atmospheric teleconnection indices and their remote response on the continent, the Pacific basin, specifically the PDO and ENSO regions mentioned by the National Center for Atmospheric Research (NCAR) (Deser, Clara &, Trenberth, 2022; Trenberth, 2024), was first defined. Subsequently, the research was geographically narrowed to Mexico.

Figure 1 shows that the PDO is located in part of the North Pacific basin (Figure 2.1B), while ENSO is situated in the tropical region of the Pacific Ocean (Figure 2.1A). Although ENSO encompasses four different regions (ENSO 1+2, ENSO 3, ENSO 3.4 and ENSO 4), the ENSO 3.4 region (Figure 2.1A) effectively captures the dynamics of SST anomalies in the other regions, making it the one used in this study. Regarding the continental area, Figure 2.1A displays the geolocation of Mexico, along with the average annual precipitation accumulation (1980 to 2012) and the main mountain ranges within the country. It is important to note that selecting Mexico contributes to the development of knowledge and the evaluation of the CORDEX experiment for the North American region. This selection also aids in studying RCMs and their response to teleconnection indices in relation to precipitation characterization.

Regarding the temporal scope of the study, the availability of data and the time periods reviewed in other studies were examined. The time interval defined for both SST and precipitation is from 1980 to 2012. This time frame meets the climatological requirements as well as the temporal window of the selected teleconnection indices.

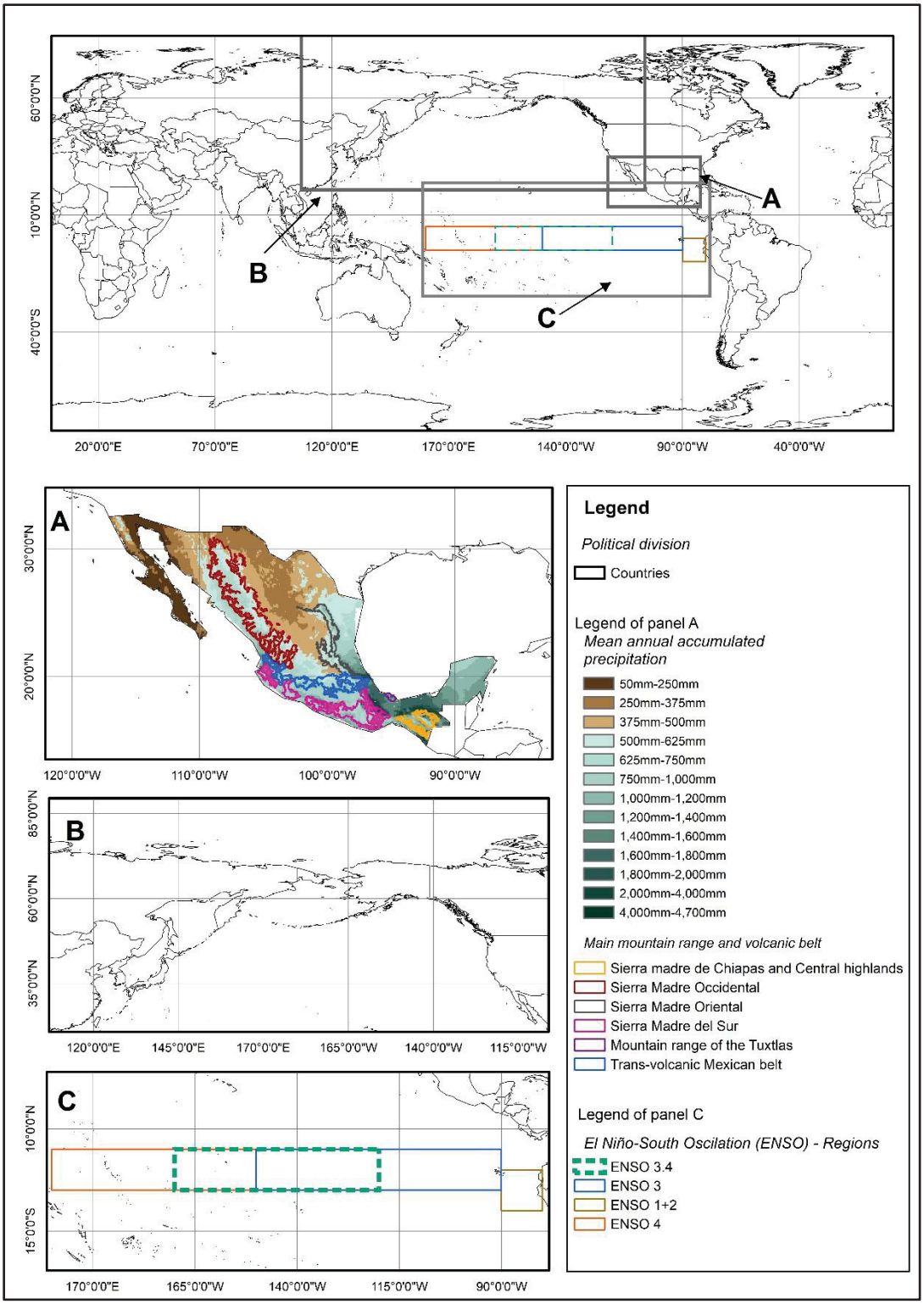

Figure 2.1 Studio area. Upper map shows the regions localization map. Panel A shows Mexico and the Mean annual accumulated precipitation and principal mountain ranges. Panel B shows de PDO region. Panel C pointed Niño regions (dotted green line ENSO 3.4)

The general diagram of the methodology for this thesis is shown in Figure 2.2 This diagram presents the consecutive stages of the research development from left to right, as well as the variables, analyses, and general calculations. Each of these stages will be described below. The first concerns the variables and data used (orange and light blue boxes in Figure 2.2), the second relates to the reproduction of each of the teleconnection indices (ENSO and PDO) and the precipitation-related indices (SPI, CDD, CWD, Rx1, and Rx5) (second stage in Figure 2.2). The final stage involves the comparison of the correlation between the teleconnection indices and the precipitation-related indices (final stage in Figure 2.2).

2.1.1 Sea Surface Temperature and Precipitation Data

After defining the study area, in the first stage, SST data were obtained from HadISST with a 1° latitude-longitude resolution, serving as observations. Additionally, ERA-Interim data (forcing data) for the same variable were acquired, with a resolution of 0.75° latitude-longitude. The SST data from ERA-Interim were adjusted to match the resolution of the observations (1° latitude-longitude) through simple spatial aggregation.

Precipitation data were obtained from Livneh et al. (2015) with a spatial resolution of 0.075° latitude-longitude, which were used as observations. Furthermore, ERA-Interim precipitation data were acquired with a resolution of 0.75° latitude-longitude, along with data from two simulations of the Canadian Regional Climate Model, fifth edition (CRCM5-ERA-Interim-0.22 and CRCM5-ERA-Interim-0.44), as well as simulations RCA4-ERA-Interim-0.5 and RegCM4-7-ERA-Interim-0.25. All simulations were forced with ERA-Interim and have different resolutions, so they were adjusted to match the resolution of the observations (0.075° latitude-longitude) through spatial disaggregation.

2.1.2 Calculation of Teleconnection Indices (ENSO and PDO), SPI, and Climate Extreme Indices

In the second stage, the teleconnection indices were calculated using data from both observations and ERA-Interim, allowing for the identification of spatial and temporal differences in their representation. ENSO was calculated using the methodology proposed by the National Center for Atmospheric Research (NCAR) (Trenberth, 2024). Meanwhile, PDO was calculated using the methodology proposed by Mantua et al. (1997).

In this same stage, the SPI and CEIs were calculated using data from both observations and ERA-Interim, as well as simulation data. SPI was calculated using the methodology by McKee, T.B., Doesken, N.J. y Kleist (1993). The CEIs were calculated using the methodology of the Expert Team on Climate Change Detection and Indices (ETCCDI) (Karl et al., 1999; Peterson et al., 2001). The SPI and CEIs calculated using ERA-Interim and the simulations were compared with those calculated from the observations.

2.1.3 Comparison and Pearson correlation

In the third stage of the methodology, the Pearson correlation was calculated (Equation 1). This calculation was performed between the time series of the teleconnection indices and each grid point of each dataset for the period defined for each case and each index.

$$\rho xy = \frac{\varepsilon((X - \mu x)(Y - \mu y))}{\sigma_X \sigma_Y} \tag{2.1}$$

In this equation, ρxy represents the correlation coefficient, and , σ_X and σ_Y are the standard deviations of "X" and "Y", respectively. It should be noted that ρxy takes values within the interval [-1,1].

In this same stage, the correlation between the teleconnection indices and the SPI was calculated (Figure 2.2, Paper 1). Since the behavior of the SPI index during the study period exhibits both wet characteristics (associated with positive threshold values) and dry characteristics (associated with negative threshold values), distinct time periods were selected based on the phases of each Oscillation. This allowed to study the correlation between each phase of the teleconnection indices under wet and dry conditions in northern and southern Mexico.

The correlation between the teleconnection indices and the CEIs (Figure 2.2, Paper 2 and Paper 3) was calculated for the entire period as well as seasonally. This was done to understand the characteristics under different atmospheric conditions, both generally and seasonally.

In the comparison stage, contrasting images were created to identify differences, underestimations, and overestimations, as well as the representation of the spatial variability for each dataset during each time period of the correlation.

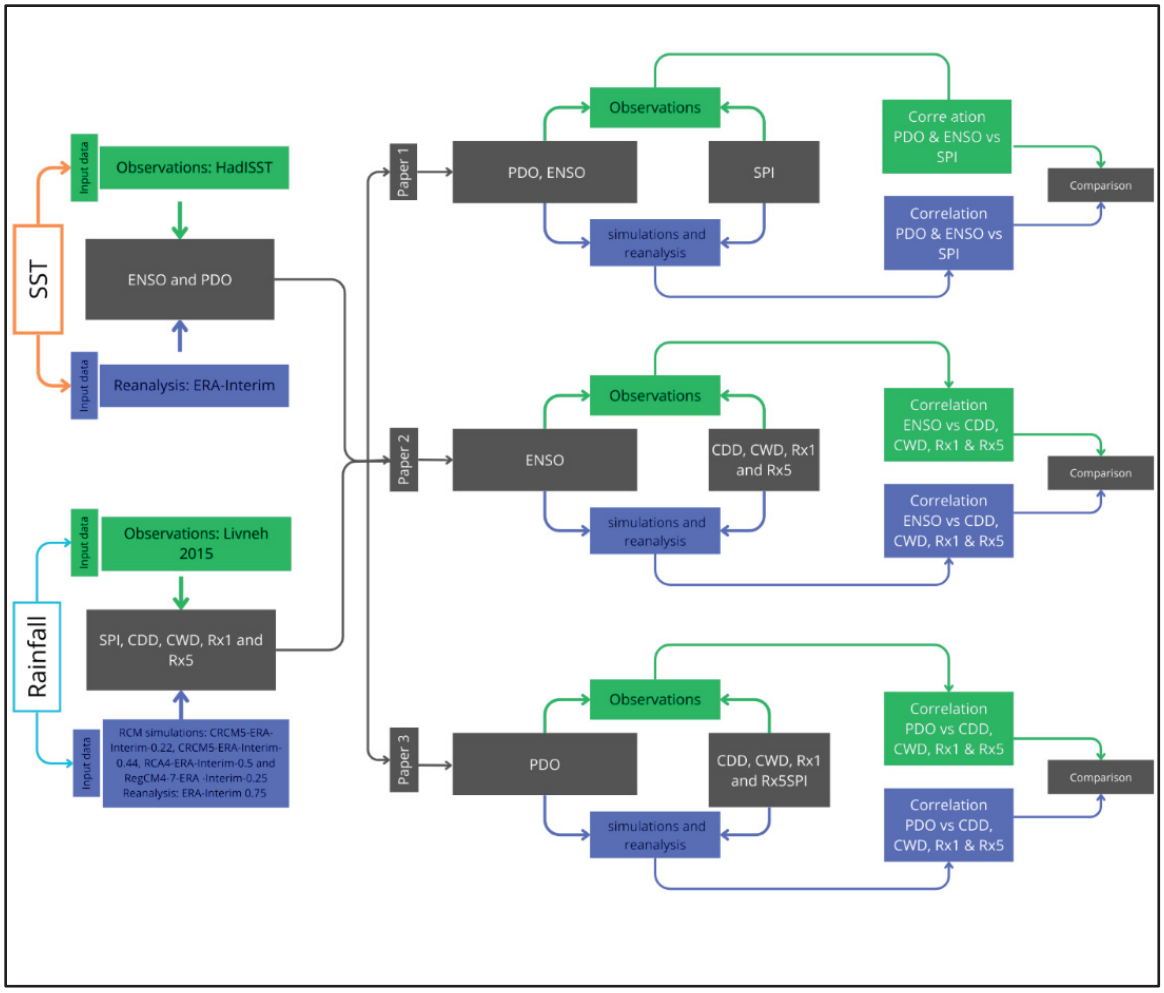

Figure 2.2 General methodology diagram of the studio

2.2 Thesis Organization

This document comprises an introduction, five chapters, a general discussion, and a conclusion, organized as follows. The first chapter provides a literature review and offers an overview of the fundamental concepts and the relevance of this study. The second chapter presents a general overview of the study's methodology. Chapters 3, 4, and 5 were submitted to international scientific journals and are described in the following paragraphs.

Chapter 3, titled *"Can Historical Regional Climate Model Simulations be Used to Study the Link Between Precipitation Patterns in Mexico and Sea Surface Temperature Oscillations"*

presents an evaluation of RCM simulations to reproduce the link between Teleconnection Indices (ENSO and PDO) and the SPI index over 24- and 60-month time windows. The results of this chapter provide a spatial and temporal perspective, not only on the relationship between SST oscillations and moisture conditions in Mexico but also on the Mexican climatology of SPI and its teleconnection with ENSO and PDO. This article was submitted to the journal *Climate Dynamics*.

Chapter 4, titled *"The Link Between ENSO and Precipitation Patterns Studied by RCM"* examines precipitation extremes and their relationship with ENSO through RCM simulations. The extremes in this chapter are represented by the Climate Extreme Indices (CEI) (CDD, CWD, Rx1, and Rx5), which provide insight into their spatial distribution in Mexico and how they are represented by RCM simulations. The results offer a climatological perspective on the correlation of these indices with ENSO and the ability of RCMs to reproduce this link. This article was submitted to the journal *Theoretical and Applied Climatology*.

Chapter 5, titled *"How Well RCM Simulations Reproduce the PDO and Precipitation Patterns Link,"* evaluates RCMs' ability to seasonally reproduce the CEI and their link with the PDO. The results provide an understanding of the simulations' accuracy and an analysis of how well the RCMs represent the link between the PDO and the CEI. This article was submitted to the journal *Theoretical and Applied Climatology*.

CHAPTER 3

CAN HISTORICAL REGIONAL CLIMATE MODEL SIMULATIONS BE USED TO STUDY THE LINK BETWEEN PRECIPITATION PATTERNS IN MEXICO AND SEA SURFACE TEMEPERATURE OSCILLATIONS

Abraham Hernandez-Garcia[1], Annie Poulin[1], Rabindranarth Romero-Lopez[2] and Dominique Paquin[3]

[1]Ecole de technologie supérieure, Department of Construction Engineering, Hydrology, Climate and Climate Change (HC3) Laboratory, Canada
[2]Universidad Veracruzana, Lomas del Estadio S/N, Zona Universitaria, Xalapa, 91000, México
[3]Ouranos Consortium, 550 Sherbrooke street West, 19th floor, West tower, Montreal, QC, Canada H3A 1B9

Paper submitted to the *Climate Dynamics*, August 2024

Abstract

Efforts to evaluate Regional Climate Model (RCM) simulations and their various uncertainties have been extensive. However, there remains a need to determine whether these simulations can accurately reproduce the links between different elements of the Climate System (CS). This study aims to assess the ability of ERA-Interim forced RCM simulations to reproduce the spatial pattern of temporal correlation between teleconnection indices (ENSO 3.4 and PDO) and the Standardized Precipitation Index (SPI24 and SPI60) over Mexico from 1980 to 2012. First, ERA-Interim's performance in reproducing Sea Surface Temperature (SST) and Teleconnection Indices (TI) was evaluated. Subsequently, both ERA-Interim forced RCM simulations and the ERA-Interim dataset itself were assessed for their ability to reproduce precipitation and the SPI in 24- and 60-month time windows. Finally, an analysis of the spatial pattern of temporal correlation between SPI24, SPI60, and TI (ENSO and PDO) was conducted. The results indicate that ERA-Interim effectively reproduces SST and TI. The simulations and forcing data also successfully reproduce the mean annual cycle of monthly accumulated precipitation. However, there is an overestimation during peak precipitation

months and in the spatial gradient of annual mean accumulated precipitation, as well as in the time series of SPI24 and SPI60, on the other hand there is a spatial underestimation in these SPI indices. Lastly, the simulations identified the north-south correlation between ENSO, PDO, and the SPI indices, though there is an underestimation in the spatial gradient of the correlation, with PDO showing the most significant correlation values.

Keywords: Teleconnection indices; Regional Climate Models; Reanalysis; ERA-Interim; Forcing data; Standardized Precipitation Index (SPI); El Niño South Oscillation (ENSO); Pacific Decadal Oscillation (PDO)

3.1 Introduction

The mechanisms underlying the behavior of the extreme precipitation patterns, both spatially and temporally, have been of scientific interest due to their potential to increase vulnerability (Zúñiga & Magaña, 2018) and have social, ecological and material repercussions and damages (Nicholls, 2012). One component of the CS that is closely linked to these precipitation patterns is the ocean (Schneider, 1992), which in addition to serving as the primary thermoregulator of the CS, transports energy from the tropics to the poles (Niiler, 1992). Ocean's behaviour and its impact on climate can be studied by using sea surface temperature (SST) data.

The SST exhibits large-scale patterns known as teleconnections, which react over different time scales and can lead to changes in precipitation patterns (Deser et al., 2010).The National and Atmospheric Administration (NOAA) defines the teleconnection patterns as "*recurring and persistent, large-scale pattern of pressure and circulation anomalies that spans vast geographical areas*" (NOAA, 2012). Several(Oviedo, 2010) patterns of SST anomalies at different time scales are considered teleconnection indices, and have been described in several studies (Deser et al., 2010). Examples include the Atlantic Multidecadal Oscillation (AMO), the Pacific Decadal Oscillation (PDO) and El Niño Southern Oscillation, to name a few (Deser et al., 2010) . These oscillations can influence precipitation patterns at the synoptic scale, particularly in Mexico and Central America (Pan 2018). Notably, droughts in northern Mexico

often coincide with abnormally wet conditions in southern Mexico and Central America, and vice versa. These associations are largely attributed to tropical sea surface temperature anomalies (PDO and AMO) (Méndez, 2010). Similarly, at a finer spatial scale, numerous studies have examined the effects of these oscillations on hydroclimatic variations within specific watersheds (Hidalgo, 2003) or droughts in specific regions(Abiy et al., 2019), including flood risks associated with the behavior of ENSO and PDO (Hamlet & Lettenmaier, 2007). In Mexico the link between ENSO and PDO with extreme precipitation, seasonal rainfall, and regional rainfall has been extensively studied (Arriaga-Ramrez & Cavazos, 2010) (Bravo-Cabrera et al., 2017)(P. J. Englehart and A. V. Douglas, 2002)(Pavia et al., 2006), In fact, Jauregui (1995) compiled a record of drought types and their associated impacts from 1535 to 1987(Jauregui, 1995), subsequently Mendez et al. (2010) studied the relation between the presence of droughts related with PDO phases Furthermore, the regional rainfall patterns have been analyzed in relation to the PDO, allowing for a comprehensive understanding of the climatic dynamics in the region(P. J. Englehart and A. V. Douglas, 2002).

Changes in precipitation patterns can have implications for extreme events such as droughts and floods. The Mexican government has developed a Drought Monitor(CONAGUA, 2024), and a National Inventory of Flood Protection Works in Natural Channels (CONAGUA, 2009). Furthermore, there is a known distinct north-south precipitation pattern, roughly divided at 20° latitude, that is, when the north experiences low values of precipitation, the south experiences high values and vice versa (Méndez & Magaña, 2010). This highlights the importance of advancing in the knowledge of the mechanisms (e.g. teleconnection indices) that trigger changes in regional precipitation patterns, and this can be done through mathematical and computational tools to improve the response capacity in the face of extreme events.

In this sense, there are studies whose objective is to analyze the ability of regional climate models (RCMs) to reproduce precipitation characteristics (Cavazos et al., 2019; Jacob, 2007; Stefanidis et al., 2020). However, despite the fact that there are efforts to analyze the response of the precipitation in the RCM simulations to the teleconnection indices (Endris et al., 2016) as well as the response of extreme precipitation at regional scale (Dittus et al., 2018), it is

necessary to further study their ability to do so in various regions of the globe. RCMs are limited-area climate models that allow simulating the climate over a given at fine spatio-temporal resolutions (in the order of 10 km). They need to be driven, at their boundaries, by global datasets inherited from reanalyses or general circulation models (also known as environmental system models in their most advanced versions (Flato, 2011; Xu et al., 2019). Several indices can be used to study the spatial and temporal variation of precipitation patterns over a given area. Among those, the standardized precipitation index (SPI) is widely used(WMO, 2012), and allows characterizing the frequency of extreme (wet or dry) conditions and defining various meteorological drought intensities on a range of timescales and across regions with climates that can differ substantially. Additionally, SPI is simple to compute as it uses only precipitation as input data (Keyantash, 2023); (Méndez & Magaña, 2010); (Schneider, 2013) (Andrade-Velázquez, 2020). SPI can be computed on timescales varying from 1 to 60 months (i.e. SPI1 to SPI60).

The main objective of this paper is to study the ability of a set of four ERA-Interim-driven climate simulations to reproduce the observed link between precipitation patterns in Mexico and two SST oscillations, ENSO and PDO.

In order to achieve this main goal, three sub-objectives are addressed:

1. Since ERA-Interim is the global climate dataset from which SST information is provided to RCMs, the ability of ERA-Interim at reproducing SST, ENSO and PDO, spatially and temporally, is first analysed;
2. Then, a comparison between observed and RCM-simulated precipitation patterns in Mexico is performed, using mean precipitation values, SPI24 and SPI60 indices which are compatible with the timescales of ENSO and PDO, respectively. ENSO occurs over a cycle of two to seven years (Santoso, 2022), while PDO has a normal cycle of a decade (Deser, 2022).

3. Finally, an analysis is conducted to assess the reproduction of the spatial pattern of temporal correlation between the SPI24 and SPI60 indices and the teleconnection indices (ENSO and PDO).

The rest of this paper is organized as follows. A short description of the study sites is presented in Section 1, followed by a description, in Section 2, of the SST data sets as well as precipitation data sets that were utilized. The third section corresponds to the methodology used for the analysis. The fourth section is dedicated to the results, and is followed by a discussion in Section 5. Finally, a conclusion is presented.

3.2 Study sites

The regions to be considered for the teleconnection indices (PDO and ENSO) are shown in Figure 3.1. The delimitation of the PDO region (grey dotted area) is from 20° latitude towards the north pole (Deser, 2022). Since the El Niño 3.4 region takes in account portions from Niño 3 and 4 regions, and also reflects the phases of ENSO (NOAA, 2024), this region was considered for ENSO (box delimited by the line dotted gray) and delimited upon the information available in the Climate Data Guide from the National Center for Atmospheric Research (NCAR) (Trenberth, 2024).

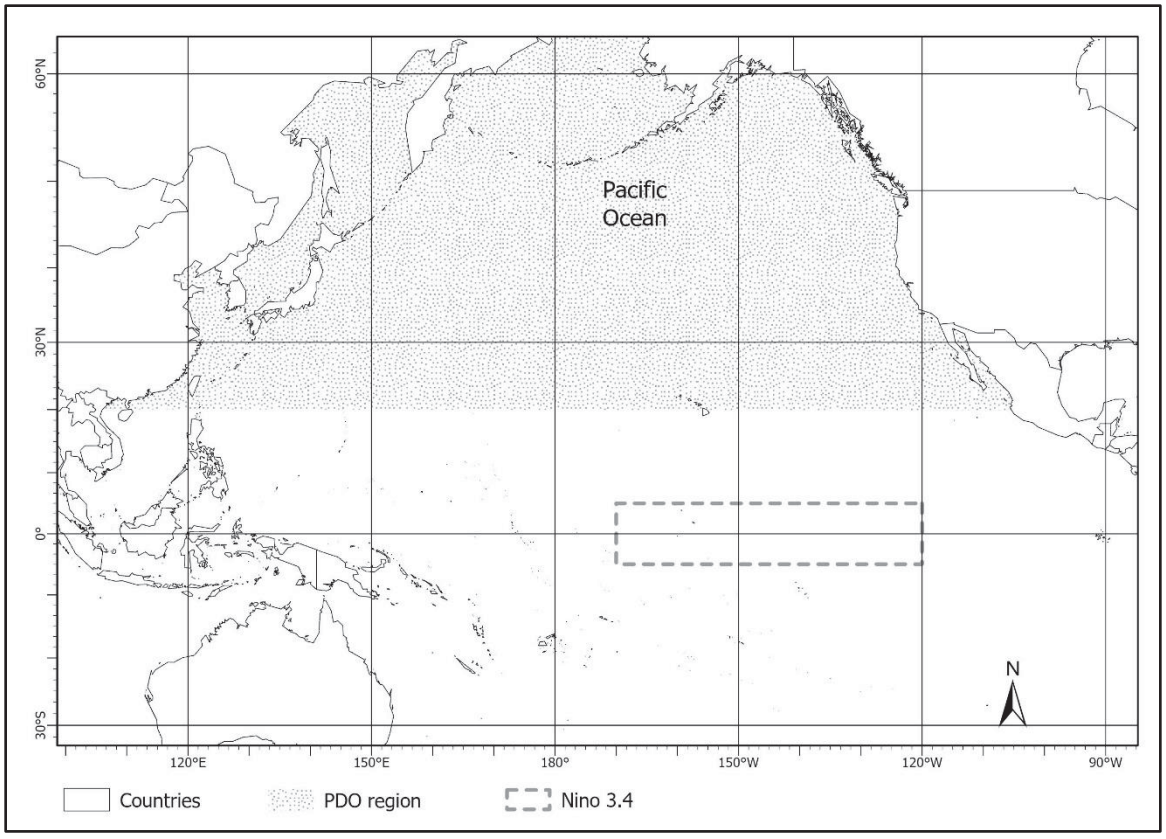

Figure 3.1 PDO and ENSO 3.4 regions used in this study

This study looks at precipitation patterns over the entire Mexican country territory, as shown in Figure 3.2. The map also shows, the mean annual accumulated precipitation computed form Livneh (2015) gridded dataset over the 1980-2012 time period (see section 2.2 hereafter for more details). The main mountain ranges in Mexico are also identified in this figure, i.e.: Sierra Madre Occidental, Sierra Madre Oriental and Sierra Madre del Sur.

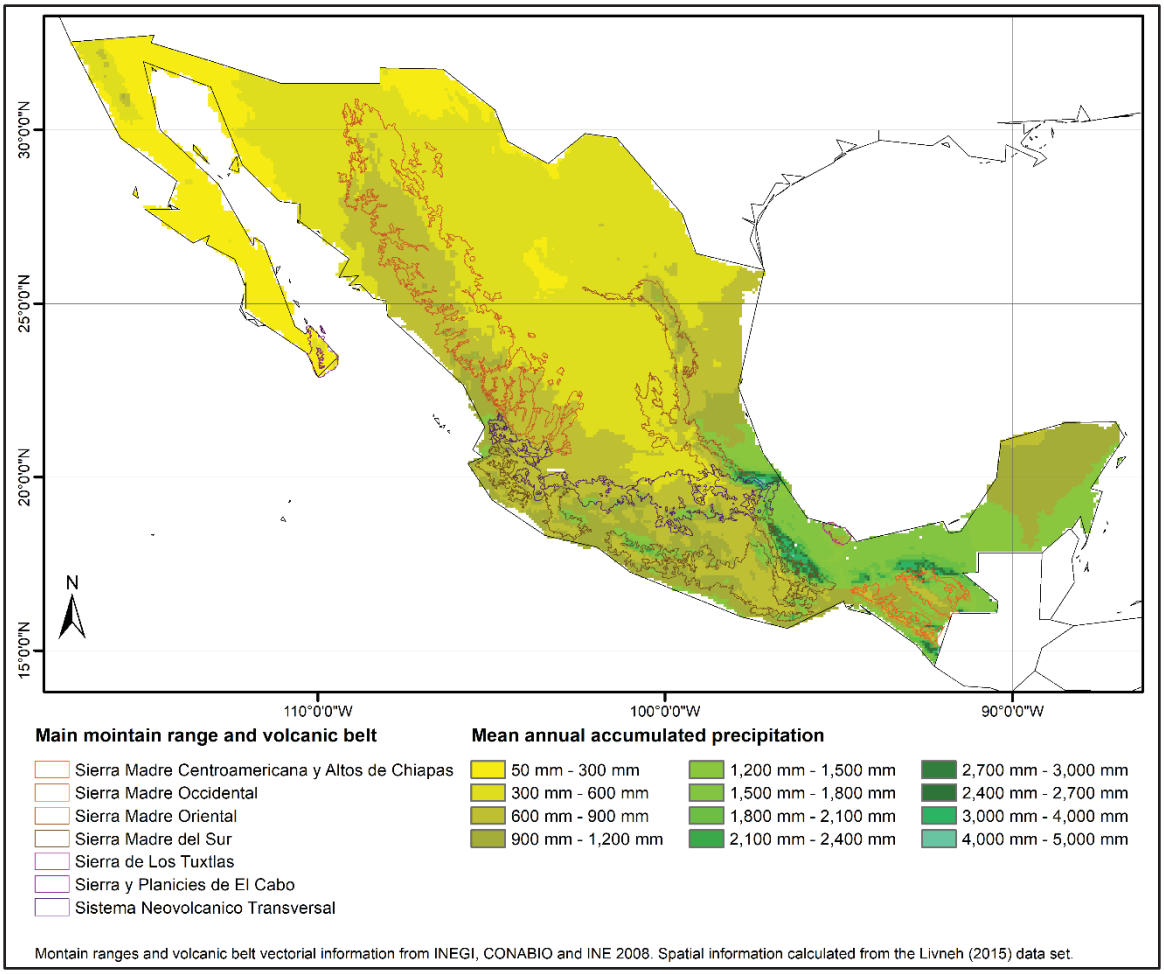

Figure 3.2 Map of Mexico showing mean annual accumulated precipitation and the main mountain ranges

3.3 Data

In this study global-scale SST data from the north and center of the Pacific Ocean, as well as regional precipitation data for Mexico were utilized. The following subsections provide a description of these datasets.

3.3.1 Sea Surface Temperature data

The SST data comes form the Met Office Hadley Centre's sea ice and Sea Surface Temperature (HadISST). This dataset combines monthly sea surface temperature and sea ice concentration

data at 1° latitude-longitude resolution (Rayner et al., 2003). Additionally, data from ERA-interim (Reanalysis) was utilized, which provides monthly averages at a resolution of 0.75° latitude-longitude. In this study, ERA-Interim is the global dataset that was used to drive the RCM simulations from which precipitation data were analysed (see section 2.2 hereafter). The ERA-Interim data can be accessed at https://apps.ecmwf.int/datasets/data/interim-full-moda/levtype=sfc/ (Berrisford et al., 2009).

3.3.2 Precipitation data

Precipitation data comes from three different sources, observations, reanalysis and RCM simulations. For the observations, the gridded data of Livneh (2015) were used, which have a spatial resolution of 1/16° ≈ 0.075° (~6km) latitude-longitude and a daily temporal resolution (Livneh et al., 2015). Regarding the reanalysis data, these come from ERA-Interim and present a spatial resolution of 0.75° latitude-longitude, with 12 hours temporal resolution (0000 and 1200 UTC). The time period considered is from 1980 to 2012, to remain coherent with the availability of RCM data (Table 1).

Four RCM simulations have been used, and are all part of the CORDEX available simulations for the Central America domain (Table 1). They were selected since: (1) they are all reanalysis-driven which allows comparison with observed data; (2) they have been produced using three RCMs at different spatial resolutions. In particular, the two Canadian Regional Climate Model version 5 (CRCM5) (Martynov et al., 2013) simulations can provide insights on the effect of spatial resolution on the results. Precipitation data were available at a daily time scale.

Table 3.1 ERA-Interim forced Simulations from RCM's considered in this paper

RCM	Data driven	Spatial resolution	Time period	Variable
CRCM5-ERA-Interim-0.22	ERA-Interim	0.22° latitude-longitude	1980 - 2012	Precipitation
CRCM5-ERA-Interim-0.44	ERA-Interim	0.44 latitude-longitude	1980 – 2012	Precipitation
RCA4-Interim-ERA-0.5	ERA-Interim	0.5 latitude-longitude	1980 – 2012	Precipitation
RegCM4-7-ERA-Interim-0.25	ERA-Interim	0.25 latitude-longitude	1980 - 2012	Precipitation

3.4 Methods

This section comprises first, the method used in adjusting the data, both precipitation and SST, due to the difference in resolutions, and second, the methodology used in the analysis.

3.4.1 Data adjustment

3.4.1.1 SST data spatial aggregation

To compare the reanalysis data (ERA-Interim) with observations (HadISST), both temporally and spatially, the ERA-Interim data were aggregated spatially to match the coarser resolution of the observations (Bierkens, 2000). The process involved averaging the information from ERA-Interim within a 0.5° square of each location of the observations and assigning this value to the corresponding observation grid tile.

To compare the reanalysis data (ERA-Interim) with observations (HadISST), both temporally and spatially, the ERA-Interim data were aggregated spatially to match the coarser resolution of the observations (Bierkens, 2000). The process involved averaging the information from

ERA-Interim within a 0.5° square of each location of the observations and assigning this value to the corresponding observation grid tile.

3.4.1.2 Precipitation data resolution adjustment

The precipitation data used in this study come from various sources with different resolutions (Table 1). Therefore, an adjustment was performed to match the resolution of the observations, which is 1/16° (~6km, ~0.075°). This adjustment involved spatial disaggregation, where the values from each dataset were distributed to the resolution of the observations while preserving the original values.

3.4.2 Analysis methods

3.4.2.1 Comparison between HadISST and ERA-Interim SST data

Temporal reproduction of SST. The temporal comparison involved aggregating spatially averaged time series, specifically focusing on the central and northern Pacific region spanning from -23.5° to the North Pole. also for assessing the anomaly variation, the time series were detrended, with mean value equal to 0 and standard deviation equal to 1. The Pearson's correlation coefficient was also computed between the two spatially averaged time series (equation 1).

$$\rho xy = \frac{\sum((X - \mu x)(Y - \mu y))}{\sigma_X \sigma_Y} \tag{3.1}$$

Where ρxy represents the correlation coefficient, and the standard deviations for “X” and “Y” are given by the expressions σ_x, σ_y respectively. Note that the correlation coefficient (ρxy) takes values in the interval [-1,1] (Storch, 1999).

The bias was also investigated by computing a simple difference between the two time series.

Spatial reproduction of SST. The root mean square error (RMSE; equation 2) and the mean absolute error (MAE; equation 3) (Chai, 2014), were computed between the ERA-Interim and HadISST time series at each grid cell.

$$MAE = \frac{1}{n}\sum_{i=1}^{n}|e_i| \tag{3.2}$$

$$RMSE = \sqrt{\frac{1}{n}\sum_{i=1}^{n}e_i^2} \tag{3.3}$$

Where "n" is the total number of days in the time series and "e" is the simple difference between the observation and the upscaled reanalysis data for each grid cell. These two errors were calculated for each grid cell over the central and northern Pacific.

3.4.2.2 Comparison of the reproduction of ENSO and PDO oscillations by HadISST and ERA-Interim.

Temporal and spatial reproduction of ENSO. The ENSO index time series was computed based on the methodology described in (K. & N. C. for A. R. S. Trenberth, 2024), which defines this index as the normalization with the standard deviation of the 5-month moving average of the SST, after subtracting the climatological average (in other words: temperature anomaly). The spatial pattern was calculated with the main empirical orthogonal function (EOF1) of the detrended anomaly of the sea surface temperature. As mentioned previously, the 3.4 ENSO region is used in this study.

The time period considered is 1980 – 2012. This methodology was used both in the observations (HadISST) and in the reanalysis data (ERA-Interim).

Temporal and spatial reproduction of PDO. The methodology mentioned in Mantua (1997) was used, which obtains the EOF from the detrended SST for each time series in each grid cell, where the EOF1 is the leading spatial pattern of the variability of PDO and the leading Principal Component is the time series of this index (Mantua et al., 1997). The above was calculated for the two data sets (HadISST and ERA-Interim) for the period of interest (1980 - 2012).

Temporal bias of the reproduction of ENSO and PDO. Simple subtraction was used to find the temporal pattern of the bias between the HadISST-derived ENSO and PDO indices times series, and the ERA-Interim-derived time series.

3.4.2.3 Comparison of precipitation from observations, ERA-Interim and RCM simulations

The precipitation comparison was conducted through spatial and temporal analysis using various representations. The mean annual cycle based on monthly accumulated precipitation values was calculated for entire Mexico, over the 1980-2012 time period, in order to assess the relationship between precipitation observations data, the reanalysis data (ERA-Interim) and the ERA-Interim-driven RCM simulations (Table 1) in reproducing temporal patterns. The correlation coefficient (equation 1) between the mean annual cycle time series was also computed. The spatial pattern assessment was done through the annual mean accumulated precipitation, for each grid cell, and was shown graphically as raster in the original datasets resolutions.

3.4.2.4 Standardized Precipitation index for 24- and 60-months time-windows.

The standardized precipitation index (SPI) was computed by fitting the normal inverse distribution to the Gamma probability distribution of the moving average of 24- and 60-months precipitation values, covering a period of 33 years (1980 - 2012) (McKee, 1993). SPI classifications system was obtained from the Standardized Precipitation Index User Guide (Table 3.2) (WMO, 2012) , which was used also for validating the results. This calculation was

applied to the spatially averaged monthly time series of the Mexican precipitation for each data set: Livneh (observations), ERA-Interim reanalysis and RCM simulations.

Table 3.2 SPI system classification
Adapted from WMO (2012)

SPI Value	Drought Category
2.0 and more	Extremely wet
1.5 to 1.99	Very wet
1.0 to 1.49	Moderately wet
-0.99 to 0.99	Near normal
-1.0 to -1.49	Moderately dry
-1.5 to -1.99	Severely dry
-2 and less	Extremely dry

Since the three types of precipitation datasets used in this study are gridded, spatial representations of SPI24 and SPI60 can be shown, by computing one mean SPI value (in each case, in specific time period) per grid cell. The time periods that were chosen in this study span 4 or 5 years in the case of the SPI24 index, and 14 years in the case of the SPI60 index. Those time periods were specifically selected because the SPI indices display opposite conditions in the north and south of Mexico (wet vs. dry and dry vs. wet).

3.4.2.5 Spatial pattern of temporal correlation of SPI24 and SPI60 indices with ENSO and PDO oscillations

The analysis of the spatial pattern of the temporal correlation was addressed by computing the correlation per grid point, through equation 1, between the SPI indices (SPI24 and SPI60) and the climatic oscillations (ENSO and PDO) time series, in selected time periods. The results are displayed as correlation maps. The choice of time periods was based on the temporal evolution of oscillations, specifically examining the SPI index at different phases of ENSO

and PDO, respectively. Observations data (Livneh and HadISST data set) were used as reference correlation pattern between SPI and the teleconnection indices, while ERA-Interim and RCM simulations data were used to study the reproduction of the pattern described by observations.

3.5 Results

The results section is divided into three parts, respectively dedicated to SST data and the ENSO and PDO oscillations, to the reproduction of precipitation patterns in Mexico and the SPI24 and SPI60 indices, and to the analysis of the correlation pattern of the temporal correlation of the ENSO and PDO with the SPI24 and SPI60 indices over Mexico.

3.5.1 Comparison between HadISST and ERA-Interim SST data

3.5.1.1 Reproduction of the sea surface temperature in the Central and North Pacific region

For having a fair comparison between the different datasets of the sea surface temperature data, the ERA-Interim data was scaled to match HadISST data resolution, hereafter we refer to this data as upscaled ERA-Interim.

Temporal reproduction of SST. In order to show the similarities between the different sea surface temperature data, as far as the covariation of the temporal behavior is concerned, the linear correlation was calculated, where the fit between each data set is quantified (ERA-Interim and upscaled ERA-Interim) with respect to observations (HadISST). The correlation that presents the highest value with HadISST is ERA-Interim, with 1, while the upscaled ERA-Interim is 0.97, however, the average of the bias between HadISST and ERA-Interim is notably greater, 5.62 ° C, while the mean bias between HadISST and upscaled ERA-Interim is only 0.23 ° C.

Figure 3.3 shows a comparison between the SST anomaly time series from HadISST and upscaled ERA-Interim datasets. It shows a high level of agreement between the two data sets. in addition to showing bias values that remain within 0.5 ° C.

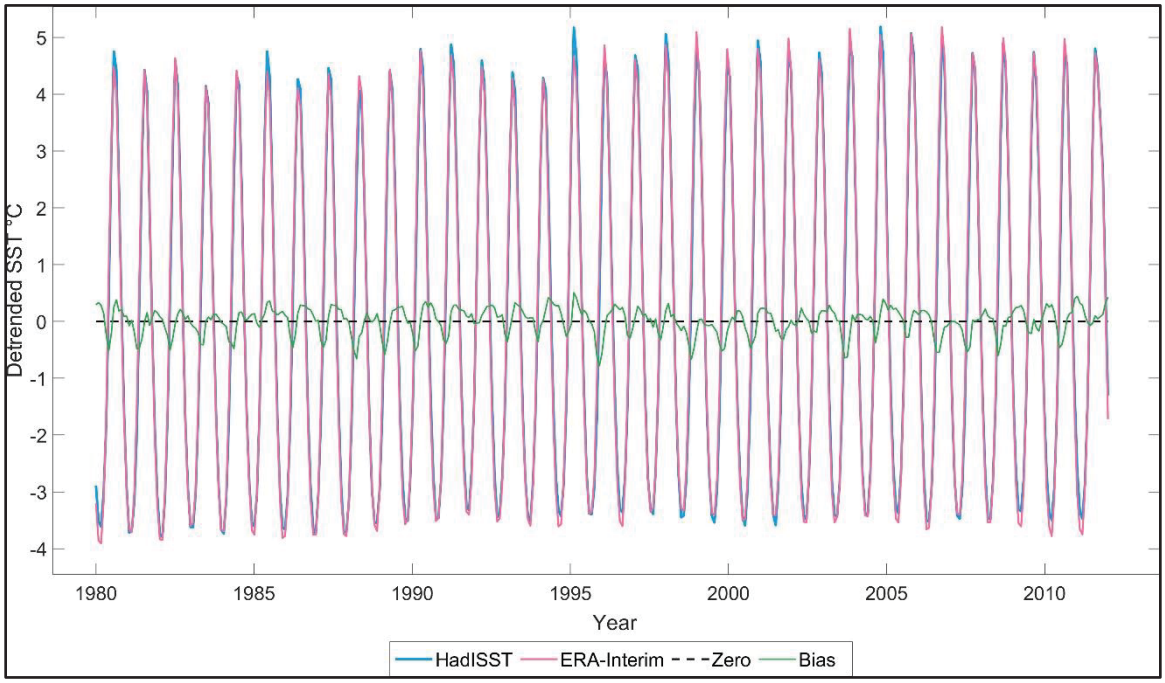

Figure 3.3 Detrended spatially averaged SSTanomaly data from HadISST (solid blue line) and upscaled ERA-Interim (solid pink line), at the center and north Pacific in the period from 1980 to 2012. The dashed black line representsthe cero value. The circle-solid green line represents the bias HadISST and upscaled ERA-Interim

Spatial reproduction of SST. The map displayed in the upper part of Figure 3.4 illustrates the RMSE between the HadISST and upscaled ERA-Interim time series, depicted on a grid cell basis. Across the majority of the depicted area, the RMSE values are approximately 0.25°C. However, there is a discernible gradient showing an increase towards the North Pole and coastlines. This can be attributed to biases in the various datasets used in ERA-Interim (Dee et al., 2011), such as a lack of information in those regions combined with water vapor, which could introduce errors in satellite sensors and result in cooler SST measurements (Luo et al., 2020) Additionally, other variables like cool skin, diurnal warm layer, salinity effects, submarine topography, coastal circulation, and vertical ocean mixing may also contribute to

these biases. Within the PDO region, demarcated by the solid black line, the RMSE values also show values around 0.25°C. Notably, there is a slight elevation of this error near the coasts of Russia and Alaska. The highest RMSE value is located in a few grid cells along the coasts of the Gulf of California in Mexico, in close proximity to the Baja California coast.

Examining the ENSO 3.4 region, denoted by the dark red line, the majority of RMSE values are in the vicinity of 0.25°C. However, there is a gradual increase in error towards the coasts of Ecuador and Peru, reaching a maximum RMSE value of 1.75°C.

The MAE, depicted in the lower map of Figure 3.4, reveals a notable feature in the central North Pacific, where values close to a 0°C error are prominent. This stands out as a distinction from the spatial distribution observed in RMSE, as these values escalate towards the north and coastlines. Within the PDO region, MAE values hover around 0.25°C, with an increase reaching 1-2°C near the coasts of Russia and western Alaska. Notably, there is a distinct region with values close to 0°C along the south coast of Alaska, the west coast of Canada, and the southern limit of the PDO region.

In ENSO 3.4 region, as seen in the lower map of Figure 3.4, MAE values predominantly approach 0°C. However, there are instances of where values hover around 0.25°C with an increase towards the coasts of Ecuador and Peru, reaching close to 1°C.

In summary, the correlation (0.97), bias (Figure 3.3), MAE, and RMSE (Figure 3.4) collectively indicate that ERA-Interim upscaled data generally provides a good representation of HadISST. Despite this overall agreement, it is crucial to acknowledge specific inconsistencies near the land coasts and towards the North Pole.

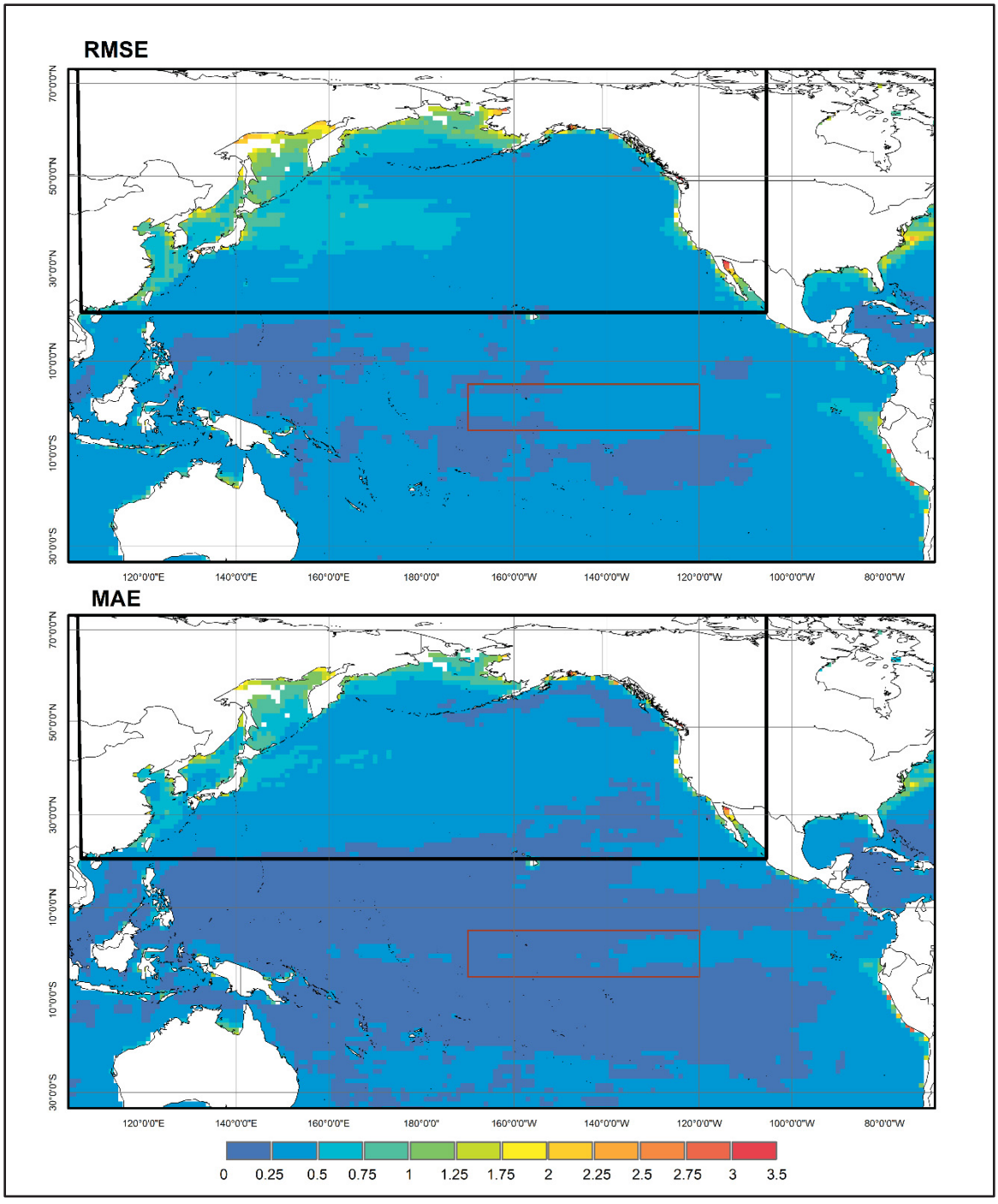

Figure 3.4 Root mean square error (RMSE), in °C in upper map. Mean absolute error (MAE), in °C in lower map. Both maps used HadISST and ERA-Interim upscaled datasets for computing the errors in the time interval from 1980 to 2012. Black line frames PDO region, dark red line frames ENSO 3.4 region

3.5.2 Comparison of the reproduction of ENSO and PDO oscillations by HadISST and ERA-Interim.

3.5.2.1 Temporal reproduction of ENSO

Upscaled ERA-Interim shows a linear correlation of 0.99, with respect to HadISST when reproducing the ENSO index time series over region 3.4. The graphical analysis over time is shown in Figure 3.5, where it is possible to notice that the simple bias (solid gray line) presents its maximum in the period from 1998 to 2002 with a value of 0.43 ° C. It is noteworthy that the ERA-Interim reproduction of ENSO index time series (dot-dashed pink line) is capable of adjusting, as well as correctly representing the extremes and the positive and negative phases of the monthly SST anomaly in the ENSO region 3.4, for the studied time period.

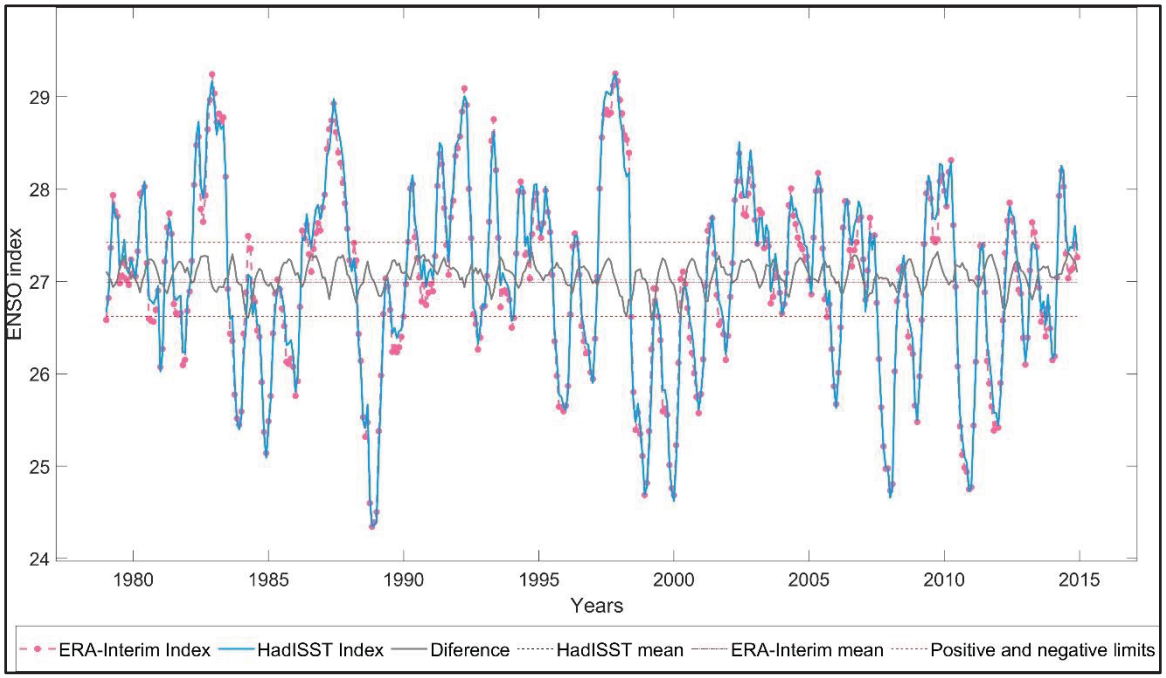

Figure 3.5 Time series of the region 3.4 ENSO index computed from upscaled ERA-Interim (pink dash-dot line) and HadISST (solid blue line) in the period from 1980 to 2012. Bias (solid gray line), the limits of positive and negative ENSO phases (red dotted lines) (CPC, 2019), as well as the averages of HadISST (gray dotted line) and ERA-Interim (dark red dotted line) are shown

3.5.3 Spatial reproduction of ENSO

The ENSO spatial pattern, as illustrated in Figure 3.6, reveals that the computations of the primary empirical orthogonal function (EOF1) of the detrended SST anomaly from both datasets are in close agreement. The difference in the variance represented by EOF1 is only 4% between HadISST (64%) and upscaled ERA-Interim (60%), indicating a similarity in variability across central Pacific Ocean. The latitudinal gradient of the EOF1, as depicted in Figure 3.6, is also very similar from one dataset to the other. Specifically the ENSO 3.4 region, shows a changes associated with positive variance values and an overestimation the spatial distribution by ERA-Interim.

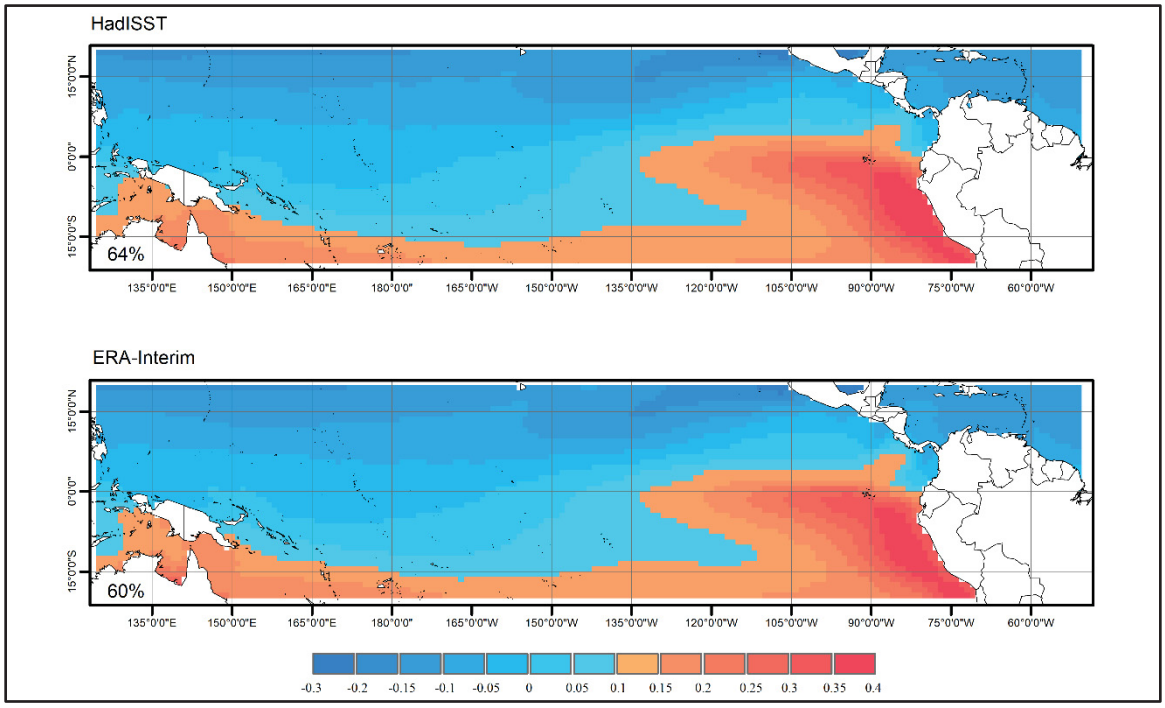

Figure 3.6 ENSO index spatial pattern in central Pacific Ocean. Main empirical orthogonal function (EOF1) of the monthly SST anomaly, based on data from HadISST (upper map) and ERA-Interim (lower map) in the time interval from 1980 to 2012. The doted line represents ENSO 3.4 region. This EOF1 mode explains 64% of variance for HadISST and 60% of variance for ERA-Interim

3.5.4 Temporal reproduction of PDO

The upscaled ERA-Interim representation of the PDO index time series has a 0.98 correlation with the times series deduced from the observations. However, upscaled ERA-Interim dataset (depicted by the pink dash-dot line in Figure 3.7) under(over)estimates the positive (negative) values, with an absolute difference of up to 1.03°C. Despite this bias, upscaled ERA-Interim reproduces the positive and negative phases of this index, as well as its inflection points, satisfactorily. The period with the most important bias between the upscaled ERA-Interim and observed PDO time series is between 1998 and 2003.

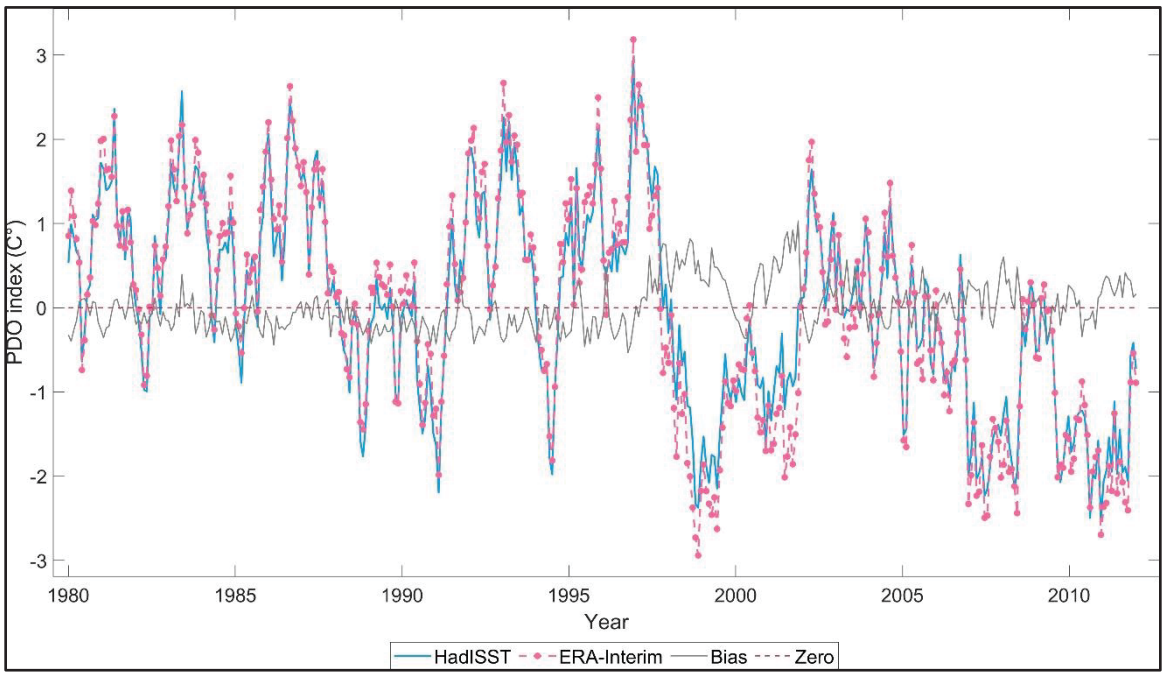

Figure 3.7 Time series of the PDO index computed from upscaled ERA-Interim (pink dash-dot line) and HadISST (solid blue line) in the period from 1980 to 2012. Bias (solid gray line)

3.5.5 Spatial reproduction of PDO

The spatial pattern of the PDO described by the leading EOF of the monthly SST anomalies is shown in Figure 3.8. It can be seen that the upscaled ERA-Interim dataset satisfactorily

reproduces the index computed from the observations. The explained variance from EOF1 is the same in both cases, i.e. 21%.

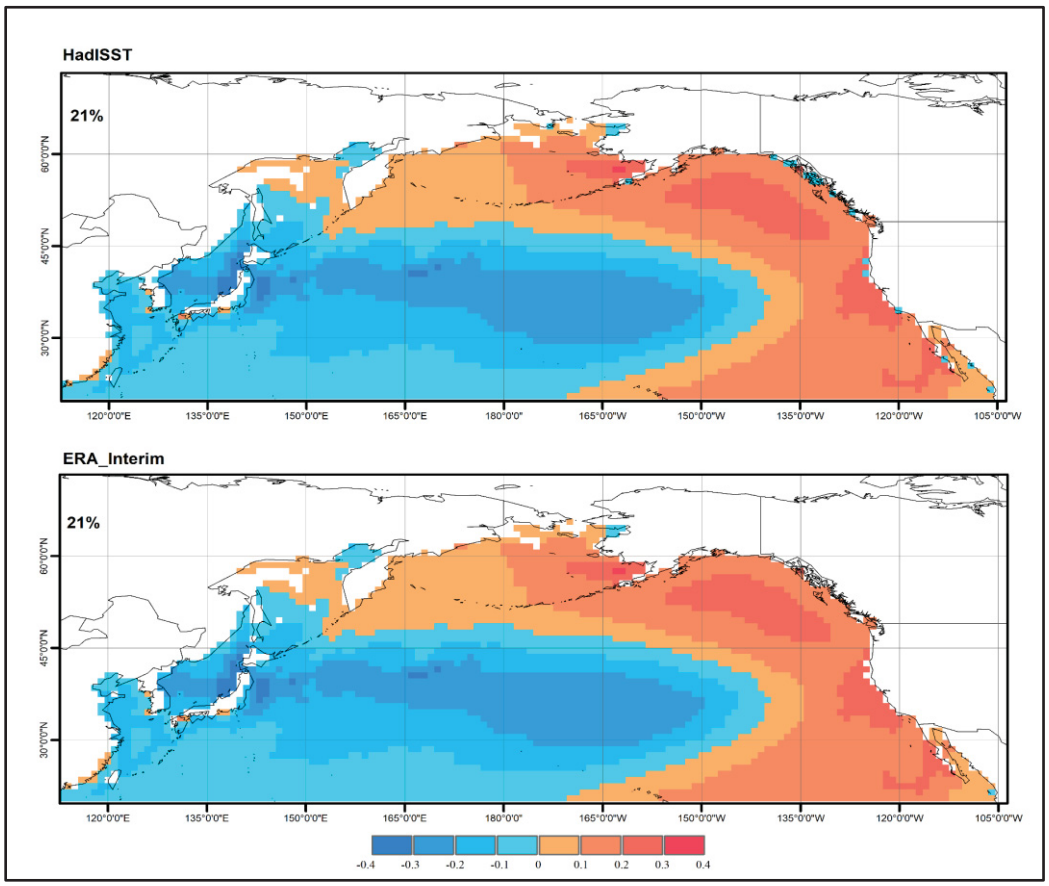

Figure 3.8 PDO index spatial pattern in Pacific Ocean. Main empirical orthogonal function (EOF1) of the monthly SST anomaly, based on data from HadISST (upper map) and ERA-Interim (lower map) in the time interval from 1980 to 2012. This EOF1 mode explains 21% of variance in both cases

3.5.6 Comparison of precipitation from observations, ERA-Interim and RCM simulations

The precipitation data used in this study is obtained from Livneh (2015) gridded dataset and serves as observations. It serves as a basis for comparison with reanalysis data from ERA-Interim and the RCM simulations. The main focus of this section is to examine the correlation

between the different precipitation datasets, as well as their temporal and spatial characteristics.

3.5.6.1 Reproduction of the temporal patterns of precipitation in Mexico

The mean annual cycle of monthly accumulated precipitation is shown if Figure 3.9 for all the datasets used in this study. They show, as can be expected, that the annual cycle is divided into two distinct periods: (1) a wet season occurring during the months of May to October; (2) a dry period occurring the rest of the year. It can be seen that RegCM4-7 and RCA4 simulations are overestimating the ERA-Interim and Livneh values through almost the entire year, while CRCM5-ERA-Interim-0.22 and CRCM5-ERA-Interim-0.44 simulations are closer to the observational datasets but still generally overestimate precipitation with the highest difference seen in the month of September. With regards to the observational datasets, ERA-Interim is generally much closer to the Livneh observations but it does underestimate the precipitation (with respect to observations) during the summer months which represent the wettest season of the year.

Next, the linear correlation was computed between the observations and the time series from the other datasets. The obtained values are, for ERA-Interim, and CRCM5-ERA-Interim-0.22, CRCM5-ERA-Interim-0.44, RCA4-ERA-Interim-0.5, and RegCM4-7-ERA-Interim-0.25 simulations, respectively: 0.98, 0.91, 0.92, 0.91 and 0.89. As can be expected from examining Figure 3.9 and analyzing the monthly and seasonal behavior of ERA-Interim, it successfully detects the inflection points over time, resulting in the highest correlation value. The four simulations show similar values, all around 0.9, which aligns with the monthly and seasonal analysis.

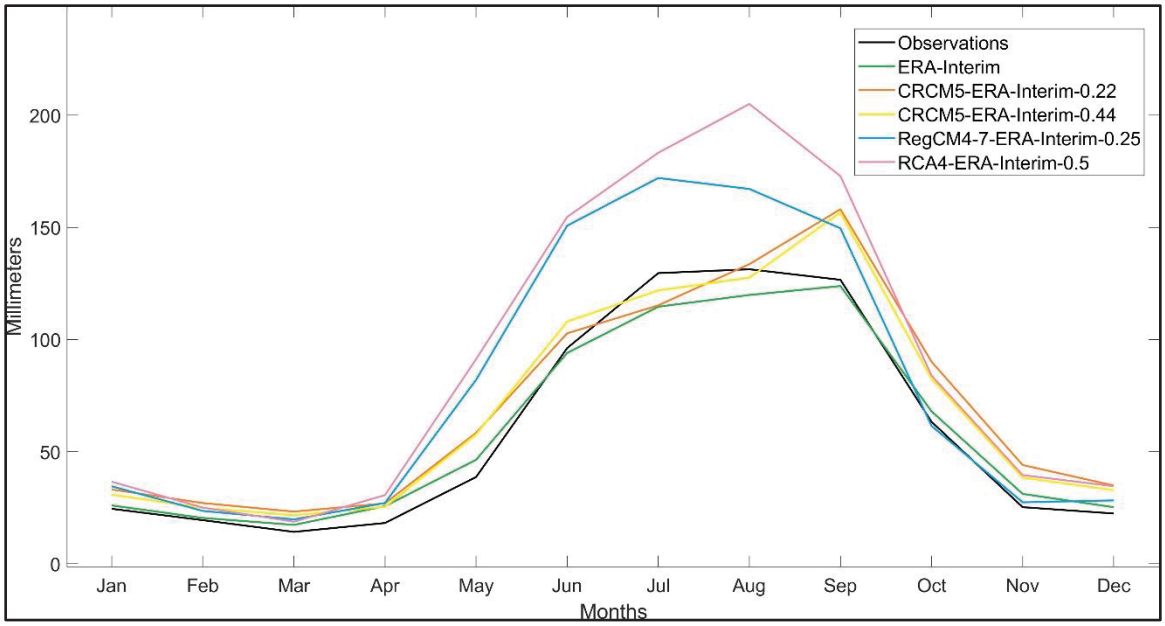

Figure 3.9 Mean annual cycle of monthly accumulated precipitation from 1980 to 2012. Black line Livneh dataset as observations, Green line ERA-Interim, orange line CRCM5-ERA-Interim-0.22, yellow line CRCM5-ERA-Interim-0.44, blue line RegCM4-7 and purple line RCA4

RegCM4-7 showed the worst seasonal reproduction of observations with a marked overestimation throughout the entire year, it can be explained by the similarity with its predecessor version (RegCM3), which regularly produce excessive precipitation as noted by Giorgi et al., (2012). The RCA4 simulation is the one showing the highest overestimation with respect to observations. This has been noted in simulations covering the European domain (Strandberg et al., 2014). One likely explanation could stem from much higher amounts of precipitation in mountainous areas, as can be seen from Figure 3.10 presented in the next section.

3.5.6.2 Reproduction of the spatial patterns of precipitation in Mexico

Regarding the spatial pattern of annual mean accumulated precipitation, the north-south (dry-wet) gradient in Mexico is generally reproduced by all the different datasets (Figure 3.10), albeit with some difficulties. On the other hand, in the south of Mexico, the mean annual

accumulated precipitation is overestimated by all the RCM simulations, with respect to Livneh observations, and by ERA-Interim to a lesser extent. RCA4 and RegCM4-7 simulations encounter challenges in representing the spatial pattern, with higher precipitation values in the mountains, i.e., the ranges of the Occidental Sierra Madre to the west and the Oriental Sierra Madre to the east (see also Figure 3.2). Those two simulations also show more precipitation along and east-west band located in the south part of the country. RegCM4-7 simulation displays the highest precipitation values in the north part of the country.

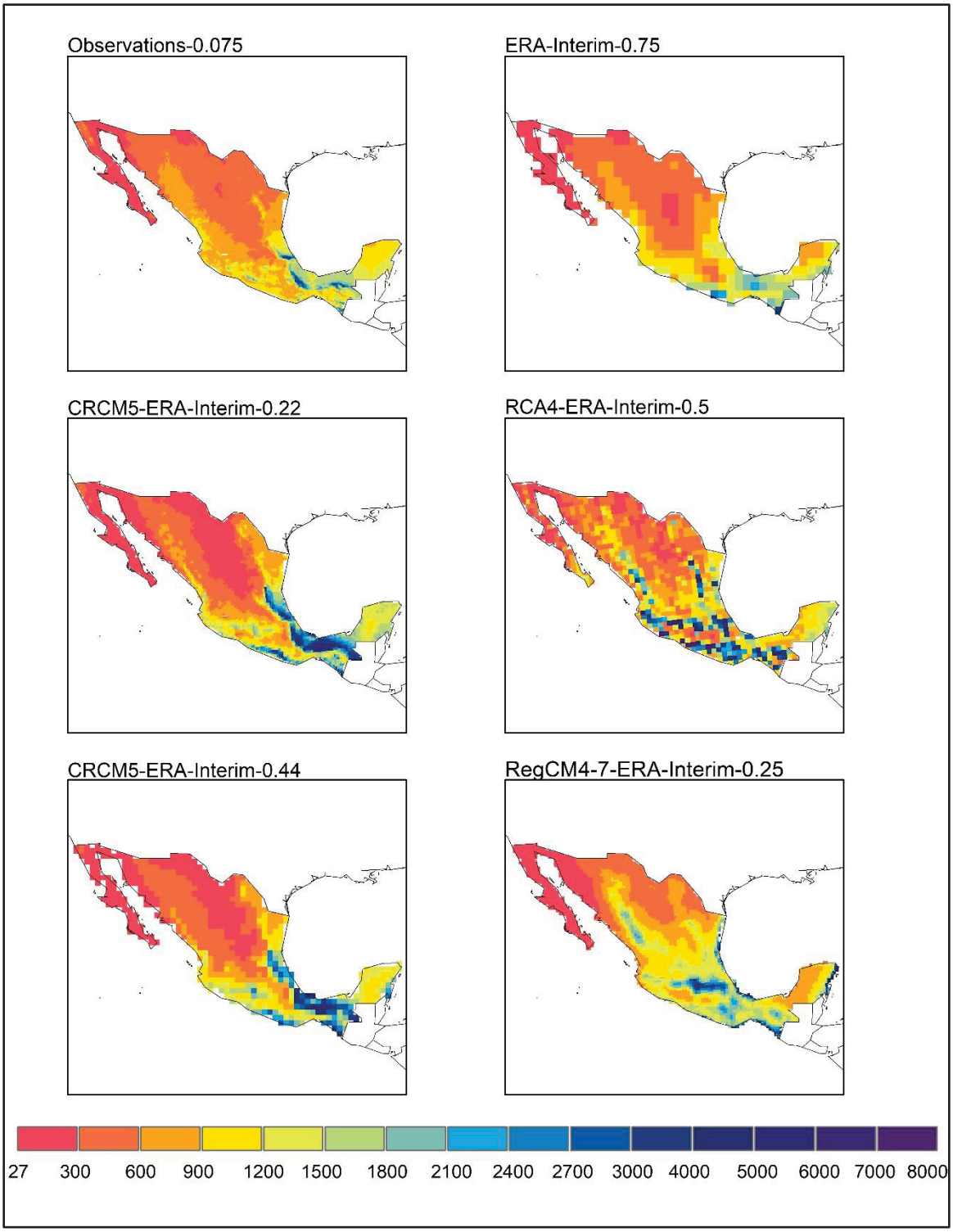

Figure 3.10 Annual mean accumulated precipitation over Mexico for each dataset (1980 to 2012)

Some differences between the RCM simulations setup can be highlighted to explain (at least partially) their different behaviors, even though they were all driven by the same global dataset, i.e., ERA-Interim reanalysis. First, they use three different RCMs with different spatial resolutions. It is known that the spatial resolution has an impact on mountains representation and therefore on mountainous processes reproduction (Antic et al., 2006). That being said, one must keep in mind that gridded datasets based on weather station data interpolation, even though they are seen here as the reference, also have their own drawbacks: (1) interpolation tends to smooth out the (high) extreme values, and (2) they often count on rare data in the mountainous areas which are difficult to access, and on a misrepresentation of orographic effect.

Another point worth noting is that the spatial domains that are covered by all four simulations are not exactly the same. The two CRCM5 simulations were ran on a smaller domain than the RegCM4-7 and RCA4 ones. The CRCM5 simulations were specifically produced for a research project focusing on Mexico, therefore, the spatial domain is limited to the Mexican territory and surroundings, whereas the RegCM4-7 and RCA4 simulations cover the regular, and larger, Central American domain as prescribed by CORDEX (CORDEX, 2016). Finally, the way the information from ERA-Interim in passed to the RCMs, at the boundaries (e.g. using spectral nudging or not), can play a significant role in how each RCM will simulate the Mexican climate and, therefore, precipitation (Schubert-Frisius et al., 2017).

3.5.7 Standardized precipitation index for 24- and 60-months time windows

The SPI24 index computed for the entire Mexican territory (Figure 3.11) is showing an oscillating time behavior with a period ranging from five-years to 7-8 years while the SPI 60 index oscillation (Figure 3.14) displays a decadal behaviour. For this study, SPI24 and SPI60 were used, due to the temporal scales of interest, which agree with those of ENSO and PDO, respectively, as mentioned in the methodology section.

Temporal reproduction of the SPI24 index in Mexico. The times series of the SPI24 index over Mexico territory were calculated with precipitation data from the Livneh dataset, from the ERA-Interim reanalysis and from the four RCM simulations. The results are shown in Figure 3.11. The correlations between the Livneh and the other time series were also computed and are: 0.73, 0.74, 0.73, 0.56 and 0.43 for ERA-Interim-0.75 and the CRCM5-ERA-Interim-0.22, CRCM5-ERA-Interim-0.44, RegCM4-7-ERA-Interim-0.25 and RCA4-ERA-Interim-0.5 simulations, respectively.

As seen previously, the RegCM4-7 and RCA4 simulations show the greatest difference with respect to observations. Although they follow well the observations until year 2000, after that they display opposite trajectories, with respect to the observations time series, and especially at the very end of the period. The datasets have biases that can reach up to 1° Celsius (due to over or underestimations or lags in the inflection points), however they follow a similar behaviour as that from the observations (wet/dry conditions transitions). Most of the time they find themselves in the same SPI category as the observations (except for the RegCM4.7 and RCA4 simulations, at the end of the studied time period). They show near normal to moderately wet conditions at the beginning of the time period (until 1986-87), then move on to drier conditions and remain in the near normal category until 1991 (except for ERA-Interim which remains on the wetter side). Generally wet conditions, oscillating between near normal and moderately wet follow until 1995, and then drier conditions are seen until 2002, reaching close to the very dry conditions, but only in the case of the ERA-Interim dataset. Finally, the datasets switch back to wetter conditions (near normal and even moderately wet) until 2010 before showing a decrease afterwards.

In general, the datasets from the reanalysis and from the simulations are reproducing the trajectory of the dry and humid conditions, however, there is a time lag, that is, the inflection points of the SPI24 index, whether in the wet or in the dry direction, are out of phase in time. Regarding the reproduction of the intensity, from the simulations (CRCM5-ERA-Interim-0.22, CRCM5-ERA-Interim-0.44, RCA4 and RegCM4-7), it is possible to observe that there is an underestimation for the first half of the time interval of this study (approximately from 1982

to 1997), while for part of the second half (approximately 1997 to 2009) there is an overestimation with respect to the observations (Figure 3.11). On the other hand, the ERA-Interim reanalysis dataset overestimates the first half and underestimates part of the second, to end in closer agreement with the observations (as of 2010).

Those figures show aggregated information for the entire Mexican country, so the amplitude of the intensity of the index can be dampened. The next step is to look into the maps of SPI24 to more closely investigate their spatial behaviours and compare the different datasets.

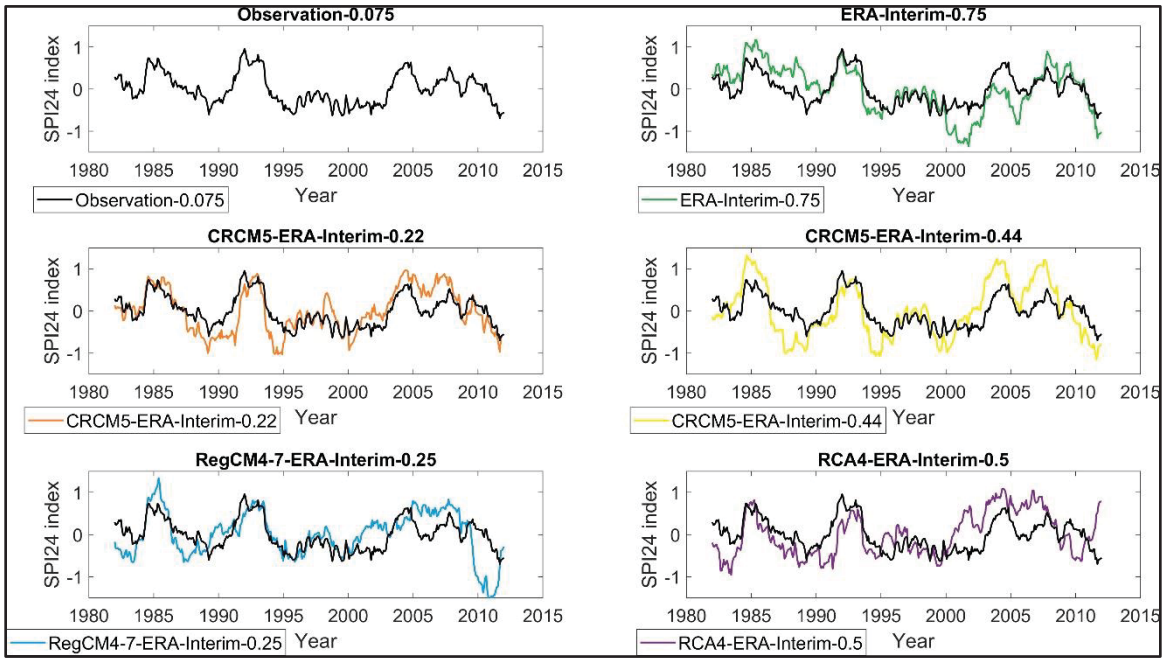

Figure 3.11 SPI24 index time series from 1980 to 2012. Black lines Livneh dataset as observations, green line ERA-Interim, orange line CRCM5-ERA-Interim-0.22, yellow line CRCM5-ERA-Interim-0.44, blue line RegCM4-7 and purple line RCA4

Spatial reproduction of the SPI24 index in Mexico from 1991 to 1994 (north wet conditions and south dry conditions). The spatial display of the SPI24 index in the time period from 1991 to 1994, for the observations (upper left map of Figure 3.12), shows humid conditions for the north of Mexico with the SPI categories of moderately humid to very humid (table 2) making a transition at approximately 20 ° latitude (Méndez & Magaña, 2010), towards the south, observing dry conditions with the category of moderately dry (Table 2). According the time

series in Figure 3.11, the Mexican SPI24 index was in a positive phase during those years, which is mainly driven by the conditions prevailing in the north of the country.

The ERA-Interim reanalysis, shown in the upper right map of Figure 3.12, is able to capture the transition of wet to dry conditions towards the south of Mexico, as well as the reproduction of some nuclei, in the center and north of Mexico, and of maximum values. However, in general terms there is a loss of details in the location and extension of the SPI24, to regional scale, as well as a reproduction of the intensity of this index, likely due to the coarser resolution of ERA-Interim.

Regarding the ERA-Interim-driven RCM simulations, it is possible to note that the previous pattern exists, where the north is humid and the south is dry (maps in the center and lower rows of Figure 3.12), however, the spatial gradient in the intensities differ for each data set. A good portion of the territory shows neutral conditions (SPI values between -0.5 and 0.5), which is not the case when looking at the observations. Yet, there are certain successes at local scale in the spatial reproduction of the SPI24 index by these data sets, as it is possible to observe in southwestern Mexico, where dry conditions are seen (from moderately dry to severely dry, Table 2), as in the observations, however ERA-Interim was not able to reproduce this pattern. With respect to the northwest RegCM4-7 simulation presented a spatial distribution of SPI24 congruent with the observations.

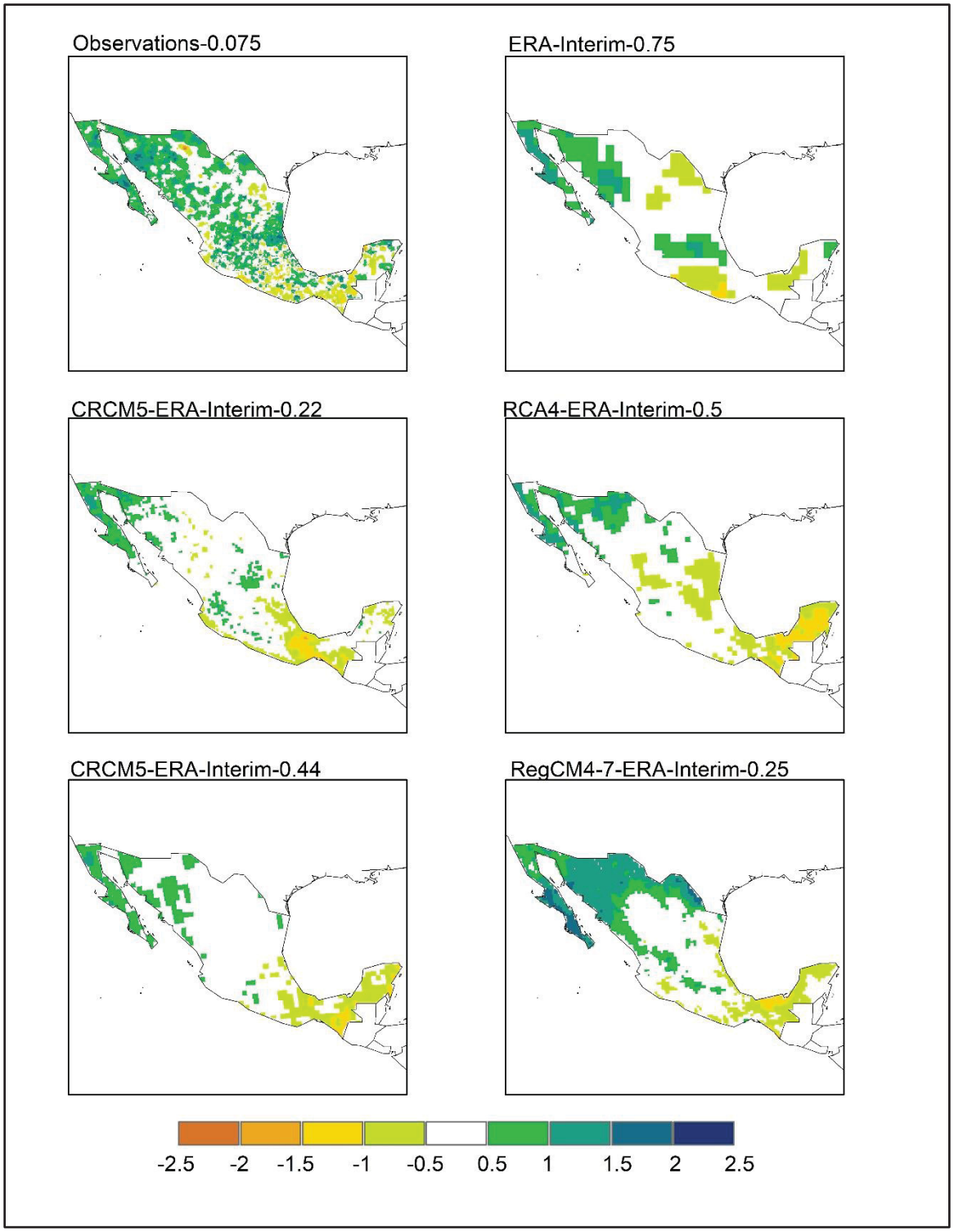

Figure 3.12 SPI24 index reproduction mean from 1991 to 1994 over Mexico of all datasets. The map legend is the system classification of SPI index

Spatial reproduction of the SPI24 index in Mexico from 2009 to 2012 (north dry conditions and south wet conditions). Contrary to the previous period, in this subsection the time interval showed a negative phase in the SPI24 time series (Figure 3.11). In the upper left corner of Figure 3.13 is shown the SPI24 index computed from the observations, where the dry conditions (from near normal to severely dry, Table 2) now occur in northern Mexico and wet conditions (from moderately wet to extremely wet) occur in the south. The Yucatan peninsula is one exception and shows dry conditions, while the rest of the south is generally wet. In the north, wet conditions extend along the Sierra Madre Occidental and Sierra Madre Oriental mountain ranges (Figure 3.2). The extent and intensity of the dry conditions is probably what led to a negative value (although of low intensity) of the index for this time period over Mexico, as shown previously in Figure 3.11. The desert part of the country (in between the mountain ranges) as well as the westernmost par of northern Mexico (encompassing Baja California) clearly show dry behaviours. On the other hand, most representative humid conditions values are seen for central and southwestern Mexico, where there are nuclei with values reaching the extremely humid category.

The SPI24 index from upscaled ERA-Interim reanalysis, shown in the upper right map of Figure 3.13, reproduces generally well the transition from dry to wet in the southern direction however, once again, with a loss of spatial details. Additionally, the south of the country and Yucatan peninsula are wetter in the ERA-Interim dataset than in the observations with a larger continuous region being seen as extremely wet.

The simulations are also able to capture the southbound dry-to-wet transition of the observations, however, none of them show the wet mountain ranges towards the north of the country, and they all display a generally clear distinction between the dry north conditions and the wet south conditions. In particular, the RegCM4.7 simulation shows a much drier north than all the other datasets. This is probably what explains the dive towards dry conditions seen in the time series of Figure 3.11 for this simulation.

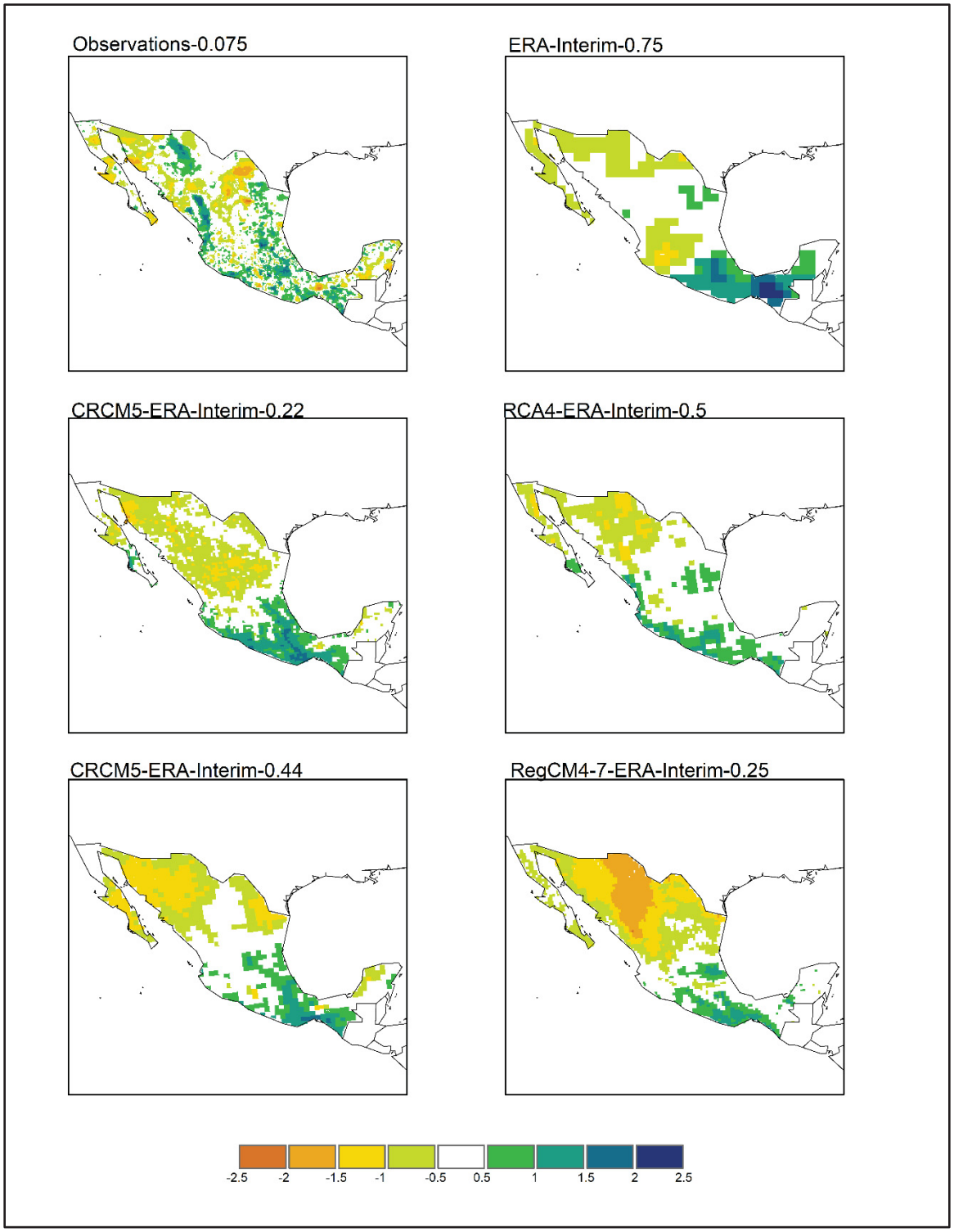

Figure 3.13 SPI24 index reproduction mean from 2009 to 2012 over Mexico of all datasets. The map legend is the system classification of SPI index

Temporal reproduction of the SPI60 index in Mexico. The reproduction of the SPI60 index from the observations was compared with that from the simulations and ERA-Interim. First, joint variation is studied through linear correlation, where it is observed that ERA-Interim and RegCM4-7 simulation presents the highest value with 0.71, followed by CRCM5-ERA-Interim-0.22 and CRCM5-ERA-Interim-0.44 with 0.65 and 0.70 respectively. RCA4 simulation presents the lowest correlation value with 0.36. From the graphical analysis in Figure 3.14, it can be seen that the reanalysis and simulations all reproduce the oscillations of the SPI60 index from the observations but with overestimation for the reanalysis data and underestimation for the simulations data for the first half of the time period (1985-2000). Opposite behaviours are seen for the period from 2000 to 2012.

The RegCM4-7 simulation shows the highest level of agreement with the observations until year 2000, while the RCA4 simulation still has the lowest level of agreement with observations. Although they have biases that can reach up to 0.95° Celsius (due to over or underestimations or lags in the inflection points), the simulations (except for RCA4) follow a similar behaviour as that from the observations (wet/dry conditions transitions). Most of the time they find themselves in the same SPI category as the observations.

Around the years 1995-1997, all the datasets display a transition from a decadal wetter phase to a decadal drier phase. Those two different time periods are studied into more details, from spatial point of view, in the next section.

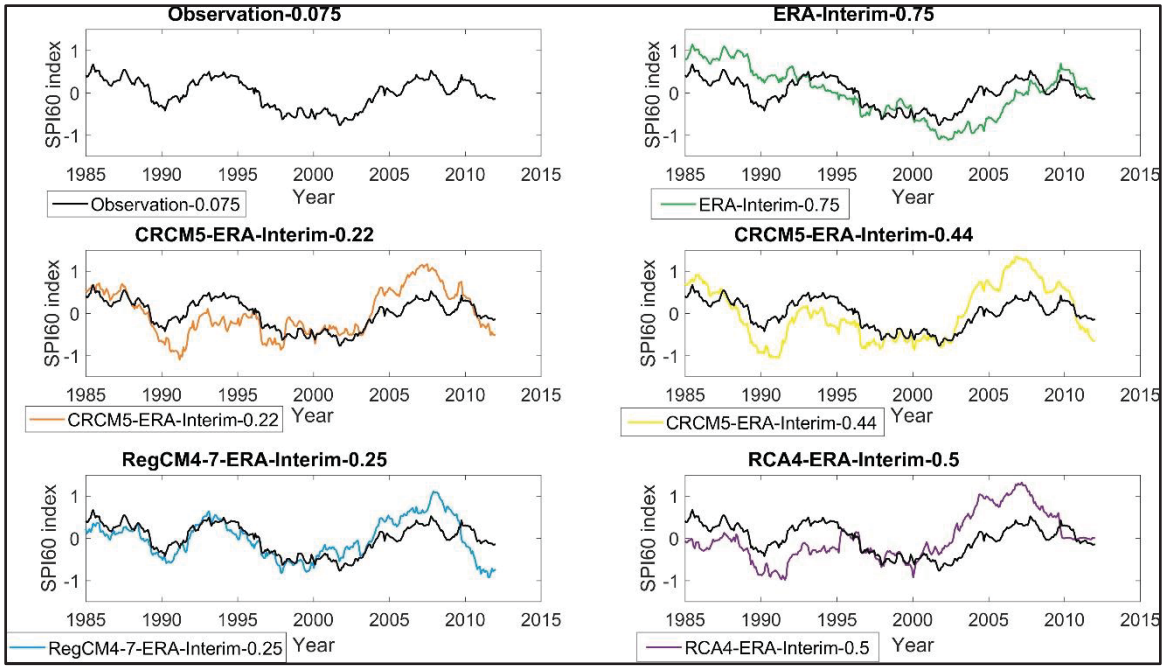

Figure 3.14 SPI60 index time series from 1985 to 2012. Black lines Livneh dataset as observations, green line ERA-Interim, yellow line CRCM5-ERA-Interim-0.44, orange line CRCM5-ERA-Interim-0.44, pink line RegCM4-7 and blue line RCA4

Spatial reproduction of the SPI60 index in Mexico from 1985 to 1998 (north wet conditions and south dry conditions). The spatial representation of the SPI60 index from the observations, in the time interval from 1985 to 1998 (upper left map of Figure 3.15), shows a contrast in humidity conditions, between the south and north of Mexico, in other words, the north reaches a value of 1 (Table 2) which means a moderately humid categorization for the SPI index, while in the south moderately dry conditions are present with a value of -1 (Table 2). The transition in the conditions displayed by theSPI60 index occurs gradually and a change is seen around 20 ° latitude.

In the case of the ERA-Interim reanalysis (upper right map in Figure 3.16), it manages to reproduce the differentiation in the humidity conditions between the north and the south of Mexico, however, there is a clear spatial overestimation of the dry conditions towards the south and an underestimation of the humid conditions for the same region.

The RCM simulations all reproduce the correct north-south gradient and show an adequate adjustment in the northwestern region of Mexico. However, in the south there is a spatial overestimation, that is, the dry conditions described by the SPI60 index are distributed in almost the entire territory of southern Mexico from 20 ° latitude and even lower latitude (RCA4 simulation). The RegCM4.7 simulation, which showed a good agreement in terms of times series (Figure 3.14) is probably the one with closest representation to that from observations.

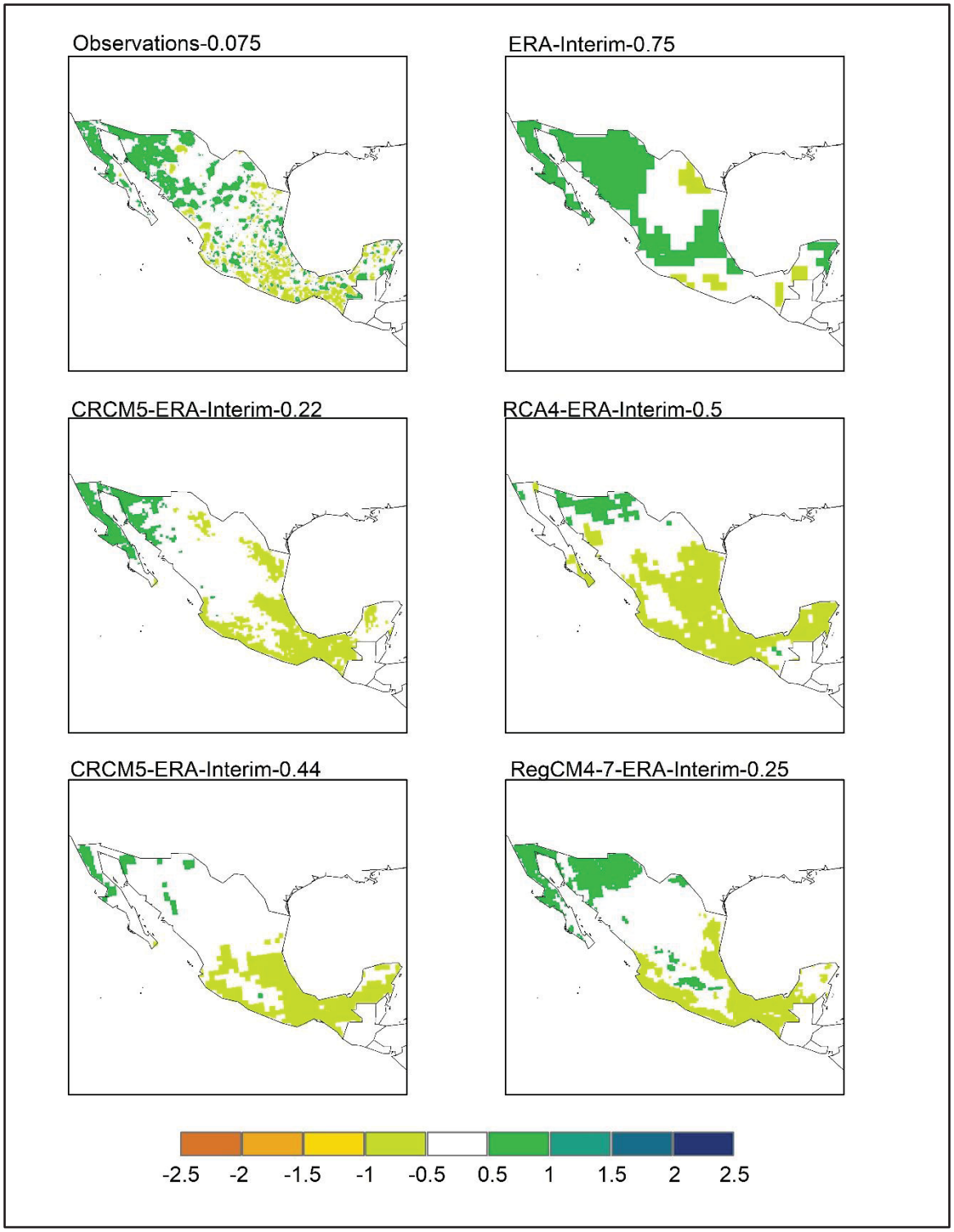

Figure 3.15 SPI60 index reproduction mean from 1985 to 1998 over Mexico of all datasets. The map legend is the system classification of SPI index

Spatial reproduction of the SPI60 index in Mexico from 1999 to 2012 (north dry conditions and south wet conditions). The calculation of the SPI60 index for this time interval (Figure 3.16), shows conditions opposite to those observed in the previous period (1985 to 1998). It should be mentioned that not only is there a category of moderately dry for the north and moderately humid for the south, but also that very similar nuclei are observed within Mexico as shown by the observations in the previous subsection (upper left map in Figure 3.16), but with a totally opposite behaviour.

The other data sets, both from the reanalysis and the simulations, repeat the same spatial pattern, but with a cleaner distinction between the north and the south of the country, a larger area with neutral conditions (values between -0.5 and 0.5) in the case of the two CRCM5 simulations and the RegCM4.7 simulations, and an overestimation of the area in humid conditions from all the simulations, which was expected as per Figure 3.14.

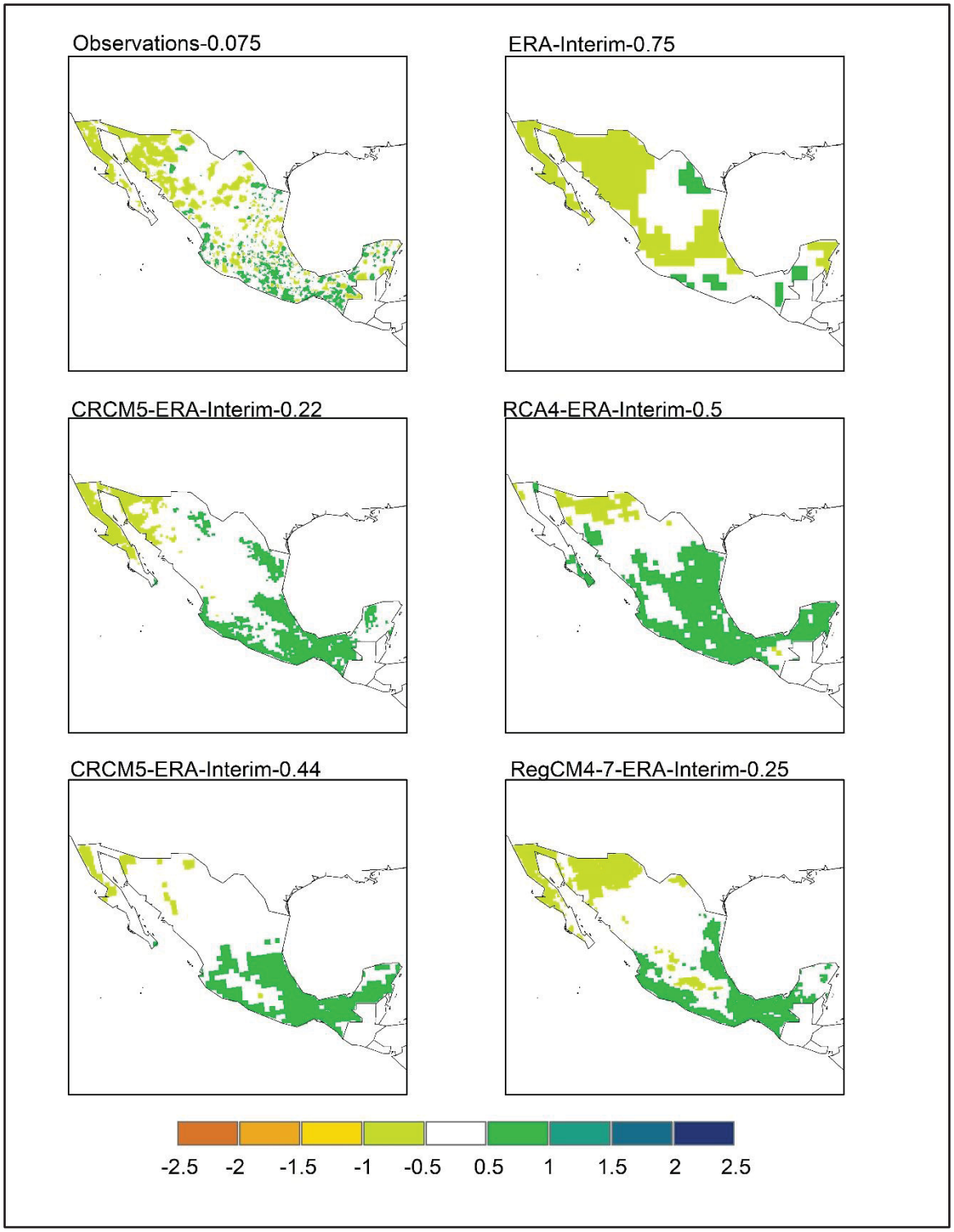

Figure 3.16 SPI60 index reproduction mean from 1999 to 2012 over Mexico of all datasets. The map legend is the system classification of SPI index

3.5.8 Spatial pattern of temporal correlation of SPI24 and SPI60 indices with ENSO and PDO oscillations

The approach to correlation analysis involved the consolidation of criteria over time for each oscillation and each SPI index. This entailed considering the phase of each teleconnection index, the overall temporal average behavior of the SPI index across Mexico (which corresponds to an oscillation), as well as detecting contrasts between wet conditions in the north (south) and dry conditions in the south (north) in the spatial pattern of the SPI. The choice of time intervals was based on the temporal evolution of oscillations, specifically examining the SPI index at different phases of ENSO and PDO, respectively. For SPI24, the period from 1991 to 1994 was chosen, as this timeframe corresponds to a positive phase of ENSO (Figure 3.5) and PDO (Figure 3.7), with SPI values above zero (Figure 3.11) which suggests a wet phase of SPI24. For SPI60 the time periods from 1985 to 1998 was chosen, which coincides with an extensive time period of positive phase of PDO and wet conditions of SPI60.

Spatial pattern of correlation from 1991 – 1994 between SPI24 and ENSO and PDO. The spatial pattern of the correlation between SPI24 and ENSO for the time period from 1991 to 1994, as described by observations (upper left corner map of figure 3.17), reveals positive correlation in the central-northern part of Mexico, and negative correlations mostly in the south and northwest parts of country. In other words, when ENSO is primarily in a positive phase (as seen in Figure 3.5), the moisture conditions described by the SPI24 index indicate a very wet event (according to the SPI classification system) in the northern part of the country (Figure 3.12). This condition is related to ENSO by up to 0.5-0.65 correlation. Conversely, the southern region shows a negative correlation (up to 0.65) with the same positive phase of ENSO, generating conditions ranging from moderately dry to severely dry, with small clusters of extremely dry conditions (Figure 3.17).

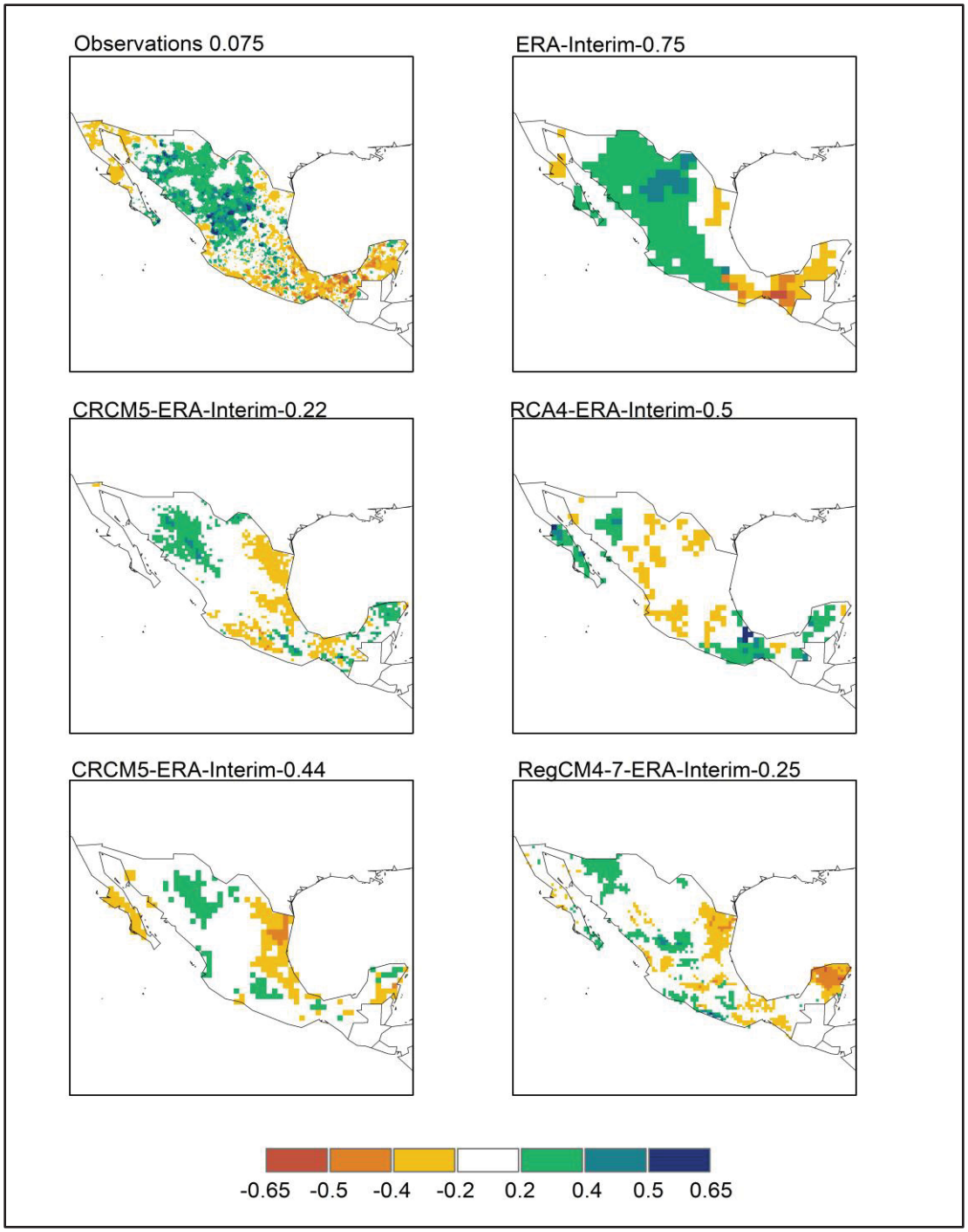

Figure 3.17 Spatial pattern of temporal correlation per grid point between SPI24 and ENSO, in the time period from 1991 to 1994, calculated with observations (upper left corner map), ERA-Interim (upper right corner map), CRCM5-ERA-Interim-0.22 (left center map), CRCM5-ERA-Interim-0.44 (lower left corner map), RCA4-ERA-Interim-0.5 (right center map) and RegCM4-7-ERA-Interim-0.25. For SPI24 simulations correlation, ENSO was calculated with ERA-Interim

The clusters exhibiting extreme conditions in the northwest and southeast of Mexico (extremely wet and severely dry, respectively: Figure 3.12) show a strong correlation of SPI24 with the positive phase of PDO in this case (upper left corner map of Figure 3.18). The correlation of PDO with the spatial behavior of the SPI24 index during this time interval (upper left corner map of Figure 3.18) is considerably higher than the values shown in correlation with ENSO (Figure 3.17). In the eastern-central and southeastern parts of the country, correlation values exceed 0.8, which are related with wet conditions for that region.

It is noteworthy that the spatial correlation behavior with both indices, at a regional scale, suggests not only a correlation with the oscillation but it is also a link with the topography for the understanding of SPI behavior.

Regarding the reproduction of the correlation between SPI24 calculated with ERA-Interim and ENSO (upper right corner map of Figure 3.17) and PDO (upper right corner map of Figure 3.18), it can be observed that the general pattern of the correlation is reproduced, correctly identifying the areas of stronger positive and negative correlation values. It also identifies certain cores of decreased or increased correlation with both ENSO and PDO. This result suggests that the spatial correlation pattern could assist reanalysis data (ERA-Interim, in this case) in improving the representation of precipitation. In other words, there is an opportunity of a reverse process creation from the spatial correlation pattern in time to the calculation of precipitation.

The correlation calculated with the RCM simulations detects a condition of increased humidity in the north and a decrease in the south (second and third lines of maps in Figures 3.17 and 3.18). However, it does so with an underestimation both in intensity and in the spatial gradient. Regarding the RCA4 simulation (right center map of Figure 3.17), the correlation with ENSO fails to represent what is described by the observations or ERA-Interim. However, the correlation with PDO (right center map of Figure 3.18) manages to identify it, similar to the other simulations.

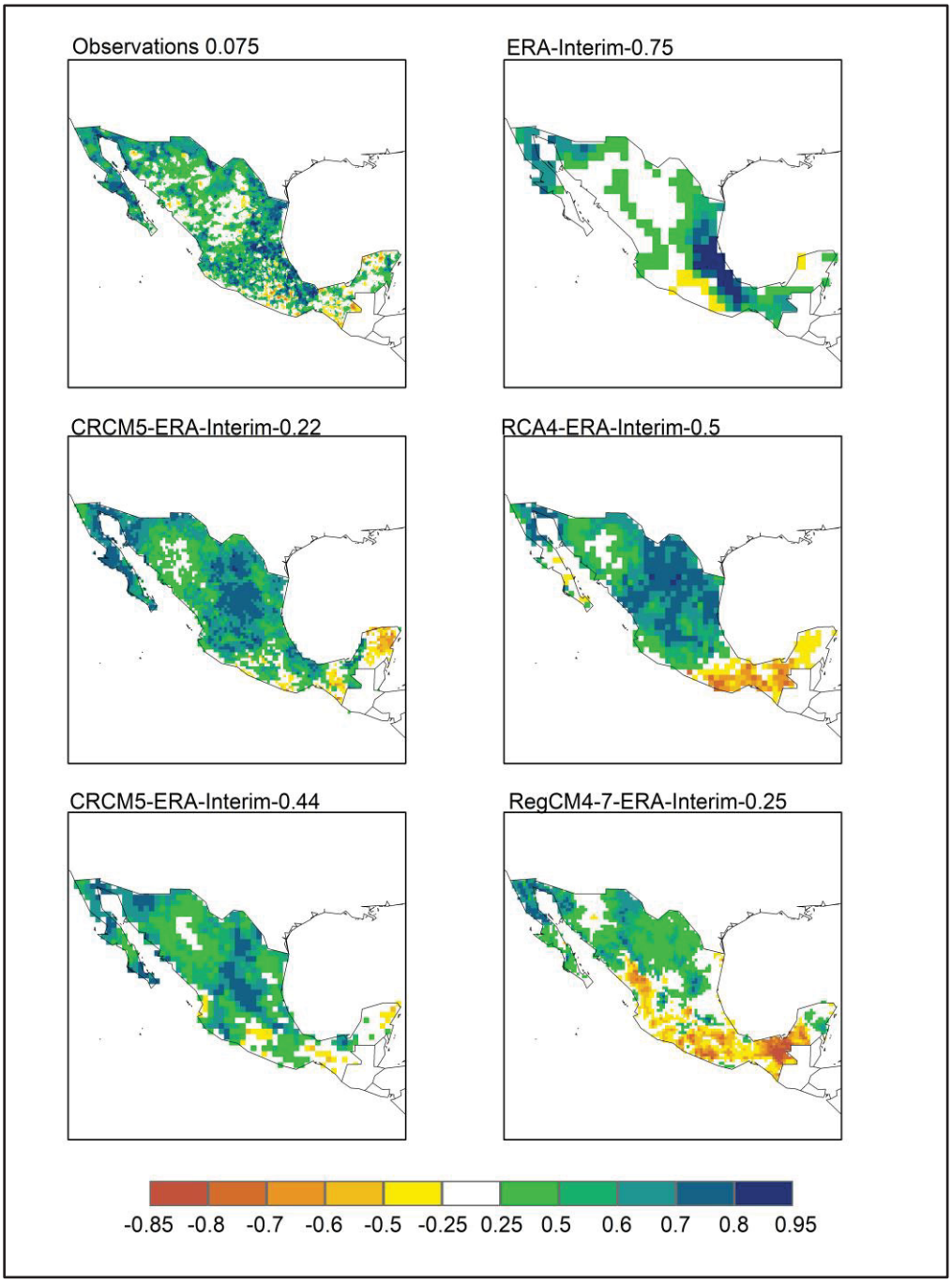

Figure 3.18 Spatial pattern of temporal correlation per grid point between SPI24 and PDO, in the time period from 1991 to 1994, calculated with observations (upper left corner map), ERA-Interim (upper right corner map), CRCM5-ERA-Interim-0.22 (left center map), CRCM5-ERA-Interim-0.44 (lower left corner map), RCA4-ERA-Interim-0.5 (right center map) and RegCM4-7-ERA-Interim-0.25. For SPI24 simulations correlation, PDO was calculated with ERA-Interim

Reproduction of the spatial pattern of correlation from 1985 – 1998 between SPI60 and PDO. Regarding the correlation over periods of more than 10 years (1985 – 1998) between SPI60 and oscillations ENSO (supplementary material) and PDO (upper left corner map of Figure 3.19), the spatial gradient in the case of ENSO shows only some scattered and very localized cores with values ranging from -0.5 (in the south) to 0.4 (in the north), with ENSO in the positive phase for most of the time interval. However, in the correlation of SPI60 with PDO, there is clearly a strong correlation pattern throughout Mexico. The central and northern parts of the country present correlation values from -0.55 to -0.5%, which transitions inversely for the rest of the country, including the Baja California Peninsula (with positive values from 0.2 to 0.6), except for certain localized cores (with negative values from -0.3 to -0.5). It is worth noting that negative correlation values are related to conditions ranging from near-normal to moderately wet in northern Mexico, considering a 60-month period for SPI calculation, and that the phase of PDO, for the most part within the considered time interval, is positive.

In the south, the behavior is opposite, meaning that correlation values are related to conditions ranging from near-normal to moderately dry for SPI60.

The reproduction of the spatial pattern of temporal correlation, this time calculated with ERA-Interim, between SPI60 and ENSO fails to emulate what is described by the observations. However, it does detect that the south exhibits negative correlation characteristics and the north positive (Figure at the supplementary material). Regarding the correlation between SPI60 and PDO, ERA-Interim (upper right corner map of Figure 3.19) manages to identify the behavior described by the observations, meaning that they present the north with a negative correlation pattern (with the exception of the Baja California Peninsula, which may be caused by the resolution and the phenomena effects associated to seasonal precipitation behavior and marine breeze input) and the south with a positive correlation pattern. However, there is an overestimation in spatial correlation for the negative values.

In the case of the simulations, it can be observed that they fail at emulating the observed correlations between SPI60 and ENSO (supplementary material). Generally, they overestimate the negative correlation in intensity and spatially. However, they manage to detect the pattern of temporal correlation with PDO (negative correlation in the central-northern region and positive in southern Mexico). It is worth mentioning that they all underestimate the negative correlations, both in terms of intensity and spatially, while RCA4 and CRCM5-0.22 simulations overestimate the intensity of positive correlation.

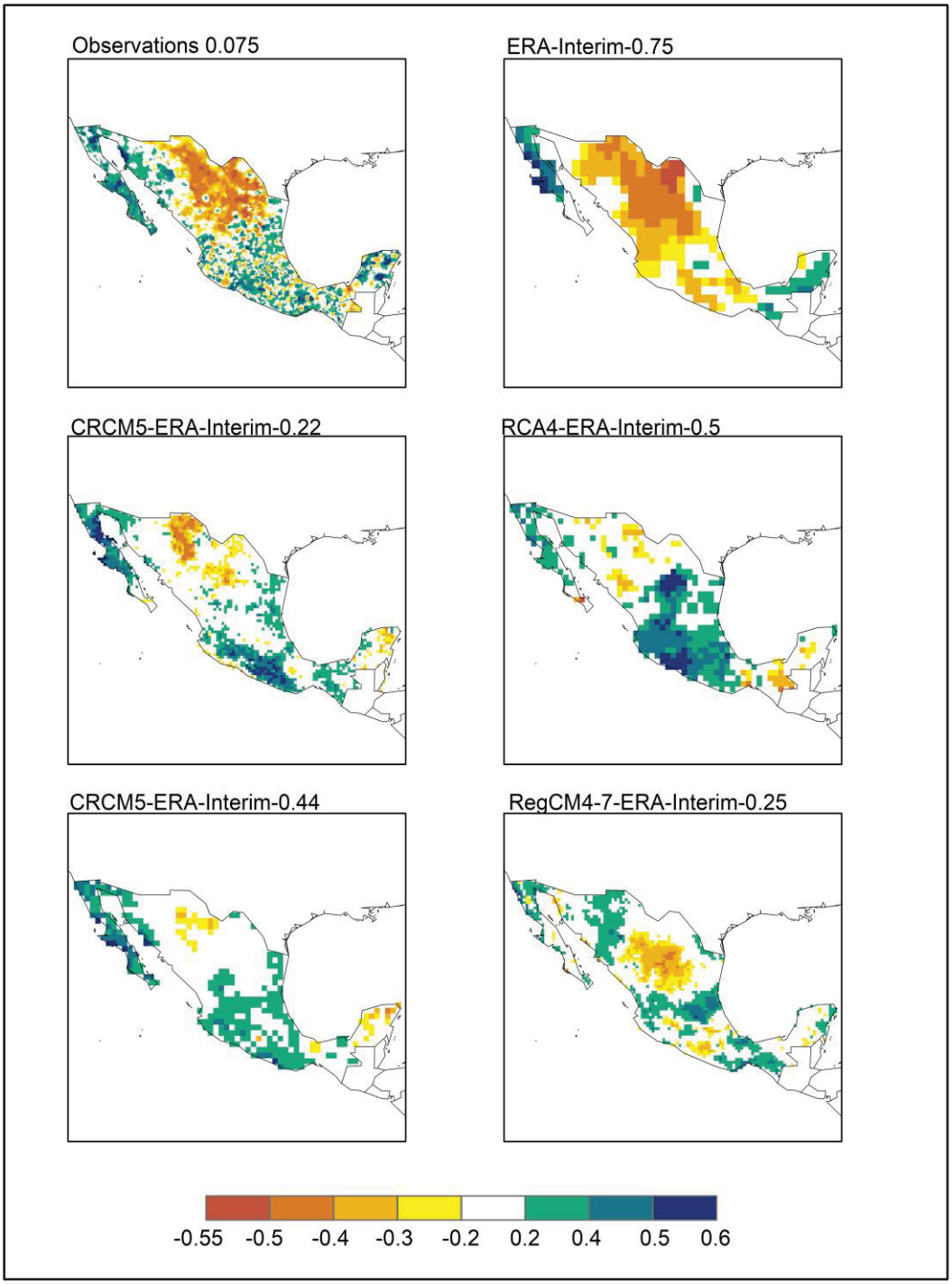

Figure 3.19 Spatial pattern of temporal correlation per grid point between SPI60 and PDO, in the time period from 1985 to 1998, calculated with observations (upper left corner map), ERA-Interim (upper right corner map), CRCM5-ERA-Interim-0.22 (left center map), CRCM5-ERA-Interim-0.44 (lower left corner map), RCA4-ERA-Interim-0.5 (right center map) and RegCM4-7-ERA-Interim-0.25. For SPI60 simulations correlation, PDO was calculated with ERA-Interim

3.6 Discussion

This section will be divided into 3 parts, 2 of them related to the spatial scale (global and regional) and one to the coupled behavior of ENSO and PDO with the SPI index for 24-, and 60-months.

3.6.1 SST, ENSO and PDO analysis

It was found that the monthly average of the SST from 1980 to 2012, from the upscaled ERA-Interim, in the central and northern Pacific Ocean, shows greater accuracy towards the tropics with RMSE and MAE values between 0 and 0.25° C, with respect to the observations. The rest of this region reaches values up to 0.5 (Figure 3.4), also presenting a temporal correlation of 0.97. However, the RMSE and MAE values increase substantially close to the coasts and the north of norther hemisphere. Despite the near-surface ocean effects schemes taken into account by ERA-Interim such as the cool skin, diurnal warm layer, and salinity effects (Luo et al., 2020), the reanalysis data could underestimate the influence of submarine topography representation, coastal circulation, and vertical ocean mixing. The resolution of the dataset could influence also the representation of the SST. Likewise, ERA-Interim in other regions and temporal scales has shown similar results, such the case over Atlantic Ocean region, where reproduced accurate fields of SST(Luo et al., 2020).

It can be seen from Figures 3.7 and 3.5 that the reproduction of PDO by ERA-Interim, in comparison with HadISST observations, is inferior to that of ENSO. This is likely due to the length of the SST time series that remains short for the computation of PDO. According to Deser, (2022) (Deser, 2022), 50+ years of data would ideally be required, while in the present case 33 years were used. Uncertainty necessarily emerges from considering this rather short time period, in both the cases of the HadISST observations and ERA-Interim data. That being said, the reproductions of ENSO and PDO in the time interval considered in this study (1980 to 2012) good level of accuracy, with linear correlations of 0.99 and 0.98, respectively.

Regarding the spatial pattern of these indices, it is possible to observe that ERA-Interim is capable of reproducing not only the spatial gradient but also the variability explained by its leading empirical orthogonal function, which in the case ENSO is 64% from the observations (HadISST) and 60% from ERA-Interim. In the case of PDO, the explained variance is lower, as can be expected, and reaches 21% for both data sets. Once again, those results align with the findings of Luo (2020).

3.6.2 Precipitation, SPI24 and SPI60 analysis

The reanalysis data (ERA-Interim) and the RCM simulations used in this investigation (CRCM5-ERA-Interim-0.22, CRCM5-ERA-Interim-0.44, RCA4-Interim-0.5 and RegCM4-7-Interim-0.25) present a varied level of correlation with observations in their mean annual cycle time series computed on a monthly basis (from 1980 to 2012), with values of 0.98, 0.91, 0.92, 0.91 and 0.89, respectively (Figure 3.9). The spatial representation of the mean annual accumulation over the Mexican country shows that both the reanalysis data and the RCM simulations detect an average increase towards the south of the country and around the mountainous areas, as do the observations, however, in general, the spatial representation shows biases. Such findings coincide with those from Cavazos et al. (2019) and Ashfaq et al. (2021), who observe that models such as RCA4 and RegCM4-7 are moderately capable of reproducing trends, observing positive biases in mountainous areas over Mexico. Then again, the reference observations are not perfect and have their own drawbacks, as mentioned in section 4.3.2. ERA-Interim, on its side, has the coarsest resolution of all the studied datasets, which is not well adapted to representing the topography and reproducing the associated orographic processes. All four RCM simulations, although to different extents, do show the orography.

Despite the differences noted in the representation of precipitation between the datasets, they all manage to reproduce the observed SPI24 and SPI60 time series (for entire Mexico), with fair levels of agreement. They also all succeed at reproducing the general north-south wet-dry

patterns drawn from observations. However, there are overestimations of both the intensity and the spatial extents of the SPI24 and SPI60 values.

3.6.3 Reproduction of the correlation between teleconnection indices and SPI indices

The reproduction of the spatial correlation pattern between time series, both for SPI indices (SPI24 and SPI60) and teleconnection indices (ENSO and PDO), by reanalysis data and RCM simulations was analyzed. The analysis, from a climatological perspective, suggests that moisture conditions in the country exhibit a correlation with the phases of teleconnection indices, which is consistent with findings from previous studies (Méndez & Magaña, 2010). However, upon delving deeper into the analysis, a teleconnection is identified not only with ENSO but also with PDO in the behavior of the SPI24 index over relatively short periods (5 to 7 years). Additionally, the correlation that exhibits higher values and a greater spatial extent is between SPI indices (SPI24 and SPI60) and PDO, despite ENSO having a temporal window of between 3 and 7 years (Trenberth, 2024). Evidence was also found suggesting that both ERA-Interim and RCM simulations can emulate the change in correlation between the north and south among oscillations and SPI indices. However, the analysis also suggests that both simulations and forcing data still exhibit some inconsistencies in attempting to reproduce the correlation described by observations. This leads us to recommend the development of analytical tools for precipitation simulations as well as resolution.

3.7 Conclusion

This study focused on studying the ability of a set of four ERA-Interim-driven regional climate simulations to reproduce the observed link between precipitation patterns in Mexico and two SST oscillations, ENSO and PDO. The analyses were divided into three steps: (1) analysing the ability of ERA-Interim at reproducing observed SST in the Pacific Ocean, as well as ENSO and PDO, spatially and temporally; (2) comparing observed, reanalysis-derived and RCM-simulated precipitation patterns in Mexico; and (3) assessing the reproduction of the spatial

pattern of temporal correlation between the SPI24 and SPI60 indices and the teleconnection indices (ENSO and PDO) in Mexico.

The main findings can be summarized as follows:

- The ERA-Interim reanalysis provides a high level of agreement with HadISST (observed SST) in the Pacific Ocean over the 1980-2012 time period, including in the ENSO3.4 and PDO regions that were the focus of the present study. Some more important differences were found towards the North Pole and closer to the coasts but those were also reported in previous studies. Despite the rather short time period that was considered (33 years), ENSO and PDO indices computation is also well reproduced by ERA-Interim, both temporally and spatially, with respect to the indices' computation based on HadISST data.

- In the precipitation temporal patterns, the ERA-Interim reanalysis data and the CRCM5-ERA-Interim-0.22, CRCM5-ERA-Interim-0.44, and RCA4-ERA-Interim-0.5 simulations showed the closest match to observations and the highest correlation values. In the spatial analysis of the average annual accumulated precipitation, both the simulations and the reanalysis data successfully identify the transition of increase in total annual precipitation towards southeastern Mexico. However, all simulations exhibit a generalized overestimation, particularly in the mountainous regions of the country. In the temporal reproduction of SPI24 index, the reanalysis data and RCM simulations successfully describe the trajectory of moisture conditions over time. In the spatial analysis, the RCM simulations generally tend to underestimate wet regions and overestimate dry regions. For the temporal representation of the SPI60 index, both the RCM simulations and the reanalysis data manage to detect, for most of the studied time period (1980-2012), the transition from one SPI category to another for the countrywide average. The spatial representation of the average SPI60, computed from both the RCM

simulations and ERA-Interim, depicts the contrast between a north with wet conditions and a south with dry conditions, and vice versa.

- In the spatial pattern of temporal correlation between the teleconnection indices ENSO and PDO and the SPI24, in the time interval from 1991 to 1994, both the reanalysis data and the RCM simulations CRCM5-ERA-Interim-0.22, CRCM5-ERA-Interim-0.44, and RegCM4-7-ERA-Interim-0.25 managed to identify that the SPI24 and teleconnection indices describe a spatial pattern of positive temporal correlation in the north of the country's center, which is related to moisture conditions in the SPI24, and a positive phase for both ENSO and PDO. In this same phase of the teleconnection indices, there is a negative correlation with ENSO in the northwest and southeast of Mexico. The above coincides with what is described by the observations; however, as mentioned in the results section, there is an underestimation in intensity of correlation and spatial distribution. Regarding the time period from 1985 to 1998, the pattern of temporal correlation between PDO and SPI60 in Mexico is captured by the simulations with an underestimation of the correlation intensity, compared to the observations, in the north of the country's center and with an overestimation by the reanalysis data. Regarding the northeast and south of Mexico, the RCM simulations manage to identify the pattern of positive correlation with an overestimation of the intensity.

Finally, the results in this study suggest that RCM simulations have the ability for reproducing the spatial characteristics of temporal correlation between SPI24 and SPI60 indices and teleconnections indices. Additionally, in this region and time interval, the RCM simulations, showed improvements over the reanalysis data at spatial pattern of temporal correlation characteristics.

3.8 Acknowledgments

We acknowledge the World Climate Research Programme's Working Group on Regional Climate, and the Working Group on Coupled Modelling, former coordinating body of CORDEX and responsible panel for CMIP5. We also thank the climate modelling groups (listed in Table XX of this paper) for producing and making available their model output. We also acknowledge the Earth System Grid Federation infrastructure an international effort led by the U.S. Department of Energy's Program for Climate Model Diagnosis and Intercomparison, the European Network for Earth System Modelling and other partners in the Global Organisation for Earth System Science Portals (GO-ESSP). We acknowledge of data taken from Livneh gridded precipitation and other meteorological variables for continental US, Mexico and southern Canada. We acknowledge of any material or data taken from Hadley Centre Sea Ice and Sea Surface Temperature data set (HadISST). We acknowledge of ERA-Interim data taken from European Centre for Medium-Range Weather Forecast. We acknowledge the grant from Consejo Nacional de Humanidades Ciencias y Tecnologías (CONAHCYT) as well as the grant from Fonds de recherche du Québec – Nature et technologies (FRQNT).

3.9 Supplementary material

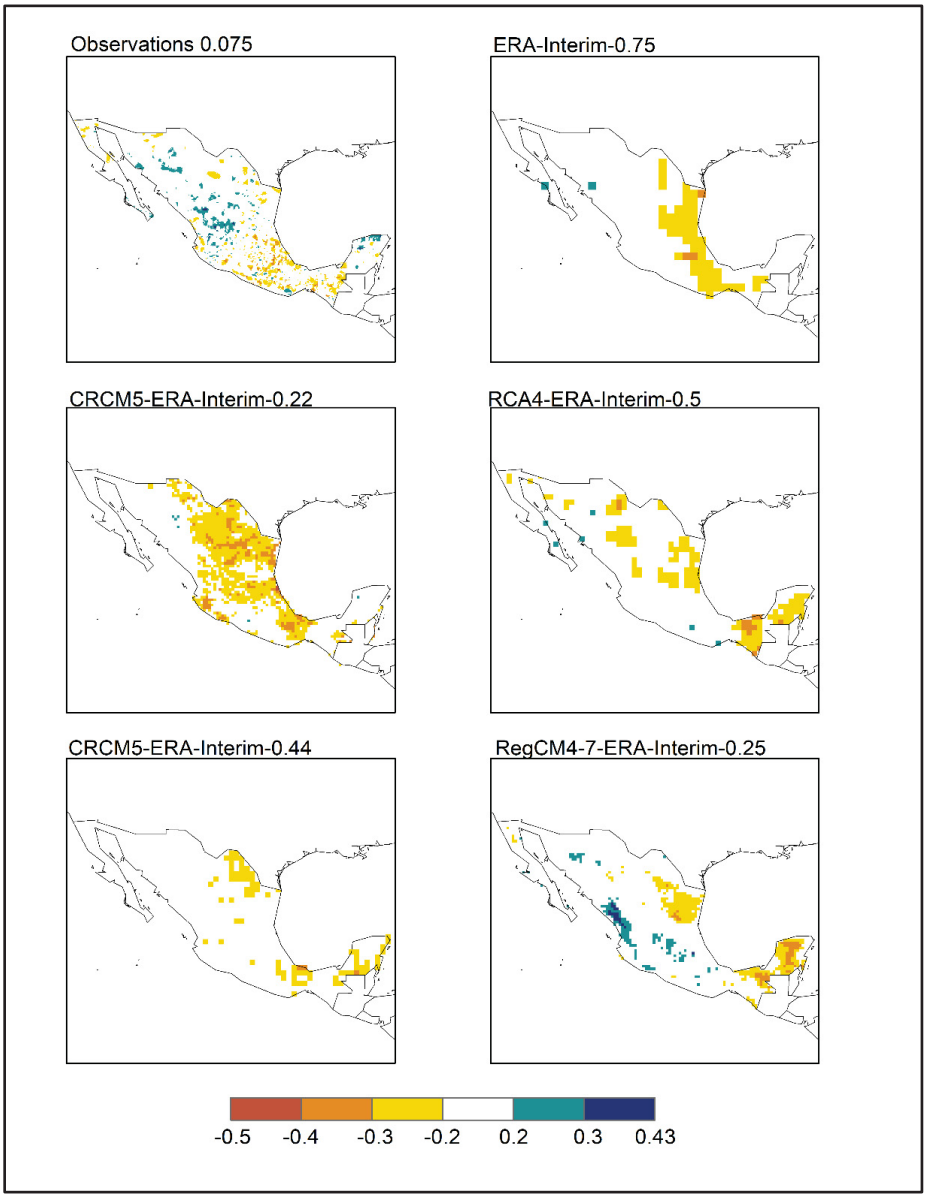

Figure 3.20 Spatial pattern of temporal correlation per grid point between SPI60 and ENSO, in the time period from 1985 to 1998, calculated with observations (upper left corner map), ERA-Interim (upper right corner map), CRCM5-ERA-Interim-0.22 (left center map), CRCM5-ERA-Interim-0.44 (lower left corner map), RCA4-ERA-Interim-0.5 (right center map) and RegCM4-7-ERA-Interim-0.25. For SPI60 simulations correlation, PDO was calculated with ERA-Interim

CHAPTER 4

ASSESSMENT OF ERA-INTERIM-DRIVEN RCM SIMULATIONS IN REPRODUCING THE LINK BETWEEN ENSO AND CLIMATE EXTREME INDICES

Abraham Hernandez-Garcia[1], Annie Poulin[1], Rabindranarth Romero-Lopez[2] and Dominique Paquin[3]

[1]Ecole de technologie supérieure, Department of Construction Engineering, Hydrology, Climate and Climate Change (HC3) Laboratory, Canada
[2]Universidad Veracruzana, Lomas del Estadio S/N, Zona Universitaria, Xalapa, 91000, Mexico
[3]Ouranos Consortium, 550 Sherbrooke street West, 19th floor, West tower, Montreal, QC, Canada H3A 1B9

Paper submitted to the *Theoretical and Applied Climatology*, October 2024

Abstract

The link between ENSO and precipitation patterns has been extensively studied. However, whether RCM simulations and their driving data can reproduce this link remains unclear. This study aims to evaluate the ability of ERA-Interim-driven RCM simulations to replicate the spatial patterns of the temporal correlation between ENSO and Climate Extreme Indices (CEI) -CDD, CWD, Rx1, and Rx5- over Mexico from 1980 to 2012. First, the accuracy of ENSO reproduction with ERA-Interim was assessed. Second, RCM simulations' performance in reproducing the CEIs was evaluated. Finally, the replication of the spatial pattern of temporal correlation between ENSO and CEIs and its statistical significance were analyzed. The findings reveal that ERA-Interim can accurately reproduce the ENSO index. Both ERA-Interim and the simulations are capable of replicating CEIs spatial representation throughout the study period, although they tend to overestimate the maximum and minimum values. Both ERA-Interim and the simulations reproduce the observed humidity conditions in Mexico, characterized by a dry north and wet south. Among the CRCM5 simulations, the 0.22 resolution shows the best agreement with the CDD and CWD indices, while the 0.44 resolution

aligns best with the Rx1 and Rx5 indices. Moreover, ERA-Interim and RCA4 simulation show better agreement in reproducing the correlation of ENSO calculated with ERA-Interim and CDD, while the CRCM5 0.22 simulation shows this for CWD. The seasonal CEIs correlation with ENSO was best represented by both CRCM5 simulations for summer in the CDD and CWD indices, whereas just the RegCM4-7 simulation was unable to reproduce this link in winter.

Keywords: Climate Extreme Indices, Regional Climate Models, El Niño South Oscillation

4.1 Introduction

The combined effects of El Niño South Oscillation (ENSO) and other Sea Surface Temperature Anomaly (SSTA) oscillations such as the Pacific decadal oscillation and the Atlantic multidecadal oscillation has been linked to trends in droughts in the southeastern United States (Abiy et al., 2019) and in extreme precipitation in Mexico and in southwestern United States (Arriaga-Ramirez & Cavazos, 2010).

In Mexico, a correlation has been observed between changes in precipitation patterns and SSTAs (Pan et al., 2018). Specifically, ENSO has historically influenced precipitation patterns across the country (Arroyo-Morales et al., 2023). ENSO phases are linked to variations in precipitation in both northern and southern Mexico (Englehart & Douglas, 2002; Méndez & Magaña, 2010), with these effects potentially amplified by the country's complex orography (Stagge et al., 2023) and extending beyond its borders (Méndez & Magaña, 2010; Ruiz-Vásquez et al., 2024).

In the pursuit of gaining a deeper understanding of the relationship between oceanic changes and precipitation patterns, various studies have assessed the reproduction of precipitation using regional climate models (RCMs) (Jacob et al., 2007; Liang et al., 2007), even when driven by different forcing data (e.g. MPI-ESM-LR, HadGEM2-ES and GFDL-ESM2M) (Endris et al., 2016), in different type of regions and physiographic conditions (e.g. Beranová & Kyselý,

2024; Rai et al., 2024; Stefanidis et al., 2020; Torrez-Rodriguez et al., 2023), including in Mexico (Costa et al., 2023; Fuentes-Franco et al., 2014; Liang et al., 2007; Mendoza-Uribe & Lugo-Morín, 2020; Morales-Velazquez et al., 2021). Additionally, efforts have been made to assess the performance of Regional Climate Models (RCMs) in reproducing precipitation patterns associated with ENSO signals, such as drought and rainfall patterns (Aryal & Zhu, 2021; De Silva et al., 2023; Torres-Alavez et al., 2021).

Given the significant impact of extreme weather events in Mexico-from humid conditions, such as floods and river overflows (CENAPRED, 2021), from dry conditions (CENAPRED, 2014) that resulted in the country's most severe drought in a decade in 2023 (NASA, 2024)-ongoing research focuses on understanding climate extremes, their trends, and the hydroclimatic contrast between the northern and southern regions of the country (Colorado-Ruiz & Cavazos, 2021; García-Cueto et al., 2019; Montero-Martínez et al., 2018; Ortiz-Gómez et al., 2020; Pita-Díaz & Ortega-Gaucin, 2020; Ruiz-Alvarez et al., 2020). However, there is a need to deepen our understanding of how well RCM historical simulations can reproduce the effects of teleconnection—derived from RCM driving data—on dryness and humidity conditions through Climate Extreme Indices (CEIs) based on simulated precipitation. The application of CEIs in Mexico, reproduced by climate models and reanalysis data, has been explored using the Coupled Model Intercomparison Project (CMIP6) by Kim et al. (2020) and over the tropical Americas, including Mexico, using the Regional Atmospheric Modeling System (RAMS) by Costa et al. (2023).

Evaluating the ability of RCM simulations to reproduce monthly and seasonal ENSO-CEIs relationships is a crucial step in validating their historical performance. This is the first step to study the RCM behaviors for their use in projections under climate change conditions. The primary objective of this work is to study the reproduction of the observed correlation between ENSO and wet or dry conditions in Mexico, from ERA-Interim reanalysis and four ERA-Interim-driven RCM historical simulations.

The primary objective is achieved through the following three secondary objectives:

1. Evaluation of Reanalysis Data: The first step involves assessing the ERA-Interim reanalysis sea surface temperatures (SSTs) in reproducing the ENSO index time series computed from HadISST observed dataset, in the 1980 to 2012 time period.

2. Assessment of Precipitation and Climate Extremes: The monthly accumulated precipitation from ERA-Interim and the four RCM simulations is compared to the values from Livneh et al. (2015) observed dataset in the 1980 to 2012 period; a comparison is also carried for four CEIs, namely maximum monthly wet spell duration, maximum monthly dry spell duration, monthly maximum 1-day precipitation depth, and monthly maximum consecutive 5-day precipitation depth.

3. Correlation Analysis: Finally, the correlation between ENSO and the monthly CEIs time series, respectively computed from ERA-Interim and the RCM simulations, is compared to the observed correlation, i.e. computed from HadISST and Livneh precipitation data.

4.1.1 Study sites and data

4.1.1.1 Study sites

In this study, the El Niño 3.4 region is used to calculate the temporal pattern of the teleconnection index, as it effectively reflects ENSO phases and includes portions of both the El Niño 3 and 4 regions (Figure 4.1). The boundaries of the El Niño 3.4 region were determined based on information available in the Climate Data Guide from the National Center for Atmospheric Research (Trenberth, 2024).

The Mexican country territory, also shown in Figure 1, panel B, is the main focus of this study. The country has two important peninsulas, the Baja California peninsula to the northwest and

the Yucatan peninsula to the southeast (a reference to those peninsulas will be made in the analysis of the results).

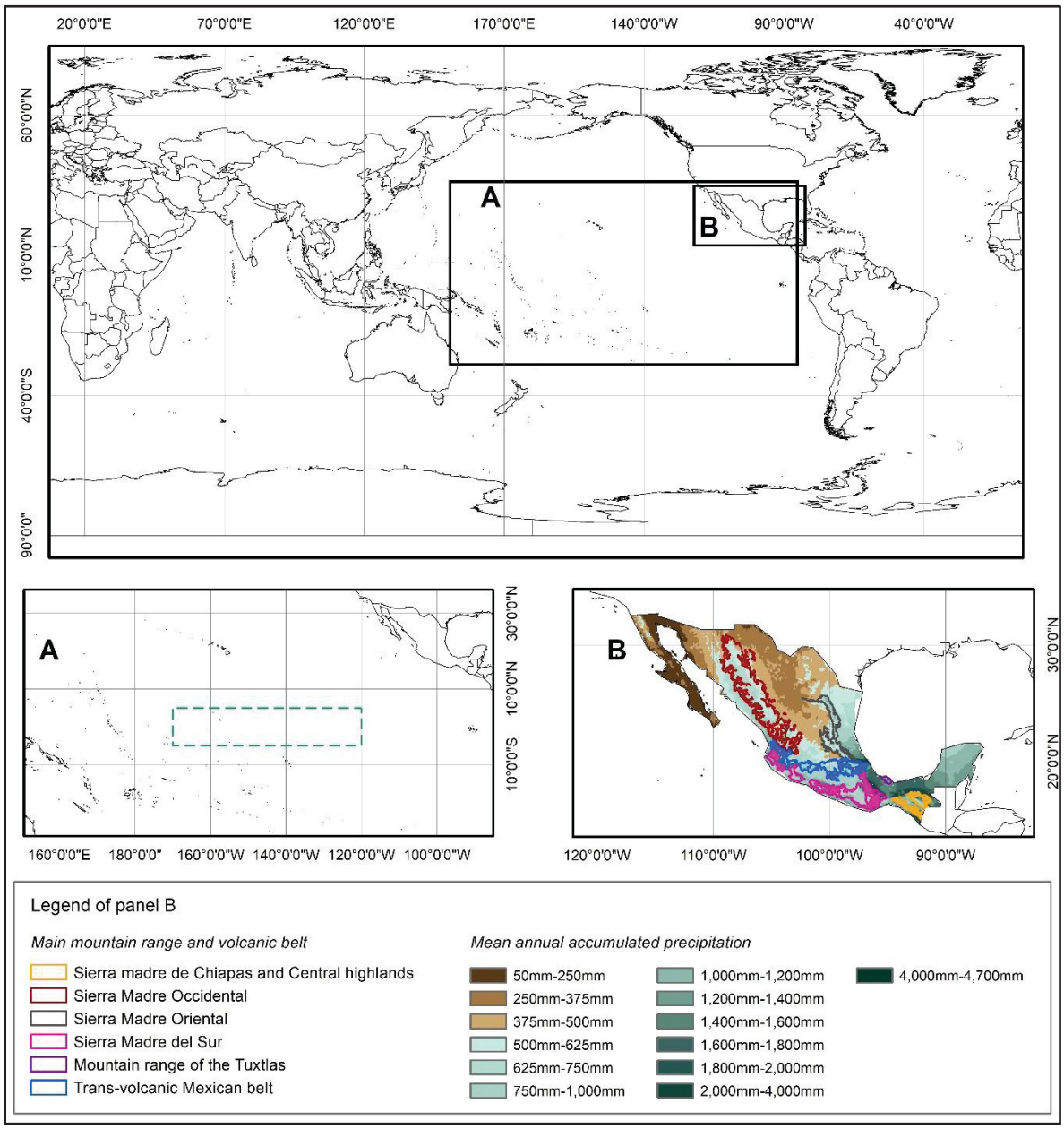

Figure 4.1 Study sites: Upper panel, localization map. Panel A, The El Niño 3.5 region (dashed green line). Panel B Mexico region

The Mexican country territory, also shown in Figure 4.1, panel B, is the main focus of this study. The country has two important peninsulas, the Baja California peninsula to the northwest and the Yucatan peninsula to the southeast (a reference to those peninsulas will be made in the results analysis).

4.1.1.2 Data

The time period taken into account is from 1980 to 2012, since it is common to all the datasets that are described hereafter.

Sea Surface Temperature Data. Two data sources were utilized in this study. The first is the Met Office Hadley Centre's Sea ice and sea surface temperature dataset (HadISST), which has a spatial resolution of 1° latitude-longitude and a daily temporal resolution, and was used as the observed reference (Rayner et al., 2003). The second dataset is the ERA-Interim reanalysis provided by the European Centre for Medium-Range Weather Forecasts (ECMWF), having a spatial resolution of 0.75° latitude-longitude and a daily temporal resolution (Berrisford et al., 2009; Dee et al., 2011). The ERA-Interim dataset was included because it serves as the driving dataset for the studied historical RCM simulations. Global information is inherited by RCMs from ERA-Interim (see section 4.2).

Precipitation Data. Data from observations, ERA-Interim reanalysis and RCM simulations were used. The dataset considered as observed reference is the Livneh et al. (2015) gridded dataset, with a spatial resolution of 1/16° ≈ 0.075° (~6km) latitude-longitude, and daily temporal resolution. It was generated from interpolating weather station observations. The ERA-Interim precipitation data has an original temporal resolution of 12 hours. In the present study, daily values were computed and used. The RCM simulations data are described in table 4.1.

Table 4.1 Description of RCM simulations characteristics

RCM	Driving data	Spatial resolution	Time period	Variable
CRCM5-ERA-Interim-0.22	ERA-Interim	0.22° latitude-longitude	1980 - 2012	Precipitation
CRCM5-ERA-Interim-0.44	ERA-Interim	0.44 latitude-longitude	1980 – 2012	Precipitation
RCA4-Interim-ERA-0.5	ERA-Interim	0.5 latitude-longitude	1980 – 2012	Precipitation
RegCM4-7-ERA-Interim-0.25	ERA-Interim	0.25 latitude-longitude	1980 - 2012	Precipitation

4.2 Methods

This section is divided into three main parts: The first part focuses on the reproduction of the ENSO 3.4 index by ERA-Interim. The second part examines the reproduction of the time series for the monthly accumulated precipitation and the Climate Extreme Indices time series for the precipitation datasets. The third part addresses the representation of the correlation between the teleconnection index (ENSO) and the Climate Extreme Indices from ETCCDI.

4.2.1 ENSO temporal pattern reproduction

The ENSO index time series was calculated using the methodology outlined by the National Center for Atmospheric Research (NCAR) (Trenberth, 2024). In this study, ENSO was analyzed for the period from 1980 to 2012, specifically focusing on the El Niño 3.4 region. The computation process involved the following steps: first, the average value of the study period was subtracted from the SST time series to obtain anomalies; these anomalies were then smoothed using a 5-month moving average; finally, the smoothed values were normalized by their standard deviation over the study period. It is important to note that the SST data from ERA-Interim were spatially aggregated to match the resolution of the observational data

(Bierkens, 2000). From this point forward, the computation of ENSO using ERA-Interim will be referred to as ERA-ENSO.

4.2.2 Precipitation and CEIs reproduction

The precipitation data used in this study have different resolutions, as seen previously, so an adjustment was made to each data set to the resolution of the observations (1/16°, ~6km, ~0.075 °). The adjustment was made by spatial disaggregation of each RCM simulation data and of ERA-Interim data to the observations' resolution. The spatial disaggregation was performed by distributing values from a coarser resolution dataset uniformly across a finer resolution grid, with each finer grid cell inheriting the same value as its corresponding coarser resolution grid cell. This approach ensures that the original data structure is preserved while aligning it with the grid of higher-resolution datasets. All the precipitation and CEIs analyses that are described hereafter were based on those spatially disaggregated datasets that have the exact same grid.

The precipitation temporal pattern analysis was done through the monthly accumulated precipitation, which was computed for each data set, and for each grid cell.

To observe the agreement of the precipitation time series between the observations and the other datasets (ERA-Interim and RCM simulations,) the Pearson correlation coefficient (equation 1) was used.

$$\rho_{XY} = \frac{\sum((X - \mu_X)(Y - \mu_Y))}{\sigma_X \sigma_Y} \tag{4.1}$$

Where ρxy is the correlation coefficient, σ_X and σ_Y are the standard deviations of X and Y, respectively. ρxy takes values between [-1,1] (Von Storch & Zwiers, 1999).

The monthly time series for each dataset were spatially aggregated by calculating the spatial average across the entire Mexican domain. These aggregated time series were then plotted to enable a temporal comparison and assess their agreement with the observations.

4.2.2.1 CEIs reproduction

The computation of climate extreme indices was conducted using the equations provided by the Expert Team on Climate Change Detection and Indices (ETCCDI) (http://etccdi.pacificclimate.org/list_27_indices.shtml) (Karl et al., 1999; Peterson et al., 2001). This study focused on four specific indices: "Maximum length of wet spell" (CWD), defined as the maximum number of consecutive days with precipitation (RR) ≥ 1mm; "Maximum length of dry spell" (CDD), defined as the maximum number of consecutive days with RR < 1mm; "Monthly maximum 1-day precipitation" (Rx1); and "Monthly maximum consecutive 5-day precipitation" (Rx5). The first two indices relate to humidity conditions in Mexico, with CWD representing wet conditions and CDD representing dry conditions, while Rx1 and Rx5 are associated with maximum precipitation values. The definitions of each of these indices are provided below.

CDD: maximum number of consecutive days in a month, with precipitation values (RR) less than 1 millimeter,

$$RR_{ij} < 1mm \tag{4.2}$$

CWD: maximum number of consecutive days in a month, with precipitation values (RR) greater than or equal to 1 millimeter,

$$RR_{ij} \geq 1mm \tag{4.3}$$

Rx1: maximum precipitation recorded on day "j" for the period of one month "i", expressed in millimeters,

$$Rx1day_j = \max\left(RR_{ij}\right) \quad (4.4)$$

Rx5: maximum precipitation recorded in 5 days (starting from day "j") consecutively within the period of one month "k", expressed in millimeters,

$$Rx5day_j = \max\left(RR_{kj}\right) \quad (4.5)$$

The indices described above were calculated each grid cell on a monthly time basis, and for each data set.

4.2.3 Reproduction of the correlation between the ENSO teleconnection index and the CEIs (CDD, CWD, Rx1 and Rx5)

Pearson correlation coefficient (equation 1) was computed between time series of the CEIs and the ENSO index, for observations, and between CEIs from ERA-Interim or simulations and ERA-ENSO. Again, the correlation was computed per grid cell and displayed spatially using maps. The correlations were first computed for the entire monthly time series, and then per season. The seasons were defined as follows: December-January-February for winter; March-April-May for spring; June-July-August for summer; September-October-November for fall. The monthly values pertaining to each season were extracted each year to create a new time series per season, per index, per dataset, and per grid cell.

The Student's t-test is employed to determine the statistical significance of the Pearson correlation coefficient (r) between ENSO index and CEIs time series per grid point. The test evaluates whether the correlation differs significantly from zero, which would suggest a meaningful linear relationship between ENSO and CEIs. The t-statistic is calculated as equation 4.6,

$$t = \frac{r\sqrt{n-2}}{\sqrt{1-r^2}} \tag{4.6}$$

where n represents the number of data and n-2 the degrees of freedom. A p-value is derived from the t -distribution based on the calculated t-statistic. The null hypothesis (H_0) assumes no correlation, while the alternative hypothesis (H_1) posits a significant correlation. A p-value less than the chosen significance level (α=0.05) leads to rejecting H_0, indicating that the correlation is statistically significant.

4.3 Results

4.3.1 ENSO time series reproduction

The Pearson correlation between the daily HadISST and daily ERA-Interim data reaches a high value of 0.97. The average bias between both time series is 0.23 °C.

4.3.1.1 Enso temporal pattern reproduction

In Figure 4.2, illustrates the temporal agreement between ERA-ENSO index (pink dashed-dotted line) and the HadISST ENSO index. ERA-ENSO effectively captures the observed oscillation and transitions from positive phase to negative phase However, slight discrepancies are noted in the extreme values, with an overestimation that peaks at 0.43°C in 1998. The bias fluctuates around zero throughout the time series, indicating a consistent yet slightly overestimated ENSO amplitude in ERA-Interim.

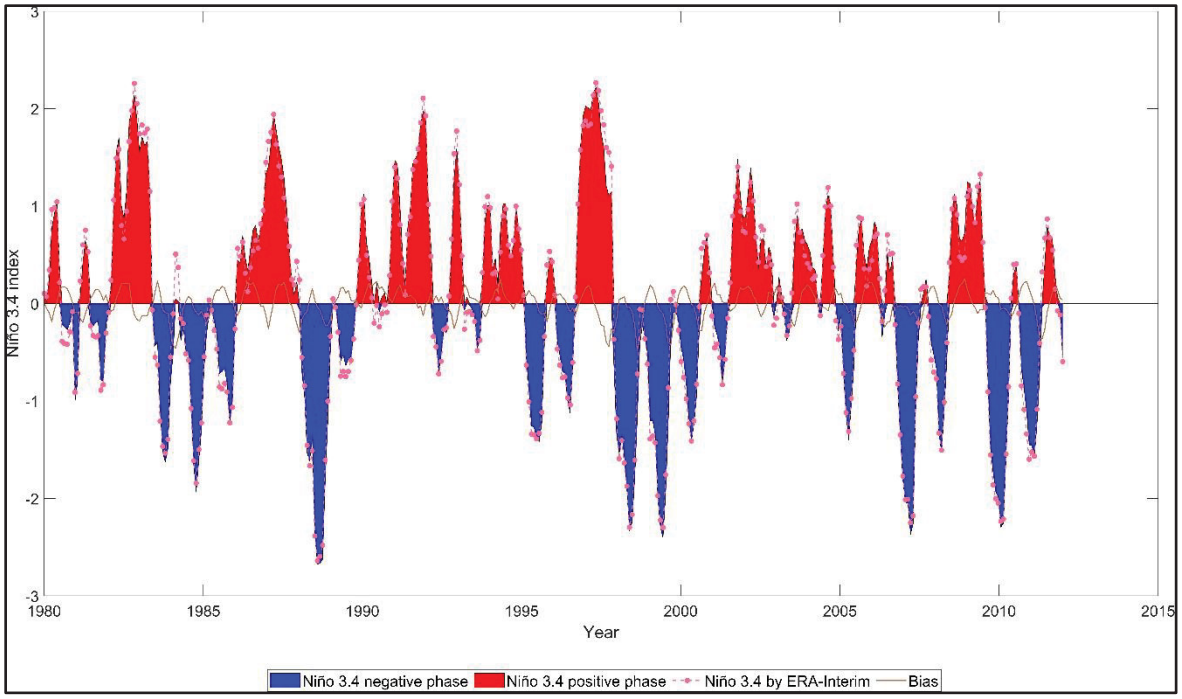

Figure 4.2 ENSO index by HadISST (red area for positive phase and blue area for negative phase), ERA-ENSO index (pink dashed line) and bias (brown solid line)

4.3.2 Precipitation patterns and CEIs reproduction

4.3.2.1 Precipitation time series reproduction

The correlation values between the observed data and the reanalysis and RCM simulations data, are shown in Table 4.2. ERA-Interim data exhibit a correlation of 0.98 with observations. Among simulations, CRCM5-ERA-Interim-0.44 achieves the highest correlation (0.92), while RegCM4-7-ERA-Interim-0.25 yields the lowest correlation (0.89). These high correlations primarily reflect the agreement in temporal patterns, despite some discrepancies in magnitudes.

Table 4.2 Correlation values between observations and ERA-Interim and ERA-Interim RCM simulations

	ERA-interim-0.75	CRCM5-ERA-Interim-0.22	CRCM5-ERA-Interim-0.44	RCA4-ERA-Interim-0.5	RegCM4-7-ERA-Interim-0.22
ERA-interim-0.75	1	0.91	0.91	0.89	0.88
Observations	0.98	0.91	0.92	0.90	0.89

Figure 4.3 shows the monthly accumulated precipitation time series over the study period (1980–2012). Observations (black line) depict wet and dry seasons occurring each year. ERA-Interim (green line) underestimates maximum precipitation values and slightly overestimates minimum values. The RCM simulations overestimate the annual maxima, with RegCM4-7-ERA-Interim-0.25 and RCA4-ERA-Interim-0.5 showing the largest biases, sometimes exceeding 100 mm. Such overestimations are consistent with findings by Giorgi et al. (2012) and Strandberg et al. (2014).

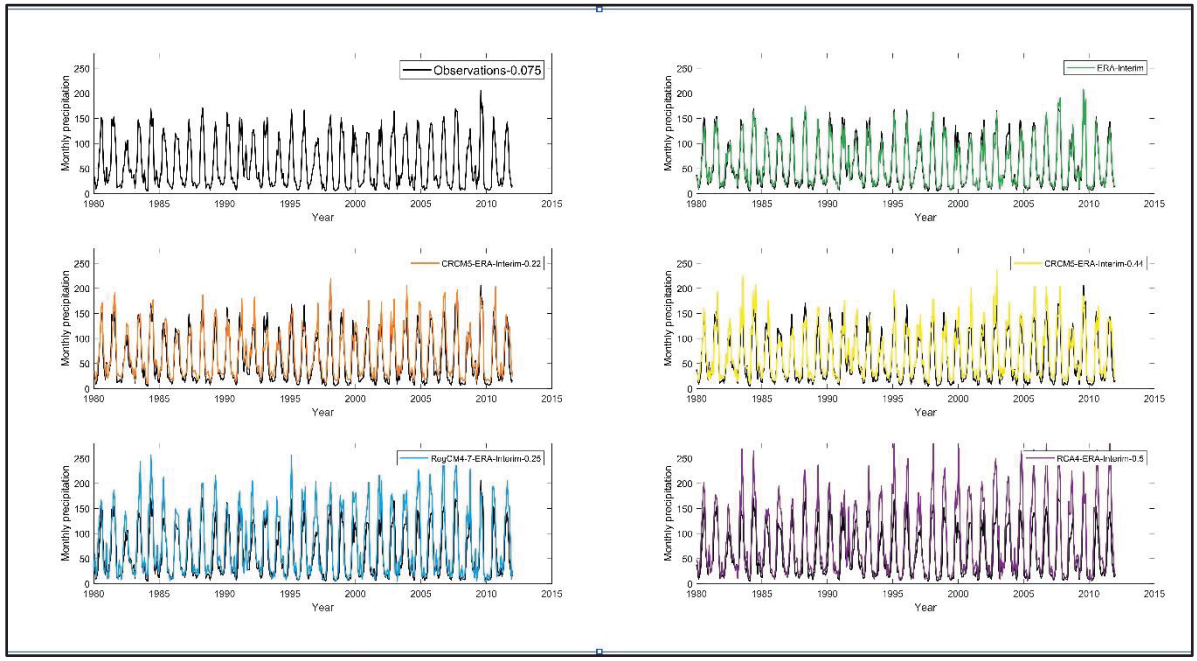

Figure 4.3 Temporal pattern of monthly accumulated precipitation for the entire Mexican domain from 1980 to 2012. Observations (black lines), ERA-Interim (green line), CRCM-ERA-Interim-0.22 (orange line), CRCM-ERA-Interim-0.44 (yellow line), RegCM4-7-ERA-Interim-0.25 (blue line), and RCA4-ERA-Interim-0.5 (purple line).

4.3.2.2 CEIs reproduction (CDD, CWD, Rx1 and Rx5)

The reproduction of CEIs was analyzed for all datasets, including observations, ERA-Interim reanalysis, and RCM simulations, over the study period (1980 - 2012). This section first examines the dry (CDD) and wet (CWD) spell duration indices, (Figures 4.4 A and 4.4 B). Subsequently, the Rx1 and Rx5 indices, which represent maximum precipitation over one and five consecutive days, respectively, are presented (Figures 4C and 4D).Each map in Figure 4 was obtained by computing the average value, in each grid cell of the Mexican domain, from the full monthly time series (1980-2012) of the different indices.

The following convention is used, throughout the paper, to present the CEIs results:

CDD-y, CWD-y, Rx1-y and Rx5-y,

where y can take the values Obs (observations), ERA (ERA-Interim reanalysis), CRCM5.22 (CRCM5-ERA-Interim-0.22 simulation), CRCM5.44 (CRCM5-ERA-Interim-0.44 simulation), RCA4.5 (RCA4-ERA-Interim-0.5 simulation), or RegCM4-7.25 (RegCM4-7-ERA-Interim-0.25 simulation).

CDD and CWD indices. In Figure 4.4A, it is possible to observe the spatial behavior of CDD-Obs (upper left panel of Figure 4.4A), which shows a decrease towards the southeast of Mexico (5 days), this decrease is related to an average decrease in dry conditions for the study period, and an average increase towards the northwest of Mexico (30 days),

The behavior previously observed in the CDD index is analogous to the behavior of the CWD-Obs index, which is shown in the map in the upper left panel of Figure 4.4B, where it is observed that the spatial gradient of the observations increases towards the southeast of Mexico, with up to 8 days on average of continuous precipitation, decreasing towards the northwest showing values close to 0 days. It is worth mentioning that an increase in humid

conditions is observed in the west of central Mexico, suggested by both indices (CDD and CWD).

Regarding CDD-ERA, (upper right panel in Figure 4.4A) it is possible to notice some similarities to what is spatially represented by the observations, such is the case of the yellow-coloured area over northern center of Mexico (which corresponds to the Chihuahua desert), where not only the geolocation is reproduced but also the intensity of this index. In addition, there is an increase in the CDD values towards the southeast of the country and a decrease in a northwest direction, however there is an overestimation both in highest and lowest values of this index, as well as in the size of the area being covered by those values. This is most likely due to the spatial resolution of the reanalysis, which is much larger than that of the observations.

CWD-ERA (upper right panel in Figure 4.4B), shows similarities with CWD-Obs, analogous to the CDD index described in the previous paragraph, in this case (in CWD-ERA index) there is an increase in the average number of wet days towards the southeast of Mexico and a decrease towards the northwest, as does the pattern of this index in the observations (upper left panel of Figure 4.4B), it is also shown an overestimation both in the highest and lowest values and in their spatial extent.

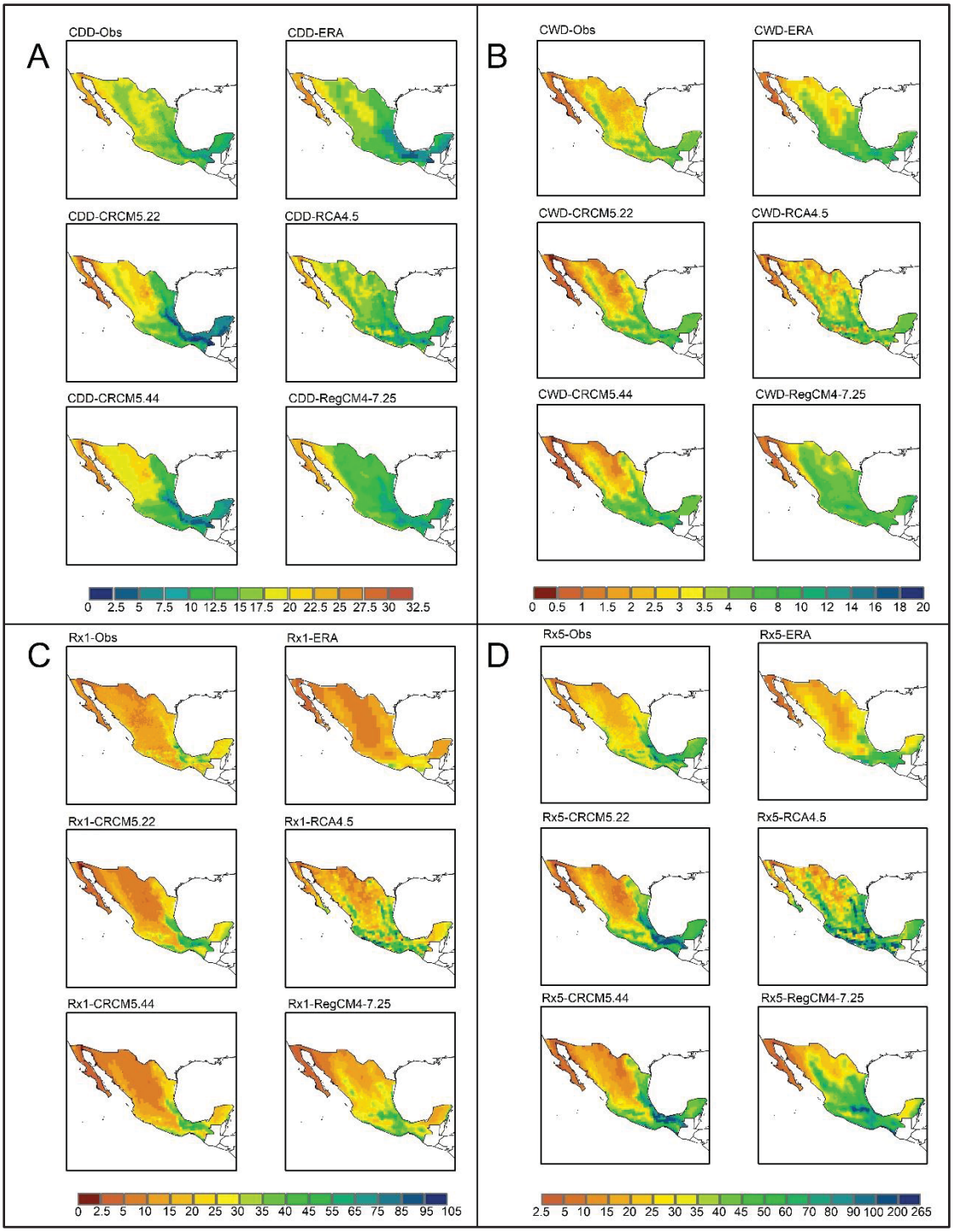

Figure 4.4 Mean monthly CEIs values over the 1980-2012 time period, CDD panel A (number of days), CWD panel B (number of days), Rx1 panel C (mm of precipitation) and Rx5 panel D (mm of precipitation). In each section are shown Observations, ERA-Interim and RCM simulations, CRCM5-ERA-Interim-0.22, CRCM5-ERA-Interim-0.44, RCA4-ERA-Inteirm-0.5 and RegCM4-7-ERA-Inteirm-0.25

CDD-CRCM5.22 (central left panel of Figure 4.4A), CWD-CRCM5.22 (central left panel of Figure 4.4B), CDD-CRCM5.44 (lower left panel of Figure 4.4A) and CWD-CRCM5.44 (lower left panel of Figure 4.4B) are able to reproduce the spatial gradient noted in CDD-Obs. However, they overestimate the spatial variability, with lower values in the northwest (down to a low mean range of 2.5-5 days) and higher values in the southwest (up to 32 days). Higher values are generally reached by CDD-CRCM5.22 and CWD-CRCM5.22 than CDD-CRCM5.44 and CRCM5.44, which can be likely be attributed to the finer resolution of CRCM5-0.22 simulation resulting in a finer representation of topography (Figure 4.1B).

CDD-RCA4.5 (central right panel of Figure 4.4A) overestimates the lower values at Sierra Madre Oriental (Figure 4.1B; 2.5 days) and higher values in the northwest of Mexico (32.5 days). This is analogous to what is observed in CWD-RCA4.5 (middle right panel of Figure 4.4B) with an overestimation in the southeast of Mexico (up to 20 days) and in the northwesterly direction (values close to 0 days of precipitation on average). These overestimations can be as a result of the resolution difference, with respect to observations, nevertheless as in the case of the other datasets, the spatial variability of the CDD and CWD values generally follow the topography of Mexico.

Regarding CDD-RegCM4-7.25 (lower right panel of Figure 4.4A), it generally underestimates the spatial variability with a narrower range of values than the other datasets. However, in northwestern Mexico, it represents similar spatial variability to observations even showing values between 25 and 30 days of this index (CDD). CWD-RegCM4-7.25 (lower right panel of Figure 4.4B) shows a similar behavior as for the RegCM4-7.25, that is, it underestimates the spatial variability in most of Mexico but in northwestern Mexico, manages to reproduce the spatial variability pattern described by observations.

The above results suggest that not only the resolution and topography have an impact on CDD and CWD indices but also the wet contrasts between the north and the south, as can be observed in Figure 4.1.

Rx1 and Rx5 indices. Rx1-Obs (upper left panel of Figure 4.4C) and Rx5-Obs (upper left panel Figure 4.4D), show their higher values towards the southeast and south of Mexico, suggesting a relationship with the topography (Sierra Madre Oriental, Sierra Madre Occidental and the Mexican Volcanic Belt, shown in Figure 4.1B) as well as the proximity with the Gulf of Mexico. The maximum values reach up to 105 mm in one day and 265 mm in five days, for Rx1-Obs and Rx5-Obs, respectively, and then the values decrease smoothly towards Yucatan Peninsula. The lower values are seen in the center and northwestern Mexico (0 mm of precipitation in one day and between 5 and 10 mm for Rx1-Obs and Rx5-Obs, respectively). In the case of Rx5-Obs, it is worth mentioning the continuous precipitation core in 5 days above 30 mm, in the north of the Baja California peninsula, which is likely related to the North American monsoon.

Rx1-ERA (upper right panel Figure 4.4C) shows a generalized overestimation with respect to Rx1-Obs, nevertheless it reproduces the general spatial pattern. Rx5-ERA (upper right panel Figure 4.4D), reproduces, in a general way, the behavior described by observations, since the values increase towards the southeast, showing values of up to 80 mm, and decrease towards the northwest of Mexico. As can be expected it shows underestimation with respect to Rx5-Obs, notably in the Yucatan peninsula as in the case of Rx1-ERA.

Rx1-CRCM5.22 (middle left panel of Figure 4.4C), manages to reproduce the contrast of conditions between the north and south of Mexico, however it overestimates the spatial variability reaching higher and lower values than Rx1-Obs. Similarly, Rx1-CRCM5.44 (lower left panel Figure 4.4C) overestimates the higher and lower values, but the spatial variability pattern fits with what is described by observations. Rx5-CRCM5.22 (middle left panel Figure 4.4D) and Rx5-CRCM5.44 (lower left panel of Figure 4.4D) present, once again, an

overestimation in the spatial variability (northeastern and southeastern Mexico). Rx5-CRCM5.44 is but closer to the observations.

Although Rx1-RCA4.5 (middle right panel Figure 4.4C) and Rx5-RCA4.5 (middle right panel Figure 4.4D), shows the contrast between the north (dry conditions) and the south (wet conditions) of Mexico, there is a large overestimation of the precipitation amounts, mainly in the middle ans south of the country. Moreover, the overestimation of higher values suggests being strongly related to the topography. Very similar comments also apply to Rx1-RegCM4-7.25 (lower right panel Figure 4.4C) and Rx5-RegCM4-7.25 (lower right panel of Figure 4.4D).

4.3.3 Reproduction of the correlation between the ENSO teleconnection index and the extreme climate indices (CDD, CWD, Rx1 and Rx5)

This section focuses on analyzing the correlation between ENSO time series and monthly CEIs time series over the Mexican territory, specifically highlighting areas where the correlations are statistically significant. The correlation between ERA-ENSO and the climate extreme indices computed from ERA-Interim and from RCM simulations is compared with the correlation between ENSO and observations. First, the entire 1980-2012 time period is looked at, and then the results are broken down into seasonal analysis.

4.3.3.1 Correlation reproduction for the 1980-2012 time period

The statistical significance of the correlation between ERA-ENSO and the CDD and CWD indices captures the general pattern observed in the data, albeit with some differences in the spatial extent. In contrast, the statistical significance of the correlation between ERA-ENSO and the Rx1 and Rx5 indices exhibits a more limited spatial extent compared to observations, which is likely associated with the underestimation of the correlation magnitude.

CDD index. The correlation between ENSO and the CDD-Obs (upper left panel of Figure 4.5A) shows negative or slightly positive (up to 0.15) values throughout the entire country. The strongest negative values, reaching -0.35, are seen along spinal pattern crossing Mexico from north to south. The above suggests that there is a pattern in the relationship between dry spell length and ENSO in some of in the driest regions of the country (see Figure 4.1B).

The ERA-ENSO correlation with the CDD-ERA index (upper right panel of Figure 4.5A), shows a similar pattern. However, there is an underestimation in amplitude of the correlation and size of the area reaching negative correlation values.

The correlation between the ERA-ENSO and CDD-CRCM5.22, shown in the central left panel of Figure 4.5A, replicates the main pattern seen in observations but with a much narrower area reaching negative correlation values. Most of the country shows close to no correlation (values between -0.15 and 0.15). One aspect worth noting is the positive correlation values appearing in the south of the country and along the coast of the Gulf of Mexico, reaching up to 0.35. A very similar spatial pattern is seen in the case of CDD-CRCM5.44. The two CRCM5 simulations showed the lowest dry spell durations, on average, in the areas where positive correlation values appear (Figure 4.4A).

The ERA-ENSO correlation with CDD-RCA4.5 (middle right panel of Figure 4.5A), manages to reproduce the pattern shown by the observations, for the north of the country, with some overestimations toward the northeast and northwest. Towards the southwest of the country, a few grid cells display positive correlation values, but with lower values and covering smaller areas than in the case of CDD-CRCM5.22 and CDD-CRCM5.44.

The correlation between the ERA-ENSO and CDD-RegCM4-7.25 (lower right panel of Figure 4.5A) detects the pattern seen in observations, but with weaker correlation values. It is also the only CDD case showing negative correlation in the Yucatan peninsula where the CRCM5 cases, on their side, displayed positive correlations. This is possibly related with the lower

DCC values and higher precipitation extremes from the RegCM4-7 simulation with respect to the CRCM5 simulations (Figures 4.4A, 4.4C, and 4.4D).

CWD index. As can be expected, results for the CWD index generally show a similar behavior to that of the CDD results in terms of spatial pattern, but with opposite (i.e., positive) correlation values. The correlation between the ENSO and CWD-Obs, (upper left panel of Figure 4.5B), reaches values up to 0.35 for the center of the north of Mexico, but the spatial extent of the positive values is more limited than in the case of CWD-Obs. This suggests, as in the case of CWD index, that ENSO may be influencing the wet spell length in the driest regions of the country.

CWD-ERA (upper left panel of Figure 4.5B) shows only one positive correlation core in the north of central Mexico, that is, there is a clear underestimation in correlation with respect to the observations both in spatial extent and in magnitude.

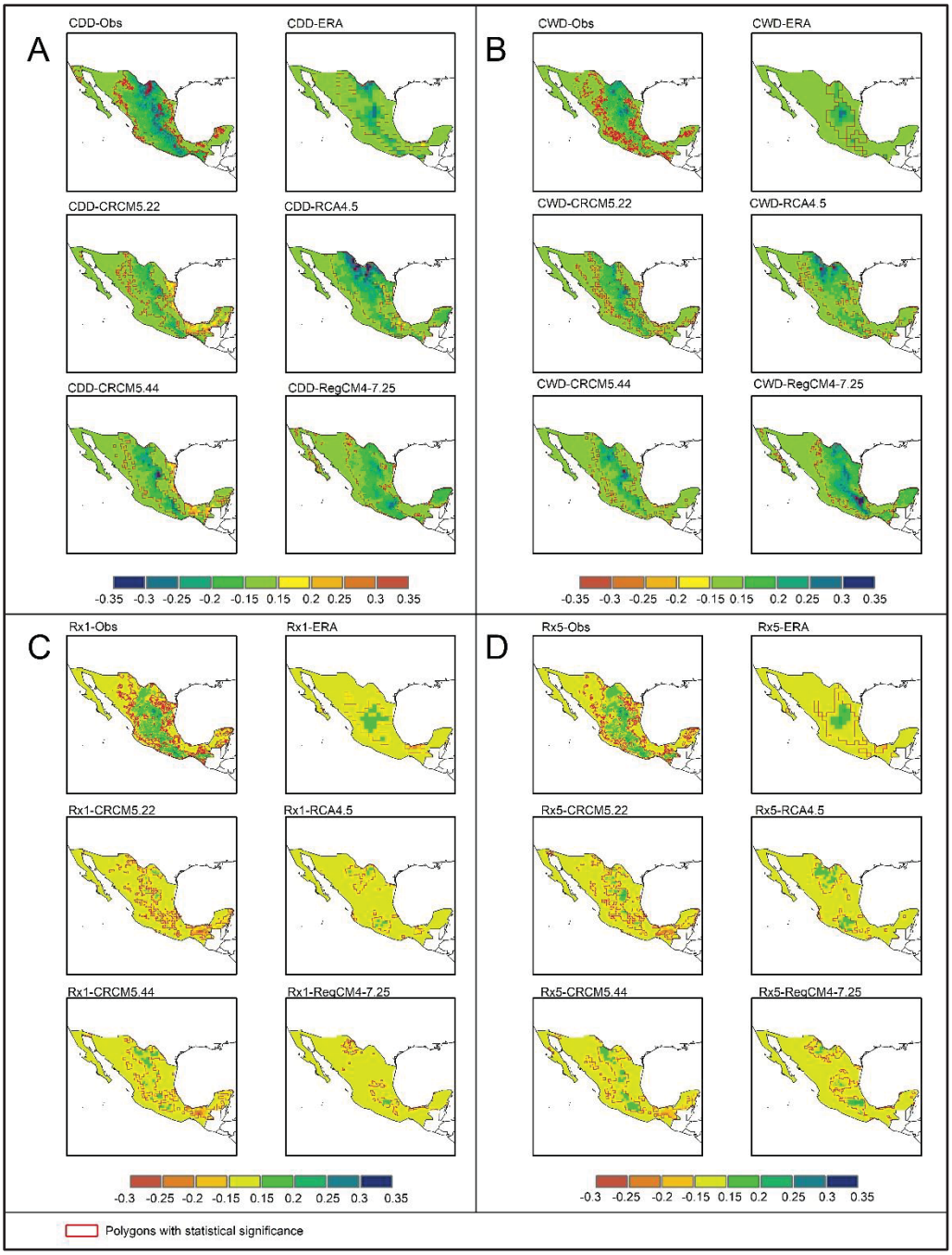

Figure 4.5 Correlation between de ENSO teleconnection index and climate extreme indices (CDD, CWD, Rx1 and Rx5). The teleconnection indices were calculated from HadISST observations (ENSO) and ERA-Interim (ERA-ENSO). The climate extreme indices were calculated from Livneh data set for observations, reanalysis (ERA-Interim-0.75) and RCM simulations (CRCM5-ERA-Interim-0.22, CRCM5-ERA-Interim-0.44, RCA4-ERA-Inteirm-0.5 and RegCM4-7-ERA-Inteirm-0.25). Section A refers to ENSO and CDD index correlation, section B refers to the ENSO and CWD index correlation, section C refers to the ENSO and Rx1 index correlation and section D refers to the ENSO and Rx5 index

The analysis of the correlation between ERA-ENSO and the CWD index from the four RCM simulations (center and bottom panels of Figure 4.5B) is similar to that for the CDD index. The most positive correlation values reached (0.25-0.35), per simulation, are mainly located in the same areas as the most negative values that were reached in the case of the CDD index. Negative correlation values are found from the two CRCM5 and the RCA4 simulations, but with smaller spatial extent than in the case of the CDD index for the same simulations. The two CRCM5 simulations showed the highest values of wet spell duration (Figure 4.4B) close to the areas where the positive correlation values are found.

Rx1 and Rx5 indices. The correlation results for those two indices are very similar. In both cases, the correlation between ENSO and observed values of the indices (RX1-Obs and Rx5-Obs; top left panels of Figure 4.5C and 4.5D) follows a north-south pattern that resembles that seen for the CDD and CWD indices. The strongest correlations are positive, reaching up to 0.35. This pattern, again, suggests the existence of a relationship between ENSO and wet conditions in the driest parts of the country.

The correlation pattern shown by the observations cannot be reproduced neither between ERA-ENSO and Rx1-ERA (upper right panel of Figure 4.5C) nor between ERA-ENSO and Rx5-ERA (upper right panel of Figure 4.5C). In both cases, only a core in central Mexico is present, with values between the 0.15 and 0.20 of correlation. It is worth mentioning that the small nuclei of negative correlation in the south, shown in the observations, move towards the north in this case and are more spatially extended.

Regarding the correlation between ERA-ENSO, and the Rx1 and Rx5 indices from the four RCM simulations, none of those cases manage to reproduce what is described by the observations. The two CRCM5 simulations overestimate, both spatially and in magnitude, the negative correlations in the south of the country, again showing the link between such correlation and the wetter CRCM5-simulated conditions (Figure 4.4) in this part of the country.

Rx1-CRCM5.44 and Rx5-CRCM5.44 are the only cases that show the appearance of the north-south spinal pattern seen in the observations.

4.3.3.2 Seasonal correlation reproduction

This section describes the reproduction of the seasonal correlation between the ENSO teleconnection index and the climate extreme indices, CDD, CWD, Rx1 and Rx5. Since winter (December, January, February) and spring (March, April, May) showed the most extensive spatial pattern correlation, this section focuses on the analysis of those seasons. Winter is a dry season in Mexico while spring sees a rise in precipitation during the months of April and May (see Figure 4.6 showing the mean annual precipitation cycle computed for the entire country). Results for summer and fall (June, July, August – wet season; September, October, November – tropical storms season followed by a decrease in precipitation) are shown in the supplementary materials. The correlation between ENSO and the CDD and CWD indices will be described together because these are related to the count of dry and wet days, respectively. This joint description helps to clarify the pattern of the relationship between ENSO and humidity conditions in Mexico by season. In the same way, the reproduction of the correlation between ENSO and the Rx1 and Rx5 indices will be described together. This allows for the analysis of precipitation intensity over a one- or five-day period and helps to observe the relationship between ENSO and the maximum precipitation values in that time. The statistical significance of the correlation between ERA-ENSO and the CDD and CWD presents an underestimation in the spatial extent with respect to observed correlation, which also is stronger when ERA-ENSO is correlated with Rx1 and Rx5 for both seasons (Spring and Winter). The spatial extent of statistical significance of the correlation encompasses the correlation values above 0.15.

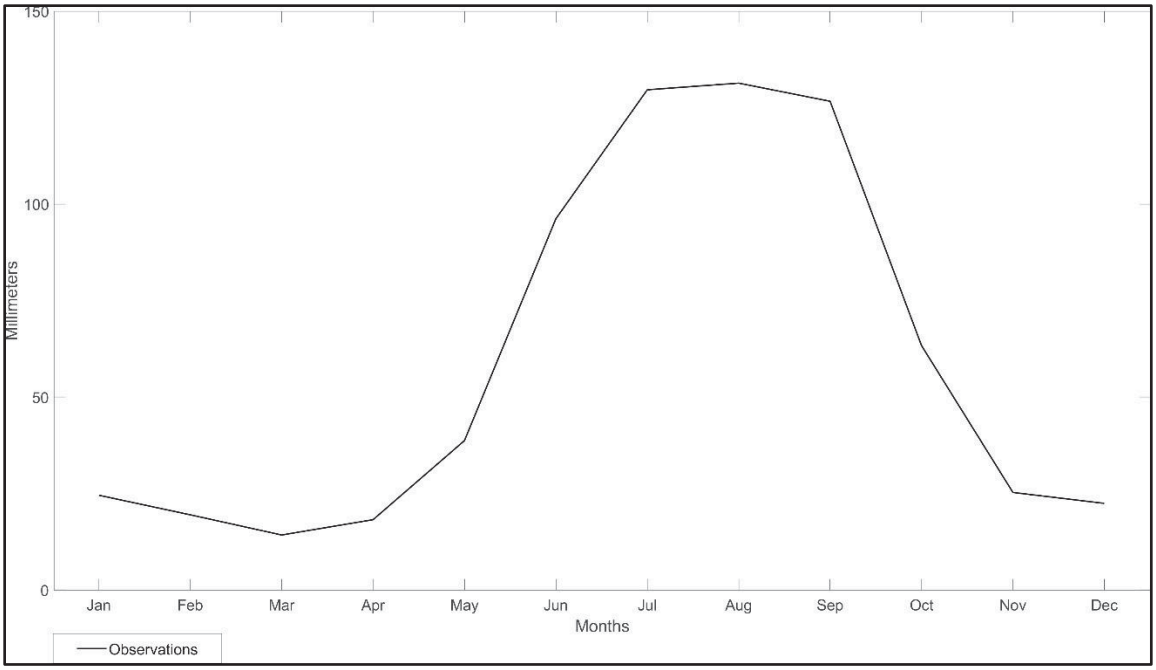

Figure 4.6 Mean monthly accumulated precipitation

Reproduction of spring correlation between ENSO time series and CDD and CWD indices.

The spring correlation between the ENSO and CDD-Obs, (upper left panel of Figure 4.7A), shows that there is a pattern of negative correlation that extends over much of the country except the southeast and northwest of Mexico. This negative correlation oscillates in most of the territory between -0.25 and -0.4, however, there are small areas where the correlation presents values up to -0.5. The stronger negative correlation values are located in the center of the northern border and in the southwest of Mexico, in addition nuclei of these values are observed in the center and east of the north of the country. The spatial pattern of the temporal correlation of the ENSO teleconnection index and the CWD-Obs (upper left panel of Figure 4.6B), reinforce what was described above, that is, in this case there is a positive correlation in the wet spell length (humid conditions) with the ENSO, which clearly extends in the center and north of the country. with some nuclei located in the south of the Sierra Madre Oriental and the Sierra Madre Occidental, as well as in the Sierra madre de Chiapas (Figure 4.1). The maximum values reach up to 0.5 correlation for the CWD index. With respect to the CWD and CDD results presented in the previous section for the entire 1980-2012 period, the spring correlations are stronger and extend to larger areas of the Mexican territory.

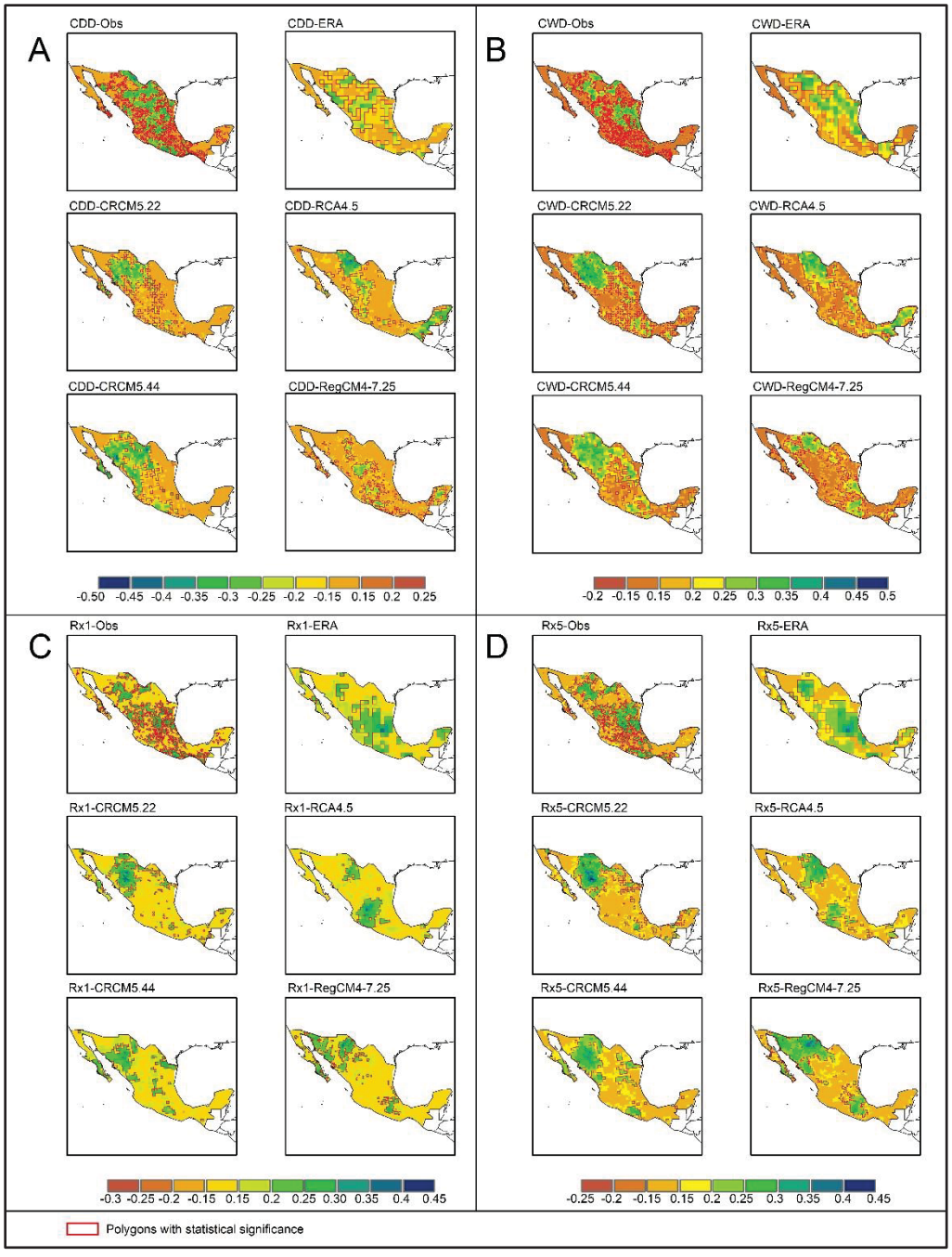

Figure 4.7 Spring correlation between de ENSO teleconnection index and climate extreme indices (CDD, CWD, Rx1 and Rx5). The teleconnection index was calculated from HadISST observations (ENSO) and ERA-Interim (ENSO-ERA). The climate extreme indices were calculated from Livneh data set for observations, reanalysis (ERA-Interim-0.75) and RCM simulations (CRCM5-ERA-Interim-0.22, CRCM5-ERA-Interim-0.44, RCA4-ERA-Inteirm-0.5 and RegCM4-7-ERA-Inteirm-0.25). Section A refers to ENSO and CDD index correlation, section B refers to the ENSO and CWD index correlation, section C refers to the ENSO and Rx1 index correlation and section D refers to the ENSO and Rx5 index

The correlation between ERA-ENSO and CDD-ERA (upper right panel of Figure 4.7A), is underestimated in its magnitude and spatial variability with respect to observations; however, it manages to reproduce the general spatial pattern that is shown by the observations. On the other hand, the correlation of the ERA-ENSO with the CWD-ERA (upper right panel of Figure 4.7B), indicates that, despite the differences inherent in the resolution and the underestimation of the magnitude of the correlation, it manages to represent the ascent of the correlation towards the north and northeast of Mexico, as shown by the observations.

In the cases of CDD-CRCM5.22 (middle left panel of Figure 4.7A) and CDD-CRCM5.44 (lower left panel of Figure 4.7A) the strength of the correlation is overestimated in the northwest of Mexico, where close to no correlation was seen in the observations (-0.15-0.15) is underestimated the center and southwest of the country. The correlation of ERA-ENSO with CWD-CRCM5.22 (middle left panel of Figure 4.7B) as well as CWD-CRCM5.44 (lower right panel of Figure 4.7B) is overestimated in magnitude in the northwest and underestimated in the east of the country.

RCA4 simulation shows more difficulties in reproducing the observed correlation pattern than the other RCM simulations. The correlation strength between the ERA-ENSO and CDD-RCA4.5 (middle right panel of Figure 4.7A) is overestimated in the north and southeast of Mexico and underestimated in the center of the country. The same analysis applies to the case of CWD-RCA4.5 (central right panel of Figure 4.7B).

The spatial variability of correlation between the ERA-ENSO and CDD-RegCM4-7.25 (lower right panel of Figure 4.7A) is underestimated, although it shows some nuclei in central Mexico similar to what is described by the observations. The correlation of ERA-ENSO with CWD-RegCM4-7.25 (lower right panel of Figure 4.7B) shares similarities with observations, but with a large area of underestimation in the west part of Mexico.

Spring correlation between ENSO time series and Rx1 and Rx5 indices. The correlation between ENSO and Rx1-Obs (upper left panel of Figure 4.7C) shows nuclei with correlation values from 0.20 to 0.35 located in central northern Mexico. The central eastern region shows small nuclei that reach up to 0.45 of correlation. The south of the Sierra Madre del Sur and Sierra Madre de Chiapas (Figure 4.1) present correlation values of up to 0.45. The pattern of the correlation between ENSO and Rx5-Obs (upper left panel of the section of Figure 4.7) is very similar to that for the Rx1-Obs index. This suggests that, in spring, the maximum intensity of precipitation in 1 day and in 5 days, as well as its spatial variability in most of the country, is related to ENSO behavior up to a correlation of 0.45. As in the case of the CWD and CDD indices, the spring correlations are stronger and extend to larger areas of the Mexican territory than when the entire 1980-2012 time period is studied. Spring generally starts with a dry month of March, followed by rainfall events occurring in April and May, and mainly related with local-scale systems throughout the country.

The correlation pattern between ERA-ENSO and both Rx1-ERA (upper right panel of Figure 4.7C) and Rx5-ERA (upper right panel of Figure 4.7D) reproduces the spatial distribution presented by the observations, with some differences inherent to the difference in resolution. This leads to an overestimation of the correlation for the Yucatan Peninsula and an overestimation in the south.

None of the four ERA-ENSO-RCM-simulations cases (middle and bottom panels of Figures 4.7C and 4.7D) manage to reproduce the spatial correlation patterns seen in observations. They all show localized albeit different areas of strong correlation, interspersed with sometimes large areas showing close to no correlation (-0.15-0.15).

The Rx1-ERA, Rx5-ERA, Rx5-CRCM50,22, Rx5-RCA4, Rx5-RegCM4.7 all present an overestimation of the magnitude of correlation in the Yucatan peninsula.

Reproduction of winter correlation between ENSO time series and CDD and CWD indices. The strongest correlation values between ENSO and the CWD-Obs and CDD-Obs indices

(upper left panel of Figures 4.8A and 4.8B) are seen in this part of the study and reach up to -0.6 and 0.6, respectively. The main spatial correlation patterns, which are also generally well reproduced in the cases of CWD-ERA and CDD-ERA, display the strongest values in the northwest of Mexico. Th correlation values then gradually decrease towards the southeast and close to the coast of the Gulf of Mexico (-0.15-0.15). A lower-correlation area appears right in the center of the north of the country, in between the Sierra Madres Occidental and Oriental Mountain ranges (Figure 4.1). Winter is the driest season of the year in Mexico. The east-west partitioning of the country suggests a relationship between the conditions occurring in the west part of the country and ENSO.

The east-west partitioning of Mexico, in terms of correlation, is also reproduced in the cases of three of the four RCM simulations, namely the two CRCM5 simulations and the RCA4 simulation (center and bottom left panels of Figures 4.8A and 4.7B). However, the size of the eastern area showing the lowest correlation values is generally overestimated in those three cases, as well as the magnitude of western correlation values (CRCM5 simulations). ERA-ENSO correlations with Rx1 and Rx5 indices from the two CRCM5 simulations display values with opposite signs than in the rest of the country. Those values are located in a similar area to the cases shown in the left middle and left center panels of Figures 4.5A and 4.5B and reach similar values in the order of -0.3 or 0.3. The correlation spatial patterns, in the case of the RegCM4.7 simulation, are very different (lower right panels of Figures 4.8A and 4.8B).

The correlation between ERA-ENSO and CDD-RegCM4-7.25 (lower right panel of Figure 4.8A) and CWD-RegCM4-7.25 (lower right panel of Figure 4.8B) is underestimated across the entire country.

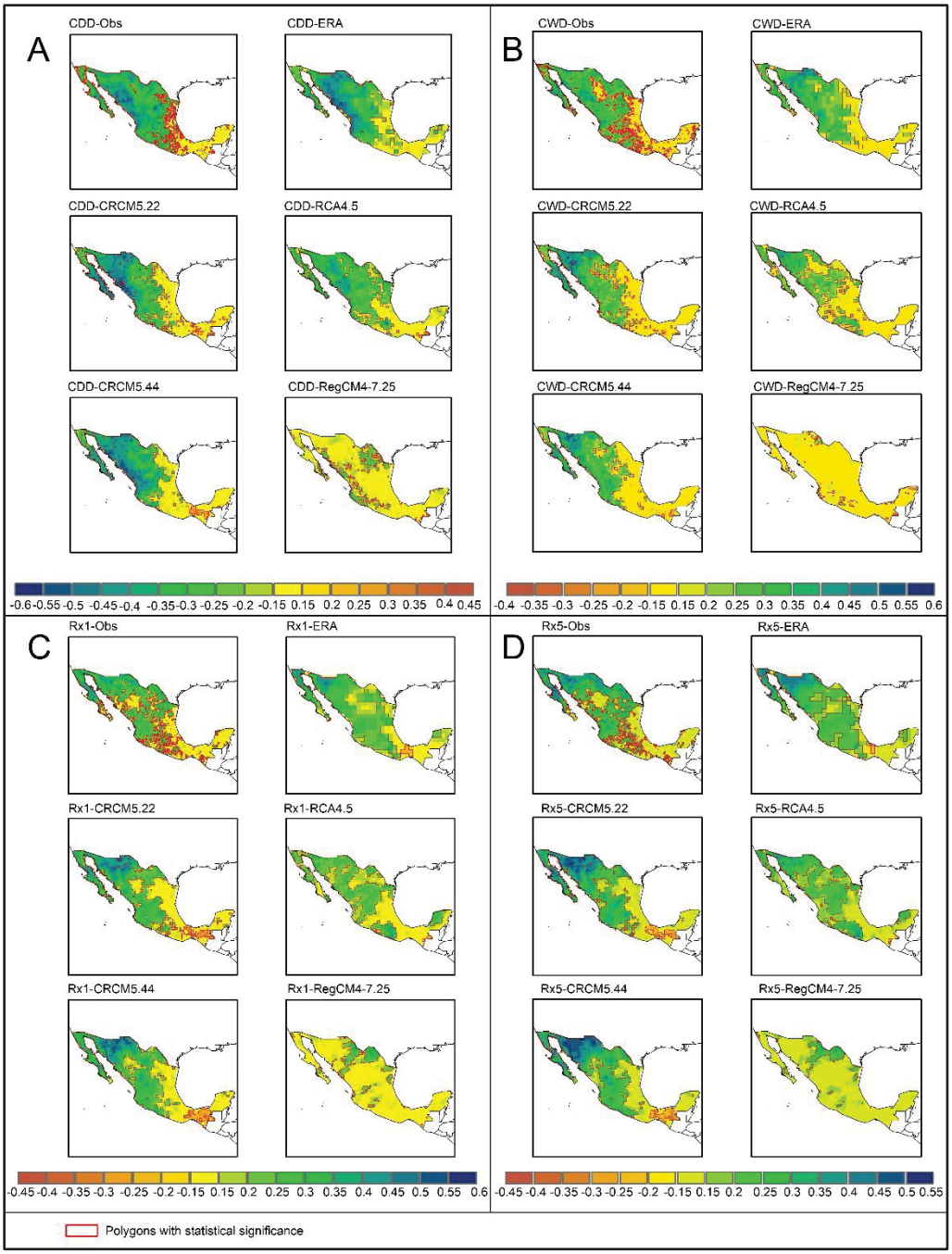

Figure 4.8 Winter correlation between de ENSO teleconnection index and climate extreme indices (CDD, CWD, Rx1 and Rx5). The ENSO teleconnection index was calculated from HadISST as observations (ERA) and ERA-Interim (ERA-ENSO). The indices were calculated from Livneh data set for observations, reanalysis (ERA-Interim-0.75) and RCM simulations (CRCM5-ERA-Interim-0.22, CRCM5-ERA-Interim-0.44, RCA4-ERA-Inteirm-0.5 and RegCM4-7-ERA-Inteirm-0.25). Section A refers to ENSO and CDD index correlation, section B refers to the ENSO and CWD index correlation, section C refers to the ENSO and Rx1 index correlation and section D refers to the ENSO and Rx5 index

Reproduction of winter correlation between ENSO time series and Rx1 and Rx5 indices. The winter correlations between ENSO and the Rx1-Obs and Rx5-Obs (upper left panels of Figures 4.8C and 4.8D) show a spatial pattern similar to that for the CDD and CWD indices. The maximum correlations values that are reached are lower in the case of the Rx1 index though (around 0.5). Winter is Mexico's driest time of the year so this analysis suggests that the dry season precipitation maxima in western and northwestern Mexico are correlated from 0.20 to 0.50 with ENSO.

The correlations between the ERA-ENSO and the Rx1-ERA and Rx5-ERA (upper right panels of Figures 4.8C and 4.8D) mostly reproduce the observed spatial correlation pattern; however, they show negative values in the south of the country and higher positive values in the Yucatan peninsula.

Three of the four simulations (CRCM5.22, CRCM5.44 and RCA4) show, as in the case of the CDD and CWD indices, an east-west partitioning (center and bottom left panels of Figures 4.8C and 4.8D) which was less evident in observed correlations for Rx1 and Rx5 indices. In the cases of the two CRCM5 simulations, higher correlation values are reaches to the northwest of Mexico and negative correlation values are reached in the south. The latter was also seen inf Figures 4.5C and 4.5C for the same two simulations. The correlations, in the case of the RegCM4.7 simulation, is again very different (lower right panels of Figures 4.8C and 4.8D).

Summer and Fall correlation reproduction of the ENSO temporal pattern with the Rx1 and Rx5 indices (supplementary material). The summer correlation between the ERA-ENSO and the CDD, CWD, Rx1, and Rx5 indices suggests that the simulations and the ERA-Interim data reproduce the spatial variability and magnitude in the northwest of the country, with certain discrepancies inherent to each simulation (see supplementary material). In autumn, the correlation between ERA-ENSO and CDD-CRCM5.22 and CWD-CRCM5.22 manages to reproduce the patterns described by observations. Finally, the spatial pattern of correlation

between the ERA-ENSO and the Rx1-ERA and Rx5-ERA indices reproduces the characteristics present in the observations (see supplementary material).

4.4 Discussion

4.4.1 ENSO and precipitation representation

The ENSO calculation with ERA-Interim (ERA-ENSO) shows a 0.99 correlation with respect to the ENSO in observations (HadISST dataset), which corresponds with previous studies (Luo et al., 2020).The maximum difference found with observations, in the studied 1980-2012 period, is 0.43 °C around 1998.

In terms of the temporal representation of monthly accumulated precipitation, after ERA-Interim, which has a correlation of 0.98, the CRCM5-ERA-Interim-0.44 simulation shows the highest correlation at 0.92 (Table 2). While ERA-Interim generally underestimates maximum values, all simulations tend to overestimate them (Figure 4.3), with respect to observations. As noted by Liu et al. (2018) who carried a study in China, ERA-Interim can show difficulties in reproducing observed precipitation in regions with complex orography which is the case for Mexico. ERA-Interim has a much lower spatial resolution than the observations and the RCM simulations which could explain the differences between the results from the analysis and the results form the other datasets.

The precipitation observations were taken as a reference, in the present study, but they also have their own drawbacks. The Livneh et al. (2015) dataset is based on weather station interpolation and one should bear in mind that: (1) interpolation tends to smooth the high (extreme) precipitation values, and (2) data is often missing in the mountainous areas which are difficult to access, therefore leading to a misrepresentation of orographic effect.

4.4.2 Climate extreme indices reproduction

ERA-Interim's spatial representations of CDD, CWD, Rx1 and Rx5 generally remain close to the observed representations but with loss of information related to the reanalysis' lower spatial resolution. The four RCM simulations tend to be wetter than ERA-Interim and the observations. While the two CRCM5 simulations are closer to the observed indices, they show higher values mainly in the mountain ranges. We hypothesize that RCMs have an advantage over (missing) observations at representing precipitation in the mountainous areas, but we cannot verify to what extent. It also depends on RCM spatial resolution and simulation settings, including atmospheric processes parameterizations and the way the information from ERA-Interim (the driving global dataset for the four simulations) is passed to the RCMs, at the boundaries (e.g. using spectral nudging or not; Schubert-Frisius, 2017).

Specifically, in terms of the spatial pattern described by the observations, the greater agreement, per index, was found by CDD-CRCM5.22, CWD-CRCM5.22, Rx1-CRCM5.44 and Rx5-CRCM5.44. When looking at the reproduction of the magnitude or precipitation amount, CDD-CRCM5.44, CWD-CRCM5.44, Rx1-CRCM5.44 and Rx5-CRCM5.44 are closer to the values described by the observations. Nevertheless, all simulations are detecting the change from dry conditions in the north and wet condition in the south of Mexico (Figure 4.4), except for the RCA4 simulation in the cases of CDD and CWD indices.

Although the spatial distribution of the CDD index (calculated globally from the HadEX3 dataset) presented by Kim et al. (2020) for Mexico aligns with the spatial variability observed in this study (computed using the Livneh dataset), there is a contrast in the magnitude of the index values, particularly in the northern part of the country where Kim's values are higher. Similarly, the Rx5 index shows a contrast in magnitude in northern Mexico compared to Kim et al. (2020)'s study, with their values being higher than those calculated using the Livneh et al. (2015) dataset. However, both the spatial variability and magnitude southward of Mexico are consistent between the two studies.

Kim et al. (2020) also noted that the magnitude of the CDD index is well reproduced by ERA-5, CMIP6 MEM (Multimodel Ensemble Median), and CMIP5 MEM. In this study, for Mexico, ERA-Interim and the simulations (CRCM-ERA-Interim-0.22, CRCM-ERA-Interim-0.44, RCA4-ERA-Interim-0.5, and RegCM4-7-ERA-Interim-0.25) are reasonably close to the observations, both in terms of spatial gradient and intensity of the indices. It is important to clarify that the time period for Kim et al. (2020)'s study is from 1981 to 2000, while this study covers the period from 1980 to 2012.

4.4.3 Reproduction of the ENSO and climate extreme indices correlation

The spatial representation of the correlation between the ERA-ENSO time series and the time series of CDD-RCA4.5 retains the characteristics from observed data, particularly in the northern part of the country, more clearly than other simulations. The correlation between the CWD-CRCM5.22 simulation and ERA-ENSO more effectively captures the spatial pattern described by observations. Although the correlation of the Rx1-Obs and Rx5-Obs indices with ENSO shows a clear north-south pattern in central Mexico, with values generally around 0.25 and reaching up to 0.35 in specific regions, neither ERA-Interim nor the RCM simulations successfully replicate this spatial correlation pattern between the two indices and ERA-ENSO.

Regarding the reproduction of correlation magnitudes for the CDD and CWD indices, the CDD-RCA4.5 and CWD-RCA4.5 simulations, as well as the ERA-ENSO, show values that align with observed patterns. However, for the Rx1 and Rx5 indices, only ERA-Interim data accurately captures the correlation strength with ERA-ENSO, and this is primarily observed in the central Mexican plateau.

Interestingly, for the CDD, Rx1 and Rx5 indices, the two CRCM5 simulations show some correlations with ERA-ENSO that have opposite signs with respect to observed correlations. The areas of opposite signs remain small and located in the in the south of Mexico and close to the coats of the Gulf of Mexico. This is possibly due the CRCM5 simulations being wetter than the observations in the areas where the correlations with opposite signs are found.

4.4.4 Seasonal reproduction of the ENSO and climate extreme indices correlation

Some authors have primarily examined the association between the ENSO and precipitation patterns in summer and in winter, due to low-latitude phenomena and the sporadic presence of tropical cyclones in the Mexico region during those seasons (Bravo-Cabrera et al., 2017; Pavia et al., 2006; Vega-Camarena et al., 2023). However, the findings of the present study indicate that a relationship also exists for fall (specifically in the central northern region of the country) and spring (central, northern, and southern Mexico). Furthermore, the reproduction of this relationship is demonstrated using the aforementioned datasets, encompassing all four seasons of the year (see supplementary material).

4.4.4.1 Spring

The correlations between the ERA-ENSO and the CDD-ERA, CWD-ERA, Rx1-ERA and Rx5-ERA indices show a fair representation of observed spatial patterns despite coarser spatial resolution. The simulations CRCM5-ERA-Interim-0.22 and CRCM5-ERA-Interim-0.44 agree with observations in in northwestern Mexico but show stronger correlations for the CWD and CDD indices. None of the simulations could reproduce the spatial correlation patterns seen in observations for the Rx1 and Rx5 indices.

4.4.4.2 Winter

In winter, the strongest correlation values are reached, up to 0.6 and -0.6. An east-west partitioning of the country appears in the observed correlation results for all four CWD, CDD, Rx1 and Rx5 indices. The west side of the country shows stronger correlation values while the east side shows close to no correlation. The two CRCM5 simulations and the ERA-Interim reanalysis are the best at reproducing the observed spatial correlation patterns but tend to overestimate the extent on the east-side area.

4.5 Conclusion

The first part of this paper focused on analysing the reproduction of (1) observed ENSO index time series, and (2) observed precipitation time series over the entire Mexican domain by ERA-Interim (ENSO and precipitation) The results demonstrated a high level of agreement between SST time series from HadISST and ERA-Interim datasets, with a correlation of 0.97. ENSO index time series computed from ERA-Interim SST (ERA-ENSO) closely aligned with those derived from HadISST, showing a maximum difference of 0.45°C over the study period (1980-2012).

The mean accumulated monthly precipitation from ERA-Interim reanalysis exhibited a correlation of 0.98 with the observed data set from Livneh et al. (2015). Among the simulations, CRCM5-ERA-Interim-0.44 demonstrated the highest correlation with observed precipitation (0.92), although all four simulations achieved correlation values above 0.89.

The second part of this paper analysed the ability of reanalysis data (ERA-Interim) and RCM simulations (CRCM-ERA-Interim-0.22, CRCM-ERA-Interim-0.44, RCA4-ERA-Interim-0.5 and RegCM4-7-ERA-Interim-0.25) to replicate the grid-cell-to-grid-cell correlation between ERA-ENSO time series and CEIs across Mexico during the time period 1980 to 2012. The selected CEIs focused on wet and dry conditions (CWD and CDD indices), as well as extreme precipitation conditions (Rx1 and Rx5 indices). Annual and seasonal correlations were examined. The results highlighted regional variations in the performance of simulations, with CRCM5 simulations generally outperforming others. Seasonal correlations further emphasized those differences, with RCA4-ERA-Interim-0.5 performing better in winter.

Building on prior findings of Méndez et al. (2010) and Pavia et al. (2006), which linked ENSO phases to shifts in precipitation patterns, this study provides additional insights into seasonal correlations across Mexico. For example, during fall, the central-northern region exhibited positive correlations (~0.3) between ENSO and wet spell indices (CWD and Rx5), while dry conditions in the northwest during summer correlated negatively (-0.35). However, biases in

simulating spatial patterns and extreme events persist, particularly in regions with complex topography.

While this study provides insights into the ability of ERA-Interim-driven RCM simulations to reproduce the link between ENSO and CEIs, several limitations should be noted. First, the structural differences among the RCMs, including parameterizations of key physical processes like convection and land-atmosphere interactions, introduce variability in the representation of ENSO signals inherited from the driving data set (Giorgi, 2019; Laprise, 2008). The study's spatial and temporal resolutions may further limit the ability to resolve localized precipitation extremes, particularly in regions with complex topography (Kim et al., 2020, Westra et al., 2014). Secund, the lack of bias correction in the analysis allows for a direct evaluation of RCM skill but may leave errors unaddressed, which could affect the interpretation of absolute values relevant for impact studies (Maraun et al., 2017; Ehret et al., 2012). Third, the simulations analyzed were selected based on availability at the time of the research. These simulations do not represent the most recent versions of their respective RCMs, which could have included updated parameterizations and improved physics (Giorgi et al., 2019; Laprise, 2008). The ERA-Interim driving data is not the most recent ECMWF reanalysis product, ERA5 is, but ERA5-driven RCM simulations are yet to be produced over the Mexican domain. Fifth, the study period (1980–2012) is relatively short for capturing the full spectrum of ENSO variability, including long-term decadal oscillations and rare extreme events. Extending the temporal coverage could enhance statistical reliability and provide a deeper understanding of ENSO's influence on CEIs (Simmons et al., 2010). Sixth, observational data used for comparison were derived from gridded, interpolated datasets, which, while comprehensive, may smooth or underestimate extreme precipitation events, limiting the evaluation of RCMs in replicating such phenomena (Livneh et al., 2015; Westra et al., 2014). Lastly, the spatial resolutions of the RCMs employed in this study, ranging from 0.22° to 0.5°, are insufficient to resolve convective processes critical for extreme precipitation events, particularly those represented by the Rx1 and Rx5 indices. Higher-resolution models, including convection-permitting simulations, are recommended to better capture these localized phenomena (Deep et al., 2024; Giorgi et al., 2012; Ban et al., 2021; Prein et al., 2015). These limitations highlight

the need for further research using more advanced models, extended datasets, and improved observational benchmarks. To reduce bias and enhance the characterization of CEIs using teleconnections, future studies should consider the inclusion of other reanalysis datasets and higher-resolution models to strengthen the robustness of these results. Also, future studies should incorporate additional oscillations or phenomena related to precipitation patterns. This type of characterization of CEIs could be further analyzed using data from additional RCMs, including simulations from convection permitting RCMs. The more recent EAR5 reanalysis could also be used.

4.6 Acknowledgments

We acknowledge the World Climate Research Programme's Working Group on Regional Climate, and the Working Group on Coupled Modelling, former coordinating body of CORDEX and responsible panel for CMIP5. We also thank the climate modelling groups (listed in Table XX of this paper) for producing and making available their model output. We also acknowledge the Earth System Grid Federation infrastructure an international effort led by the U.S. Department of Energy's Program for Climate Model Diagnosis and Intercomparison, the European Network for Earth System Modelling and other partners in the Global Organisation for Earth System Science Portals (GO-ESSP). We acknowledge of data taken from Livneh gridded precipitation and other meteorological variables for continental US, Mexico and southern Canada. We acknowledge of any material or data taken from Hadley Centre Sea Ice and Sea Surface Temperature data set (HadISST). We acknowledge of ERA-Interim data taken from European Centre for Medium-Range Weather Forecast. We acknowledge the grant from Consejo Nacional de Humanidades Ciencias y Tecnologías (CONAHCYT) as well as the grant from Fonds de recherche du Québec – Nature et technologies (FRQNT).

4.7 Supplementary Material

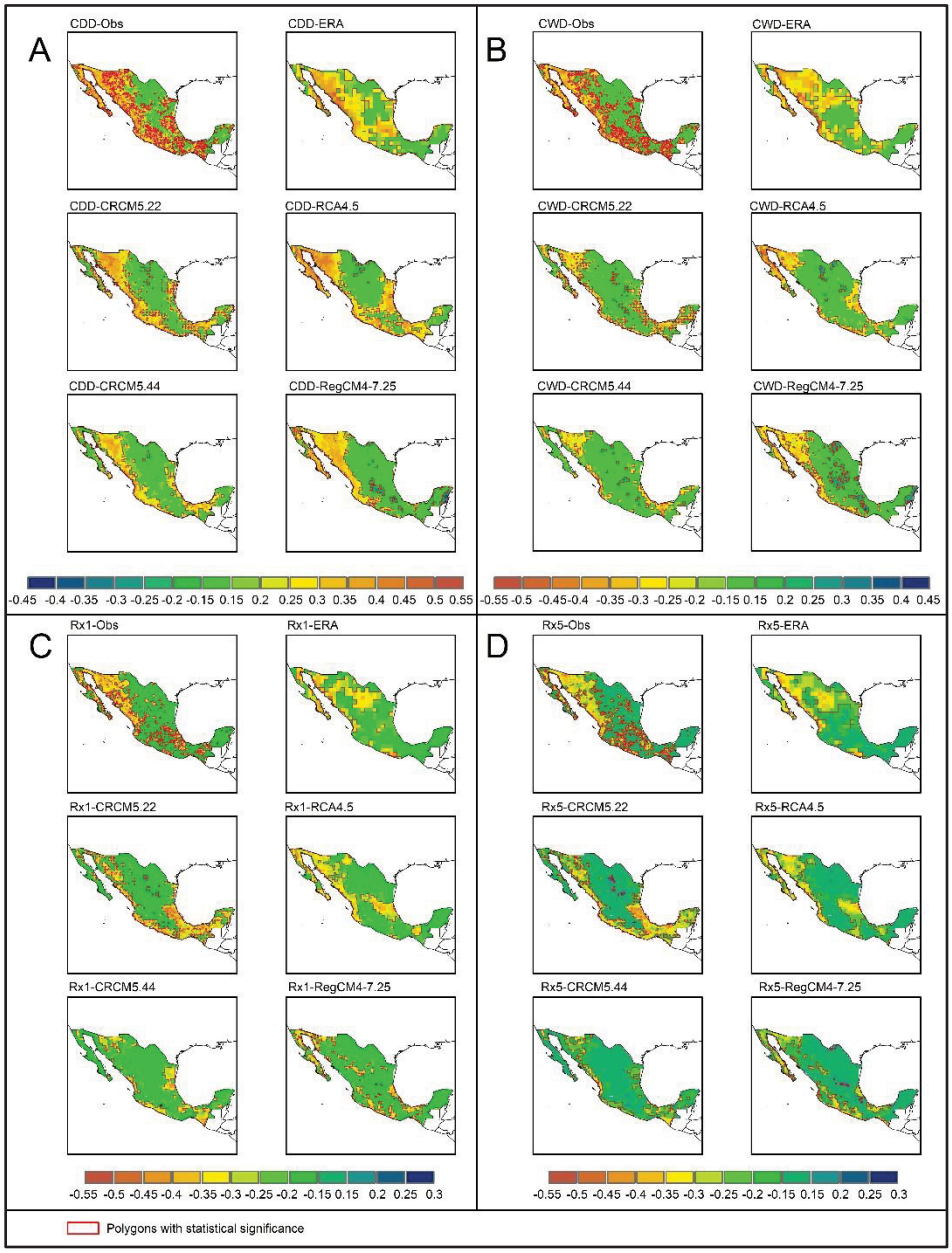

Figure 4.9 Summer correlation reproduction between de ENSO teleconnection index and climate change indices (CDD, CWD, Rx1 and Rx5). The ENSO teleconnection index were calculated by HadISST as observations and ERA-Interim. The climate change indices were calculated by Livneh data set for observations, reanalysis (ERA-Interim-0.75) and RCM's simulations (CRCM5-ERA-Interim-0.22, CRCM5-ERA-Interim-0.44, RCA4-ERA-Inteirm-0.5 and RegCM4-7-ERA-Inteirm-0.25). Section A refers to ENSO and CDD index correlation, section B refers to the ENSO and CWD index correlation, section C refers to the ENSO and Rx1 index correlation and section D refers to the ENSO and Rx5 index

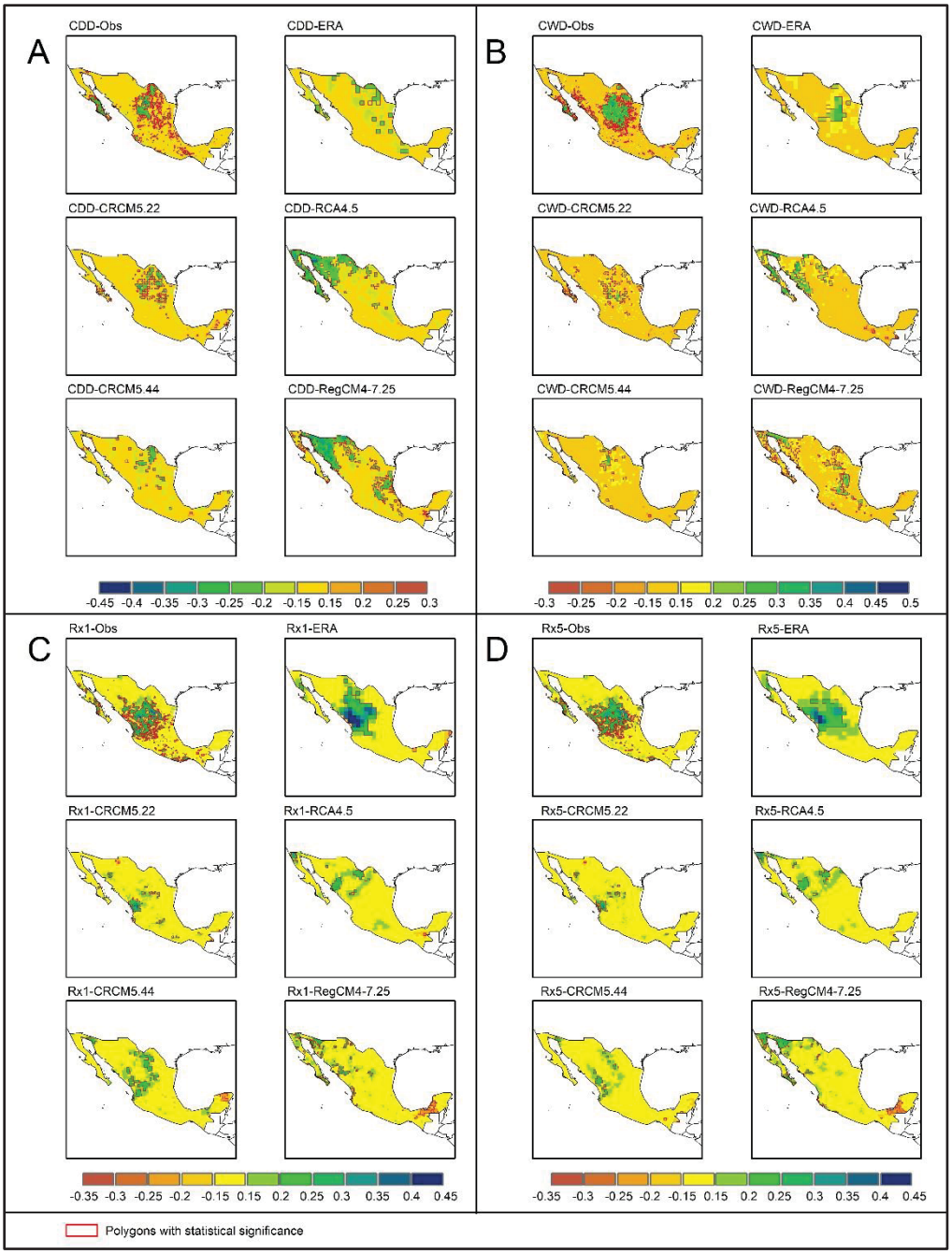

Figure 4.10 Fall correlation reproduction between de ENSO teleconnection index and climate change indices (CDD, CWD, Rx1 and Rx5). The ENSO teleconnection index was calculated by HadISST as observations and ERA-Interim. The climate change indices were calculated by Livneh data set for observations, reanalysis (ERA-Interim-0.75) and RCM's simulations (CRCM5-ERA-Interim-0.22, CRCM5-ERA-Interim-0.44, RCA4-ERA-Inteirm-0.5 and RegCM4-7-ERA-Inteirm-0.25). Section A refers to ENSO and CDD index correlation, section B refers to the ENSO and CWD index correlation, section C refers to the ENSO and Rx1 index correlation and section D refers to the ENSO and Rx5 index

CHAPTER 5

ASSESSMENT OF REGIONAL CLIMATE MODEL SIMULATIONS AT REPRODUCING THE LINK BETWEEN PDO AND CLIMATE EXTREME PRECIPITATION INDICES IN MEXICO

Abraham Hernandez-Garcia[1], Annie Poulin[1], Rabindranarth Romero-Lopez[2] and Dominique Paquin[3]

[1]Ecole de technologie supérieure, Department of Construction Engineering, Hydrology, Climate and Climate Change (HC3) Laboratory, Canada
[2]Universidad Veracruzana, Lomas del Estadio S/N, Zona Universitaria, Xalapa, 91000, Mexico
[3]Ouranos Consortium, 550 Sherbrooke street West, 19th floor, West tower, Montreal, QC, Canada H3A 1B9

Paper submitted to the *Theoretical and Applied Climatology*, October 2024

Abstract

The primary objective of this study is to evaluate whether Regional Climate Models (RCM)-simulations and their driving dataset (ERA-Interim) can reproduce the spatial pattern of the temporal correlation between the Pacific Decadal Oscillation (PDO) and four Climate Extreme Indices –CDD, CWD, Rx1, and Rx5– over Mexico from 1980 to 2012. First the ERA-Interim dataset's ability to reproduce the PDO index time series were assessed. Next, both ERA-Interim and four ERA-Interin-driven RCM simulations (CRCM5-0.22, CRCM5-0.44, RCA4-0.5, and RegCM4-7-0.25) were evaluated for their representation of the average monthly accumulated precipitation and the seasonal spatial patterns of the climate extreme indices. Finally, the study assessed how well ERA-Interim and RCM simulations reproduced the spatial pattern of the temporal correlation between the PDO and climate extreme indices. The findings indicate that ERA-Interim effectively reproduces the PDO. Both ERA-Interim and RCM simulations capture the main features of monthly accumulated precipitation, although some overestimation occurs in summer and spring. The CRCM5 and RCA simulations perform better in reproducing the seasonal spatial patterns of the climate extreme indices. Spatial correlation patterns, with

statistical significance, were found during the two driest seasons in Mexico, winter and spring, and mainly relate to moisture conditions in the north-west part of the country (spring) and in the northern central part of the country (winter). Given the location of the Sierra Madre Occidental Mountain range, the spring moisture conditions could also be associated with orography. The ERA-I dataset as well as the two CRCM5 simulations generally perform best at reproducing the observed correlations.

Keywords: Teleconnection Indices, Regional Climate Models, Pacific Decadal Oscillation, ERA-Interim.

5.1 Introduction

Each component of the climate system—the atmosphere, hydrosphere, cryosphere, continents, and biosphere—has a different heat capacity, meaning that its ability to absorb or emit thermal energy varies. These differences lead to contrasts and energy exchanges between the components. The ocean, as part of the climate system, acts as a vast reservoir of thermal energy due to its high heat capacity. This allows it to exchange energy with the atmosphere through processes such as shortwave radiative flux, longwave infrared flux, and turbulent fluxes of moisture and heat, which result in the ocean cooling or warming (Niiler, 1992). These energy exchanges play a critical role in transporting moisture toward land, altering precipitation patterns, and influencing the intensity of cyclonic systems in the tropics and other regions (Stewart, 1997). A key aspect of this dynamic is the variation in the temperature of the millimeter-scale surface layer of the ocean, known as Sea Surface Temperature (SST) (Deser et al., 2010). SST anomalies, defined as deviations from average SST values (NOAA, 2010), occur at different time scales across various oceanic regions, ranging from five-year (quinquennial) to multi-decadal oscillations.

One example of such an oscillation is the Pacific Decadal Oscillation (PDO), a decadal-scale fluctuation of SST in the northern Pacific. The PDO has been linked to widespread changes in the atmosphere, ocean, marine ecosystems, hurricanes, and precipitation extremes (Deser et

al., 2010; Hamlet & Lettenmaier, 2007; Hidalgo & Dracup, 2003; Mantua et al., 1997; Senna et al., 2023; Tootle & Piechota, 2006; Wang et al., 2014). Its effects have been observed in hydroclimatic conditions across different regions of the world, such as the Upper Colorado River Basin (Hidalgo & Dracup, 2003) and flood risks in the western United States (Hamlet & Lettenmaier, 2007). The PDO has also influenced inter-decadal summer precipitation patterns in eastern China (Chen et al., 2024) and has been linked to variations in Indian precipitation (Xavier et al., 2023). Furthermore, the interaction between oceanic indices like the Atlantic Multidecadal Oscillation (AMO), PDO, and 500 mb geopotential height has been shown to influence streamflow in various parts of the U.S. (Sagarika et al., 2015).

In Mexico, the relationship between the PDO and precipitation patterns has been explored in numerous studies (Gonzalez et al., 2010; Llanes-Cárdenas et al., 2020; Pavia et al., 2006b). Research has focused on the PDO's influence during different phases (Gonzalez et al., 2010) and on its connection to seasonal precipitation (Englehart & Douglas, 2002). The PDO has been associated with droughts in northern Mexico and wetter conditions in the southern regions (Méndez & Magaña, 2010). Additionally, links have been found between oceanic oscillations (such as the PDO, AMO, and North Atlantic Oscillation [NAO]) and the non-stationarity of certain seasonal precipitation series in Mexico (Alvarez-Olguin & Escalante-Sandoval, 2017). The PDO also affects tropical cyclone activity and Mexican precipitation anomalies (Llanes-Cárdenas et al., 2020). Importantly, Mexico's seasonal precipitation patterns, particularly in summer and winter, are shaped by the combined effects of the El Niño-Southern Oscillation (ENSO) and the PDO (Pavia et al., 2006a).

The diversity of impacts in Mexico caused by climate extreme events and their demographic implications, as well as implications for water and food availability, governance (SEGOB, 2015), risk and vulnerability (Rivera-Arriaga et al., 2023), has prompted the development not only of studies to enhance resilience (Rivera-Arriaga et al., 2023) but also of national strategies to address these events. The National Drought Monitor (CONAGUA, 2024), as well as the National Water Information System (SINA) (SEMARNAT, 2018) are examples. This has led

to various analyses of climate processes to deepen our understanding of the behavior of extreme events and the phenomena associated with them.

Precipitation patterns in different regions of the world, with various hydroclimatic characteristics (e.g., subtropical and semi-arid) and physiographic features (e.g., complex orography and vast plains), have been studied using Regional Climate Models (RCMs) (Al-Hilali et al., 2024; Torrez-Rodriguez et al., 2023; Zhao et al., 2024). Additionally, RCMs have been used to study climate extremes through the indices from the Expert Team on Climate Change and Indices (ETCCDI), also called climate extreme indices (Kim et al., 2020; Lagos-Zúñiga et al., 2022; Rai et al., 2024; Xiong et al., 2019). In Mexico these indices have been used to study the north (Arriaga-Ramrez & Cavazos, 2010) and the center of the country (Ortiz-Gómez et al., 2020; Ruiz-Alvarez et al., 2020).

This paper brings together the study of PDO in conjunction with wet and dry conditions in Mexico through the use of ERA-Interim reanalysis and historical regional climate simulations. The main objective is to investigate the reproduction of the observed correlation between PDO and climate extreme indices (CWD, CDD, Rx1 and Rx5) over entire Mexico, by ERA-Interim and four ERA-Interim-driven RCM simulations (CRCM5-ERA-Interim-0.22, CRCM5-ERA-Interim-0.44, RCA4-ERA-Interim-0.5, and RegCM4-7-ERA-Interim-0.25) over the 1980-2012 time period. This main objective will be achieving through the following secondary objectives:

1. Evaluation of the ability of ERA-Interim reanalysis SSTs to replicate the PDO index time series derived from the HadISST observed dataset for the period 1980 to 2012.

2. Comparison of monthly accumulated precipitation data from ERA-Interim and the four RCM simulations against the observed values from the Livneh et al. (2015) dataset for the same 1980–2012 period. Additionally, a comparison is conducted for four climate extreme indices: maximum monthly wet spell duration, maximum monthly dry spell

duration, monthly maximum 1-day precipitation depth, and monthly maximum consecutive 5-day precipitation depth (CDD, CWD, Rx1 and RX5).

3. Comparison of the correlation between PDO and climate extreme indices, as calculated from ERA-Interim and the RCM simulations, with the observed correlation, which is derived from the HadISST and Livneh datasets.

5.1.1 Study Site

The region considered for computing the PDO index time series is depicted in map A of Figure 5.1, delimited poleward from the 20° latitude in the northern basin of the Pacific Ocean (Deser, Clara &, Trenberth, 2022).

Precipitation- and climate extreme indices-related analyses are conducted over the Mexican territory, depicted in map B of Figure 1. Map B also shows the mean annual accumulated precipitation in Mexico, computed form the Livneh et al. (2015) dataset (see the Data section hereafter) and the mountain ranges found on the country's territory. The most elevated point in the country reaches 5636 m and is located in the Trans-volcanic Mexican belt. The country has two important peninsulas, the Baja California peninsula to the northwest and the Yucatan peninsula to the southeast (reference to those peninsulas will be made in the results analysis).

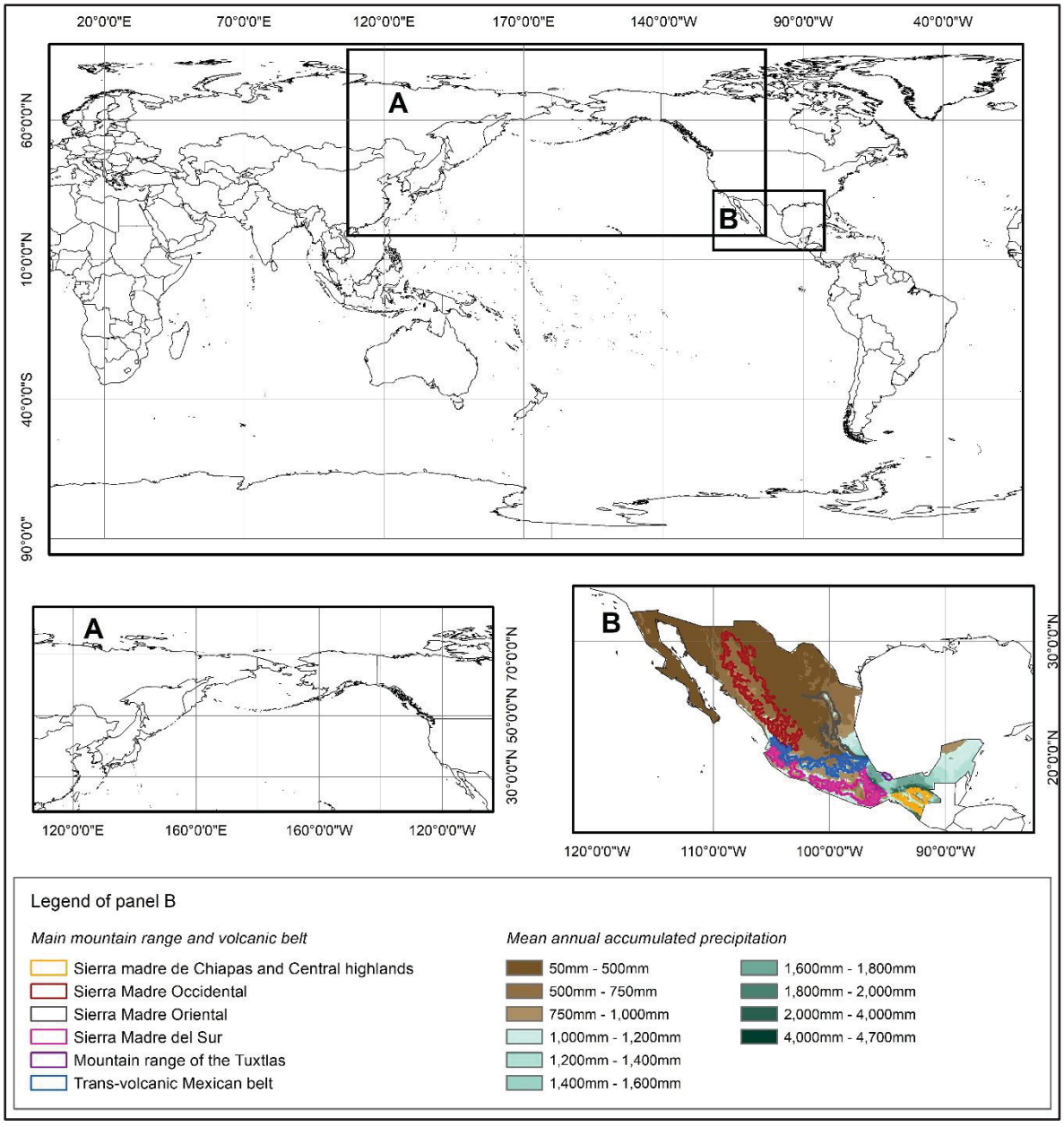

Figure 5.1 Map depicting the complete region taken in account in this study, northern basin of the Pacific Ocean and Mexico (top map).Map A depicting the PDO region and map B depicting Mexico with the mean accumulated precipitation and the principal mountains

5.2 Data

5.2.1 Sea Surface Temperature Data

The SST observation data are sourced from the Met Office Hadley Center's sea ice and sea surface temperature dataset (HadISST), which has a resolution of 1° latitude-longitude and a daily temporal resolution (Rayner et al., 2003). Additionally, SST data from the European Centre for Medium-Range Weather Forecasts (ECMWF)'s global reanalysis ERA-Interim (hereafter called ERA-I) were utilized. These data are available at a spatial resolution of 0.75° latitude-longitude and a daily temporal resolution (accessible at https://apps.ecmwf.int/datasets/data/interim-full-moda/levtype=sfc/) (Berrisford et al., 2009).

5.2.2 Precipitation Data

For the precipitation analysis and calculation of climate extreme indices, data from observations, reanalysis, and RCM simulations, from Coordinated Regional Climate Downscaling Experiment (CORDEX), were employed (Table 1). Observation data were sourced from Livneh gridded data, which have a spatial resolution of 1/16° ≈ 0.075° (~6km) latitude-longitude and a daily temporal resolution (Livneh et al., 2015). Reanalysis data were obtained from ERA-Interim and possess a spatial resolution of 0.75° latitude-longitude, with a temporal resolution of 2 daily data points (0000 UTC and 12 UTC). They can be downloaded from https://apps.ecmwf.int/datasets/data/interim-full-moda/levtype=sfc/ (Berrisford et al., 2009). The RCM simulations are presented in Table 1; all four were driven by the ERA-Interim global dataset. The availability of HadISST data limited the studied time period to 1980-2012.

Table 5.1 Characteristics of the observations, forcing data and RCMs used in this study

ID	Complete name	Spatial Resolution	Temporal Resolution	Source	Time period	Spatial Domain
Obs	Observations	0.075° latitude-longitude	Daily	Livneh et al., (2015)	1980-2012	North America, south of 50° latitude
ERA-I	ERA-Interim	0.75° latitude-longitude	Daily	Berrisford et al., 2009	1980-2012	Global
CRCM5-0.22	CRCM5-ERA-Interim-0.22	0.22° latitude-longitude	Daily	CORDEX	1980-2012	CORDEX North America Domain, extended to include Mexico
CRCM5-0.44	CRCM5-ERA-Interim-0.44	0.44° latitude-longitude	Daily	CORDEX	1980–2012	CORDEX North America Domain, extended to include Mexico
RCA4-0.5	RCA4-ERA-Interim-0.5	0.44° latitude-longitude	Daily	CORDEX	1980–2012	CORDEX Central America Domain
RegCM4-7-0.25	RegCM4-7-ERA-Interim-0.25	0.22° latitude-longitude	Daily	CORDEX	1980 - 2012	CORDEX Central America Domain

5.3 Methods

This section comprises three main parts. The first part pertains to the reproduction of observed PDO by the ERA-Interim reanalysis. The second part is associated with the analysis of the time series of monthly accumulated precipitation, as well as the seasonal spatial reproduction of observed climate extreme indices by ERA-Interim and the four RCM simulations (CRCM5-0.22, CRCM5-0.44, RCA4-0.5, and RegCM4-7-0.25). The third and final part addresses the computation of the correlation between the PDO and climate extreme indices in Mexico.

5.3.1 Reproduction of the temporal patter of PDO

First, the SST data from ERA-Interim were spatially aggregated to match the resolution of the observational data (Bierkens, 2000). The PDO, calculated using both observed and reanalysis data, is defined as the first empirical orthogonal function of the SST anomaly field based on the covariance matrix (Mantua et al., 1997). This matrix was built using monthly anomalies from the region depicted in map A of Figure 1. PDO was computed for the time period from 1980 to 2012. From this point forward, the PDO computed with ERA-Interim will be referred to as ERA-PDO.

5.3.2 Reproduction of precipitation patterns and seasonal climate extreme indices

This subsection first outlines the method used to analyze the similarity between the precipitation time series from observations and the data derived from ERA-Interim and RCM simulations. The second part focuses on how well these datasets reproduce the selected extreme climate indices. It is important to note that spatial disaggregation was applied to adjust the resolution of the ERA-Interim and simulation datasets to match the resolution of the observed data (Bierkens, 2000).

5.3.2.1 Temporal analysis of monthly precipitation accumulation

The Pearson linear correlation was computed between observed monthly precipitation times series and the same time series each from each one of the ERA-Interim and RCM simulation datasets, using equation (5.1):

$$\rho xy = \frac{\sum((X - \mu x)(Y - \mu y))}{\sigma_X \sigma_Y} \quad (5.1)$$

Where ρxy represents the correlation coefficient; σ_X and σ_Y denote the standard deviations of X and Y time series, respectively; μx and μy are the mean values of the X and Y time series, respectively. ρxy takes values between [-1, 1] (Storch & Zwiers, 1999). A correlation matrix with histograms and scatter plots was generated, along with box plots for the entire time period and seasonally, to visually assess the fit of each dataset with the observations. The seasons were defined as winter (December, January and February), spring (March, April, May), summer (June, July and August) and fall (September, October and November). Finally, box plot graphs were generated to compare the empirical distributions of monthly precipitation time series from all the studies datasets, again for the entire time period and then on a seasonal basis.

5.3.2.2 Reproduction of seasonal Climate Extreme Indices

In this article, four indices from the Expert Team on Climate Change Detection and Indices (ETCCDI) were utilized (http://etccdi.pacificclimate.org/list_27_indices.shtml) (Karl et al., 1999; Peterson et al., 2001). Two of these indices are related to maximum duration of dry (CDD) and wet (CWD) spell, while the other two indices are related to the maximum intensity of rainfall in one day (Rx1) and in five consecutive days (Rx5). All four indices were computed, FOR Mexican domain, on a monthly basis for the enitre time period. Winter includes the months of December, January and February; Spring includes the months of March, April and May; Summer includes the months of June, July and August; and finally, Fall

includes the months of September, October and November. The equations of each index are presented below.

The CDD Index, "Maximum length of dry spell," is defined as the maximum number of consecutive days with $RR < 1\ mm$: *Let*RR_{ij} *be the daily precipitation amount on day* i *in period* j*"* (Karl et al., 1999; Peterson et al., 2001):

$$RR_{ij} < 1mm \tag{5.2}$$

This index is significant for understanding and quantifying the length of dry periods, i.e. with very low or no precipitation.

The CWD Index, "Maximum length of wet spell," is defined as: *"maximum length of wet spell, maximum number of consecutive days with* $RR \geq 1\ mm$*: Let,* RR_{ij} *be the daily precipitation amount on day* i *in period* j*"* (Karl et al., 1999; Peterson et al., 2001):

$$RR_{ij} \geq 1mm \tag{5.3}$$

This index is useful for characterizing and quantifying prolonged periods of wet conditions or important precipitation events.

The Rx1day Index, "Monthly maximum 1-day precipitation," is defined as maximum value of daily precipitation in a month. *"Let RRij be the daily precipitation amount on day* i *in period* j*"* (Karl et al., 1999; Peterson et al., 2001), then the Rx1day index is calculated as:

$$Rx1day_j = \max\left(RR_{ij}\right) \tag{5.4}$$

This index is relevant for assessing extreme precipitation events within a specific time period, as it represents the highest amount of precipitation recorded in a single day during a given month.

The Rx5day Index, "Monthly maximum consecutive 5-day precipitation," is defined as the maximum value of accumulated precipitation over a period of 5 consecutive days in a month. *"Let RR_{kj} be the precipitation amount for the 5-day interval ending k, in period j Then maximum 5-day values for period j are" (Karl et al., 1999; Peterson et al., 2001)*:

$$Rx5day_j = \max\left(RR_{kj}\right) \tag{5.5}$$

This index is relevant for assessing intense and prolonged precipitation events within a specific time period, as it represents the highest accumulated precipitation over 5 consecutive days in a given month.

5.3.3 Correlation between PDO and Climate Extreme indices (CDD, CWD, Rx1 and Rx5)

The Pearson correlation index (equation 1) was computed in each grid cell of the studied domain (map B in Figure 1): (1) between observed PDO time series and the indices times series computed from precipitation observations; (2) between ERA-PDO time series and the indices computed from ERA-I and from the four RCM precipitation time series. The correlation was fist analysed for the entire 19080-2012 time period and then on a seasonal basis. This allowed for a comparison of the spatial correlation patterns form the different datasets.

The Student's t-test is utilized to assess the statistical significance of the Pearson correlation coefficient (r) between the PDO index and CEIs time series at each grid point. This test determines whether the correlation differs significantly from zero, indicating a meaningful linear relationship between PDO and CEIs. The t-statistic is computed using equation 5.6,

$$t = \frac{r\sqrt{n-2}}{\sqrt{1-r^2}} \tag{5.6}$$

where n denotes the number of data and $n-2$ represents the degrees of freedom. A p-value is derived from the t -distribution based on the calculated t-statistic. The null hypothesis (H_0) assumes no correlation, while the alternative hypothesis (H_1) asserts a significant correlation. If the p-value is smaller than the predefined significance level (α=0.05), H_0 is rejected, confirming that the correlation is statistically significant.

5.4 Results

This section is mainly composed of three parts. The first part concerns the reproduction of the observed PDO by ERA-PDO. The second part deals with the reproduction of the observed time series of precipitation and climate extreme indices using data from ERA-Interim and RCM simulations. The third and final part focuses on the spatial pattern of temporal correlation between PDO and climate extreme indices.

5.4.1 PDO Temporal Pattern

The ERA-PDO index time series (pink dashed line in Figure 2) effectively captures the phases of the PDO index (red and blue areas in Figure 5.2), as calculated from HadISST data. However, some discrepancies emerge in replicating the magnitude of the index. The most notable overestimation occurs between 1998 and 2003, as illustrated by the solid brown line in Figure 2, reaching a positive bias value of 0.67°C.

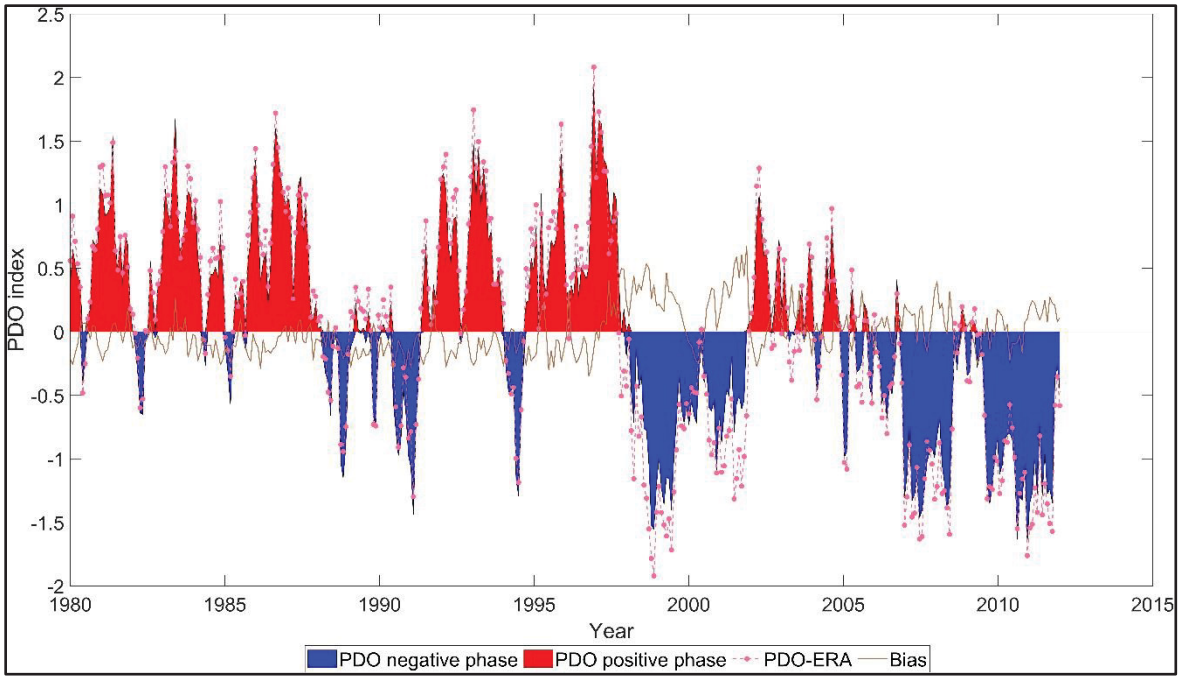

Figure 5.2 Time pattern of PDO (red and blue areas) from 1980 to 2012. ERA-PDO (dashed and dotted pink line). Bias between PDO and ERA-PDO (solid brown line)

5.4.2 Precipitation Patterns and Climate Extreme Indices

This section outlines the reproduction of the time series of monthly accumulated precipitation. Furthermore, since the seasonal patterns of climate extreme indices are distinguishable, this section elaborates on the replication of the seasonal spatial patterns of climate extreme indices (CDD, CWD, Rx1, and Rx5) as described by observations, and by ERA-Interim and RCM simulations.

5.4.2.1 Mexican Monthly Accumulation Precipitation

Figure 5.3 and table 2 show that the closest fit with the observations is achieved using ERA-I, yielding a correlation value of 0.98 and with the lowest value of RMSE (10.58 mm). The second-best correlated dataset with the observations is the CRCM5-0.44 simulation, at 0.92 and second lowest RMSE value of 22.77 mm, then follow the CRCM5-0.22 and RCA4-0.5 simulations, both showing a correlation value of 0.91, however RCA-0.5 shows the highest

RMSE value (46.70 mm) of all datasets. Finally the RegCM4-7-0.25 simulation shows a 0.89 correlation and RMSE of 36.62 mm. The correlation between ERA-I and the four RCM precipitation time series follow the same order, with slightly lower values (not shown). The ERA-I and RCM datasets all show asymmetrical (positively-skewed) histograms as in the case of observations, but with some differences in shape, and dispersion.

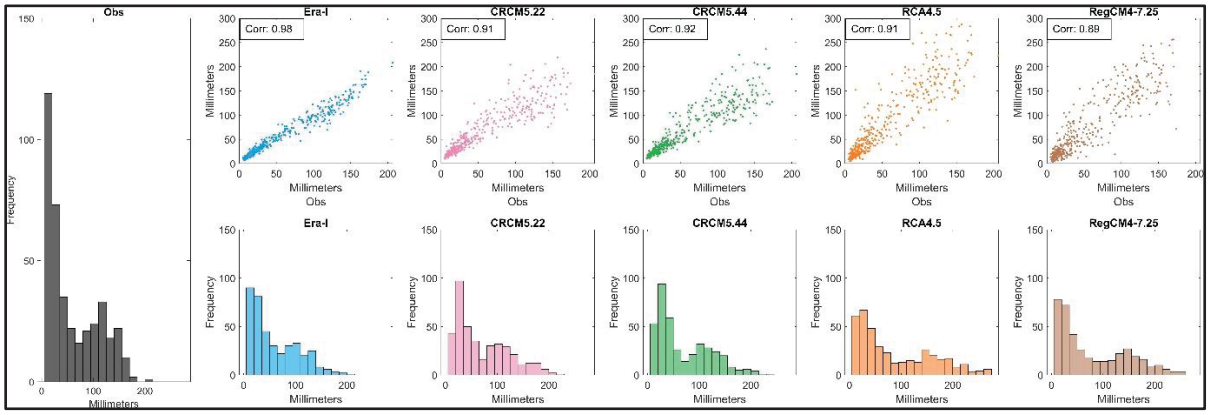

Figure 5.3 Monthly accumulated precipitation correlation graph, for the 1980-2012 time period. The first column shows the histogram of observations (grey bars). The rest of the columns show the scatter plot (upper row) and histograms (bottom row) of ERA-I (blue dots and blue bars), CRCM5-0.22 (pink dots and pink bars), CRCM5-0.44 (green dots and green bars), RCA4-0.5 (orange dots and orange bars) and RegCM-7-0.25 (brown dots and brown bars).

The right panel in Figure 4 suggests a widespread overestimation of dispersion in the simulations compared to the observations (as could be expected form the histograms in Figure 3). All four simulations also have higher medians than the observations, and the RCA4 and RegCM4-7 simulations have wider interquartile ranges.

Table 5.2 Correlation, statistical significance and Root Mean Square Error (RMSE) between observations and ERA-Interim and simulations.

Data set ID	Correlation	Statistical significance	RMSE
ERA-I	0.98	p-value < 0.05	10.58 mm
CRCM5-0.22	0.91	p-value < 0.05	23.50 mm
CRCM5-0.44	0.92	p-value < 0.05	22.77 mm
RCA-0.5	0.91	p-value < 0.05	46.70 mm
RegCM4-7-0.25	0.89	p-value < 0.05	36.62 mm

The left panel in figure 4 shows the seasonal empirical distributions of monthly accumulated precipitation. The most important differences, among all the datasets, are from the RCA4 and RegCM4-7 simulations, which: generally, overestimate the median values and the interquartile ranges with respect to the observations and even with respect to the other simulations and ERA-I in winter, spring and summer; strongly overestimate the monthly precipitation values in winter, with respect to all other datasets. ERA-I remains closer to the observations in all seasons, followed by CRCM5-0.44 and CRCM5-0.22 simulations.

Winter is the driest season across all of Mexico. Spring is generally dry and sees the start of an increase in precipitation during the months of April and May. Summer and fall are the wet seasons and also correspond to the hurricane seasons.

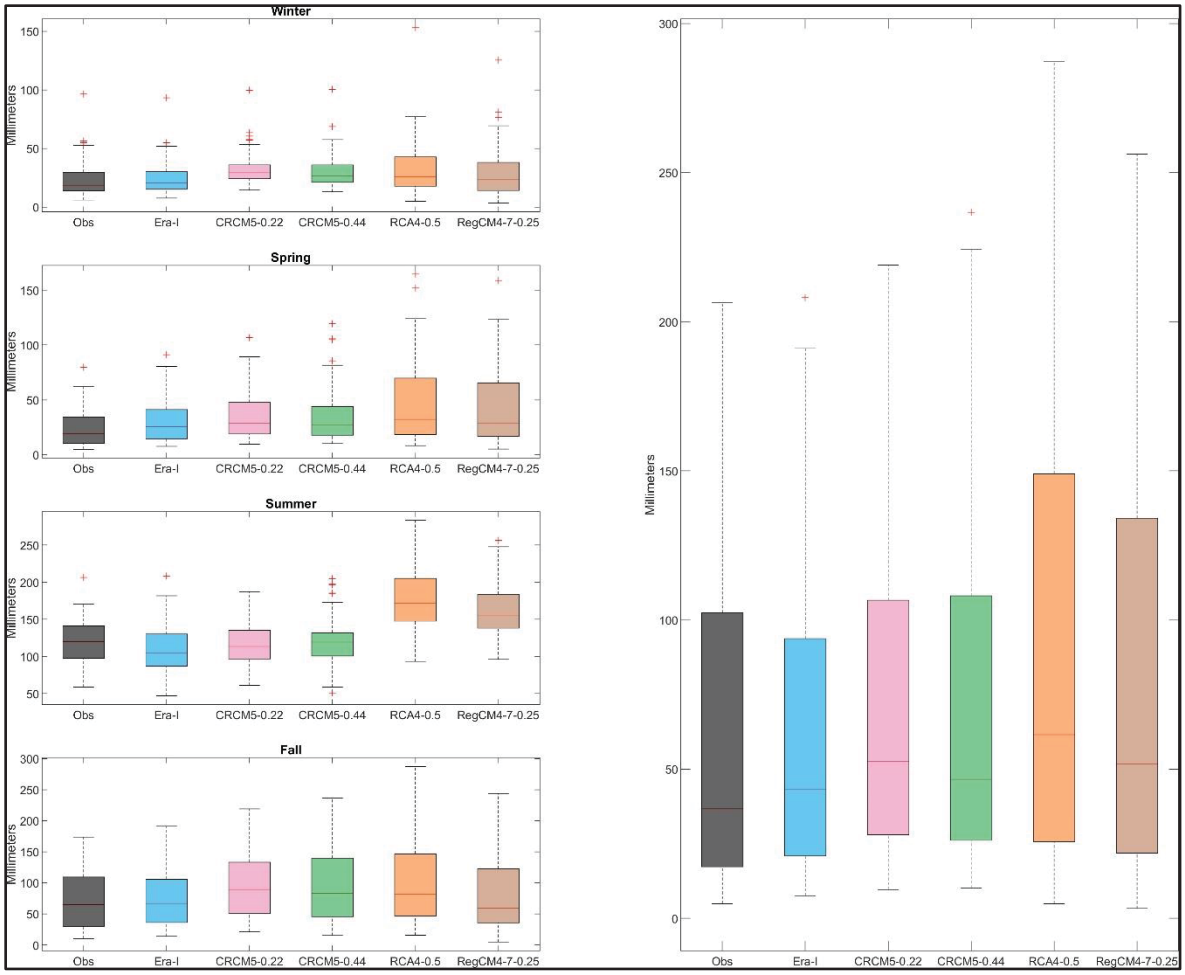

Figure 5.4 Monthly and seasonal accumulated precipitation of Observations (black box), ERA-Interim (blue box), CRCM5-0.22 (pink box), CRCM5-0.44 (green box), RCA4-0.5 (orange box) and RegCM-7-0.25 (brown box)

5.4.2.2 Seasonal reproduction of Climate Extreme Indices

The analysis of climate extreme indices (CDD, CWD, Rx1, and Rx5), in each season, is divided in two parts. It first addresses the CDD and CWD indices which refer to wet and dry conditions duration, and then the Rx1 and Rx5 indices which refer to extreme precipitation events.

The nomenclature hat is adopted, in the rest of the paper, to present climate extreme indices-related results, is as follows:

CDD-y-z, CWD-y-z, Rx1-y-z and Rx5-y-z,

where y can take the values Obs (observations), ERA (ERA-Interim reanalysis), CRCM5.22 (CRCM5-ERA-Interim-0.22 simulation), CRCM5.44 (CRCM5-ERA-Interim-0.44 simulation), RCA4.5 (RCA4-ERA-Interim-0.5 simulation), or RegCM4-7.25 (RegCM4-7-ERA-Interim-0.25 simulation); and z can take the values w (winter), s (spring), su (summer) and f (fall).

Winter reproduction of CDD and CWD Indices. The lowest CDD-Obs-w values (top left panel in Figure 5.5A) are reached in the southeast region located around the Gulf of Mexico (including the effect of the mountain ranges; Figure 5.1) and in the Yucatan peninsula, with an average of down to 3 consecutive days without precipitation in winter over the study period. The southwestern and southernmost regions of Mexico show the highest maximum dry spell length, as well as the central-northern part of the country, with values reaching up to 27 and 30 days. For CWD-Obs-w (top left panel in Figure 5.5B), complementing the above description, most of the country observes a maximum of 0 to 2 days consecutive with precipitation on average during winter; however, the southeast shows the highest average values, with up to 6 consecutive days with precipitation. It is worth noting that in the northwest, some localized areas show lower values of CWD index (between 2 and 4 days).

CDD-RCA4-0.5-w (middle right panel in Figure 5.5A) and CDD-RegCM4-7-0.25-w (lower right panel of Figure 5.5A) manage to capture the observed spatial variability and magnitude in southeast Mexico. However, they underestimate the magnitude of the index in most of the country. DCC-ERA-I-w (top left panel in Figure 5A), CDD-CRCM5-0.22-w (middle left panel in Figure 5.5A), and CDD-CRCM5-0.44-w (lower left panel in Figure 5.5A) all overestimate the observed values in the region located around the Gulf of Mexico. ERA-I and all four RCM simulations are able to detect the effect of the Sierra Madre Occidental Mountain range (Figure 1) in the north, with the two CRCM5 simulations being closer to observations. CWD-ERA-I-w (top left panel in Figure 5.5B) overestimates the observed spatial variability and magnitude of the index, while CWD-CRCM5-0.22-w (middle left panel in Figure 5.5B) and CWD-

CRCM5-0.44-w (lower left panel in Figure 5.5B) detect the spatial variability in the east and center of Mexico with some overestimations, although they underestimate the spatial variability in the northwest. The indices CWD-RCA4-0.5-w (middle right panel in Figure 5.5B) and CWD-RegCM4-7-0.25-w (lower right panel in Figure 5.5B) diverge from with what is described by CWD-Obs-w.

Winter Rx1 and Rx5 indices. Rx1-Obs-w (top left panel in Figure 5.5C) and Rx5-Obs-w (top left panel in Figure 5.5D) show that precipitation magnitude remains low throughout the country, with slight increases in the east and northwest of the country. Some very localized grid areas can reach values up to 60-90 mm for Rx1-Obs-w and 100-125 mm for Rx5-Obs-w in the south, close to the border of the Gulf of Mexico and in the Baja California peninsula.

Rx1-ERA-I-x and Rx5-ERA-I-w (top right panels in Figures 5.5C and 5.5D, respectively) manage to capture the spatial patterns from the observed indices, however without the localized higher values, most likely because of ERA-I's coarser resolution. Rx1-CRCM5-0.22-w (middle left panel in Figure 5.5C), Rx1-CRCM5-0.44-w (lower left panel in Figure 5.5C), Rx5-CRCM5-0.22-w (middle panel in of Figure 5.5D), and Rx5-CRCM5-0.44-w (lower left panel in Figure 5.5D), despite showing an overestimation in magnitude and spatial variability, manage to detect the increasing gradient of these indices in the southeast and northwest of the country, even emulating the lower values in the center of the entire country. Rx1-RCA4-0.5-w (middle right panel in Figure 5.5C), Rx1-RegCM4-7-0.25-w (lower right map of Figure 5.5C), Rx5-RCA4-0.5-w (middle right panel in Figure 5.5D), and Rx5-RegCM4-7-0.25-w (lower right panel in Figure 5.5D) are unable to reproduce the spatial pattern and magnitude described by the observations.

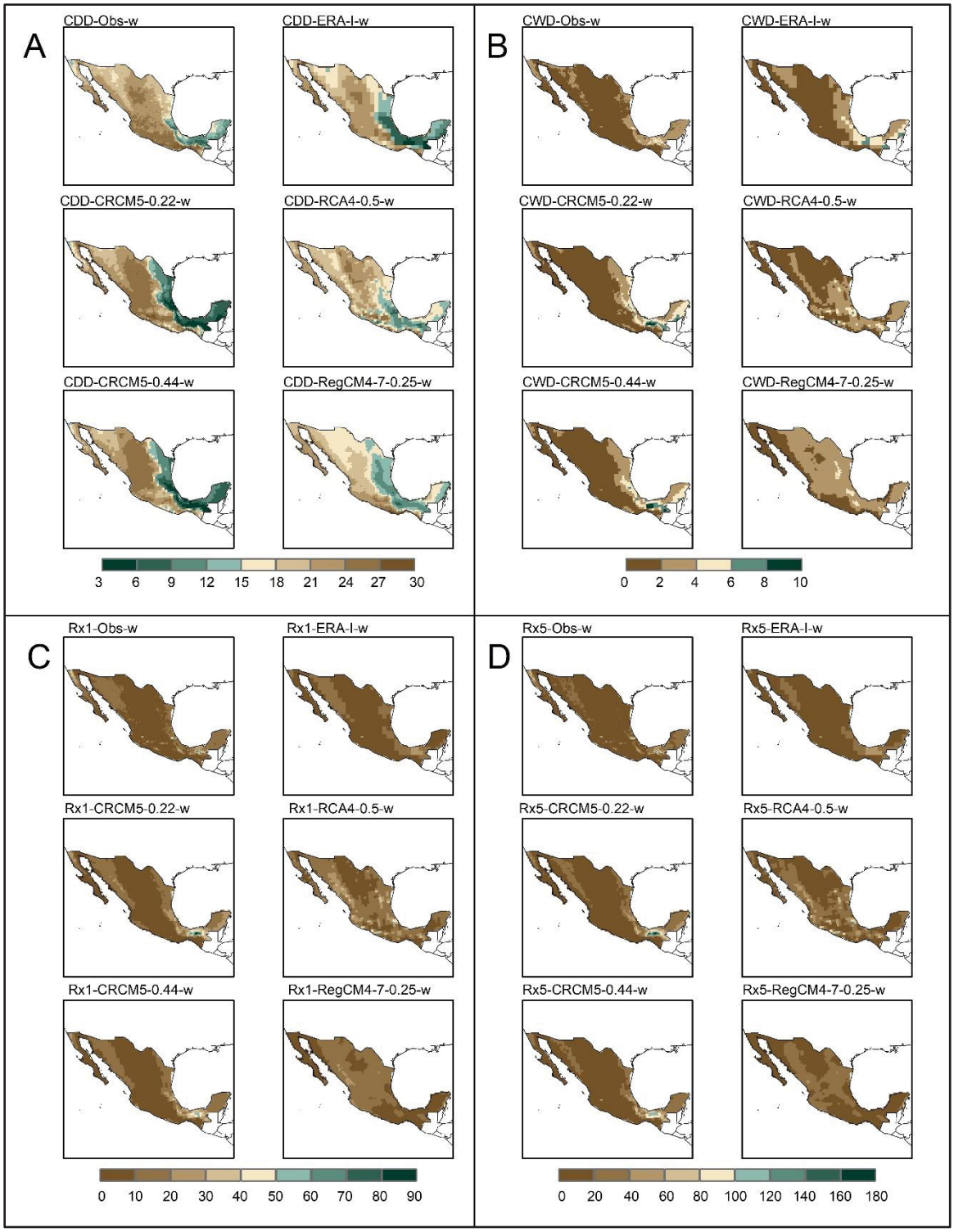

Figure 5.5 Winter computation for CDD (Panel A), CWD (Panel B), Rx1(Panel C) and Rx5 (Panel D) indices. The computation was done for ERA-I as well as simulations

Spring CDD and CWD indices. CDD-Obs-s (top left panel in Figure 5.6A) in spring shows a clear east-west partition of the country. The eastern region presents the lowest values of the index, with the minimum values located in the Sierra Madre Oriental, the eastern Sierra Madre del Sur, and the Central Highlands. The highest values of the index extend towards the west, reaching maximum values on the west coast and in the southern part of the Baja California peninsula. Similarly, for CWD-Obs-s (top left panel in Figure 5.6B), there is a differentiated behavior between the east and west of Mexico. However, the entire country falls within the range of 2 to 8 days maximum wet spell duration.

All other datasets manage to reproduce the observed differentiation between the east and west of Mexico. CDD-ERA-I-s (top right panel in Figure 5.6A) and CWD-ERA-I-s (top right panel in Figure 5.6B), as well as CDD-CRCM5-0.22-s (middle left panel in Figure 5.6A), CDD-CRCM5-0.44-s (lower left panel in Figure 5.6A), CWD-CRCM5-0.22-s (middle left map of Figure 5.6B), and CWD-CRCM5-0.44-s (lower left map of Figure 5.6B) show spatial patterns that resemble the observed pattern, however they underestimate the magnitude of the CDD index and overestimate the magnitude of the CWD index on the east side of the country. ERA-I also shows underestimation of CDD index magnitude on the west side of the country. In the case of CDD-RCA4-0.5-s (middle right panel in Figure 5.6A), CDD-RegCM4-7-0.25-s (lower right panel in Figure 5.6A), CWD-RCA4-0.5-s (middle right panel in Figure 5.6B), and CWD-RegCM4-7-0.25-s (lower left panel in Figure 5.6B), the east-west partition is moved towards the west side of the country resulting in underestimation of the CDD index values and overestimation of the CWD index values.

Spring Rx1 and Rx5 indices. The east-west partition seen previously is still present for those two indices, but less marked in the case o observed spring Rx5. Rx1-Obs-s (top left panel in Figure 5.6C) shows the highest values of Rx1 index in the east and south of Mexico, with values ranging from 20 mm to 40 mm. Both the north and the west of the country have average values between 0 and 10 mm. Rx5-Obs-s (top left panel in Figure 5.6D) shows values between 0 and 25 mm of precipitation for most of Mexico; however, there is a strip in the east of the country with the highest values of maximum average precipitation in 5 consecutive days,

ranging from 25 mm in the northeast to 70 mm in the Sierra Madre del Sur and the Central Highlands.

Rx5-ERA-I-s (top right panel in Figure 5.6D), Rx1-CRCM5-0.22-s (middle left panel in Figure 5.6C), Rx1-CRCM5-0.44-s (lower left panel in Figure 5.6C), Rx5-CRCM5-0.22-s (middle left panel in Figure 5.6D), and Rx5-CRCM5-0.44-s (lower left panel in Figure 5.6D) manage to reproduce the spatial pattern described by the observations, showing a slight overestimation in magnitude. Rx1-ERA-I-s (top right panel in Figure 5.6C) shows an underestimation in east part of the country. In contrast, Rx1-RCA4-0.5-s (middle right panel in Figure 5.6C), Rx1-RegCM4-7-0.5-s (lower right panel in Figure 5.6C), Rx5-RCA4-0.5-s (middle right panel in Figure 5.6D), and Rx5-RegCM4-7-0.5-s (lower right panel in Figure 5.6D) overestimate both magnitude and spatial variability compared to the observations. The spatial pattern of overestimation in all datasets suggests it is related to the Mexican topography.

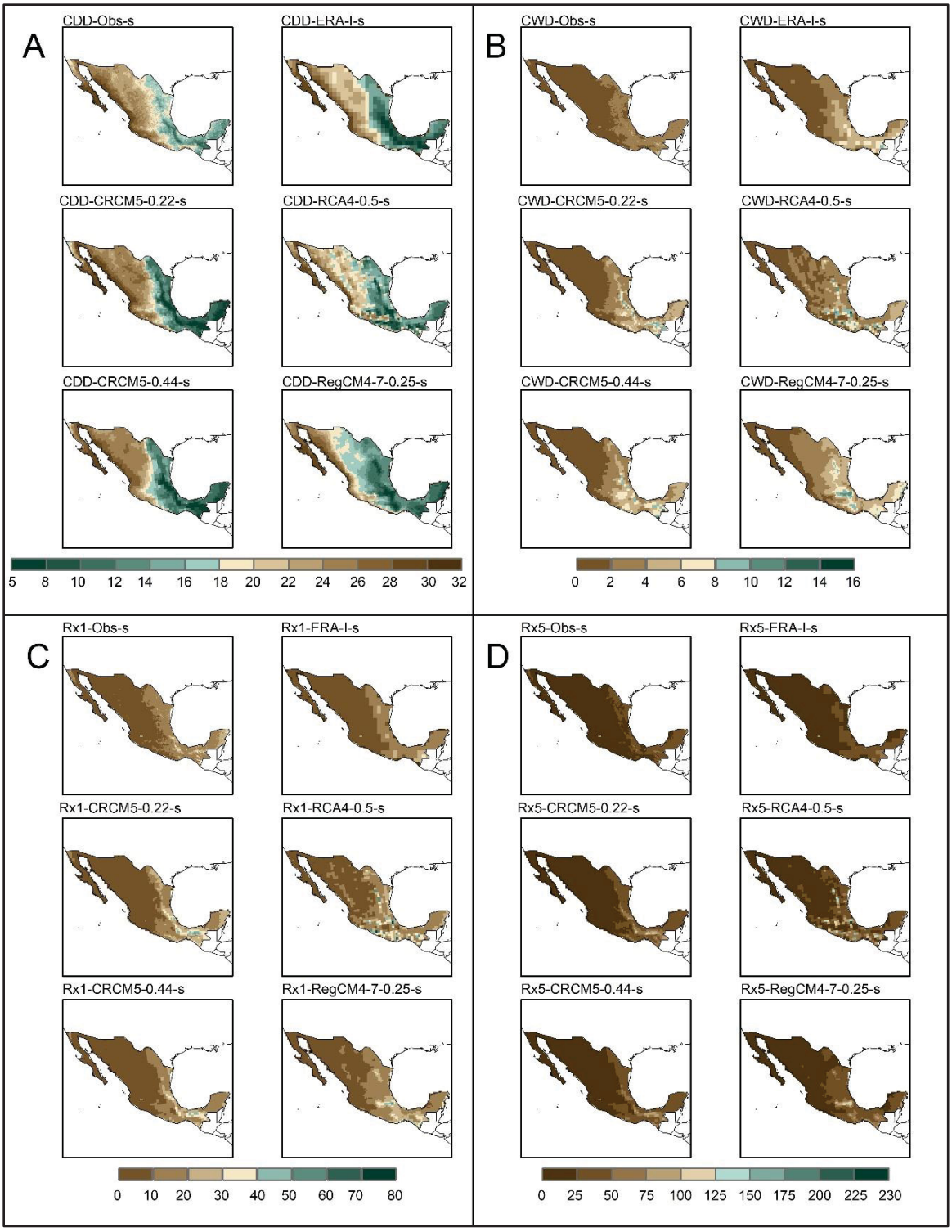

Figure 5.6 Same as Figure 5.5 but for spring

Summer CDD and CWD indices. As would be expected, lower dry spell duration values (CDD index) and higher wet spell duration values (CWD index) are reached throughout Mexico during the wetter summer season than during the drier winter and spring seasons. CDD-Obs-su (top left panel in Figure 5.7A) reaches its maximum values in the Baja California peninsula, with averages ranging from 18 to 31 days, and a small core in the eastern part of northern Mexico with values between 16 and 18 days. The rest of the country ranges from 1 to 16 days in the mountainous areas (Sierra Madre Oriental, Sierra Madre Occidental, Sierra Madre del Sur, Trans-Mexican Volcanic Belt, Tuxtla Mountains, Sierra Madre de Chiapas, and Central Highlands) and between 4 and 16 days for the rest of the country. Similarly, CWD-Obs-su (top left map in Figure 5.7B) shows the highest values of the number of the index in the mountainous areas in Mexico. The CDD index values decrease towards the coasts, presenting values between 2.5 and 7 days, and towards the north-west and north-central parts of the country, with values between 0 and 1.25 days in summer. As seen in Figure 5.1, the northern central part of Mexico and the Baja California peninsula are the driest parts of the country, on average.

All ERA-I and RCM simulation datasets manage to emulate the spatial pattern described by the observations for the CDD and CWD indices (Figures 5.7A and 5.7B, respectively). However, CDD-CRCM5-0.22-su (middle left panel in Figure 5.7A) and CDD-CRCM5-0.44-su (lower left panel in Figure 5.7A) overestimate the spatial variability in the eastern part of northern Mexico. CDD-ERA-I-su (upper right panel in Figure 5.7A), CDD-RCA4-0.5-su (middle right panel in Figure 5.7A), and CDD-RegCM4-7-0.25-su (lower right panel in Figure 5.7A) underestimate the number of days in the northeast of the country. On the other hand, CWD-CRCM5-0.22-su (middle left panel in Figure 5.7B), CWD-CRCM5-0.44-su (lower left panel in Figure 5.7B), and CWD-RCA4-0.5-su (middle right panel in Figure 5.7B) reproduce the spatial pattern shown by CWD-Obs-su, but overestimate the number of days in the mountainous areas. CWD-ERA-I-su (upper right panel in Figure 5.7B) and CWD-RegCM4-7-0.25-su (lower right panel in Figure 5.7B) show an important overestimation in the southwest of Mexico. In northern Mexico, all datasets emulate the lower values of the CWD index.

Summer Rx1 and Rx5 indices. Rx1-Obs-su (top left panel in Figure 5.7C) and Rx5-Obs-su (top left panel in Figure 5.7D) show the highest values in southern Mexico, where the average Rx1 index values range from 60 to 120 mm, and the Rx5 index values range from 75 to 250 mm in the southeastern coast of the country and the Sierra Madre del Sur. It is noteworthy that the north presents the lowest values, with 0.3 mm in the Baja California peninsula.

Rx1-ERA-I-0.75 (top right panel in Figure 5.7C), Rx1-CRCM5-0.22-su (middle left panel in Figure 7C), Rx1-CRCM5-0.44-su (bottom left panel in Figure 5.7C), Rx1-RCA4-0.5-su (middle right panel in Figure 5.7C), Rx5-ERA-I-0.75 (top right panel in Figure 5.7D), Rx5-CRCM5-0.22-su (middle left panel in Figure 5.7D), Rx5-CRCM5-0.44-su (bottom panel in Figure 5.7D), and Rx5-RCA4-0.5-su (middle right panel in Figure 5.7D) maintain the spatial pattern described by the observations; however, they overestimate the magnitude in the mountainous areas. The overestimation is mostly marked for the RCA4 simulation. ERA-I and the CRCM5 simulations also show underestimations central northern (desert) area of the country. On the other hand, Rx1-RegCM4-7-0.25-su (bottom right panel in Figure 5.7C) and Rx5-RegCM4-7-0.25-su (bottom right panel in Figure 5.7D), fail to identify the spatial pattern described by the observations.

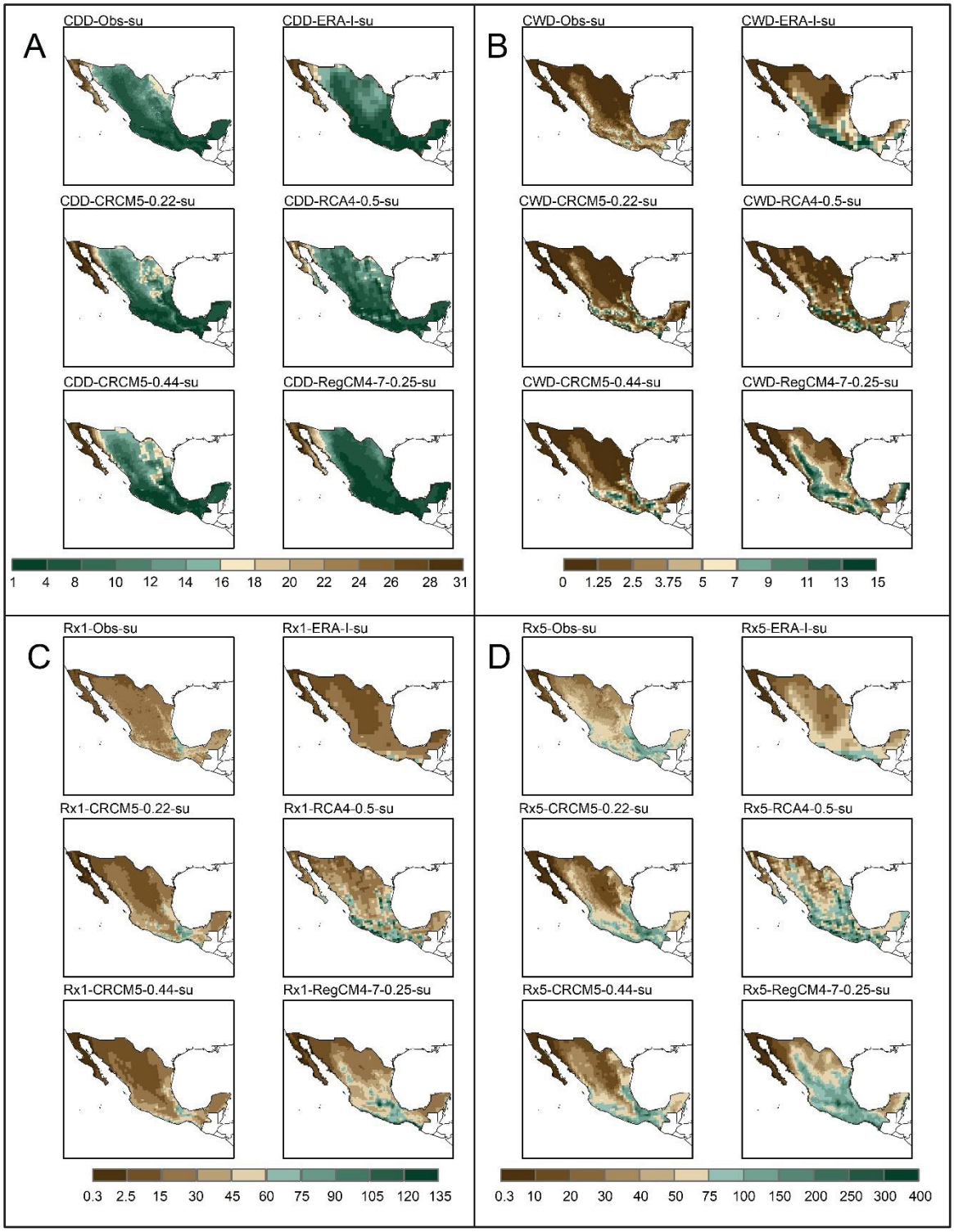

Figure 5.7 Same as Figure 5.5 but for summer

Fall CDD and CWD indices. The lowest values of the CDD-Obs-f index (upper left panel in Figure 5.8A) are located over the mountainous regions of Mexico (Sierra Madre Occidental, Sierra Madre Oriental, Sierra Madre del Sur, Trans-Mexican Volcanic Belt, Mountain Range of the Tuxtlas, Sierra Madre de Chiapas, and Central Highlands). The number of days for the CDD index decreases towards the southeast of the country, with an average of only 2.5 in fall. The highest number of days are found in the dry north and northwest of Mexico (Figure 5.1), with values reaching up to 31. Complementarily, the CWD-Obs-f index (upper left panel in Figure 5.8B) shows the highest values over the mountainous regions of Mexico. These values increase in the southeast of Mexico, with up to 13 days. The lowest values are located in the north and northwest of the country.

All the other datasets are able to reproduce, to some extent, the spatial pattern shown by the observations, however with underestimations of CDD index and overestimations of CWD index mainly in the Gulf of Mexico coastal area and in the mountainous areas. CDD-RegCM4-7-0.25-f (lower right map of Figure 5.8A) presents the most widely spread underestimation of observed CDD values. CDD-ERA-I-0.75 and CWD-ERA-I-0.75 also present underestimation and overestimation of observed values, respectively, in the south-west coast area of Mexico.

Fall Rx1 and Rx5. Both Rx1-Obs-f (top left panel in Figure 5.8C) and Rx5-Obs-f (top left panel in Figure 5.8D) reach their highest values in southeastern Mexico, which coincides with the Sierra Madre Oriental and the eastern Sierra Madre del Sur (up to 120 mm for Rx1-Obs-f and 250 mm for Rx5-Obs-f). The lowest values extend across the central and northern regions of the country, with values as low as 2.5 mm of maximum average precipitation in 1 day (Rx1-Obs-f) and 3.5 mm of maximum average precipitation in 5 consecutive days (Rx5-Obs-f). The west coast of Mexico shows an increase in Rx5-Obs-f, which coincides with the beginning of the mountain range in that region (Sierra Madre Occidental and Sierra Madre del Sur).

The five other datasets detect high values in southeastern Mexico and low values in the central and northern regions of the country. However, Rx1-CRCM5-0.22-f (middle left panel in Figure 5.8C), Rx1-CRCM5-0.44-f (lower left panel in Figure 5.8C), Rx5-RCA-0.5-f (middle left

panel in Figure 5.8D), Rx5-CRCM5-0.22-f (lower left panel in Figure 5.8D), Rx5-CRCM5-0.44-f (middle right panel in Figure 5.8C), and Rx5-RCA4-0.5-f (middle right panel in Figure 5.8D) overestimate the values in the south, southwest and west of the country. Rx1-ERA-I-f (top right panel in Figure 5.8C) and Rx5-ERA-I-f (top right panel in Figure 5.8D) detect the magnitude of the highest values in the southeast; however, there is a generalized overestimation in the south in the case of Rx5, which is also reflected by Rx1-RegCM4-7-0.25-f (lower right panel in Figure 5.8C) and Rx5-RegCM4-7-0.25-f (lower right panel in Figure 8D).

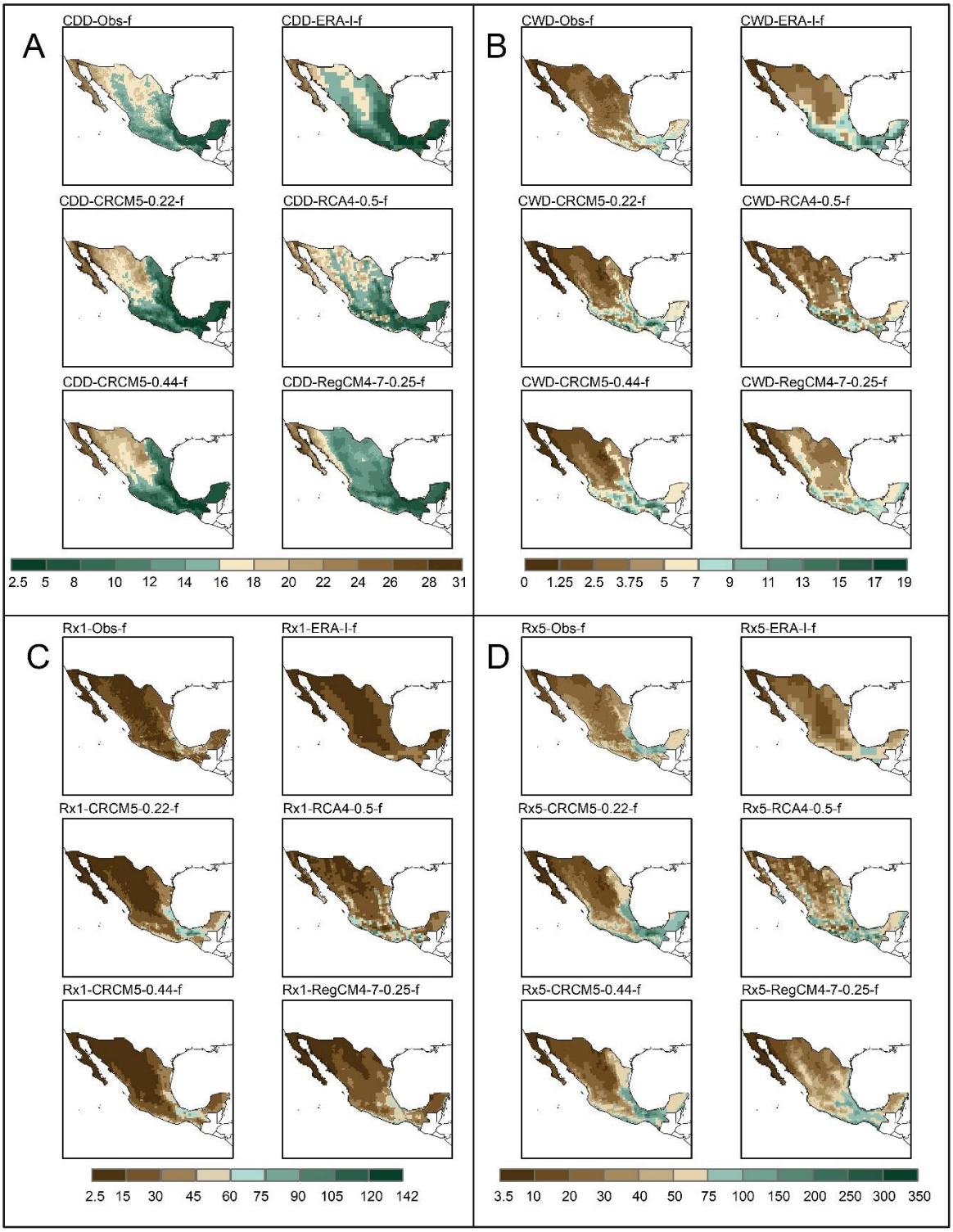

Figure 5.8 Same as Figure 5.5 but for fall

5.4.3 Correlation between PDO and Climate Extreme Indices (CDD, CWD, Rx1, and Rx5)

5.4.3.1 Analysis for the entire 1980-2012 time period

When considering the entire time period, no distinctive spatial pattern was found above 0.2 of correlation value, neither in the correlation between observed PDO and observed indices (except for tiny nuclei in center northern Mexico), nor in the correlation between ERA-PDO and the indices computed from ERA-I and the RCM simulations. Nevertheless, there are areas that show statistical significance. The results are shown in the supplementary materials. However, as mentioned by Brito-Castillo et al. (2002) and Méndez et al. (2010), the link between the PDO and moisture conditions in Mexico becomes evident when considering the phases of the PDO and/or the season of the year. For example, the northwest of Mexico is associated with wet winters during the positive phase of the PDO, whereas the negative phase is linked with drier conditions during that season.

5.4.3.2 Seasonal Analysis

The results are presented for the winter and spring (dry) seasons, which showed the most distinctive spatial correlation patterns with statistical significance. Summer and fall results have been included in the supplementary materials. The correlation is analysed according to two groups: the correlation of the PDO with CDD and CWD indices, and the correlation of the PDO with Rx1 and Rx5 indices. This grouping is structured to address humidity conditions in Mexico in the first group and precipitation extremes in the second.

Spring Correlation Patterns of PDO with CDD and CWD Indices. The correlation between PDO and the CDD-Obs-s index (top left panel in Figure 5.9A), displays the most negative correlation values in the northwest of Mexico, over the Sierra Madre Occidental. The correlation values are in the range of -0.2 to -0.45, with scattered cores at -0.5 and show statistical significance. As for the correlation between the PDO and CWD-Obs-s index (top

left panel in Figure 5.9B), it coincides with the aforementioned, but with positive correlation values. This suggests that the PDO may influence the moisture conditions in the northwest of the country, which also possibly has a link with the orography.

The ERA-I and RCM simulation datasets identify the magnitude of the correlation values between ERA-PDO and the CDD and CWD indices in northwestern Mexico. However, the correlation between ERA-PDO and the indices CDD-ERA-I-s (top right panel in Figure 5.9A) and CWD-ERA-I-s (top right panel in Figure 5.9B) is overestimated in magnitude, with respect to observations, in the southeastern coast of the country. The correlation between ERA-PDO and the indices CDD-CRCM5-0.22-s (left center panel in Figure 5.9A), CDD-CRCM5-0.44-s (lower left panel in Figure 5.9A), CDD-RegCM4-7-0.25-s (lower right panel in Figure 5.9A), CWD-CRCM5-0.22-s (left center panel in Figure 5.9B), CWD-CRCM5-0.44-s (lower left panel in Figure 5.9B), and CWD-RegCM4-7-0.25-s (lower right panel in Figure 5.9B) shows an underestimation in magnitude in the most negative values. The correlation between ERA-PDO and the indices CDD-RCA4-0.5-s (right center panel in Figure 5.9A) and CWD-RCA4-0.5-s (right center panel in Figure 5.9B) shows an overestimation in the central part of the country and an underestimation in the northeast, respectively. The results in Figure 5.6A did show a distinctive pattern in the CDD values in the north-western part of the country, while such a pattern was present but less clear in Figure 5.6B (CWD index).

Reproduction of Spring Correlation Patterns of PDO with Rx1 and Rx5 Indices. The spatial pattern of correlation with statistical significance between the PDO and the Rx1-Obs-s index (top left panel in Figure 5.9C) and Rx5-Obs-s index (top left panel in Figure 5.9D), displays the highest values (0.15 to 0.45) in the northwest of Mexico, over the north of the Sierra Madre Occidental, which again supports the relationship with moisture conditions. Maximum values (0.45) are observed at the center of the northwest border of the country. In the center northern Mexico there are also correlation values above 0.25. The southern part of the country presents small localized cores with negative correlation values of up to -0.35. This suggests that, despite the PDO's time window spanning decades, it does impact precipitation extremes during spring in the northwest of Mexico.

All the other datasets are able to detect the highest values in northwestern Mexico, although with underestimations. The correlation between ERA-PDO and the indices Rx1-ERA-I-s (top right panel in of Figure 5.9C) and Rx5-ERA-I-s (top right panel in Figure 5.9D) shows less details in the spatial pattern, which is likely related with its coarser resolution. The correlation between ERA-PDO and the indices Rx1-CRCM5-0.22-s (center left panel in Figure 5.9C), Rx1-CRCM5-0.44-s (lower left panel in Figure 5.9C), Rx5-CRCM5-0.22-s (center left panel in Figure 5.9D), and Rx5-CRCM5-0.44-s (lower left panel in 5.9D), present more negative values in the south and an in the center of Mexico. The correlation between ERA-PDO and the indices Rx1-RegCM4-0.25-s (lower right panel in Figure 5.9C) and Rx5-RegCM4-0.25-s (lower right panel in Figure 5.9D) presents an overestimation in the northern Baja California peninsula, as well as stronger negative correlation in the northeast of the country. The correlations between ERA-PDO and the indices Rx1-RCA4-0.5-s (center right panel in Figure 5.9C) and Rx5-RCA4-0.5-s (center right panel in Figure 5.9D) show close to no correlation (between -0.15 and 0.15) in most of the country. The results in Figure 6C and 6D (Rx1 and Rx5 indices, respectively) suggested a modestly distinctive pattern in the north-west area of Mexico.

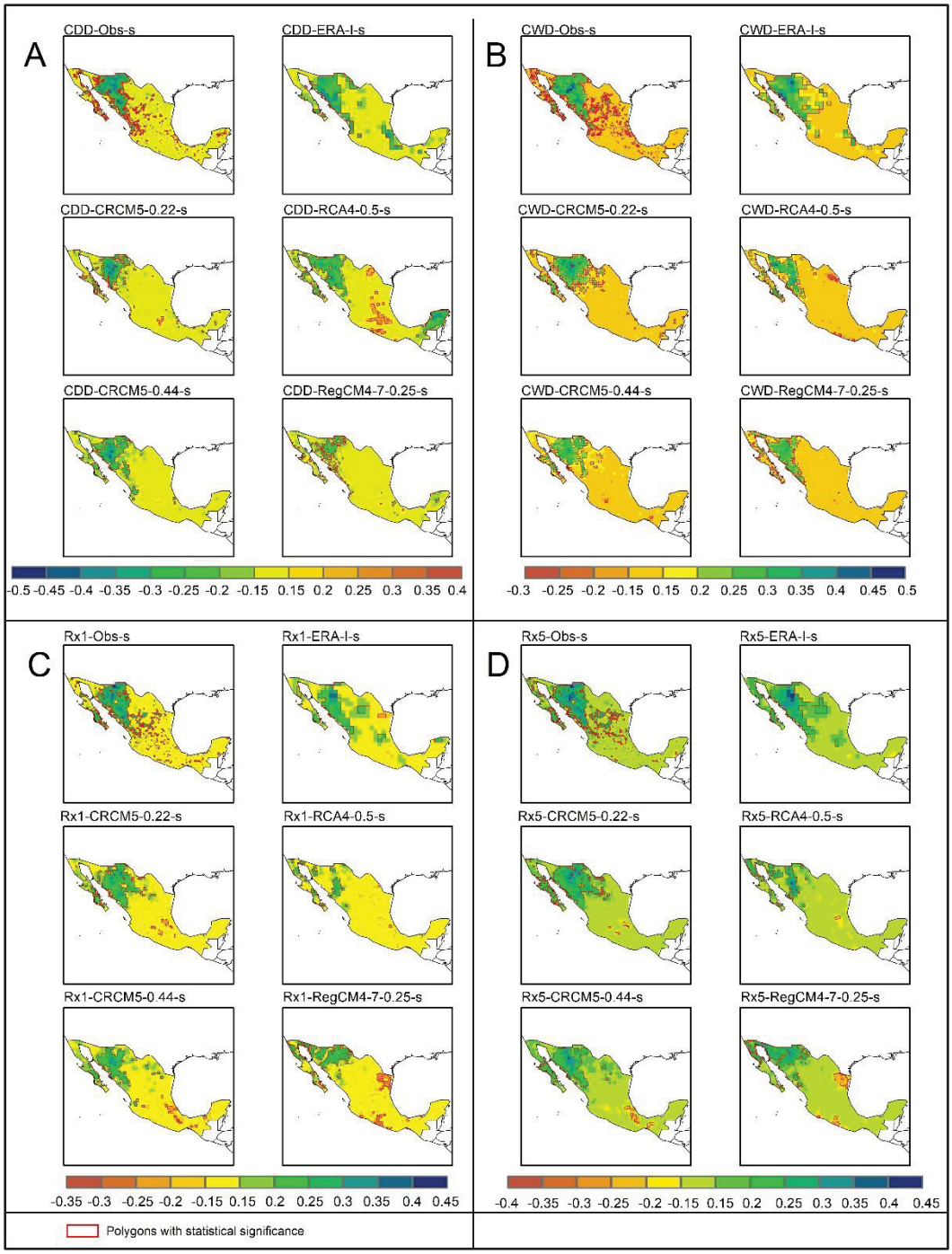

Figure 5.9 Spring correlation reproduction between de PDO teleconnection index and Climate Extreme Indices (CDD, CWD, Rx1 and Rx5). The teleconnection index was calculated by HadISST as observations and ERA-Interim. The Climate Extreme Indices were calculated by Livneh data set for observations, reanalysis (ERA-I) and RCM's simulations (CRCM5-0.22, CRCM5-0.44, RCA4-0.5 and RegCM4-7-0.25). Section A refers to PDO and CDD index correlation, section B refers to the PDO and CWD index correlation, section C refers to the PDO and Rx1 index correlation and section D refers to the PDO and Rx5 index

Reproduction of Winter Correlation Patterns of PDO with CDD and CWD Indices. The winter correlation between PDO and CDD-Obs-w (top left panel in Figure 5.10A) shows the strongest (negative) values in the western and central northern regions of Mexico with statistical significance. These observed values range from -0.25 to -0.50, and encompass the Sierra Madre Occidental Mountain range. Smaller and scattered cores, especially in the south and southeast coast (Sierra Madre de Chiapas), show positive correlation with values up to 0.40. A very similar spatial correlation pattern is seen between PDO and CWD-Obs-w, but this time with the opposite sign. As in the case of spring, this suggests an influence of PDO on moisture conditions in the northwest of the country, which also possibly has a link with the orography. One difference, though, pertains to a large northern area, in the case of winter, where weak (-0.15-0.15) correlations are found.

The correlations between ERA-PDO and CDD-ERA-I-w (top right panel in Figure 5.10A) and between ERA-PDO and CWD-ERA-I-w (top right panel in Figure 5.10B) show an overestimation of the spatial spread of the strongest values, with respect to observations. The respective positive and negative correlation values form the observations in the south and in the Yucatan peninsula are also not reproduced. The correlation of ERA-PDO with CDD-CRCM5-0.22-w (center left panel in Figure 5.10A) and CDD-CRCM5-0.44-w (lower left panel in Figure 5.10A), as well as with CWD-CRCM5-0.22-w (center left panel in Figure 5.10B) and CWD-CRCM5-0.44-w (lower left panel in Figure 5.10B) presents an underestimation in magnitude in the north-western part of the country. The extent of the more strongly correlated areas is also smaller with respect to observations, although the small cores with opposite correlation signs are reproduced. The correlation of ERA-PDO with the CDD-RCA4-0.5-w (center right panel in Figure 5.10A) and CWD-RCA4-0.5-w (center right panel in Figure 5.10B) shows a lack of accuracy in the spatial pattern with respect to observations, with the highest values not coinciding to same the region of the country. The correlation between ERA-PDO and CDD-RegCM4-7-0.25-w (lower right panel in Figure 5.10A), and CWD-RegCM4-7-0.25-w (lower right panel in Figure 5.10B), completely misses the spatial pattern seen in the observations, with weak values throughout almost the entire country.

In central northern Mexico, the regions that had shorter wet spell duration and longer dry spell duration in Figures 5.5A and 5.5B are to some extent noticeable in the strongest correlations. However, these correlation values are negative for the CDD index and positive for the CWD index, which suggests that the PDO in winter contributes to an longer dry spells and hence shorter wet spells. This behavior is detected by CDD-ERA-I-w, CWD-ERA-I-w, CDD-CRCM5-0.22-w, CWD-CRCM5-0.22-w CDD-CRCM5-0.44-w, and CWD-CRCM5-0.44-w.

Reproduction of Winter Correlation Pattern between PDO and Rx1 and Rx5 Indices. The correlation between PDO and Rx1-Obs-w (top left panel in Figure 5.10C) and Rx5-Obs-w (top left panel in Figure 5.10D), with statistical significance, shows the strongest (positive) values, ranging from 0.35 to 0.45, in the central west coast and central north of Mexico. Negative correlation values are also found in the southeastern coast of the country, with values reaching up to -0.5. This indicates that, for these regions, the PDO influences the magnitude of maximum precipitation, not only over a single day but also in five consecutive days, which aligns with what is described by Brito-Castillo et al. (2002) about stability between the precipitation and the oceanic conditions under PDO conditions.

The five other datasets show an underestimation of correlation magnitude for this season compared to the observations. Specifically, the correlation between ERA-PDO and Rx1-ERA-I-w (top right panel in Figure 5.10C) and Rx5-ERA-I-w (top right panel in Figure 5.10D) underestimate the maximum values. The correlation between ERA-PDO and Rx1-CRCM5-0.22-w (middle left panel in Figure 5.10C), Rx1-CRCM5-0.44-w (lower left panel in Figure 5.10C), Rx5-CRCM5-0.22-w (middle left panel in Figure 5.10D), and Rx5-CRCM5-0.44-w (lower left panel in Figure 5.10D) is underestimated, in magnitude, in the center of the country, and shows stronger negative values in the south. The correlations between ERA-PDO and Rx1-RCA-0.5-w (middle right panel in Figure 5.10C) and Rx5-RCA-0.5-w (middle right panel in Figure 5.10D) do not capture the spatial pattern described by the observations, nor do the correlations between ERA-PDO and Rx1-RegCM4-7-0.25-w (lower right panel in Figure 5.10C) and Rx5-RegCM4-7-0.25-w (lower right panel in Figure 5.10D). In the latter cases, the

spatial variability is very low with respect to observations, and most of the country shows weak correlation values, between -0.15 and 0.15.

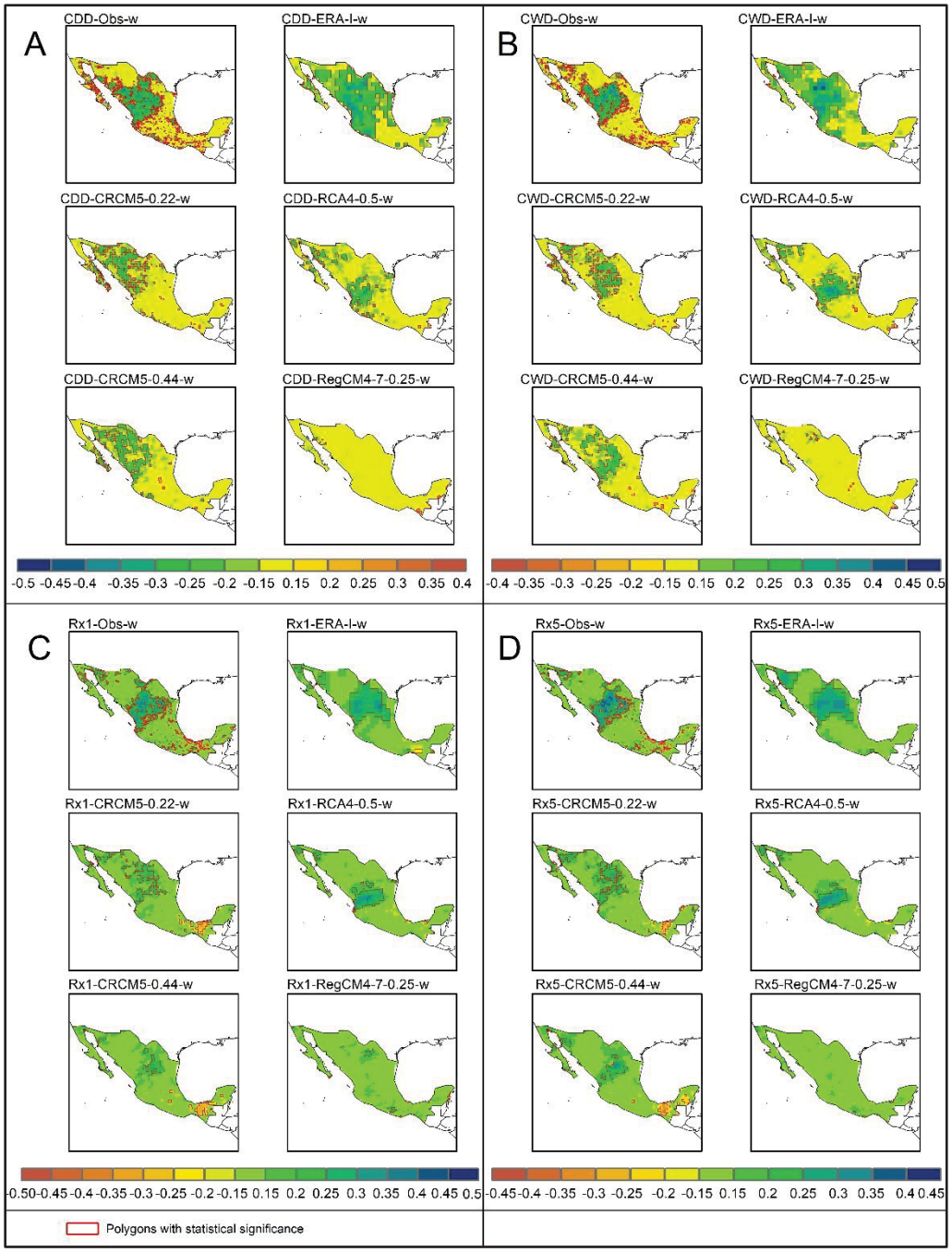

Figure 5.10 Winter correlation reproduction between de PDO teleconnection index and Climate Extreme Indices (CDD, CWD, Rx1 and Rx5). The PDO teleconnection index were calculated by HadISST as observations and ERA-Interim (ERA- PDO). The Climate Extreme Indices were calculated by Livneh data set for observations, reanalysis (ERA-I) and RCM's simulations (CRCM5-0.22, CRCM5-0.44, RCA4-ERA-Inteirm-0.5 and RegCM4-7-0.25). Section A refers to PDO and CDD index correlation, section B refers to the PDO and CWD

index correlation, section C refers to the PDO and Rx1 index correlation and section D refers to the PDO and Rx5 index

5.5 Discussion

5.5.1 PDO and Precipitation Representation

The calculation of the correlation between the time series of the PDO generated using the ERA-I data and the PDO generated from the observations is 0.98, which aligns with findings related to SST by Luo et al. (2020). This suggests that ERA-Interim is capable of reproducing the PDO. Additionally, the maximum difference value between these two time series is only 0.67°C around the year 2002.

The monthly accumulated precipitation results indicate that ERA-I and the four RCM simulations are well correlated with the observations, with ERA-I showing the highest value of 0.98. The simulations tend to overestimate the precipitation, particularly in the cases of RCA4-0.5 and RegCM4-7-0.25. Such findings coincide with those from Cavazos et al. (2019) and Ashfaq et al. (2021). The monthly accumulated precipitation results also vary on a seasonal basis, with the most important differences between the observations and the two aforementioned simulations occurring during summer (see Figure 5.4). This is a wet season in Mexico and this is where the RCA4 and RegCM4-7 simulations show the highest overestimation in precipitation throughout the year.

5.5.2 Reproduction of Climate Extreme Indices

ERA-I manages to capture the spatial patterns seen in the observations but with differences that can most likely be attributed to the coarser ERA-I spatial resolution. The simulations perform fairly well in general, with a more clearly defined spatial pattern in the mountainous areas of Mexico. We hypothesize that RCMs have an advantage over possibly missing observations in accurately representing precipitation in mountainous regions, although we cannot determine the extent of this advantage. This capability also depends on the spatial resolution of the RCMs and their simulation settings, including the parameterizations of

atmospheric processes and the methods used to transfer information from ERA-I – the global dataset driving the four simulations – to the RCMs at their boundaries (e.g., whether or not spectral nudging is employed; Schubert-Frisius, 2017).

Amongst the four studied RCM simulations, the ones that generally performed best at reproducing the observed climate extreme indices on a seasonal basis are the CRCM5-0.22 and CRCM5-0.44 simulations, according to the statistical significance testing as well as correlation magnitude and the spatial extent of the correlation. The RegCM-4-7-0.25 simulation was the one showing the most difficulty in reproducing the observed indices spatial patterns over Mexico. However, all simulations did at least show some good performances in specific seasons and in specific areas of the country (Cavazos et al., 2020, Mendez et al., 2010).

5.5.3 Reproduction of Seasonal Correlation between PDO and Climate Extreme Indices.

Since there is not a defined spatial pattern of correlation between PDO and Climate Extreme Indices in summer and fall (see supplementary material), this study focused the winter and spring seasons.

Spring. In spring, the correlation between the observations between PDO and climate extreme indices exhibits a clear spatial pattern with stronger values towards the northwest of Mexico. The correlation, in spring, between ERA-PDO and the RCM simulations-computed indices (CDD, CWD, Rx1, and Rx5) does show the observed increase towards the northwest of Mexico but with different levels of underestimation in magnitude. The most notable underestimation is between ERA-PDO and Rx1-RCA4-0.5 and Rx5-RCA4-0.5 indices in spring (Diro et al., 2012; Giorgi et al., 2012).

Winter. In winter, there is a spatial pattern of correlation between PDO and the climate extreme indices in the west-central part of Mexico as described by the observations (top left panels in Figure 10A, 10B, 10C and 10D). This pattern is identified in the cases of the ERA-PDO-ERA-

I and ERA-PDO-CRCM5 simulations correlations. The correlations between ERA-PDO and the RegCM4-7 indices fail at reproducing any of the observed correlations, while in the case of the RCA4 simulation the spatial patterns are different than what is exhibited by the observations. The spread of the area, in the case of the ERA-I dataset, is generally overestimated. In the case of the two CRCM5 simulations, the magnitude of the correlation described by the observations tends to be underestimated (Prein et al., 2015).

5.5.4 Positioning of the present study with respect to existing literature

This study contributes to analyzing whether the simulations are sensitive to oceanic conditions around the world. Diasso et al. (2015) mention that different drought modes, calculated using the Standardized Precipitation Evapotranspiration Index (SPEI), in West Africa, are related to SST anomalies. These modes are only reproduced by two RCM simulations from CORDEX. Hernandez-Garcia et al. (2024, under revision) found that certain RCMs driven by ERA-Interim are able to detect the influence of ENSO on climate extreme indices. Cavazos et al. (2020) mention that three CORDEX RCM simulations (PRECIS-HadRM3P, RCA4, and RegCM4) are capable of emulating, especially in winter, precipitation trends in northwestern Mexico, which are correlated with the Atlantic Multidecadal Oscillation and ENSO. On the other hand, Jiang et al. (2013) observed that the precipitation time series simulated with GCM/RCM do not align with ENSO and PDO. This highlights the ongoing need for studies that further explore simulations and their characteristics related to teleconnection indices in different regions of the world.

5.5.5 Main limitations

In the development of this research, it was found that the diversity in resolutions among the RCM simulations leads to differences in the representation of precipitation and the indices that aim to characterize it (e.g., climate extreme indices). Additionally, the driving dataset for the RCM simulations (ERA-Interim in this case) contribute to, but do not determine, the ability of the RCMs to reproduce precipitation features. The use of RCM simulations provides valuable

insights into historical simulations and enhances the credibility of future projections, aiding decision-makers in managing climate extremes. Nevertheless, several limitations must be acknowledged:

1. Models Structure and Representation: Differences in the internal structure and parameterization schemes of the RCMs used in this study—CRCM5-0.22, CRCM5-0.44, RCA4-0.5, and RegCM4-7-0.25—introduce variability in their ability to represent PDO-related signals. Variations in how physical processes like convection, land-atmosphere interactions, and orographic influences are modeled can impact the accuracy of simulated CEIs, especially in regions with complex topography (Laprise, 2008; Giorgi et al., 2019).

2. Bias Correction: This analysis evaluates RCM simulations directly without applying bias correction. While this approach allows for an unaltered assessment of the models' raw performance, it may leave some systematic errors unaddressed, which may influence the interpretation of extreme precipitation magnitudes and other CEIs in applied contexts (Maraun et al., 2017; Ehret et al., 2012).

3. Data Availability and Model Updates: The RCM simulations employed in this study were selected based on their availability at the time of research. These simulations may not reflect recent advancements in model physics and parameterizations. Similarly, ERA-Interim, the driving dataset for the simulations, has been superseeded by ERA5, a more advanced reanalysis product. Future studies should incorporate simulations driven by ERA5 to leverage improved accuracy in boundary conditions (Hersbach et al., 2020).

4. Temporal Coverage: The study period of 1980–2012 may not capture the full range of PDO variability, particularly its longer-term decadal phases and rare extreme events. Extending the temporal window could yield more robust statistical assessments and offer a deeper understanding of PDO's influence on CEIs (Simmons et al., 2010).

5. Observed Data Limitations: Observed datasets used for model evaluation were derived from gridded and interpolated sources. While comprehensive, these datasets may smooth or underrepresent extreme precipitation events, making it challenging to evaluate the RCMs' ability to reproduce localized and high-intensity events accurately (Livneh et al., 2015; Westra et al., 2014).

6. Spatial Resolution Constraints: The RCM resolutions employed in this study range from 0.22° to 0.5°, which may be insufficient to resolve fine-scale convective processes that drive extreme precipitation. This limitation particularly affects the representation of indices such as Rx1 and Rx5. High-resolution and convection-permitting models are recommended for future studies to enhance the fidelity of simulated extreme events (Ban et al., 2021).

These limitations underscore the need for further research that incorporates higher-resolution simulations, advanced reanalysis products, and more comprehensive observed datasets. Future studies should also explore additional climate indices and their teleconnection patterns to improve our understanding of CEI variability and its drivers in Mexico.

When using climate extreme indices instead of precipitation, some characteristics of extreme behavior related to teleconnection indicess are lost. On the other hand, conducting a spatiotemporal covariability analysis would help understand whether these variables exhibit a coupled behavior. And finally, there is still a need to develop climatological studies that contribute to the understanding of the influence of TIs on precipitation patterns and moisture conditions.

5.6 Conclusion

The main objective of this article is to investigate the capacity of four ERA-I-driven simulations (CRCM5-0.22, CRCM5-0.44, RCA4-0.5, and RegCM4-7-0.25) to replicate the

grid-cell-to-grid-cell correlation described by the observations between PDO and climate extreme indices from the ETCCDI in Mexico, in the time period of 1980 – 2012. The indices were selected to describe the wet (CWD) and dry (CDD) conditions of Mexico, as well as the maximum precipitation in one day (Rx1) and sustained over five days (Rx5).

Correlations were computed (1) between HadISST-computed PDO and Livneh et al. (2015) derived indices (observations); (2) between ERA-I-computed PDO and ERA-I derived indices; and (3) between ERA-I-computed PDO and the four RCM simulations derived indices. Spatial correlation patterns were found during the two driest seasons in Mexico, winter and spring, and mainly relate to moisture conditions in the north-west part of the country (spring) and in the northern central part of the country (winter). Given the location of the Sierra Madre Occidental Mountain range, the spring moisture conditions could also be associated with orography. The ERA-I dataset as well as the two CRCM5 simulations generally perform best at reproducing the observed correlations. Similar results were also found in a previous study that looked at the correlations between ENSO and the same climate extreme indices (Hernandez-Garcia et al., 2024, under review). Those results align well with the findings from the present study and from Hernandez-Garcia et al. (2024) that: (1) ERA-I-computed PDO is in close agreement with the HadISST observations-computed PDO which reinforces the reliability of ERA-Interim in representing large-scale oceanic processes; (2) ERA-I and the two CRCM5 simulations can represent fairly well the observed monthly accumulated precipitation amount, in terms of correlation and empirical distributions, as well as the spatial patterns (considering spatial extent and magnitude) of the mean climate extreme indices over the Mexican domain on a seasonal basis. However, biases related to RCM spatial resolution and parameterizations persist, particularly in regions of complex topography and for extreme precipitation indices (Rx1 and Rx5).

The understanding of the relationship between SST anomaly oscillations and dry and humid in Mexico suggests further analysis of the oceanic context and the continental response related to it. The development of knowledge around RCM simulations allows for an improved historical description and, consequently, better projections from the models. This provides decision-

makers with an information that can contribute to dealing with extreme situations. In future studies, it should be considered to use climate extreme indices to understand moisture conditions and extremes in RCM projections. This can also be related to the outputs of earth system models, and the coupled ocean-atmosphere behavior should be investigated.

5.7 Acknowledgments

We acknowledge the World Climate Research Programme's Working Group on Regional Climate, and the Working Group on Coupled Modelling, former coordinating body of CORDEX and responsible panel for CMIP5. The CRCM5 data has been generated and supplied by Ouranos and computations were made on the supercomputers beluga and narval managed by Calcul Québec and the Digital Research Alliance of Canada (alliancecan.ca). The operation of this supercomputer received financial support from Innovation, Science and Economic Development Canada and the Ministère de l'Économie et de l'Innovation du Québec. The Canadian Regional Climate Model (CRCM5;Martynov et al. 2013, Separovic et al. 2013) was developed by the ESCER Centre at UQAM (Université du Québec à Montréal) with the collaboration of Environment and Climate Change Canada. We also thank the climate modelling groups (listed in Table 5.1 of this chapter) for producing and making available their model output. We also acknowledge the Earth System Grid Federation infrastructure an international effort led by the U.S. Department of Energy's Program for Climate Model Diagnosis and Intercomparison, the European Network for Earth System Modelling and other partners in the Global Organisation for Earth System Science Portals (GO-ESSP). We acknowledge of data taken from Livneh gridded precipitation and other meteorological variables for continental US, Mexico and southern Canada. We acknowledge of any material or data taken from Hadley Centre Sea Ice and Sea Surface Temperature data set (HadISST). We acknowledge of ERA-Interim data taken from European Centre for Medium-Range Weather Forecast. We acknowledge the grant from Consejo Nacional de Humanidades Ciencias y Tecnologías (CONAHCYT) as well as the grant from Fonds de recherche du Québec – Nature et technologies (FRQNT).

CHAPTER 6

GENERAL DISCUSSION

This section will be organized into three parts. The first part will focus on the analysis of the representation of SST and the teleconnection indices (ENSO and PDO) using data from ERA-Interim. The second part will address the analysis of the representation of precipitation, SPI, and CEIs using data from both ERA-Interim and RCM simulations. The final part will evaluate the representation of the spatial pattern of the temporal correlation between the teleconnection indices and the SPI and CEIs.

6.1 Sea surface temperature and Oscillation Indices

The spatial representation of sea surface temperature in the northern Pacific Ocean basin, using upscaled ERA-Interim data, shows the greatest spatial bias near the coasts and towards the poles, as indicated by the RMSE and MAE error maps in Figure 3.4. In contrast, the lowest bias is found in the central northern Pacific basin for MAE, while RMSE detects the lowest bias only in certain delineated areas. It is important to mention that these biases may be mainly related to two sources: the first concerning the underestimation of the submarine topography present in the reanalysis data (Luo et al., 2020), and the second related to the difference in resolution. This behavior aligns with what was described by Luo et al. (2020) but in the Atlantic Ocean.

The adjustment of the temporal pattern representation of SST, using ERA-Interim data, as shown in Figure 3.3, indicates that despite observing an underestimation of the maximum and minimum values, the change in direction and the intersection throughout the detrended SST mean is accurately detected. Additionally, the correlation is 0.97, and the bias value remains consistently below 0.5°C.

6.1.1 ENSO

The spatial representation of ENSO using upscaled ERA-Interim data aligns well with what is described by the observations, with a slight overestimation in the positive spatial variability and the intensity of the index. The difference in the spatial variability captured by the leading EOF of the ENSO spatial pattern between the observations and ERA-Interim is only 4%. Specifically, while HadISST shows 64%, ERA-Interim shows 60%. The temporal pattern of ERA-ENSO compared to the observations matches the phase movements of the index with a correlation of 0.99 (O'Reilly, 2018).

6.1.2 PDO

The spatial pattern of PDO calculated using ERA-Interim data successfully emulates all the characteristics shown by HadISST. Deser et al. (2010) indicate that more than 50 years are required to obtain a representation of the PDO, but this study only considered 33 years (1980 to 2012). However, regarding the spatial variability captured by both HadISST and ERA-Interim data when computing PDO, it is 21%.

The time series calculation of PDO using ERA-Interim data shows a good fit with the observations, which aligns with previous descriptions (Luo et al., 2020). Similarly, the correlation between the PDO time series calculated from each dataset has a value of 0.98, with a maximum bias of 0.68°C.

6.2 Precipitation and indices

All data from the RCM simulations overestimate the spatial representation of the average monthly accumulated precipitation. The simulations RCA4-ERA-Interim-0.5 and RegCM4-7-ERA-Interim-0.25 show the least adjustment in spatial variability. However, the remaining simulations and ERA-Interim, despite showing better spatial adjustment, exhibit a strong influence from the Sierra Madre mountain ranges, as is suggest by Colorado-Ruiz et al. (2020).

Overall, all simulations are strongly influenced by the Mexican mountain systems, leading to an overestimation in these regions. This suggests that the simulated convective processes and moisture advection are affecting the precipitation calculations. Additionally, as mentioned previously, differences in resolutions might influence the results, as some authors note positive biases in the mountainous areas of the RCA4-ERA-Interim-0.5 and RegCM4-7-ERA-Interim-0.25 simulations (Ashfaq et al., 2021; Cavazos et al., 2019).

Regarding the Temporal Representation of Precipitation, the ERA-Interim data exhibit the highest correlation with observations (0.98), while among the simulations, CRCM5-ERA-Interim-0.44 retains the highest value (0.92). However, the other simulations are not far from this correlation value, with all generally around 0.9. All simulation data overestimate the intensity of precipitation for the period considered in this study. This overestimation persists in the seasonal analysis, with RCA4-ERA-Interim-0.5 and RegCM4-7-ERA-Interim-0.25 showing the greatest overestimation in spring and summer, this also was mention by Colorado-Ruiz et al. (2020) for RegCM4-7-ERA-Interim-0.44. In winter and autumn, the overestimation is mitigated by the characteristic atmospheric behavior of these seasons, leading to a smoothing of the overestimation. This suggests that the phenomena associated with precipitation in spring and summer might be related to the orographic forcing response for the simulations with the highest overestimation (Ashfaq et al., 2021; Cavazos et al., 2019). It is important to mention that Livneh et al. (2015) data are derived from interpolation, which might smooth extremes and areas with limited or difficult-to-access measurements. All the overestimations may be influenced by ERA-Interim, as was mention for Barella-Ortiz et al. (2019), but for Spain and a different simulation forced by ERA-Interim.

6.2.1 SPI

In the time intervals defined for each index, SPI24 (from 1991 to 1994 and from 2009 to 2012) and SPI60 (from 1985 to 1998 and from 1999 to 2012), both ERA-Interim and the simulations aligned with the observations in detecting the dry (wet) north and the wet (dry) south in each

case. However, they encountered issues in determining the spatial variability and intensity of the index.

The adjustment of reanalysis and simulation data in representing SPI24 and SPI60 shows some agreement in the temporal behavior of these indices. Throughout most of the time interval considered in this thesis (1980 to 2012), they are able to detect the shift from wet to dry conditions. However, there is a generalized underestimation of the highest and lowest values. It is worth mentioning that, for aggregated data across all of Mexico, the RegCM4-7-ERA-Interim-0.25 simulation showed the closest adjustment during most of the temporal behavior of these indices.

6.2.2 Climate Extreme Indices

The spatial representation of the average Climate Extreme Indices (CEI) from the simulations, successfully identifies the spatial gradient described by the observations, which coincides with the precipitation analysis of Alvarez-Olguin (2017) and Arriaga-Ramirez et al. (2012), where the south is wetter than the north. However, simulations from CRCM5 generally show the highest adjustment for each index. Additionally, the RCA4-ERA-Interim-0.5 simulation exhibits the lowest adjustment for the CDD and CWD indices. It is worth noting that this finding aligns with the results reported by Kim et al. (2020), although there are some contrasts in the northwest of Mexico. However, it should be considered that the time periods and observational data used are different.

Regarding the seasonal representation of the Climate Extreme Indices (CEI), it can be observed that the RegCM4-7-ERA-Interim-0.25 simulation does not represent seasonal behavior as well as its counterparts, showing the lowest adjustment compared to what is described by the observations in each season. Once again, simulations from CRCM5 represent the CEI more accurately on a seasonal basis. However, specifically for the CDD index in winter, the RCA4-ERA-Interim-0.5 simulation shows a better approximation. It is worth noting that the correlation in the temporal representation of precipitation indicates that the CRCM5

simulations have the best adjustment. This suggests that the correlation in the monthly average between observations and simulations may provide insight into the quality of the spatial representation of the indices over a defined time period.

6.3 Climate oscillations and precipitation indices correlation

This section discusses the representation of the spatial pattern of temporal correlation between the Climate Extreme Indices (CEI) and the Teleconnection Indices (TI). The ability of both simulations and ERA-Interim data to reproduce this representation is evaluated, not only in terms of how correlated they are but also whether they accurately depict the spatial pattern as observed in reality. This evaluation will be conducted for both the complete time interval and seasonal periods.

6.3.1 Climate oscillations and SPI correlation

When analyzing the representation of the correlation between the Teleconnection Indices (calculated with ERA-Interim) and SPI24 and SPI60 (calculated with ERA-Interim and the simulations), it is observed that these data are capable of emulating the relationship between wet and dry conditions in Mexico and the Teleconnection Indices, mentioned also by Mendez & Magaña (2010). However, inconsistencies with observations are noted. As mentioned by Méndez & Magaña (2010), the contrast in humidity between northern and southern Mexico in correlation with the Teleconnection Indices, as observed, is emulated by the simulations in detecting this contrast, as demonstrated in this thesis. Nevertheless, despite differences in time windows, the PDO showed a higher correlation with both SPI24 and SPI60.

6.3.2 Climate Oscillations and climate extreme indices correlation

Regarding the correlation between the CEI and ENSO for the study period (1980 to 2012), simulations from CRCM5 demonstrate a better fit in representing the relationship between the CDD and CWD indices. However, concerning the correlation of ENSO with the Rx1 and Rx5

indices, none of the simulations clearly emulated the observations, neither in spatial variability nor in intensity. Additionally, the correlation between PDO and CEI does not show any defined pattern when considering the entire study period.

Regarding the seasonal analysis, although studies show that the correlation between ENSO and precipitation patterns primarily occurs in summer and winter (Bravo-Cabrera et al., 2017; Pavia et al., 2006; Vega-Camarena et al., 2023), this thesis found that spring and autumn also exhibit correlation with the teleconnection indices. Specifically, in spring, the CEI calculated from simulations provided by CRCM5 better emulate the observations in terms of correlation with ENSO for the CDD and CWD indices. However, there is an overestimation in both spatial variability and intensity. None of the simulations can accurately reproduce the observations regarding the correlation between ENSO and the Rx1 and Rx5 indices. In winter, despite the overestimation, the CEI calculated from CRCM5 simulations show a better fit in representing the correlation with ENSO calculated from ERA-Interim.

In spring, the representation of the correlation between the PDO, calculated with ERA-Interim, and the CEI, calculated with ERA-Interim and the simulations, indicates that all datasets manage to emulate the correlation pattern observed. However, the RCA4-ERA-Interim-0.5 simulation exhibits a notable underestimation, specifically in the correlation between the RX1 and Rx5 indices and the PDO calculated with ERA-Interim. In winter, the correlation between the CEI calculated with the RegCM4-7-ERA-Interim simulation fails to reproduce the observations. Conversely, the correlation shown between the reanalysis data demonstrates overestimation, while the correlation with the CEI calculated from simulations underestimates the intensity of this correlation.

6.4 Main Limitations

While this thesis provides valuable insights into the relationship between teleconnection indices (ENSO and PDO) and climate extreme indices (CEIs), along with the ability of ERA-

Interim-driven RCM simulations to reproduce these relationships, several limitations must be acknowledged, which will be addressed in the next subsections.

6.4.1 Model Structure and Representation

Variations in the internal structure and parameterization schemes of the RCMs used in this study—CRCM5-ERA-Interim-0.22, CRCM5-ERA-Interim -0.44, RCA4-ERA-Interim -0.5, and RegCM4-ERA-Interim -7-0.25—introduce differences in their ability to replicate teleconnection-related signals. Disparities in how physical processes, such as convection, land-atmosphere interactions, and orographic effects, are modeled can significantly influence the accuracy of simulated CEIs, particularly in regions with complex topography (Laprise, 2008; Giorgi et al., 2016).

6.4.2 Bias Correction

The analysis was conducted on raw RCM outputs without applying bias correction, allowing for a direct evaluation of the models' inherent skill. However, this approach may leave systematic errors unaddressed, potentially affecting the interpretation of extreme precipitation magnitudes and their associated indices in applied contexts (Maraun et al., 2017; Ehret et al., 2012).

6.4.3 Data Availability and Model Updates

The RCM simulations were selected based on their availability at the time of the research, and they may not reflect the latest advancements in model physics and parameterizations. Furthermore, ERA-Interim, the dataset driving these simulations, has since been superseded by ERA5, a more advanced reanalysis product with higher temporal and spatial resolution (Hersbach et al., 2020). Incorporating ERA5-driven simulations could enhance future analyses. Nevertheless there are not yet simulations driven by ERA5 in Mexican domain.

6.4.4 Temporal Coverage:

The study period of 1980–2012 may not encompass the full range of ENSO and PDO variability, including longer-term decadal oscillations and rare extreme events. Extending the temporal range could improve statistical reliability and offer deeper insights into teleconnection influences on CEIs (Simmons et al., 2010).

6.4.5 Observational Data Limitations

The observed precipitation dataset used for comparison was derived from a gridded interpolated source. While comprehensive, this dataset may smooth or underrepresent extreme precipitation events, complicating the evaluation of RCMs' ability to replicate localized and high-intensity phenomena accurately (Livneh et al., 2015; Westra et al., 2014).

6.4.6 Spatial Resolution Constraints

The spatial resolutions of the RCMs (0.22° and 0.44°) may not adequately resolve convective processes critical for extreme precipitation events, particularly those captured by the Rx1 and Rx5 indices. High-resolution and convection-permitting models are recommended for future studies to better capture localized phenomena and improve the representation of extreme precipitation events (Ban et al., 2015; Prein et al., 2017).

6.4.7 Limitations of the SPI Indices:

While the use of SPI24 and SPI60 indices provides valuable insights into wet and dry conditions over different temporal scales, these indices rely solely on precipitation data and do not account for other variables influencing dry and wet conditions, such as temperature, evapotranspiration, and soil moisture. Indices such as the Standardized Precipitation Evapotranspiration Index (SPEI), which incorporates evapotranspiration data, or the Palmer Drought Severity Index (PDSI), which accounts for soil moisture balance, could offer a more

comprehensive assessment of dry and wet conditions (Vicente-Serrano et al., 2010; Palmer, 1965). Additionally, combining CEIs with indices like the Effective Drought Index (EDI) or the Aridity Index could help explore the broader impacts of teleconnections on water availability and climatic extremes (Byun et, al., 1999; Dai, 2011).

6.4.8 Covariability Analysis

While this study investigates correlations between teleconnection indices and CEIs, it does not fully explore the spatial and temporal covariability of these variables. A spatiotemporal covariability analysis could provide deeper insights into the coupled behavior of teleconnections and precipitation extremes (Kumar, et al., 2013).

These limitations underscore the need for continued research leveraging advanced models, extended datasets, and additional indices to further understand the teleconnection-CEI relationships in Mexico. Such efforts will help enhance climate projections and improve decision-making in managing climate extremes.

CONCLUSION

Efforts to understand both climate variability and the mechanisms associated with precipitation extremes (droughts and heavy rainfall) have been made globally, including documenting, describing, and projecting their impacts on society and nature. These worldwide efforts have been captured by the WMO and the specialized reports from IPCC, which address not only the physical mechanisms associated with precipitation patterns but also the substantial losses incurred (IPCC, 2007a, 2012, 2014, 2022; WMO, 2019). This thesis focuses on evaluating Regional Climate Models (RCMs) as tools for reproducing the linkage between Climate Oscillations (ENSO and PDO) and precipitation patterns through SPI and CEI. Specifically, it aims to (1) Study the ability of RCM simulations to reproduce the observed link between SPI wet and dry conditions and ENSO and PDO; (2) Assess the reproduction of the observed correlation between ENSO and CEI in Mexico with RCM simulations and (3) Evaluate the reproduction of the observed correlation between PDO and CEI in Mexico with RCM simulations. Additionally, since most of the reviewed studies use simulations to represent CEI or examine the response of different variables to TI, this project seeks to contribute knowledge regarding the applications and limitations of simulations. Specifically, it aims to assess the differences in the responses of various RCMs forced with ERA-Interim data, as well as to examine the reproduction of the influence of TIs on precipitation extremes and moisture conditions.

In analyzing the performance of ERA-Interim in emulating the spatial and temporal patterns of both SST and the teleconnection indices ENSO and PDO, it was found that despite RMSE and MAE errors showing biases near continental coasts and towards the poles, ERA-Interim satisfactorily represents the Teleconnection Indices both spatially and temporally, as well as in the captured spatial variability. These indices were calculated for the time period defined in this study (1980 to 2012).

The representation of precipitation shows the best fit for simulations from CRCM5, which not only exhibit a correlation of around 91% but also display the lowest temporal overestimation. The highest overestimations, however, occur in summer and spring with the RCA4-ERA-

Interim-0.5 and RegCM4-7-ERA-Interim-0.25 simulations. Regarding spatial representation, the behavior of the simulations in the annual precipitation average suggests a strong influence of topography in reproducing precipitation. Nevertheless, both ERA-Interim and the CRCM5 simulations present the best spatial fit.

Despite the generalized underestimation across all datasets in representing the time series of the SPI24 and SPI60 indices, they successfully identify the time intervals associated with wet and dry thresholds. The RegCM4-7-ERA-Interim-0.25 simulation showed the best temporal fit in representing these indices. However, despite the overestimation of spatial variability and intensity, all simulations were able to detect the contrast between wet and dry conditions in the north and south, and vice versa.

The reproduction of the Climate Extreme Indices (CEI) shows that the simulations are capable of replicating the main spatial features over the study period. However, the simulations derived from CRCM5 provide more accurate information compared to observations. Regarding the seasonal analysis of CEI representation, it was concluded that the simulations successfully reproduce the general characteristics of the observations. However, in the seasonal reproduction of the Rx1 and Rx5 indices, the CRCM5 simulations exhibit significant overestimation, while the other two simulations fail to clearly emulate the spatial features described by the observations.

In terms of the correlation between the Teleconnection indices (calculated with ERA-Interim) and SPI24 (calculated with the simulations), both the CRCM5 simulations and the RegCM4-7-ERA_Interim-0.25 simulation successfully identified the moisture conditions associated with the positive phase of ENSO and PDO during the period from 1991 to 1994, though with an underestimation of the correlation's intensity. The simulations identify the contrast between positive and negative correlations in the south and north, respectively, with an underestimation in the north and an overestimation in northwestern Mexico. Due to its resolution, the ERA-Interim data exhibited the greatest overestimation of the negative correlation and the most significant underestimation of the positive correlation among all datasets.

This thesis not only aligns with the climatological characteristics presented by other authors but also contributes and delves deeper into the climatological behavior of extremes and their relationship with TIs. This makes this work a valuable reference not only for climate modeling studies but also for climatology. Therefore, the main contribution of this thesis is not only to examine the ability of simulations to represent the link between TIs and CEIs, but also to verify the climatic behavior of this connection and analyze the performance of the simulations at the latitude of Mexico. Specifically, it aims to innovate by deepening the understanding of the differences in the responses of various RCMs forced with ERA-Interim data, as well as to examine the reproduction of the influence of TIs on precipitation extremes and moisture conditions.

RECOMMENDATIONS

Research on the link between Oceanic Oscillations and precipitation patterns is still an evolving field. However, the need to study this teleconnection through RCMs could provide crucial insights into understanding the atmospheric response and interrelated variables. RCMs are continuously being improved, increasing in precision and resolution for various applications. In this document, one of the challenges was finding simulations from different RCMs forced with the same data while maintaining the same resolution.

One of the limitations of this study is related to the varying responses of each model. Although the models are generated under controlled conditions, they retain different resolutions. Additionally, each model exhibits a different level of reliability in simulating each variable. In the case of precipitation, the response of each model depends on the complexity of the orography.

From a climatological perspective, there is a need to continue researching atmospheric teleconnection processes to more clearly establish the associated mechanisms, both theoretically and numerically. Additionally, it was found necessary to develop research that represents precipitation patterns through various indices. Further investigation into the relationship between teleconnection indices and not only precipitation patterns but also related indices and extremes of this variable is recommended. Moreover, Mexico's unique geolocation necessitates documenting the response of precipitation patterns to various teleconnection indices, beyond those presented in this thesis.

Another limitation encountered when working with interpolated observational data is the necessity of replicating this study using direct observation data, in order to assess the overestimation or underestimation of the RCMs when emulating observations.

To further this research, it is recommended to apply methodologies aimed at explaining the spatiotemporal relationship between teleconnection indices and various precipitation patterns,

as well as potentially other related variables. This approach seeks to contribute to the understanding of the covariability between these two phenomena.

LIST OF BIBLIOGRAPHICAL REFERENCES

Abiy, A. Z., Melesse, A. M., & Abtew, W. (2019). Teleconnection of regional drought to ENSO, PDO, and AMO: Southern Florida and the Everglades. *Atmosphere*, *10*(6), 1–15. https://doi.org/10.3390/atmos10060295

Al-Hilali, S. S., Hassan, A. A., Moussa, A. M., Hassan, S. A. E. F., & Zahran, S. A. (2024). Performance evaluation of six RCMs for precipitation and temperature in a semi-arid region. *Modeling Earth Systems and Environment*, *10*(3), 4223–4235. https://doi.org/10.1007/s40808-024-02006-2

Alvarez-Olguin, G., & Escalante-Sandoval, C. (2017). Modes of Variability of Annual and Seasonal Rainfall in Mexico. *Journal of the American Water Resources Association*, *53*(1), 144–157. https://doi.org/10.1111/1752-1688.12488

Andrade-Velázquez, M., & Medrano-Pérez, O. R. (2020). Patrones de precipitación en las cuencas Usumacinta yGrijalva (sur de México) bajo un clima cambiante. *Revista Bio Ciencias*, *7*, 905. https://doi.org/10.15741/revbio.07.e905

Antic, S., Laprise, R., Denis, B., & de Elí, R. (2006). Erratum: Testing the downscaling ability of a one-way nested regional climate model in regions of complex topography (Climate Dynamics (2005) vol. 23 (473-493) 10.1007/s00382-004-0438-5). *Climate Dynamics*, *26*(2–3), 305–325. https://doi.org/10.1007/s00382-005-0046-z

Arriaga-Ramirez, S., & Cavazos, T. (2010). Regional trends of daily precipitation indices in northwest Mexico and southwest United States. *Journal of Geophysical Research Atmospheres*, *115*(14), 1–10. https://doi.org/10.1029/2009JD013248

Arriaga-Ramrez, S., & Cavazos, T. (2010a). Regional trends of daily precipitation indices in northwest Mexico and southwest United States. *Journal of Geophysical Research Atmospheres*, *115*(14), 1–10. https://doi.org/10.1029/2009JD013248

Arriaga-Ramrez, S., & Cavazos, T. (2010b). Regional trends of daily precipitation indices in northwest Mexico and southwest United States. *Journal of Geophysical Research Atmospheres*, *115*(14), 1–10. https://doi.org/10.1029/2009JD013248

Arroyo-Morales, S., Astudillo-Sánchez, C. C., Aguirre-Calderón, O. A., Villanueva-Díaz, J., Soria-Díaz, L., & Martínez-Sifuentes, A. R. (2023). A precipitation reconstruction based on pinyon pine tree rings from the northeastern Mexican subtropic. *Theoretical and Applied Climatology*, *151*(1–2), 635–649. https://doi.org/10.1007/s00704-022-04303-1

Aryal, Y., & Zhu, J. (2021a). Evaluating the performance of regional climate models to simulate the US drought and its connection with El Nino Southern Oscillation. *Theoretical and Applied Climatology*, *145*(3–4), 1259–1273. https://doi.org/10.1007/s00704-021-03704-y

Aryal, Y., & Zhu, J. (2021b). *Spatial and Temporal Variability of Drought Patterns over the Continental United States*. *35*(April). https://doi.org/10.1007/s13351-021-0045-

y.1.Introduction

Ashfaq, M., Cavazos, T., Reboita, M. S., Torres-Alavez, J. A., Im, E. S., Olusegun, C. F., Alves, L., Key, K., Adeniyi, M. O., Tall, M., Sylla, M. B., Mehmood, S., Zafar, Q., Das, S., Diallo, I., Coppola, E., & Giorgi, F. (2021). Robust late twenty-first century shift in the regional monsoons in RegCM-CORDEX simulations. *Climate Dynamics*, *57*(5–6), 1463–1488. https://doi.org/10.1007/s00382-020-05306-2

Balling, R. C., Keikhosravi Kiany, M. S., Sen Roy, S., & Khoshhal, J. (2016). Trends in Extreme Precipitation Indices in Iran: 1951-2007. *Advances in Meteorology*, *2016*. https://doi.org/10.1155/2016/2456809

Ban N., Caillaud C., Coppola E., Pichelli E., Sobolowski S., Adinolf M.,Ahrens B., Alias A., Anders I., Bastin S., Belušić D., Berthou S., Brisson E., Cardoso R. M., Chan S. C., Christensen O. B., Fernández j., Fita L., Frisius T.,Gašparac G., Giorgi F., Goergen K., Haugen J. E.,Hodnebrog O., Kartsios S., Katragkou E., Kendon E. J., Keuler K., Lavin-Gullon A., Lenderink G., Leutwyler D., Lorenz T., Maraun D., Mercogliano P., Milovac J., Panitz H., Rafa M., Remedio A. R., Schär C., Soares P. M. M., Srnec L., Steensen B. M., Stocchi P., Tölle M. H., Truhetz H., Vergara-Temprado J., Vries H., Warrach-Sagi K. Wulfmeyer V., & Zander M. J. (2021). The first multi-model ensemble of regional climate simulations at kilometer-scale resolution, part I: evaluation of precipitation. Climate Dynamics. 275-302. https://doi.org/10.1007/s00382-021-05708-w

Ban, N., Schmidli, J., & Schär, C. (2015). Heavy precipitation in a changing climate: Does short-term summer precipitation increase faster? Geophysical Research Letters, 42(4), https://doi.org/10.1002/2014GL062588

Bayissa, Y., Melesse, A., Bhat, M., Tadesse, T., & Shiferaw, A. (2021). Evaluation of regional climate models (Rcms) using precipitation and temperature-based climatic indices: A case study of florida, usa. *Water (Switzerland)*, *13*(17). https://doi.org/10.3390/w13172411

Bellenger, H., Guilyardi, E., Leloup, J., Lengaigne, M., & Vialard, J. (2014). ENSO representation in climate models: From CMIP3 to CMIP5. *Climate Dynamics*, *42*(7–8), 1999–2018. https://doi.org/10.1007/s00382-013-1783-z

Beobide-Arsuaga, G., Bayr, T., Reintges, A., & Latif, M. (2021). Uncertainty of ENSO-amplitude projections in CMIP5 and CMIP6 models. *Climate Dynamics*, *56*(11–12), 3875–3888. https://doi.org/10.1007/s00382-021-05673-4

Beranová, R., & Kyselý, J. (2024). Large-scale heavy precipitation over the Czech Republic and its link to atmospheric circulation in CORDEX regional climate models. *Theoretical and Applied Climatology*. https://doi.org/10.1007/s00704-024-04907-9

Berrisford, P., Dee, D., Fielding, K., Fuentes, M., Kallberg, P., Kobayashi, S., & Uppala, S. (2009). *The ERA-Interim Archive*. http://www.ecmwf.int/publications/library/do/references/list/782009%5Cnhttp://centaur.reading.ac.uk/1997/

Bierkens, M.F.P. Finke, P.A. Willigen, P. de willigen. (2000). *Upscaling and downscaling*

methods for environmental research (Kluwer Aca).

Bravo-Cabrera, J. L., Azpra-Romero, E., Zarraluqui-Such, V., & Gay-García, C. (2017). Effects of El Niño in Mexico during rainy and dry seasons: An extended treatment. *Atmosfera*, *30*(3), 221–232. https://doi.org/10.20937/ATM.2017.30.03.03

Brito-Castillo, L., Leyva-Contreras, A., Douglas, A. V., & Lluch-Belda, D. (2002). Pacific Decadal Oscillation and the filled capacity of dams on the rivers of the gulf of Califronia continental watershed. Atmósfera, 15, 121–138.

Byun, H. R., & Wilhite, D. A. (1999). Objective quantification of drought severity and duration. Journal of Climate, 12(9), 2747-2756.

Campos-Aranda, D. F. (2015). Contraste de los índices DPP, SPI y RDI para clasificación de sequías, en la estación climatológica Zacatecas, México. *Tecnologia y Ciencias Del Agua*, *6*(1), 183–193.

Cao, T. W., Xu, Y. R., Zheng, F., & Yang, R. W. (2024). Skillful prediction of boreal winter-spring seasonal precipitation in Southern China based on machine learning approach and dynamical ENSO prediction. *Theoretical and Applied Climatology*, *0123456789*. https://doi.org/10.1007/s00704-024-05011-8

Cárdenas, O. L. (2023). Predictive association between meteorological drought and climate indices in the state of Sinaloa, northwestern Mexico. *Arabian Journal of Geosciences*, *16*(1). https://doi.org/10.1007/s12517-022-11146-7

Casanueva, A. (2013). *teleconnection patterns Variability of extreme precipitation over Europe and its relationships with teleconnection patterns*. *October*. https://doi.org/10.5194/hess-18-709-2014

Cavazos, T., Cerezo-mota, R., & Meteorological, S. (2019). *Climatic trends and regional climate models intercomparison over the CORDEX - CAM (Central America , Caribbean and Mexico) domain Climatic trends and regional climate models intercomparison over the CORDEX-CAM (Central America , Caribbean and Mexico) . August*. https://doi.org/10.1002/joc.6276

CENAPRED. (2014). *SEQUÍAS SERIE Fascículos* (V. Ramos-Radilla (ed.)). www.cenapred.gob.mx

CENAPRED. (2021). SERIE Fasículos: INUNDACIONES. In *Secretaria de Seguridad y Protección Ciudadana, Centro Nacional de Prevención de Desastres* (Vol. 6). https://www.cenapred.unam.mx/es/Publicaciones/archivos/3-FASCCULOINUNDACIONES.PDF

Chai, T., & Draxler, R. R. (2014). Root mean square error (RMSE) or mean absolute error (MAE)? -Arguments against avoiding RMSE in the literature. *Geoscientific Model Development*, *7*(3), 1247–1250. https://doi.org/10.5194/gmd-7-1247-2014

Chen, G., Li, X., Xu, Z., Liu, Y., Zhang, Z., Shao, S., & Gao, J. (2024). PDO influenced interdecadal summer precipitation change over East China in mid-18th century. *Npj*

Climate and Atmospheric Science, *7*(1), 1–11. https://doi.org/10.1038/s41612-024-00666-6

Cheval, S. (2016). *The Standardized Precipitation Index – an overview*. *February*.

Colorado-Ruiz, G., & Cavazos, T. (2021). Trends of daily extreme and non-extreme rainfall indices and intercomparison with different gridded data sets over Mexico and the southern United States. *International Journal of Climatology*, *41*(11), 5406–5430. https://doi.org/10.1002/joc.7225

CONAGUA. (2009). Inventario Nacional de Obras de Protección contra Inundaciones en Cauces Naturales. In *Inventario Nacional de Obras de Protección contra Inundaciones en Cauces Naturales*. https://www.gob.mx/cms/uploads/attachment/file/105616/2_PRESENTACION.pdf

CONAGUA. (2024a). *Índice Estandarizado de Precipitatción (SPI)*. https://smn.conagua.gob.mx/es/climatologia/monitor-de-sequia/spi

CONAGUA. (2024b). *Monitor de Sequía*. https://smn.conagua.gob.mx/es/climatologia/monitor-de-sequia/monitor-de-sequia-en-mexico

CORDEX. (2016). *About CORDEX*. https://www.icrc-cordex2016.org/index.php/about/what-is-cordex

Costa, A. A., Guimarães, S. O., Sales, D. C., das Chagas Vasconcelos Junior, F., Marinho, M. W. S., Pereira, J. M. R., Martins, E. S. P. R., & da Silva, E. M. (2023). Precipitation extremes over the tropical Americas under RCP4.5 and RCP8.5 climate change scenarios: Results from dynamical downscaling simulations. *International Journal of Climatology*, *43*(2), 787–803. https://doi.org/10.1002/joc.7828

Dai, A. (2011). Drought under global warming: A review. Wiley Interdisciplinary Reviews: Climate Change, 2(1), 45-65. https://doi.org/10.1002/wcc.81

de Lima, M. I. P., Santo, F. E., Ramos, A. M., & Trigo, R. M. (2015). Trends and correlations in annual extreme precipitation indices for mainland Portugal, 1941–2007. *Theoretical and Applied Climatology*, *119*(1–2), 55–75. https://doi.org/10.1007/s00704-013-1079-6

De Silva, Y. K., Babel, M. S., Abatan, A. A., Khadka, D., & Shanmugasundaram, J. (2023). Evaluation of ENSO in CMIP5 and CMIP6 models and its significance in the rainfall in Northeast Thailand. *Theoretical and Applied Climatology*, *154*(3–4), 881–906. https://doi.org/10.1007/s00704-023-04585-z

Dee, D. P., Medium, F., Weather, R., Poli, P., France, M., Kobayashi, S., Andrae, U., & Meteorological, S. (2011). *The ERA-Interim reanalysis : configuration and performance of*. *April*. https://doi.org/10.1002/qj.828

Dee, D. P., Uppala, S. M., Simmons, A. J., Berrisford, P., Poli, P., Kobayashi, S., Andrae, U., Balmaseda, M. A., Balsamo, G., Bauer, P., Bechtold, P., Beljaars, A. C. M., van de Berg, L., Bidlot, J., Bormann, N., Delsol, C., Dragani, R., Fuentes, M., Geer, A. J., … Vitart, F.

(2011). The ERA-Interim reanalysis: Configuration and performance of the data assimilation system. *Quarterly Journal of the Royal Meteorological Society*, *137*(656), 553–597. https://doi.org/10.1002/qj.828

Deep G., & Verma J. (2024). Deep Learning Models for Fine-Scale Climate Change Prediction: Enhancing Spatial and Temporal Resolution Using AI. Springer Nature. 81-100.

DeFlorio, M. J., Pierce, D. W., Cayan, D. R., & Miller, A. J. (2013). Western U.S. extreme precipitation events and their relation to ENSO and PDO in CCSM4. *Journal of Climate*, *26*(12), 4231–4243. https://doi.org/10.1175/JCLI-D-12-00257.1

Deng, K., Yang, S., Fan, K., Wang, Z., Yu, W., Huang, Z., Xia, M., Chen, D., Lian, T., & Tian, B. (2024). A dry-wet teleconnection between southwestern and northeastern China in winter and early spring. *Climate Dynamics*. https://doi.org/10.1007/s00382-024-07228-9

Deser, Clara &, Trenberth, K. & N. C. for A. R. S. (2022). *The Climate Data Guide: Pacific Decadal Oscillation (PDO): Definition and Indices*. https://doi.org/https://doi.org/10.1002/2013eo130001

Deser, C., Alexander, M. A., Xie, S. P., & Phillips, A. S. (2010). Sea surface temperature variability: Patterns and mechanisms. In *Annual Review of Marine Science* (Vol. 2, Issue 1). https://doi.org/10.1146/annurev-marine-120408-151453

Diasso, U., & Abiodun, B. J. (2017). Drought modes in West Africa and how well CORDEX RCMs simulate them. Theoretical and Applied Climatology, 128(1–2), 223–240. https://doi.org/10.1007/s00704-015-1705-6

Diro, G. T., Tompkins, A. M., & Bi, X. (2012) Dynamical downscaling of ECMWF Ensemble seasonal forecasts over East Africa with RegCM3. Journal of Geophysical Research, 117(D16). https://doi.org/10.1029/2011JD016997

Dittus, A. J., Karoly, D. J., Donat, M. G., Lewis, S. C., & Alexander, L. V. (2018). Understanding the role of sea surface temperature-forcing for variability in global temperature and precipitation extremes. *Weather and Climate Extremes*, *21*(June), 1–9. https://doi.org/10.1016/j.wace.2018.06.002

Do, Q. Van, Do, H. X., Do, N. C., & Ngo, A. Le. (2020). *Changes in Precipitation Extremes across Vietnam and Its Relationships with Teleconnection Patterns of the Northern Hemisphere*.

Duan, K., & Mei, Y. (2014). Comparison of Meteorological, Hydrological and Agricultural Drought Responses to Climate Change and Uncertainty Assessment. *Water Resources Management*, *28*(14), 5039–5054. https://doi.org/10.1007/s11269-014-0789-6

Edwards, P. N. (2011). History of climate modeling. *Wiley Interdisciplinary Reviews: Climate Change*, *2*(1), 128–139. https://doi.org/10.1002/wcc.95

Ehret, U., Zehe, E., Wulfmeyer, V., Warrach-Sagi, K., & Liebert, J. (2012). HESS Opinions "Should we apply bias correction to global and regional climate model data?" Hydrology

and Earth System Sciences, 16, 3391–3404. https://doi.org/10.5194/hess-16-3391-2012

Endris, H. S., Hewitson, B., & Nikulin, G. (2016). Teleconnection responses in multi-GCM driven CORDEX RCMs over Eastern Africa. *Climate Dynamics*, *46*(9), 2821–2846. https://doi.org/10.1007/s00382-015-2734-7

Englehart, P., & Douglas, A. (2002). Mexico's summer rainfall patterns: an analysis of regional modes and changes in their teleconnectivity. *Atmosfera*, *15*, 147–164. https://doi.org/https://www.scielo.org.mx/pdf/atm/v15n3/v15n3a2.pdf

Flato, G. M. (2011). *Earth system models : an overview*. *2*(December), 783–800. https://doi.org/10.1002/wcc.148

Frajka-Williams, E., Beaulieu, C., & Duchez, A. (2017). Emerging negative Atlantic Multidecadal Oscillation index in spite of warm subtropics. *Scientific Reports*, *7*(1), 1–8. https://doi.org/10.1038/s41598-017-11046-x

Fuentes-Franco, R., Coppola, E., Giorgi, F., Graef, F., & Pavia, E. G. (2014). Assessment of RegCM4 simulated inter-annual variability and daily-scale statistics of temperature and precipitation over Mexico. *Climate Dynamics*, *42*(3–4), 629–647. https://doi.org/10.1007/s00382-013-1686-z

Fuentes-Franco, R., Giorgi, F., Coppola, E., & Kucharski, F. (2016). The role of ENSO and PDO in variability of winter precipitation over North America from twenty first century CMIP5 projections. *Climate Dynamics*, *46*(9–10), 3259–3277. https://doi.org/10.1007/s00382-015-2767-y

Gajić-Čapka, M., Cindrić, K., & Pasarić, Z. (2015). Trends in precipitation indices in Croatia, 1961–2010. *Theoretical and Applied Climatology*, *121*(1–2), 167–177. https://doi.org/10.1007/s00704-014-1217-9

García-Cueto, O. R., Santillán-Soto, N., López-Velázquez, E., Reyes-López, J., Cruz-Sotelo, S., & Ojeda-Benítez, S. (2019). Trends of climate change indices in some Mexican cities from 1980 to 2010. *Theoretical and Applied Climatology*, *137*(1–2), 775–790. https://doi.org/10.1007/s00704-018-2620-4

Gebre, T., Abraha, Z., Zenebe, A., & Zeweld, W. (2024). Precipitation variability and its teleconnection with the global SST and ENSO indices in the food-insecure rural areas of Tigray. *Theoretical and Applied Climatology*, *155*(3), 1699–1711. https://doi.org/10.1007/s00704-023-04717-5

Gibbs, W.J. and J.V. Maher, (1967): Rainfall Deciles as Drought Indicators. Bureau of Meteorology Bulletin No. 48, Melbourne, Australia.

Giddings, L., & Soto, M. (2005). *Standardized Precipitation Index Zones for México*. 33–56.

Gimeno-Sotelo, L., Bevacqua, E., & Gimeno, L. (2023). Combinations of drivers that most favor the occurrence of daily precipitation extremes. *Atmospheric Research*, *294*(April), 106959. https://doi.org/10.1016/j.atmosres.2023.106959

Giorgi F. (2019). Thirty Years of Regional Climate Modeling: Where Are Weand Where Are

We Going next?. Journal of Geophysical Research, 124, 5696-5723. https://doi.org/10.1029/2018JD030094

Giorgi, F., Coppola, E., Solmon, F., Mariotti, L., Sylla, M. B., Bi, X., Elguindi, N., Diro, G. T., Nair, V., Giuliani, G., Turuncoglu, U. U., Cozzini, S., Güttler, I., O'Brien, T. A., Tawfik, A. B., Shalaby, A., Zakey, A. S., Steiner, A. L., Stordal, F., … Brankovic, C. (2012). RegCM4: Model description and preliminary tests over multiple CORDEX domains. *Climate Research*, *52*(1), 7–29. https://doi.org/10.3354/cr01018

Giorgi, F., Hewitson, B., Christensen, J., Hulme, M., Von Storch, H., Whetton, P., Jones, R., Mearns, L., & Fu, C. (2001). Regional Climate Information Evaluation and Projections. *Climate Change 2001: The Scientific Basis. Contribution of Working Group I to the Third Assessment Report of the Intergovernmental Panel on Climate Change*.

Giorgi, F., & Jr, W. J. G. (2015). Regional Dynamical Downscaling and the CORDEX Initiative. *Annual Reviews*, 467–490. https://doi.org/10.1146/annurev-environ-102014-021217

Giorgi, F., Torma, C., Coppola, E., Ban, N., Schär, C., & Somot, S. (2016). Enhanced summer convective rainfall at Alpine high elevations in response to climate warming. Nature Geoscience, 9, 584-589. https://doi.org/10.1038/ngeo2761

Gonzalez, J. M., Leyva, A. R., Oviedo, E. C., Lupercio, A. Z., & Perez, T. C. (2010). Teleconexiones de la Oscilaci??n Decadal del Pac??fico (PDO) a la precipitaci??n y temperatura en M??xico. *Investigaciones Geograficas*, *73*(1923), 57–70.

Grassi, B., Redaelli, G., Canziani, P. O., & Visconti, G. (2012). Effects of the PDO phase on the tropical belt width. *Journal of Climate*, *25*(9), 3282–3290. https://doi.org/10.1175/JCLI-D-11-00244.1

Guttman, N. B. (1999). ACCEPTING THE STANDARDIZED PRECIPITATION INDEX: A CALCULATION ALGORITHM. *Journal Of The American Water Resources Association*, *35*(2).

Hamlet, A. F., & Lettenmaier, D. P. (2007). Effects of 20th century warming and climate variability on flood risk in the western U.S. *Water Resources Research*, *43*(6), 1–17. https://doi.org/10.1029/2006WR005099

Hayes, M.J., (2006): Drought Indices. Van Nostrand's Scientific Encyclopedia, John Wiley & Sons, Inc. DOI: 10.1002/0471743984.vse8593.

Hernandez-Garcia, A., Poulin, A. et Romero Lopez, R. (2024). What can we learn from ERA-Interim-driven RCM simulations on the relationship between ENSO and climate extreme indices in Mexico? Theoretical and applied climatology (under review).

Hersbach, H., Bell, B., Berrisford, P., Hirahara, S., Horányi, A., Muñoz-Sabater, J., Nicolas, J., Peubey, C., Radu, R., Schepers, D., Simmons, A., Soci, C., Abdalla, S., Abellan, X., Balsamo, G., Bechtold, P., Biavati, G., Bidlot, J., Bonavita, M., De Chiara, G., Dahlgren, P., Dee, D., Diamantakis, M., Dragani, R., Flemming, J., Forbes, R., Fuentes, M., Geer, A., Haimberger, L., Healy, S., Hogan, R. J., Hólm, E., Janisková, M., Keeley, S.,

Laloyaux, P., Lopez, P., Lupu, C., Radnoti, G., de Rosnay, P., Rozum, I., Vamborg, F., Villaume, S., & Thépaut, J. (2020). The ERA5 global reanalysis. Quarterly Journal of the Royal Meteorological Society, 146, 1999–2049. https://doi.org/10.1002/qj.3803

Hidalgo, H. G., & Dracup, J. A. (2003). ENSO and PDO Effects on Hydroclimatic Variations of the Upper Colorado River Basin. *Journal of Hydrometeorology*, *4*(1), 5–23. https://doi.org/10.1175/1525-7541(2003)004<0005:EAPEOH>2.0.CO;2

Houghton, J. T. (1986). *The physics of atmospheres* (Cambridge). https://archive.org/search?query=external-identifier%3A%22urn%3Alcp%3Aphysicsofatmosph0000houg%3Alcpdf%3A7e8c7e43-234e-4f13-b9b0-8f137201025c%22

Huang, C., Liu, H., Li, H., Zuo, J., & Wang, R. (2024). Combined effects of ENSO and PDO on activity of major hurricanes in the eastern North Pacific. *Climate Dynamics*, *62*(2), 1467–1486. https://doi.org/10.1007/s00382-023-06973-7

Hurwitz, M. M., Calvo, N., Garfinkel, C. I., Butler, A. H., Ineson, S., Cagnazzo, C., Manzini, E., & Peña-Ortiz, C. (2014). Extra-tropical atmospheric response to ENSO in the CMIP5 models. *Climate Dynamics*, *43*(12), 3367–3376. https://doi.org/10.1007/s00382-014-2110-z

IPCC. (2001). The Scientific Basis. Contribution of Working Group I to the Third Assessment Report of the Intergovernmental Panel on Climate Change. In *[Houghton, J.T., Y. Ding, D.J. Griggs, M. Noguer, P.J. van der Linden, X. Dai, K. Maskell, and C.A. Johnson (eds.)]* (Vol. 12, Issue 3). https://doi.org/10.1016/S1058-2746(02)86826-4

IPCC. (2007a). Climate Change 2007: Impacts, Adaptation and Vulnerability. In *Contribution of Working Group II to the Fourth Assessment*. https://doi.org/10.1016/B978-008044910-4.00250-9

IPCC. (2007b). Climate Change 2007 Synthesis Report. In *Chemicals, Environment, Health: A Global Management Perspective*. https://doi.org/10.1201/b11064-39

IPCC. (2012). Managing the Risks of Extreme Events and Disasters to Advance Climate Change Adaptation. In *A Special Report of Working Groups I and II of the Intergovernmental Panel on Climate Change*. https://doi.org/10.1017/CBO9781139177245.009

IPCC. (2014). Cambio Climático 2014: Impactos, adaptación y vulnerabilidad. In *Contribución del Grupo de trabajo II al Quinto Informe de Evaluación del Grupo Intergubernamental de Expertos sobre el Cambio Climático*. https://www.ipcc.ch/site/assets/uploads/2018/02/ar5_wgII_spm_en.pdf

IPCC. (2022). Impacts, Adaptation, and Vulnerability. In *Working Group II Contribution to the IPCC Sixth Assessment Report of the Intergovernmental Panel on Climate Change* (Issue August). https://doi.org/10.1017/9781009325844.Front

IPCC. (2024). *Data Distribution Centre*. What Is a GCM? https://ipcc-data.org/guidelines/pages/gcm_guide.html

Jacob, D., Bärring, L., Christensen, O. B., Christensen, J. H., & De, M. (2007). *An inter-comparison of regional climate models for Europe : Model performance in Present-Day Climate An inter-comparison of regional climate models for Europe : Model performance in Present-Day Climate*. *May*. https://doi.org/10.1007/s10584-006-9213-4

Jauregui, E. (1995). Rainfall fluctuations and tropical storm activity in Mexico. *Erdkunde*, *49*(1), 39–48. https://doi.org/https://doi.org/10.3112/erdkunde.1995.01.04

Jiang, P., Gautam, M. R., Zhu, J., & Yu, Z. (2013). How well do the GCMs/RCMs capture the multi-scale temporal variability of precipitation in the Southwestern United States? *Journal of Hydrology*, *479*, 75–85. https://doi.org/10.1016/j.jhydrol.2012.11.041

Jiang, P., Gautam, M. R., Zhu, J., & Yu, Z. (2013). How well do the GCMs/RCMs capture the multi-scale temporal variability of precipitation in the Southwestern United States? Journal of Hydrology, 479, 75–85. https://doi.org/10.1016/j.jhydrol.2012.11.041

Karl, T. R., Nicholls, N., & Ghazi, A. (1999). CLIVAR/GCOS/WMO Workshop on Indices and Indicators for Climate Extremes Workshop Summary BT - Weather and Climate Extremes: Changes, Variations and a Perspective from the Insurance Industry. In *Weather and Climate Extremes* (pp. 3–7). http://link.springer.com/10.1007/978-94-015-9265-9_2%0Ahttps://doi.org/10.1007/978-94-015-9265-9_2

Karmalkar, A. V., Bradley, R. S., & Diaz, H. F. (2011). Climate change in Central America and Mexico: Regional climate model validation and climate change projections. *Climate Dynamics*, *37*(3), 605–629. https://doi.org/10.1007/s00382-011-1099-9

Kashki, A., Karami, M., & Hosseini, S. M. (2022). Analysis of El Niño–Southern Oscillation and its impact on precipitation distribution over Iran. *Arabian Journal of Geosciences*, *15*(14). https://doi.org/10.1007/s12517-022-10452-4

Keyantash, John, N. C. for A. R. S. (2023). *Standardized Precipitation Index (SPI)*. https://doi.org/https://doi.org/10.1002/2013eo130001

Khan, J. A., & Arsalan, M. H. (1966). *General Climatology*. https://doi.org/10.2307/1792587

Kim, Y., Min, S., Zhang, X., Sillmann, J., & Sandstad, M. (2020). Evaluation of the CMIP6 multi-model ensemble for climate extreme indices. *Weather and Climate Extremes*, *29*, 100269. https://doi.org/10.1016/j.wace.2020.100269

Kumar, S., Kinter, J., Dirmeyer, P. A., Pan, Z., & Adams, J. (2013) Multidecadal Climate Variability and the "Warming Hole" in North America: Results from CMIP5 Twentieth- and Twenty-First-Century Climate Simulations. Journal of Climate. 3511-3527. https://doi.org/10.1175/JCLI-D-12-00535.1

Lagos-Zúñiga, M., Balmaceda-Huarte, R., Regoto, P., Torrez, L., Olmo, M., Lyra, A., Pareja-Quispe, D., & Bettolli, M. L. (2022). Extreme indices of temperature and precipitation in South America: trends and intercomparison of regional climate models. *Climate Dynamics*, *0123456789*. https://doi.org/10.1007/s00382-022-06598-2

Laprise, R. (2008). Regional climate modelling. Journal of Computational Physics, 227(7), 3641–3666. https://doi.org/10.1016/j.jcp.2006.10.024

Li, P., Yu, Z., Jiang, P., & Wu, C. (2021). Spatiotemporal characteristics of regional extreme precipitation in Yangtze River basin. *Journal of Hydrology*, *603*(PA), 126910. https://doi.org/10.1016/j.jhydrol.2021.126910

Liang, X.-Z., Xu, M., Kunkel, K. E., Grell, G. A., & Kain, J. S. (2007). Regional Climate Model Simulation of U . S .– Mexico Summer Precipitation Using the Optimal Ensemble of Two Cumulus Parameterizations. *Journal of Climate*, *20*(20), 5201–5207. https://doi.org/https://doi.org/10.1175/JCLI4306.1

Liu, Z., Liu, Y., Wang, S., Yang, X., Wang, L., Baig, M. H. A., Chi, W., & Wang, Z. (2018). Evaluation of spatial and temporal performances of ERA-interim precipitation and temperature in Mainland China. *Journal of Climate*, *31*(11), 4347–4365. https://doi.org/10.1175/JCLI-D-17-0212.1

Livneh, B., Bohn, T. J., Pierce, D. W., Munoz-Arriola, F., Nijssen, B., Vose, R., Cayan, D. R., & Brekke, L. (2015). A spatially comprehensive, hydrometeorological data set for Mexico, the U.S., and Southern Canada 1950-2013. *Scientific Data*, *2*, 1–12. https://doi.org/10.1038/sdata.2015.42

Llanes-Cárdenas, O., Norzagaray-Campos, M., Gaxiola, A., & González, G. E. G. (2020). Regional precipitation teleconnected with PDO-AMO-ENSO in northern Mexico. *Theoretical and Applied Climatology*, *140*(1–2), 667–681. https://doi.org/10.1007/s00704-019-03003-7

Llano, A. V. (2018). *Ninth ICTP Workshop on the Theory and Use of Regional Climate Models Added Value of RegCM4 simulations over Central America and the Caribbean . Authors : Alejandro Vichot Llano Dr . Daniel Martinez Castro*. *June*.

Luo, B., Minnett, P. J., Szczodrak, M., Nalli, N. R., & Morris, V. R. (2020). Accuracy Assessment of MERRA-2 and ERA-Interim Sea Surface Temperature, Air Temperature, and Humidity Profiles over the Atlantic Ocean Using AEROSE Measurements. *Journal of Climate*, *33*(16), 6889–6909. https://doi.org/10.1175/JCLI-D-19-0955.1

Magallanes-Quintanar, R., Blanco-Macías, F., Galván-Tejada, E. C., Galván-Tejada, J., Márquez-Madrid, M., & Valdez-Cepeda, R. D. (2019). Negative regional standardized precipitation index trends prevail in the Mexico's state of Zacatecas. *Terra Latinoamericana*, *37*(4), 487–499. https://doi.org/10.28940/terra.v37i4.563

Magallanes-Quintanar, R., Galván-Tejada, C. E., Galván-Tejada, J. I., de Jesús Méndez-Gallegos, S., Blanco-Macías, F., & Valdez-Cepeda, R. D. (2023). Artificial Neural Network Models for Prediction of Standardized Precipitation Index in Central Mexico. *Agrociencia*, *57*(1), 177–207. https://doi.org/10.47163/agrociencia.v57i1.2655

Magallanes-Quintanar, R., Galván-Tejada, C. E., Galván-Tejada, J. I., Gamboa-Rosales, H., Méndez-Gallegos, S. de J., & García-Domínguez, A. (2024). Auto-Machine-Learning Models for Standardized Precipitation Index Prediction in North–Central Mexico. *Climate*, *12*(7), 102. https://doi.org/10.3390/cli12070102

Mantua, N. J., Hare, S. R., Zhang, Y., Wallace, J. M., & Francis, R. C. (1997a). A Pacific

Interdecadal Climate Oscillation with Impacts on Salmon Production. *Bulletin of the American Meteorological Society*, *78*(6), 1069–1079. https://doi.org/10.1175/1520-0477(1997)078<1069:APICOW>2.0.CO;2

Mantua, N. J., Hare, S. R., Zhang, Y., Wallace, J. M., & Francis, R. C. (1997b). *A Pacific Interdecadal Climate Oscillation with Impacts on Salmon Production *. January*.

Maraun, D., Wetterhall, F., Ireson, A. M., Chandler, R. E., Kendon, E. J., Widmann, M., Brienen, S., Rust, H. W., Sauter, T., Themeßl, M., Venema, V. K. C., Chun, K. P., Goodess, C. M., Jones, R. G., Onof, C., Vrac, M., & Thiele-Eich, I. (2010). Precipitation downscaling under climate change: Recent developments to bridge the gap between dynamical models and the end user. Reviews of Geophysics, 48(3). https://doi.org/10.1029/2009RG000314

Maraun, D, Shepherd T. G., Widmann M., Zappa G., Walton D., Gutierrez J. M., Hagemann S., Richter I., 785 Soares P. M. M., Hall A., & Mearns L. O.. (2017). Towards process-informed bias correction of climate 786 change simulations. Nature Climate Change, 7(11), 764-773. https://doi.org/10.1038/nclimate3418

Martynov, A., Laprise, R., Sushama, L., Winger, K., Šeparović, L., & Dugas, B. (2013). Reanalysis-driven climate simulation over CORDEX North America domain using the Canadian Regional Climate Model, version 5: Model performance evaluation. *Climate Dynamics*, *41*(11–12), 2973–3005. https://doi.org/10.1007/s00382-013-1778-9

Mccabe, G. J., Palecki, M. A., & Betancourt, J. L. (2004). *Pacific and Atlantic Ocean influences on multidecadal drought frequency in the United States*. *April*. https://doi.org/10.1073/pnas.0306738101

McKee, T.B., Doesken, N.J., Kleist, J. (1993). The relationship of drought frequency and duration to time scales. In In Proc. 8th Conf. on Applied Climatology (Ed.), *In Proc. 8th Conf. on Applied Climatology* (pp. 179–184). American Meteorological Society. https://www.droughtmanagement.info/literature/AMS_Relationship_Drought_Frequency_Duration_Time_Scales_1993.pdf

Meher, J. K., & Das, L. (2019). Skill of CMIP5 climate models to reproduce the stability indices in identifying thunderstorms over the Gangetic West Bengal. *Atmospheric Research*, 172–180. https://doi.org/https://doi.org/10.1016/j.atmosres.2019.04.006

Méndez, M., & Magaña, V. (2010). Regional aspects of prolonged meteorological droughts over Mexico and central America. *Journal of Climate*, *23*(5), 1175–1188. https://doi.org/10.1175/2009JCLI3080.1

Mendoza-Uribe, I., & Lugo-Morín, D. R. (2020). Performance of the WRF model with different physical parameterizations in the precipitation simulation of the state of Puebla. *Atmosfera*, *33*(4), 357–383. https://doi.org/10.20937/ATM.52640

Meque, A., & Abiodun, B. J. (2015). *Simulating the link between ENSO and summer drought in Southern Africa using regional climate models*. 1881–1900. https://doi.org/10.1007/s00382-014-2143-3

Montero-Martínez, M. J., Santana-Sepúlveda, J. S., Pérez-Ortiz, N. I., Pita-Díaz, Ó., & Castillo-Liñan, S. (2018). Comparing climate change indices between a northern (arid) and a southern (humid) basin in Mexico during the last decades. *Advances in Science and Research*, *15*(2014), 231–237. https://doi.org/10.5194/asr-15-231-2018

Morales-Velazquez, M. I., del Socorro Herrera, G., Aparicio, J., Rafieeinasab, A., & Lobato-Sanchez, R. (2021). Evaluating reanalysis and satellite-based precipitation at regional scale:A case study in southern Mexico. *Atmosfera*, *34*(2), 189–206. https://doi.org/10.20937/ATM.52789

NASA. (2024). *Drought Parches Mexico*. 1–5. https://earthobservatory.nasa.gov/images/152908/drought-parches-mexico

NCAR. (2024). *Standardized Precipitation Index (SPI)*. https://climatedataguide.ucar.edu/climate-data/standardized-precipitation-index-spi

Newman, M., Alexander, M. A., Ault, T. R., Cobb, K. M., Deser, C., Di Lorenzo, E., Mantua, N. J., Miller, A. J., Minobe, S., Nakamura, H., Schneider, N., Vimont, D. J., Phillips, A. S., Scott, J. D., & Smith, C. A. (2016). The Pacific decadal oscillation, revisited. *Journal of Climate*, *29*(12), 4399–4427. https://doi.org/10.1175/JCLI-D-15-0508.1

Niiler, P. (1992). The Ocean Circulation. In K. E. Trenberth (Ed.), *Climate System Modeling* (First edit, pp. 117–148). Cambridge University press.

Niiler, P. P. (1992). The ocean circulation. In *Climate System Modeling* (Kevin E. T, pp. 117–148). Cambridge University Press.

NOAA. (2010). *Sea Surface Temperature Anomaly - Real-time*. https://sos.noaa.gov/catalog/datasets/sea-surface-temperature-anomaly-real-time/#:~:text=Sea surface temperature anomaly is the difference between,indicate that the ocean is warmer than average.

NOAA. (2012). *Teleconnection Introduction*. https://www.cpc.ncep.noaa.gov/data/teledoc/teleintro_body.html

NOAA. (2024a). *El Niño/Southern Oscillation*. https://www.ncei.noaa.gov/access/monitoring/enso/technical-discussion

NOAA. (2024b). *El Niño Suthern Oscillation,*. Introduction and Technical Discussion. https://www.ncei.noaa.gov/access/monitoring/enso/

Ohba, M., & Sugimoto, S. (2022). Dynamic and thermodynamic contributions of ENSO to winter precipitation in Japan: frequency and precipitation of synoptic weather patterns. *Climate Dynamics*, *59*(5–6), 1489–1504. https://doi.org/10.1007/s00382-021-06052-9

O'Reilly, C. H. (2018). Interdecadal variability of the ENSO teleconnection to the wintertime North Pacific. Climate Dynamics, 51(9–10), 3333–3350. https://doi.org/10.1007/s00382-018-4081-y

Ortiz-Gómez, R., Muro-Hernández, L. J., & Flowers-Cano, R. S. (2020). Assessment of extreme precipitation through climate change indices in Zacatecas, Mexico. *Theoretical*

and Applied Climatology, *141*(3–4), 1541–1557. https://doi.org/10.1007/s00704-020-03293-2

Oviedo, E. C. (2010). *Teleconexiones de la Oscilación Decadal del Pacífico (PDO) a la precipitación y temperatura en México Teleconnection of the Pacific Decadal Oscillation (PDO) to the precipitation and temperature in Mexico*. *1923*, 57–70.

Palmer, W. C. (1965). Meteorological drought. US Department of Commerce, Weather Bureau Research Paper 45.

Pan, Y., Zeng, N., Mariotti, A., Wang, H., & Kumar, A. (2018). Covariability of Central America / Mexico winter precipitation and tropical sea surface temperatures. *Climate Dynamics*, *50*(11), 4335–4346. https://doi.org/10.1007/s00382-017-3878-4

Pavia, E. G., Graef, F., & Reyes, J. (2006a). Notes and correspondence PDO – ENSO Effects in the Climate of Mexico. *Journal of Climate*, *19*, 6433–6438.

Pavia, E. G., Graef, F., & Reyes, J. (2006b). *PDO-ENSO effects in the climate of Mexico PDO – ENSO Effects in the Climate of Mexico*. *December*. https://doi.org/10.1175/JCLI4045.1

Peterson, T. C., Folland, C. C., Gruza, G., Hogg, W., Mokssit, A., & Plummer, N. (2001). Report on the activities of the Working Group on Climate Change Detection and Related Rapporteurs 1998–2001. *Rep. WCDMP-47, WMO-TD 1071*, *March*, 143. http://etccdi.pacificclimate.org/docs/wgccd.2001.pdf

Pita-Díaz, O., & Ortega-Gaucin, D. (2020). Analysis of anomalies and trends of climate change indices in Zacatecas, Mexico. *Climate*, *8*(4). https://doi.org/10.3390/cli8040055

Prein A. F., Langhans W., Fosser G., Ferrone A., Ban N., Goergen K., Keller M., Tölle M., Gutjahr O., Feser F., Brisson E., Kollet S., Schmidli J., van Lipzig N. P. M., Leung R. (2015). "A review on regional convection-permitting climate modeling: Demonstrations, prospects, and challenges." Reviews of Geophysics, 53(2), 323-361. https://doi.org/10.1002/2014RG000475

Prein, A. F., Liu, C., Ikeda, K., Bullock, R., Rasmussen, R. M., Holland, G. J., & Clark, M. (2017). Simulating North American mesoscale convective systems with a convection-permitting climate model. Climate Dynamics, 55, 95-110. https://doi.org/10.1007/s00382-017-3993-2

Rai, P., Bangelesa, F., Abel, D., Ziegler, K., Huang, J., Schaffhauser, T., Pollinger, F., Disse, M., & Paeth, H. (2024). Extreme precipitation and temperature indices under future climate change in central Asia based on CORDEX-CORE. *Theoretical and Applied Climatology*. https://doi.org/10.1007/s00704-024-04976-w

Randall, D.A., Wood, R. A., Bony, S., Colman, R., Fichefet, T., Fyfe, J., Kattsov, V., Pitman, A., Shukla, J., Srinivasan, J., Stouffer, R. J., Sumi, A., & Taylo, K. E. (2007). Climate Models and Their Evaluation. In *IPCC* (Vol. 323). https://doi.org/10.1016/j.cub.2007.06.045

Rayner, N. A., Parker, D. E., Horton, E. B., Folland, C. K., Alexander, L. V, Rowell, D. P.,

Kent, E. C., & Kaplan, A. (2003). *Global analyses of sea surface temperature , sea ice , and night marine air temperature since the late nineteenth century*. *108*. https://doi.org/10.1029/2002JD002670

Rivera-Arriaga, E., Silva, R., Cruz-Ramírez, C. J., Azuz-Adeath, I., Vega-Serratos, B. E., & Vanegas, G. P. (2023). Risk Management of Extreme Precipitation in Mexico: Building Resilience. *Disaster Risk Reduction for Resilience: Climate Change and Disaster Risk Adaptation*, 273–302. https://doi.org/10.1007/978-3-031-22112-5_12

Ruiz-Alvarez, O., Singh, V. P., Enciso-Medina, J., Ontiveros-Capurata, R. E., & dos Santos, C. A. C. (2020). Observed trends in daily extreme precipitation indices in Aguascalientes, Mexico. *Meteorological Applications*, *27*(1), 1–20. https://doi.org/10.1002/met.1838

Ruiz-Vásquez, M., Arias, P. A., & Martínez, J. A. (2024). Enso influence on water vapor transport and thermodynamics over Northwestern South America. *Theoretical and Applied Climatology*, *155*(5), 3771–3789. https://doi.org/10.1007/s00704-024-04848-3

S.I., N. Nicholls, D. Easterling, C.M. Goodess, S. Kanae, J. Kossin, Y. Luo, J. Marengo, K. McInnes, M. Rahimi, M. Reichstein, A. Sorteberg, C. Vera, and X. Z. (2012). 2012: Changes in climate extremes and their impacts on the natural physical environment. In: Managing the Risks of Extreme Events and Disasters to Advance Climate Change Adaptation [Field, C.B., V. Barros, T.F. Stocker, D. Qin, D.J. Dokken, K.L. Ebi, M.D. In *IPCC*.

Sagarika, S., Kalra, A., & Ahmad, S. (2015). Interconnections between oceanic-atmospheric indices and variability in the U.S. streamflow. *Journal of Hydrology*, *525*, 724–736. https://doi.org/10.1016/j.jhydrol.2015.04.020

Salas-Martínez, F., Valdés-Rodríguez, O. A., Palacios-Wassenaar, O. M., & Márquez-Grajales, A. (2021). Analysis of the evolution of drought through spi and its relationship with the agricultural sector in the central zone of the state of Veracruz, Mexico. *Agronomy*, *11*(11). https://doi.org/10.3390/agronomy11112099

Salathé, E. P., Leung, L. R., Qian, Y., & Zhang, Y. (2020). *Regional Climate Model*. 45–67. https://cig.uw.edu/wp-content/uploads/sites/2/2020/12/wacciach2rcm643.pdf

Santoso, A. & N. C. for A. R. S. (2022). *The Climate Data Guide: Asymmetry and Diversity in the pattern, amplitude and duration of El Niño and La Niña*. https://doi.org/https://doi.org/10.1002/2013eo130001 Key Figures

Schneider, DP, Deser, C, Trenberth, K. (2013). Climate Data Guide Spurs Discovery and Understanding. *AGU, Advancing Earth and Sciences*, *94*(13), 121–122. https://doi.org/https://doi.org/10.1002/2013EO130001

Schneider, S. (1992). Introduction to climate modeling. In K. Trenberth (Ed.), *Climate System Modeling* (First edit, pp. 3–26). Cambridge University press.

Schubert-Frisius, M., Feser, F., von Storch, H., & Rast, S. (2017). Optimal spectral nudging for global dynamic downscaling. *Monthly Weather Review*, *145*(3), 909–927. https://doi.org/10.1175/MWR-D-16-0036.1

SEGOB, S. de G. (2015). *DOF - Diario Oficial de la Federación DOF - Diario Oficial de la Federación*. 1. https://www.dof.gob.mx/nota_detalle.php?codigo=5178126&fecha=15/02/2011#gsc.tab=0.

SEMARNAT. (2018). Sistema Nacional de Información del Agua. *Comisión Nacional Del Agua*, 1. https://sinav30.conagua.gob.mx:8080/

Senna, M. C. A., França, G. B., Pereira, M. F., da Silva, M. S., de Souza, E. P., Dragaud, I. C. D. A. V., de Souza, L. S., Moraes, N. O., de Almeida, V. A., de Almeida, M. V., Frota, M. N., de Araujo, A. A. M., do Nascimento Cardozo, K., & Viana, L. Q. (2023). A teleconnection study between oceanic oscillations and trends in precipitation extremes in the Paraíba do Sul River Basin. *Theoretical and Applied Climatology*, *152*(3–4), 1095–1113. https://doi.org/10.1007/s00704-023-04451-y

Sierra-Soler, A., Adamowski, J., Malard, J., Qi, Z., Saadat, H., & Pingale, S. (2016). Assessing agricultural drought at a regional scale using LULC classification, SPI, and vegetation indices: case study in a rainfed agro-ecosystem in Central Mexico. *Geomatics, Natural Hazards and Risk*, *7*(4), 1460–1488. https://doi.org/10.1080/19475705.2015.1073799

Simmons, A. J., Uppala, S. M., Dee, D., & Kobayashi, S. (2007). ERA-Interim: New ECMWF reanalysis products from 1989 onwards. ECMWF Feature article.

Simmons A. J,, Willett K. M., Jones P. D., & Dee D. P. (2010). Low-frequency variations in surface atmospheric humidity, temperature, and precipitation: Inferences from reanalyses and monthly gridded observational data sets. Journal of Geophysical Research, 115. https://doi.org/10.1029/2009JD012442

Song, X., Peng, L., Zhihong, J., & Jun, C. (2021). Simulation Evaluation ofAMO and PDO with CMIP5 and CMIP6 Models in Historical Experiment. *Advances in Earth Science*, *36*(1), 58–68.

Stagge, J. H., Torbenson, M. C. A., Sung, K., Phillips, B., & Kingston, D. G. (2023). Orographic amplification of El Niño teleconnections on winter precipitation across the Intermountain West of North America. *Nature Water*, *1*(12), 1016–1026. https://doi.org/10.1038/s44221-023-00163-9

Stefanidis, S., Dafis, S., & Stathis, D. (2020). Evaluation of regional climate models (Rcms) performance in simulating seasonal precipitation over mountainous central pindus (greece). *Water (Switzerland)*, *12*(10). https://doi.org/10.3390/w12102750

Stewart, R. H. (1997). *Physical Oceanography*.

Storch, H. Von, & Zwiers, F. W. (1999). Statistical Analysis in Climate Research. *Journal of the American Statistical Association*, *95*, 1375. https://doi.org/10.1017/CBO9780511612336

Strandberg, G., Bärring, L., Hansson, U., Jansson, C., Jones, C., Kjellström, E., Michael Kolax, Marco Kupiainen, G., Nikulin, P. S., & Wang, A. U. and S. (2014). CORDEX scenarios for Europe from the Rossby Centre regional climate model RCA4. *Rep. Meteorol.*

Climatol., *116*(116), 1–84. https://www.smhi.se/polopoly_fs/1.90273!/Menu/general/extGroup/attachmentColHold/mainCol1/file/RMK_116.pdf

Strandberg, G., Kjellström, E., Poska, A., Wagner, S., Gaillard, M. J., Trondman, A. K., Mauri, A., Davis, B. A. S., Kaplan, J. O., Birks, H. J. B., Bjune, A. E., Fyfe, R., Giesecke, T., Kalnina, L., Kangur, M., Van Der Knaap, W. O., Kokfelt, U., Kuneš, P., Lataowa, M., … Sugita, S. (2014). Regional climate model simulations for Europe at 6 and 0.2 k BP: Sensitivity to changes in anthropogenic deforestation. *Climate of the Past*, *10*(2), 661–680. https://doi.org/10.5194/cp-10-661-2014

Teutschbein, C., & Seibert, J. (2010). *Regional Climate Models for Hydrological Impact Studies at the Catchment Scale : A Review of Recent Modeling Strategies*. *7*, 834–860.

Tootle, G. A., & Piechota, T. C. (2006). Relationships between Pacific and Atlantic ocean sea surface temperatures and U.S. streamflow variability. *Water Resources Research*, *42*(7), 1–14. https://doi.org/10.1029/2005WR004184

Torres-Alavez, J. A., Giorgi, F., Kucharski, F., Coppola, E., & Castro-García, L. (2021). ENSO teleconnections in an ensemble of CORDEX-CORE regional simulations. *Climate Dynamics*, *57*(5–6), 1445–1461. https://doi.org/10.1007/s00382-020-05594-8

Torrez-Rodriguez, L., Goubanova, K., Muñoz, C., & Montecinos, A. (2023). Evaluation of temperature and precipitation from CORDEX-CORE South America and Eta-RCM regional climate simulations over the complex terrain of Subtropical Chile. *Climate Dynamics*, *61*(7–8), 3195–3221. https://doi.org/10.1007/s00382-023-06730-w

Tramblay, Y., El Adlouni, S., & Servat, E. (2013). Trends and variability in extreme precipitation indices over maghreb countries. *Natural Hazards and Earth System Sciences*, *13*(12), 3235–3248. https://doi.org/10.5194/nhess-13-3235-2013

Trenberth, K. & N. C. for A. R. S. (2024). *The Climate Data Guide: Nino SST Indices (Nino 1+2, 3, 3.4, 4; ONI and TNI)*. https://doi.org/https://doi.org/10.1002/2013eo130001

Vega-Camarena, J. P., Brito-Castillo, L., Pineda-Martínez, L. F., & Farfán, L. M. (2023). ENSO Impact on Summer Precipitation and Moisture Fluxes over the Mexican Altiplano. *Journal of Marine Science and Engineering*, *11*(5). https://doi.org/10.3390/jmse11051083

Vicente-Serrano, S. M., Beguería, S., & López-Moreno, J. I. (2010). A multiscalar drought index sensitive to global warming: The standardized precipitation evapotranspiration index. Journal of Climate, 1696-1718. https://doi.org/10.1175/2009JCLI2909.1

Vicente-Serrano, S. M., & López-Moreno, J. I. (2005). Hydrological response to different time scales of climatological drought: an evaluation of the standardized precipitation index in a mountainous mediterranean basin. *Hydrology and Earth System Sciences Discussions*, *2*(4), 1221–1246. https://doi.org/10.5194/hessd-2-1221-2005

Vu, T. M., & Mishra, A. K. (2016). *SPATIAL AND TEMPORAL VARIABILITY OF STANDARDIZED PRECIPITATION INDEX OVER INDOCHINA PENINSULA*. *42*(1),

221–232. https://doi.org/10.18172/cig.2928

Wallace, J. M., & Hobbs, P. V. (2006). Atmospheric Science: An Introductory Survey: Second Edition. In *Atmospheric Science: An Introductory Survey: Second Edition*. https://doi.org/10.1016/C2009-0-00034-8

Wang, S., Huang, J., He, Y., & Guan, Y. (2014). Combined effects of the Pacific Decadal Oscillation and El Niño-Southern Oscillation on Global Land Dry-Wet Changes. *Scientific Reports*, *4*, 1–8. https://doi.org/10.1038/srep06651

Wang, T., & Miao, J.-P. (2018). Twentieth-century Pacific Decadal Oscillation simulated by CMIP5 coupled models. *Atmospheric and Oceanic Science Letters*, *11*(1), 94–101. https://doi.org/10.1080/16742834.2017.1381548

Westra, S., Fowler H. J., Evans J. P., Alexander L. V., Berg P., Johnson F., Kendon E. J., Lenderink G., & Roberts N. M. (2014). Future changes to the intensity and frequency of short-duration extreme rainfall. *Reviews of Geophysics*, 52(3), 522-555. https://doi.org/10.1002/2014RG000464

WMO. (2012a). *Índice Normalizado de Precipitación. Guía del usuario*. 1–23.

WMO. (2012b). SPI user guide. In *World Meteorological Organization* (Vol. 1090).

WMO. (2019). *WMO atlas of mortality and economic losses from weather, climate and water extremes*.

WMO, & GWP. (2017). *Handbook of Drought Indicators and Indices (M. Svoboda and B.A. Fuchs)* (Integrated, Issue 1173). https://doi.org/10.1201/9781315265551-12

Xavier, A. K., Varikoden, H., Babu, C. A., & Reshma, T. (2023). Influence of PDO and ENSO with Indian summer monsoon rainfall and its changing relationship before and after 1976 climate shift. *Climate Dynamics*, *61*(11–12), 5465–5482. https://doi.org/10.1007/s00382-023-06865-w

Xiao, M., Zhang, Q., & Singh, V. P. (2017). Spatiotemporal variations of extreme precipitation regimes during 1961–2010 and possible teleconnections with climate indices across China. *International Journal of Climatology*, *37*(1), 468–479. https://doi.org/10.1002/joc.4719

Xiong, J., Yong, Z., Wang, Z., Cheng, W., Li, Y., Zhang, H., Ye, C., & Yang, Y. (2019). Spatial and temporal patterns of the extreme precipitation across the Tibetan Plateau (1986-2015). *Water (Switzerland)*, *11*(7). https://doi.org/10.3390/w11071453

Xu, Z., Han, Y., & Yang, Z. (2019). Dynamical downscaling of regional climate: A review of methods and limitations. *Science China Earth Sciences*, *62*(2), 365–375. https://doi.org/10.1007/s11430-018-9261-5

Yan, J., Zhang, W., Hu, S., & Jiang, F. (2024). Different ENSO Impacts on Eastern China Precipitation Patterns in Early and Late Winter Associated with Seasonally-Varying Kuroshio Anticyclonic Anomalies. *Advances in Atmospheric Sciences*. https://doi.org/10.1007/s00376-023-3196-1

Zhang, X., Wang, J., Zwiers, F. W., & Groisman, P. Y. (2010). The influence of large-scale climate variability on winter maximum daily precipitation over North America. *Journal of Climate*, *23*(11), 2902–2915. https://doi.org/10.1175/2010JCLI3249.1

Zhao, Y., Xue, M., Jiang, J., Hu, X. M., & Huang, A. (2024). Assessment of Wet Season Precipitation in the Central United States by the Regional Climate Simulation of the WRFG Member in NARCCAP and Its Relationship with Large-Scale Circulation Biases. *Advances in Atmospheric Sciences*, *41*(4), 619–638. https://doi.org/10.1007/s00376-023-2353-x

Zúñiga, E., & Magaña, V. (2018). Vulnerability and risk to intense rainfall in Mexico: The effect of land use cover change. *Investigaciones Geograficas*, *95*. https://doi.org/10.14350/rig.59465